Investigation of Strategies to Enhance the Delivery of Oncolytic Vaccinia Virus



Claudia A. P. Hill

Linacre College

University of Oxford

A thesis submitted for the degree of

Doctor of Philosophy

Hilary Term 2020

Abstract

Vaccinia Virus (VV) is an attractive vector for oncolytic virotherapy given its potential for tumour-selective tropism, efficient cell-to-cell spread, rapid replication in cancer cells, large transgene coding capacity and stimulation of anti-tumour immunity. It has a well-defined safety profile and is being assessed in late-stage clinical trials.

Systemic delivery of VV has shown limited clinical success in patients due to a knockdown in infectivity, as a result of rapid immune-mediated neutralisation, and poor penetration into tumours. These factors have often restricted its route of delivery to intratumoural (IT) injection. For VV to become applicable across a wider range of patients/cancer indications, amenability to systemic delivery is required. This may be achieved using strategies that modulate VV by genetic or chemical means and/or that alter the physiology of target tumours. Chemical stealthing has not previously been applied to enhance the pharmacokinetics (PK) of enveloped viruses such as VV. Ultrasound (US)-mediated cavitation has been previously shown to effectively enhance the delivery of therapeutics, including VV, to solid tumours.

In this thesis, US-mediated cavitation was applied to DLD and CAPAN-2 xenografts after IT administration of VV with the aim of producing more homogenous intratumoural infection. The limited success observed in the IT context provided motivation to instead enhance the stability of VV for improved IV administration. Flow virometry demonstrated that VV could be effectively modified using an amphiphilic polymer (to create PCVV). This PCVV showed reduced natural tropism, a 20% decrease in anti-VV antibody binding and could be used as a platform for the attachment of an antibody to permit retargeting of infection to the tumour associated antigen mucin-1 (MUC1).

PK analysis of VV, PCVV and aMUC1-PCVV showed circulation kinetics for PCVV and aMUC1-PCVV were enhanced at two different doses (approximately 5-fold higher circulating dose at 5 minutes vs VV). The hypothesis that the application of US-mediated cavitation during this 5 minute window could be used to enhance extravasation of PCVV and aMUC1-PCVV into and throughout tumours, was explored. When samples were administered IV and US-mediated cavitation was applied to CAPAN-2 xenografts, increased infection (as assessed by transgene expression) was observed. The impact of cavitation on aMUC1-PCVV transgene expression was highest (a mean increase of 530-fold compared to non US exposed tumours). Tumour growth studies showed that combining aMUC1-PCVV, SSPs and US enabled substantial and significant tumour regression (-73%).

The work presented in this thesis brings to light the challenges of achieving effective and uniform delivery to tumours after both IT and IV administration of VV and contributes to the necessary progress VV needs to make if it is going to achieve its full clinical potential.

Statement of Originality

I hereby declare that this submission is my own work and, to the best of my knowledge, it contains no materials previously published or written by another person, or substantial proportions of material which have been accepted for the award of any other degree or diploma at the University of Oxford or any other educational institution, except where due acknowledgement is made in the thesis. Any contribution made to the research by others, with whom I have worked at the University of Oxford or elsewhere, is explicitly acknowledged in the thesis. I also declare that the intellectual content of this thesis is the product of my own work, except to the extent that assistance from others in the project's design and conception or in style, presentation and linguistic expression is acknowledged.

Claudia Hill
July 2020

Acknowledgements

This thesis would not have been possible without the kindness and generous support of so many people.

First and foremost I would like to thank my supervisor Prof. Robert Carlisle, without whom I would never have had the confidence to pursue a DPhil. I thank him for entrusting me with this research and guiding me through the successes and challenges that this project has encountered. I am additionally grateful for the unofficial supervision and advice I have received from Prof. Constantin Coussios and Prof. Eleanor Stride during many years of cluster meetings.

I am extremely grateful for the whole BUBBL group who have made this experience wonderful in so many ways. In particular I would like to thank Dr. Megan Grundy who has been there for me since day one and is the best mentor I could have asked for. I would also like to thank Dr. Luca Bau for helping me persevere with organic chemistry challenges and Sheena Wallington for her advice, rigorous planning and calming influence during challenging experimental days.

I would like to express my deepest gratitude to my family for their love, support and encouragement through out. Also, I want to say a special thank you to Katherine Phillips, Vicky Pugh and Anthony Pugh who have shown more kindness than I could have imagined and provided unending support to me during my time as a DPhil student. I would also like to thank all my friends near and far who have given constant reassurance, spurred me on and have taken the time to proof-read this thesis. In particular I would wish to thank Caitlin Farrar, Myfanwy Williams, Bethany Cutmore-Scott, Silviu Rad, Alec Thomas, Kristen Thomas, Isabel Stainsby, Alice Attlee, Alice Billington and Dr. Catherine Paverd.

Finally, I would like to thank Engineering and Physical Sciences Research Council, Linacre College (Brewer Street Scholarship donors) and OxCD3 for sponsoring my research. Transgene SA and OxSonics Ltd are gratefully acknowledged for their advice and provision of Vaccinia and SSPs respectively.

Statement of Contributions

I gratefully acknowledge the following who contributed to the research presented in this thesis:

Chapter 3

- Sheena Wallington: Performed the tumour inoculations for CAPAN-2 xenografts.
- Dr Megan Grundy: Performed the tumour inoculations for DLD xenografts.
- Prof. Robert Carlisle: Performed IT dosing of mice for in vivo experiments.
- Cameron Smith: Re-processed PAM data so as to calculate cavitation dose.

Chapter 4

- Dr Megan Grundy: Performed the tumour inoculations for HepG2 xenografts.
- Dr Paul Lyons: Performed phlebotomy to obtain blood from donor.
- Prof. Robert Carlisle: Performed IV dosing and bleeding of mice for in vivo experiments.
- Dr Victor Ramos: Synthesised the Chol-PEG(8K) polymer used in studies presented in this thesis.

Chapter 5

- Dr Megan Grundy: Synthesised the Chol-PEG(8K)-COOH polymer.
- Dr Luca Bau: Contributed significantly to synthesis of Chol-PEG-NHS and conducted H-NMR analysis of Chol-PEG-NHS. Optimized method for UPLC analysis of antibody-polymer constructs.
- Sheena Wallington: Performed the tumour inoculations for CAPAN-2 xenografts and performed bleeding of mice for in vivo pharmacokinetic studies.
- Prof. Robert Carlisle: Performed IV dosing and bleeding of mice for in vivo for in vivo pharmacokinetic studies.

Chapter 6

- Sheena Wallington: Performed the tumour inoculations for CAPAN-2 xenografts. Performed the DCE-MRI protocol.
- Prof. Robert Carlisle: Performed IV dosing of mice for in vivo experiments.
- Cameron Smith: Re-processed PAM data so as to calculate cavitation dose.

Dissemination

Publications

Hill, C., Bau L. and Carlisle, R. *Methods for Modification of Therapeutic Viruses.* Edited by Christine Engeland, Humana, New York, NY, 2020, pp. 7–29.

Hill, C., and Carlisle, R. "Achieving Systemic Delivery of Oncolytic Viruses." *Expert Opinion on Drug Delivery*, vol. 16, no. 6, Taylor and Francis Ltd, 3 June 2019, pp. 607–20.

Hill, C., Grundy, M., Bau, L., Wallington, S., Ramos, V., Fisher, K., Seymour, L., Coussios, C. and Carlisle, R. (2020) Polymer Stealthing and Mucin-1 (MUC1) Retargeting for Enhanced Pharmacokinetics of an Oncolytic Vaccinia Virus. *In review*

Conference Presentations

Hill, C., Grundy, M., and Carlisle, R. "Polymer Coating of Vaccinia Virus for Enhanced Bloodstream Stability", Poster presented at the 11^{th} International Oncolytic Virotherapy Conference, Oxford, UK

Hill, C., Grundy, M., Bau, L., Coussios C., and Carlisle, R. "Polymer Coating to Enhance the Delivery of Oncolytic Vaccinia Virus to Tumours", Presented at the OxCD3 Oncological Drug Delivery Conference 2019, Oxford, UK

Contents

List of Abbreviations **xiv**

1 Introduction and Literature Review **1**

1.1 Introduction . . . 1
1.2 Oncolytic Virotherapy: Benefits and Current Restrictions . . . 2
1.2.1 Oncolytic Vaccinia Virus For Cancer Treatment . . . 4
1.3 Enhancing Oncolytic Virus Efficacy by Overcoming Delivery Limitations . . . 11
1.3.1 Pharmacokinetics and anti-viral neutralisation . . . 12
1.3.1.1 Directed Evolution and Genetic Modification . . . 13
1.3.1.2 Chemical Modification . . . 15
1.3.1.2.1 Polymer stealthing viruses for enhanced blood stability . . . 15
1.3.1.2.2 Active Retargeting of Oncolytic Viruses . . . 19
1.3.1.2.3 Lipid Membrane and Lipid Anchors . . . 20
1.3.1.3 Flow Virometry for Virus Particle Detection . . . 21
1.3.1.4 Tumour-associated antigen Mucin-1 . . . 22
1.3.2 Improving Delivery within Solid Tumours . . . 23
1.3.2.1 Modification of Intratumoural Physiology . . . 24
1.3.2.1.1 Vascular Normalisation . . . 24
1.3.2.1.2 Altering the Internal Pressure Gradient . . . 27
1.3.2.2 Ultrasound . . . 28
1.3.2.2.1 Acoustic Cavitation . . . 28
1.3.2.2.2 Ultrasound Mediated Cavitation for Enhanced Drug Delivery . . . 29
1.3.2.2.3 Monitoring Cavitation Events . . . 31
1.4 Implications for Current Work . . . 32
1.4.1 Research Questions . . . 32

2 Methods and materials **34**

2.1 Chemicals and Equipment . . . 34
2.1.1 Polymers . . . 34
2.1.2 Blood Work, DNA extraction and qPCR . . . 35
2.1.3 In Vitro studies . . . 35
2.1.4 Vaccinia Viruses . . . 36
2.1.5 In Vivo studies . . . 37
2.2 Polymer Coating VV . . . 37
2.2.1 Purification of coated VV . . . 37

2.3 Retargeting VV . . . 39
2.3.1 Cholesterol-PEG-NHS synthesis . . . 39
2.3.1.1 Testing the efficiency of conversion of COOH to NHS esters on Chol-PEG-NHS . . . 39
2.3.2 Cholesterol-PEG(10K)-NHS reaction with amine groups of IgG or anti-MUC1 antibody . . . 40
2.3.2.1 HPLC analysis of PEGylated anti-MUC1 . . . 41
2.3.2.2 SDS-PAGE . . . 41
2.3.3 ELISA analysis of PEGylated aMUC1 . . . 41
2.3.3.1 Ability for Chol-PEG-aMUC1 to bind target . . . 41
2.3.3.2 Characterising Chol-PEG-aMUC1 by assaying for presence of PEG . . . 42
2.3.4 aMUC1-PCVV, IgG-PCVV and MUC1-aMUC1-PCVV formation . . . 43
2.3.5 qPCR of aMUC1-PCVV bound to immobilised MUC1 target peptide . . . 43
2.4 Flow virometry . . . 44
2.4.1 Using YOYO-1 nucleic stain to identify a VV FSC/SSC population . . . 44
2.4.2 Confirmation of Chol-PEG coating VV on BD FACS Calibur 45
2.4.3 Confirmation of Chol-PEG and Chol-PEG-aMUC1 coating VV on Attune NxT . . . 45
2.5 In Vitro Cell Work . . . 45
2.5.1 Cell culture . . . 46
2.5.2 Adherent Cell Culture assays . . . 46
2.5.3 Suspension Cell Culture Assays . . . 47
2.5.4 Lysing Cells and Luciferin Assay . . . 47
2.5.5 MTS Assay . . . 48
2.5.6 Fluorescent Microscopy . . . 48
2.5.7 Flow Cytometry . . . 49
2.5.7.1 Determining infection of cells with VV-GFP . . . 49
2.5.7.2 Determining cellular MUC1 expression of A549 and CAPAN-2 cells . . . 49
2.6 In Vitro Blood Work . . . 50
2.6.1 Evaluation of the impact of PCVV on Antibody Binding when compared to VV . . . 50
2.6.2 Human Blood Component Separation . . . 50
2.7 DNA Extraction and Quantitative Polymerase Chain Reaction (qPCR) 51
2.8 In Vivo Studies . . . 51

2.8.1 Assessment of the use of US mediated cavitation to enhance the infection intensity and spread after IT administration . . 52
2.8.1.1 Subcutaneous tumour inoculation: DLD bilateral xenografts 52
2.8.1.2 Injection and treatment: IT administered VV-GFP infection of DLD bilateral xenografts 52
2.8.1.3 IVIS Imaging: IT administered VV-GFP infection of DLD bilateral xenografts 52
2.8.2 Assessment of the use of US mediated cavitation to enhance the infection intensity and spread of pre-seeded VV infection 53
2.8.2.1 Subcutaneous tumour inoculation: CAPAN-2 unilateral xenografts 53
2.8.2.2 Injection and treatment: IT administered VV-GFP infection of CAPAN-2 unilateral xenografts 53
2.8.2.3 IVIS Imaging and tissue processing: IT administered VV-GFP infection of CAPAN-2 xenografts 54
2.8.3 CAPAN-2 tumourigenicity 54
2.8.3.1 Western blot analysis to determine MUC1 expression in CAPAN-2 human xenograft 54
2.8.3.2 DCE MRI 55
2.8.4 Pharmacokinetic studies 56
2.8.4.1 Pharmacokinetic study: VV and unwashed PCVV 56
2.8.4.1.1 Injection and treatment 56
2.8.4.2 Pharmacokinetic studies: VV, PCVV and aMUC1-PCVV 56
2.8.4.2.1 Injection and treatment 56
2.8.4.3 Blood Collection and Sample processing 57
2.8.5 In Vivo Model for Delivery of VV, PCVV, aMUC1-PCVV and IgG-PCVV 57
2.8.5.1 Injection and treatment 57
2.8.6 In Vivo Model for Tumour Volume Change of VV, aMUC1-PCVV and Glucose +/- US 58
2.8.7 Ultrasound Treatment of Tumours 58
2.8.8 IVIS Imaging and tissue processing: VV-luc infection of CAPAN-2 xenografts 59

3 Investigating the use of US-mediated cavitation to enhance the dissemination of VV-GFP after intratumoural administration 60
3.1 Introduction . . . 60
3.2 Results: Experiment 1- Bilateral DLD xenograft model with IT administered VV-GFP . . . 62
3.2.1 Experiment 1: Experimental Design . . . 62
3.2.2 Experiment 1: Acoustic Feedback . . . 64
3.2.3 Experiment 1: Assessment of US mediated cavitation with VV on tumour infection levels . . . 65
3.2.4 Experiment 1: Relationship between PAM and delivery of VV-GFP (DLD xenograft model) . . . 68
3.3 Results: Experiment 2- Unilateral CAPAN-2 xenograft model with IT administration and pre-seeded VV infection foci . . . 69
3.3.1 Experiment 2: Experimental Design . . . 69
3.3.2 Experiment 2: Acoustic Feedback . . . 71
3.3.3 Experiment 2: Assessment of US mediated cavitation with VV and pre-seeded VV infection on tumour infection levels . 75
3.3.3.1 Intervention 1 . . . 75
3.3.3.2 Intervention 2 . . . 78
3.3.3.3 Ex vivo assessment of excised tumours . . . 84
3.4 Discussion . . . 86
3.5 Summary and Conclusions . . . 91

4 Polymer Coating for Enhanced Blood Stability of Oncolytic VV 94
4.1 Introduction . . . 94
4.2 Results: Polymer Coating . . . 96
4.2.1 Determining optimum PEG-Cholesterol embedding conditions 97
4.2.2 Confirming coating with Flow Virometry . . . 100
4.3 Results: Interaction of VV and PCVV with Human Blood Components 109
4.3.1 Impact of PEG-Cholesterol Coating on VV Binding of Neutralising Antibodies . . . 110
4.3.2 Distribution Of VV and PCVV In Human Blood Components 111
4.3.3 Investigating the stability of VV and PCVV in Human Plasma 112
4.4 Results: Investigating the impact of polymer coating on circulation kinetics in murine models . . . 119
4.5 Discussion . . . 121
4.6 Summary and Conclusions . . . 127

5 Retargeting VV to tumours over expressing Mucin-1 129
5.1 Introduction . . . 129
5.2 Results: Formulation of an aMUC1 retargeted VV . . . 131
5.2.1 Cholesterol-PEG-NHS synthesis . . . 131
5.2.2 Forming Cholesterol-PEG-NHS antibody conjugates . . . 132
5.2.2.1 IgG + Chol-PEG-NHS . . . 132
5.2.2.2 aMUC1 + Chol-PEG-NHS . . . 137
5.2.3 Attachment of aMUC1 retargeting ligand to VV via PEG-Cholesterol . . . 142
5.2.4 Determining ability for aMUC1-PCVV to bind MUC1 target 144
5.3 Results: Determining the impact of MUC1 retargeting of PCVV on virus infectivity in cancer cell lines *in vitro* . . . 145
5.3.1 Confirmation of aMUC1 antibody binding to high and low MUC1 expressing cell line . . . 145
5.3.2 VV-GFP Infectivity of A549 and CAPAN-2 cells . . . 146
5.3.3 aMUC1 retargeting of VV-GFP in CAPAN-2 cells . . . 149
5.3.4 aMUC1 retargeting of VV-luc in high MUC1 expression cell line CAPAN-2 . . . 151
5.4 Results: Circulation kinetics of VV, PCVV and aMUC1-PCVV in murine models . . . 157
5.5 Discussion . . . 162
5.6 Summary and Conclusions . . . 170

6 In vivo assessment of cavitation-mediated delivery of VV, PCVV and aMUC1-PCVV 172
6.1 Introduction . . . 172
6.2 Results: Experiment 1- Assessment of suitability of CAPAN-2 xenograft model for ultrasound mediated cavitation studies . . . 175
6.2.1 Experiment 1: DCE-MRI Imaging to assess perfusion . . . 175
6.2.2 Experiment 1: Determination of MUC1 expression in xenograft CAPAN-2 tumours . . . 181
6.3 Results: Experiment 2- Assessment of the viral dose to use in combination with ultrasound-mediated cavitation . . . 183
6.3.1 Experiment 2: Experimental design . . . 183
6.3.2 Experiment 2: Luciferase imaging to determine infection levels 184
6.4 Results: Experiment 3- In vivo delivery study- VV, PCVV, aMUC1-PCVV and IgG-PCVV with ultrasound-mediated cavitation . . . 186
6.4.1 Experiment 3: Experimental design . . . 186
6.4.2 Experiment 3: Acoustic Feedback . . . 188

6.4.3 Experiment 3: Assessment of infection of VV, PCVV, aMUC1-PCVV and IgG-PCVV +/- ultrasound treatment 191
6.4.4 Relationship between PAM and delivery of VV, PCVV, aMUC1-PCVV and IgG-PCVV 201
6.5 Results: Experiment 4- Tumour growth study- VV, aMUC1-PCVV or glucose, with or without ultrasound mediated cavitation 204
6.5.1 Experiment 4: Acoustic Feedback 206
6.5.2 Experiment 4: Luciferase imaging on Day 7 and 21 to monitor infection levels 207
6.5.3 Experiment 4: Tumour growth control 210
6.5.4 Experiment 4: Relationship between PAM and tumour volume at end point 213
6.6 Discussion 215
6.6.1 Summary and Conclusions 222

7 Conclusions and Future Work **225**
7.1 Summary of findings and conclusions 225
7.2 Future work 231

References **235**

List of Abbreviations

VV . . . . . Oncolytic vaccinia virus

aVV . . . . . Neutralising anti-VV antibody

MUC1 . . . . . Mucin-1

aMUC1 . . . . Anti-mucin-1 antibody

PK . . . . . Pharmacokinetics

US . . . . . Focused ultrasound

IVIS . . . . . *in vivo* imaging system

PEG . . . . . Polyethylene glycol

Chol . . . . . Cholesterol

FITC . . . . . Fluorescein isothiocyanate

NHS . . . . . N-hydroxysuccinimide

PAM . . . . . Passive acoustic mapping

GFP . . . . . Green fluorescent protein

luc . . . . . Luciferase protein

PRFP . . . . . Peak rarefactional focal pressure

RT . . . . . Room temperature

ELISA . . . . . Enzyme-linked Immunosorbent assay

qPCR . . . . . Quantative polymerase chain reaction

HRP . . . . . Horseradish peroxidase

IT . . . . . Intratumoural

IV . . . . . Intravenous

HIFU . . . . . High intensity focused ultrasound

DC . . . . . Duty cycle

SSP . . . . . Sonosensitive particles

SDS-PAGE . . Sodium-dodecyl sulfate polyacrylamide gel electrophoresis

Chapter 1

Introduction and Literature Review

1.1 Introduction

Traditional cancer treatments are not optimally effective; their mechanism of action commonly relies on specificity solely derived from the enhanced division rate of cancerous cells. Consequently, any rapidly dividing cells are targeted, which results in dose-limiting side effects that can exacerbate the suffering caused by the disease itself. Examples of the healthy cells in the body that share a high division rate include hair cells, bone marrow cells and cells in the gut [1] and so these are also impacted upon during chemotherapy treatments, commonly leading to hair loss, myelosuppression and vomiting. Fortunately, as our understanding of cancer has improved, treatment modalities for cancer have begun to move far beyond these traditional approaches. While there have been several advances in the last 10 years that have seen increased survival rates in some common solid tumours, the most significant change has come from understanding the genetic and molecular basis of cancer. [2] This enhanced knowledge has led to the development of new types of therapy including biologics and gene therapies, which have allowed the biomedical community to start to treat cancer in a more targeted way. Such research has led to the development of more powerful and selective approaches which do not instigate the same off-target toxicity profiles observed with conventional small drug chemotherapies. One novel biologic gene-based therapy is known as 'oncolytic

virotherapy' whereby viruses with a natural or engineered ability to infect and kill cancer cells are utilised.

Parts of this chapter have been published in an alternate form in either (Hill *et al* 2020) *Methods in Molecular Biology*, Oncolytic Virotherapy or "Expert Opinion of Drug Delivery and Devices" (Hill and Carlisle, 2019). [3, 4]

1.2 Oncolytic Virotherapy: Benefits and Current Restrictions

References to the use of viruses to treat cancer patients, dating back to the early 1900s, report that cancer regression prevailed when patients became the subject of naturally occurring viral infections. This led to trials in which bodily fluids containing human or animal viruses were administered to cancer patients. The outcomes of these studies were largely negative due to viral neutralisation by the host immune system which prevented cancer cell infection and therefore tumour regression from occurring. In certain immunosuppressed patients, tumour regression was reported, however due to the lack of specificity and understanding of the viruses used, a number of patients died as a results of viral infection of normal tissue. [5] Oncolytic virotherapy has since advanced as a result of a greater understanding of virology, an ability to scale-manufacture higher quality oncolytic virus (OV) batches, and less reliance on the natural tumour tropism with more genetic modification utilised to achieve improved selectivity of viruses for cancer cells. In 1989 it was first reported that a herpes simplex virus type 1 (HSV-1) with an inactivated Thymidine Kinase (TK) gene led to tumour control without associated encephalitis in mice. [6] This study was the inspiration for many more investigations into oncolytic virotherapy. [7, 8] Since this work the range of vectors tested and variety of mechanisms used to instigate therapy has burgeoned.

Viruses are now commonly used in medical treatments as vectors for gene delivery [9] and as therapeutics for targeted cancer treatment either via cell destruction or by stimulation of an immune-response against the cancer cells or a combination of both these events. [2, 7, 8, 10] Four key benefits of virotherapy [11] can be summarised

as selectivity, replication, arming potential and provision of extra/alternative death mechanisms. Viruses can be made selective in at least three ways, (a) modification of their surface so their infection can be directed away from natural tropism towards target disease cells (b) placement of important genes downstream of cancer specific promoters (c) deletion of genes which are required to allow replication in normal cells but have limited effect on replication in cancer cells. [6, 12, 13] An OV can self-amplify intratumourally, hence increasing its dose in situ, and so even a low dose of delivered active virus has the potential to generate a powerful response provided it is initially well-distributed within the tumour. Viruses can also be armed to produce a huge range of proteins from within the tumour which can increase the anti-cancer effect. [14] Finally, viruses can provide mechanisms of death (e.g. necrosis [15]) which are not reliant on the activity of mediators of apoptosis such as p53 or Rb. Mutations to p53 and Rb are very commonly part of the process of cancer development as they prevent apoptotic death mechanisms, which consequently leads to loss of growth regulation. Many small molecule chemotherapy drugs rely on apoptotic death mechanisms to achieve their effect i.e they rely on the function of a process to treat a disease which is often defined by the loss of that process. [16]

With so many advantages it is not surprising that in recent years there has been a surge in the development and testing of OVs for cancer treatment. Results from a plethora of pre-clinical and clinical studies using HSV [17–21], vaccinia virus (VV) [22–29] and adenovirus (Ad) [30–39] for cancer treatment, have provided exciting evidence which has led to strengthened clinical and commercial interest in OV. [40] There are now two OV which have been approved for clinical use: H101 and Talimogene Laherparevec (Imlygic®). In 2005 the China Food and Drug Administration (CFDA) approved H101, an E1B-deleted serotype 5 adenovirus, for intratumoural (IT) administration in combination with chemotherapy in the treatment of head and neck cancer. [41] Imlygic®, was first described in 2003 [42], as an HSV type 1 (HSV-1) derived by functional deletion of ICP34.5 and ICP47 and insertion of the coding sequence for human granulocyte macrophage colony-stimulating factor (GM-CSF). In 2015, Imlygic® was the first OV to gain FDA

approval, for IT administration in patients with inoperable malignant melanoma. When administered every two weeks IT into accessible lesions, Imlygic® produced systemic responses in 16% of patients and longer overall survival of 23.3 months in the Imlygic® arm compared to 18.9 months in the control arm. [43]

CAVATAK, a bio-selected genetically unmodified oncolytic Cocksackievirus A21 (CVA21) [44], has also been the subject of Phase I and II clinical trials. A Phase II (NCT01227551) study looking at the use of CAVATAK in patients with late stage melanoma showed that intratumoural delivery of CVA21 was safe (no Grade 3 or 4 product related adverse effects) and resulted in an overall response rate of 28.1%. [45] Two further Phase 1b and Phase 1 clinical investigations into the intratumoural administration of CVA21 in combination therapy with impilimumab (NCT02307149) and pembrolizumab (NCT02565992) in patients with advanced melanoma are completed and results are pending.

Reolysin®, a serotype 3 oncolytic reovirus, has also shown safety and activity in Phase 1 and 2 studies against breast cancer (NCT01656538), multiple myeloma (NCT02514382), and non-small cell lung cancer (NCT01708993). The first phase II randomized breast cancer study (NCT01656538) assessed the intravenous (IV) administration of Reolysin in combination with a chemotherapeutic (paclitaxel). [46] The study showed that there was no significant increase in progression free survival (PFS) or response rate (RR) between those treated with paclitaxel alone and those treatment with a combination of Reolysin and paclitaxel. Treatment with the combination of Reolysin and paclitaxel did however provide extended overall survival (from 10.4 months to 17.4 months). Data determining the number of viral particles in the tumours were not reported and so it is not known whether poor delivery was a factor in the failure to improve PFS or RR. [46]

1.2.1 Oncolytic Vaccinia Virus For Cancer Treatment

Vaccinia virus (VV) virions are large, enveloped and complex, providing them with certain advantages for use as oncolytic viruses. Their large (192 kbp) double-stranded genome allows 25 kbp of foreign DNA to be inserted into VV without

deleting any of its viral sequence [47] and their strong promoters allow them to drive high levels of transgene expression [2].

The quick and efficient 8 hour life cycle of VV means it rapidly destroys the cells it infects and spreads effectively between surrounding cells. [48, 49] This is ideal in solid tumour treatment, where target cells are densely packed. VV only replicates in the cytoplasm of host cells [50] outside the nucleus, and therefore has relatively few interactions with host cellular proteins, or crucially, the host genome, removing concerns about mutagenesis. This allows for rapid replication and production of extracellular enveloped virion (EEV), the type of virion responsible for its efficient cell to cell spread. [48, 49] The host-derived envelope encapsulating EEV contains several host complement control proteins which enable it to be more resistant to the impact of host defences. [51–54] The genome of VV encodes proteins which are able to inhibit the innate immunity and the development T helper 1 (Th1) immune response. Examples of these include at least 3 genes that are able to block the function of the interferon (IFN) family members IFN-α and IFN-β [55–58] and at least 3 that can directly block the function of IFN-γ, a potent Th1 cytokine. [59, 60] After infection, cells secrete VV complement control proteins which bind to inactive C4b and C3b thereby preventing further activation of both the classical and alternative complement activation pathways. [61–63]

VV has a natural tropism for tumours and with the deletion of certain genes, can be made even more selective. [64] The literature describes various theories as to the mechanisms behind VV's tumour selectivity. One in particular suggests that as VV is so large, diameter of 350 nm, it is able to enter tumours because of their leaky vasculature. [64] Another suggests that VV preferentially infects sites, such as tumours, which have vascular endothelial growth factor production. [65] Furthermore, rapidly dividing cells generate a pool of nucleotides which can be used by VV to self-amplify its own genetic code and produce more virions, and hence, VV preferentially replicates in proliferating cells where the nucleotide supply is abundant. [66] Pexa-Vec (pexastimogene devacirepvec; JX-594) is a derivative of the Wyeth vaccinia strain and has been engineered to enhance natural cancer

tropism by deletion of its thymidine kinase (TK) gene, and encoding GM-CSF, thus making it dependent on the cellular TK, which is expressed at persistently high levels in cancer cells. [67] Notably, once it has infected a cell, VV secretes vaccinia growth factor (VGF), a peptide with sequence homology to human EGF, which then binds to surrounding cells, stimulating them to divide and therefore become more amenable to infection. Hence, deletion of this gene from the VV can prevent its ability to spread into non-proliferating cells. [67]

A common concern with virotherapy is that viruses can cause serious illness. Notably, the VV is derived from the poxvirus family and was used in the 1970 immunisation program which lead to worldwide eradication of smallpox. It therefore has an extensive safety profile. One concern with genetically modifying a virus for selective replication in dividing cells is the potential for harm to naturally dividing cells in vivo. However, previous murine, rat, rabbit and primate studies have shown that known sites of dividing cells (eg. bone marrow and gastrointestinal mucosa) are not affected by systemic VV administration. [64]

The rationale for use of oncolytic VV is therefore strong and it has shown promise and has been tested in hundreds of cancer patients in late stage clinical trials to date. These trials have determined how oncolytic VV can be administered safely and efficiently in multiple types of cancer. Pexa-Vec was first investigated in clinical trials in 1999 by Mastrangelo *et al.* [27] In 2005 in a Phase I study the maximum tolerated dose (MTD) of IT injection in patients with metastatic or primary liver cancer was determined to be 1 x10^9 pfu. [28] Grade III hyperbilirubinemia was the dose-limiting toxicity. [28] Clinical studies investigating the safety and efficacy of IV administration of Pexa-Vec were first reported in 2011. [22] The trial administered escalating doses of Pexa-Vec in 23 patients with treatment-refractory solid tumours with the primary aim of determining the safety and MTD. No dose limiting toxicities (DLT) were reported at the highest dose administered of 2 x10^9 pfu which was concluded to be the maximum feasible dose (MFD) based on manufacturing limits. Of significance, it was determined during this trial that the viremic threshold for tumour infectivity after IV injection was 1 x10^9 pfu, below which there was no

evidence of Pexa-Vec infection. The outcomes of both the IT and IV Phase I clinical trials [22, 28] provided support for further late stage clinical trials with Pexa-Vec. A randomized Phase II trial [68] investigating IT administered Pexa-Vec in 30 patients with liver cancer was conducted to compare the outcomes of a high and low dose arm. The higher dose arm had a median survival of 14.1 months compared with 6.7 months at the lower dose. This was the first randomized clinical trial of an OV which demonstrated improvement in survival duration linked to the administered dosage. Another Phase II trial (Jennerex & Transgene SA, n.d.) in patients with Hepatocellular carcinoma (HCC) reported the safety and efficacy of a combined treatment of Pexa-Vec via IV and repeated IT injection, followed by the Tyrosine Kinase Inhibitor (TKI) Sorafenib. After treatment with Pexa-Vec alone 62% of patients had disease control (as determined by RECIST criteria) and after 6 - 12 weeks 59% of patients had disease control. Both these clinical studies presented the clear therapeutic benefit of Pexa-Vec in patients with HCC. Further investigations into IV administration of oncolytic VV, the Phase IIa (NCT01636284) "FLASH" and large Phase IIb (NCT01387555) "TRAVERSE" studies, have now been completed. The results of these trials are yet to be published, however in the TRAVERSE trial, it was noted that patients with advanced liver cancer did not reach their primary survival endpoint even in the high-dose cohort. [69]

Recently, the Phase III trial (NCT02562755) "PHOCUS" investigating the benefits of the combination of Pexa-Vec + Sorafenib compared to Sorafenib alone was stopped as it became clear that the trial would not meet its primary end point of overall survival. These trials are summarised in Table 1.1.

Trial name	National Clinical Trial number	Phase	Number of patients	Disease	Dose	Frequency	Delivery	Random-ised	Status
Intratumoral recombinant GM-CSF-encoding virus as gene therapy in patients with cutaneous melanoma		1	7	Cutaneous Melanoma	dose escalation (pfu/dose): 10^4 - 8x10^7	2 /week (up to 6 weeks)	IT	NO	completed
Use of a targeted oncolytic poxvirus, JX-594, in patients with refractory primary or metastatic liver cancer: a phase I trial	NCT00629759	1	14	Liver metastases	dose escalation (pfu/dose): 1 x 10^8 - 3 x 10^9	1 /3 week X4	IT	NO	completed
A Mechanistic Proof-of-concept Clinical Trial With JX-594, a Targeted Multi-mechanistic Oncolytic Poxvirus, in Patients With Metastatic Melanoma	NCT00429312	1/2	10	Metastatic Melanoma	10^8 pfu/dose	1 /week X9	IT	NO	completed
Intravenous delivery of a multi-mechanistic cancer-targeted oncolytic poxvirus in humans	NCT00625456	1	23	Solid tumours	dose escalation (pfu/dose): 1x10^5 or 3x10^7 pfu/kg	1	IV	NO	completed
Randomized dose-finding clinical trial of oncolytic immunotherapeutic vaccinia JX-594 in liver cancer	NCT00554372	2a	30	HCC	dose escalation (pfu/dose): 1x10^5 - 3x10^7 pfu/kg	1 /2weeks X3	IT	NO	completed
A Phase 2 Study of HCC Patients Treated IV & IT with JX-594 Prior to Sorafenib	NCT01171651	2	25	HCC	1x10^9 pfu/dose	1 /week X3	1 IV and 2 IT	NO	analysis ongoing
A Phase 2a Study of Modified Vaccinia Virus to Treat Sorafenib-naïve Advanced Liver Cancer (FLASH)	NCT01636284	2a	16	HCC	1x10^9 pfu/dose	1 /week X5	IV	NO	analysis ongoing
A Phase 2b Study of Modified Vaccinia Virus to Treat Patients Advanced Liver Cancer Who Failed Sorafenib (TRAVERSE)	NCT01387555	2b	129	HCC	1x10^9 pfu/dose	1 /3weeks X6	1 IV and 5 IT	YES 2:1	completed
Hepatocellular Carcinoma Study Comparing Vaccinia Virus Based Immunotherapy Plus Sorafenib vs Sorafenib Alone (PHOCUS)	NCT02562755	3	recruiting	HCC	1x10^9 pfu/dose	3/ 2weeks X3	IT	NO	stopped
Phase 1 Study of Intratumoral Pexa-Vec (JX-594), an Oncolytic and Immunotherapeutic Vaccinia Virus, in Pediatric Cancer Patients	NCT01169584	1	6	pediatric tumours	10^6 or 10^7 pfu/kg	1	IT	NO	stopped

Table 1.1: Summary of Pexa-Vec clinical trials to date.

	Phase 1b Trial of Biweekly Intravenous Pexa-Vec (JX-594), an Oncolytic and Immunotherapeutic Vaccinia Virus in Colorectal Cancer	NCT01469611	1b	15	CRC	dose escalation (pfu/dose): 1x10^6, 1x10^7 or 3x10^7 pfu/kg	1 /2weeks X2	IV	NO	completed
	A phase 1/2a Study of Patients with Metastatic, Refractory Colorectal Carcinoma with Advanced Colorectal Cancer Treated Intravenously (IV) with JX-594 Alone and in combination with Irinotecan	NCT01394939	1/2a	52	CRC	dose escalation (pfu/dose): 3x10^8 - 1x10^9 pfu/dose /or combo	1 /week X5	5 IV and 3 IV boosts	NO	analysis ongoing
	A Phase I Dose Escalation Trial Evaluating the Impact of an in Situ Immunization Strategy With Intra-Tumoral Injections of Pexa-Vec in Combination With Ipilimumab in Metastatic / Advanced Solid Tumors With Injectable Lesions.	NCT02977156	1	recruiting	Solid tumours	1x10^9 pfu/dose	1 /3weeks X5	IT	NO	enrollement ongoing
	A Phase I/IIa Trial to Evaluate the Safety and Efficacy of the Combination of the Oncolytic Immunotherapy Pexa-Vec With the PD-1 Receptor Blocking Antibody Nivolumab in the First-line Treatment of Advanced Hepatocellular Carcinoma (HCC)	NCT03071094	1/2a	recruiting	HCC	1x10^9 pfu	1 /2weeks X3	IT	NO	enrollement ongoing
	A Phase I/II Study of Metronomic Cyclophosphamide and Oncolytic Poxvirus JX-594 in Patients With Advanced Breast Cancer and Advanced Soft Tissue Sarcoma (METROmaJX)	NCT02630368	1/2	recruiting	Breast Cancer/ soft tissue sarcoma	unknown	unknown	IV	YES	enrollement ongoing
	A Phase 1b, Dose-escalation Study of Pexa-Vec in Combination With REGN2810 (Anti-PD-1) in Patients With Metastatic or Unresectable Renal Cell Carcinoma (RCC)	NCT03294083	1b	recruiting	RCC	dose escalation: $3x10^8$ - $1x10^9$ pfu/dose	IV: 1/weekX4 IT: 1/2weeks X3	IV/IT	YES	enrollement ongoing
	A Phase I/II Study of Pexa-Vec Oncolytic Virus in Combination With Immune Checkpoint Inhibition in Refractory Colorectal Cancer	NCT03206073	43862	recruiting	RCC	dose escalation: $3x10^8$ - $1x10^9$ pfu/dose	1/2weeks	IV	YES	enrollement ongoing

Table 1.1: Summary of Pexa-Vec clinical trials to date.

Five trials for multimodal therapy involving Pexa-Vec are currently recruiting. First is a Phase I/II trial (NCT03071094) evaluating the combination of Pexa-Vec with Nivolumab, a PD-1 immune-checkpoint inhibitor (ICI) antibody, for first-line treatment of HCC. Second is a Phase I trial evaluating the combination of Pexa-Vec with Ipilimumab (anti-CTLA4 antibody) delivered IT for patients with metastatic or advanced solid tumours. Third is a Phase I/II clinical trial (NCT02630368) to determine the MTD, safety and efficacy of Pexa-Vec (IV injection) and metronomic cyclophosphamide in patients with advance soft-tissue sarcoma and advanced breast cancer. Fourth is a Phase Ib trial (NCT03294083) to determine the MTD, safety and efficacy of Pexa-Vec in combination with REGN2810 (monoclonal antibody to Programmed Death-1, PD-1) for patients with non-resectable Renal Cell Carcinoma (RCC). Of interest here, in this trial there are two arms for Pexa-Vec + REGN2810; one in which Pexa-Vec is administered IV and the other where it is delivered IT. This will give the opportunity to compare the anti-tumour effects as a result of these two different administration routes, providing information on how limiting poor circulation and tumour delivery are. Fifth is a Phase I/II clinical trial to determine the MTD, safety and efficacy of Pexa-Vec in combination with Durvalumab (monoclonal antibody directed against PD-L1) or Tremelimumab (monoclonal antibody that binds to CTLA-4).

There are two other oncolytic VV derivatives of note in early stage clinical investigation GL-ONC1 (an attenuated version of the Lister strain with the deletion of F14.5L, A56R and J2R) and the vvDD (a Western Reserve derivative with TK and VGF deletions). [29, 70–74]

Crucially, out of the 25 studies reported investigating Oncolytic VV clinically, only 11 used IV administration. As improved survival has only been shown with IT administration, this may be the reason that most ongoing or recruiting trials are using IT administration (NCT02562755, NCT02977156, NCT03071094). Hence, while IT administration of oncolytic VV has shown a safe profile with promising anti-tumour response, these trials have also indicated that effective dissemination throughout the body to treat metastatic sites of disease is still an area which needs

improvement. At the MTD, IV administration of Pexa-Vec showed infection of tumours but the number of infectious VV virions that were able to reach tumour sites was limited and insufficient to produce significant tumour regression as a mono-therapy. It is also notable that both H101 and Imlygic®, the two oncolytic viruses approved for clinical use, are administered IT.

Hence, there are still important challenges to overcome before the use of OVs as therapeutic agents in cancer treatment becomes a standard clinical approach for treatment of metastatic disease. This restriction to IT administration is the result of several challenges faced by OV. Firstly, there is the challenge of delivering the virus via the bloodstream so that all the distant sites of cancer deposition can potentially be reached. When injected into the body, most viruses are recognised as xenogens and are attacked and cleared from the body before they are able to reach the desired location(s). This immune-mediated clearance dramatically impedes the efficiency of OV. [22, 75, 76] If the virus does manage to reach the tumour site, it then needs to maintain a sufficient level of activity to be able to infect and kill cancer cells. This leads to the second challenge; the virus needs to be stable in the blood and retain a high level of infectivity. Thirdly, dysfunctional vascularization, dense stromal tissue and poor lymphatic drainage within tumours make them high pressure environments comprised of a dense disorganised collection of cells. [7] This means solid tumours often have no convective flow passing through them, making it difficult for particulates, especially large ones such as viruses, to penetrate into and distribute throughout the whole tumour. Therefore mechanisms to help the virus continue to infect, propagate and spread until the entire tumour has been eradicated may be required. [77]

1.3 Enhancing Oncolytic Virus Efficacy by Overcoming Delivery Limitations

Oncolytic viruses (OV) have shown efficacy when delivered by direct IT injection both locally through direct tumour cell lysis and systemically by stimulating an anti-tumour immune responses [43, 78] (detailed in section 1.2). However, in order

for OV to become an established easily administered tool in pan-cancer treatment, able to optimally infect primary and metastatic tumours, they will need to be delivered via IV injection. [10, 77] Indeed, IV injection may enhance the generation of anti-tumour immune responses compared to intralesional delivery. [79] Bourgeois-Daigneault *et al* reported that IV infusion of the Maraba virus was more efficient than IT administration at preventing tumour growth in a murine model rechallenge setting, with 40% of the mice disease-free for the duration of the experiment after IV administration when compared with 20% after IT administration. The anti-tumour effect was then tested on mice bearing different primary (CT26) and secondary (4T1) tumours (i.e. mice bearing CT26 tumours were treated with IT administered Maraba virus and then rechallenged with 4T1 tumours). IT administration of Maraba virus was performed as previously and there was no impact on 4T1 tumour volume or survival benefits seen, thereby highlighting that the anti-tumour effect observed was tumour specific. [79] The reported genetic differences between primary tumours and matched metastatic cancer are therefore worth considering in this context. [80, 81] In those cases where metastatic variants have lost or changed their neoepitope landscape, treatment resistance to neoepitope specific treatments presents a challenge. [82] Hence, reliance on the abscopal effect of anti tumour-associated antigen activity could also be limited by metastatic variation, supporting the need for systemic infection in metastatic cancer.

Moreover, IV administration is the standard, and more standardisable, means of therapeutic delivery worldwide and cancer treatment centres are setup with IV infusion equipment accordingly. Therefore, whilst IT delivery will continue to provide a viable option for many patients, achieving systematic bioavailability in local and disseminated cancer will be critical to the expansion of the utility and efficacy of OV.

1.3.1 Pharmacokinetics and anti-viral neutralisation

Providing better circulation kinetics following IV injection will enable more effective treatment of metastatic disease and hence widen the number of patients that can be treated with these powerful and selective agents. It has been shown in pre-clinical

models that the bloodstream stability and tumour accumulation of OV can be improved using modification or shielding techniques including those which rely on genetic and/or chemical engineering. [11]

1.3.1.1 Directed Evolution and Genetic Modification

Directed evolution, a technique which was the subject of the 2018 chemistry Nobel Prize, has been used as an alternative approach to producing highly selective and efficacious OV. It was first used in the OV field by Kuhn *et al* for the creation of an oncolytic adenovirus that was not based on adenovirus type 5, namely ColoAd1. [83] Here the authors pooled a variety of serotypes of adenovirus, which showed lower sero-prevalence in humans, and passaged them under conditions which closely mirrored those of the human cancer microenvironment. The viruses which thrived in these selective culturing environments were tested and those which showed increased potency and enhanced tumour tropism were selected. In the case of ColoAd1, the specific conditions were those of the colon cancer cell line, HT29. Tests were performed to determine ColoAd1's activity in whole human blood and showed that compared with the Ad5 based OV ONYX-015, the inhibition of infection in 20 % (v/v) human serum was just 10-fold as opposed to 1000-fold. Both *in vitro* and *in vivo* investigations of ColoAd1 showed a 2-3 logs higher potency and a 3-4 log increase in therapeutic window, when compared with Ad5 vectors. [83] The success reported with ColoAd1 opens up the opportunities that directed evolution could have when used on different cancer types and with a range of different viruses. Due to the high potency reported here, one consideration which should be noted is that restriction of replication tropism to cancer cells needs to be achieved to ensure off target toxicity is avoided. [84]

As discussed previously, it has been shown that enhancing tumour selectivity of OVs through genetic modification can lead to enhanced efficacy and reduced adverse effects with more virions reaching and infecting target cells in murine models. [85] Gene silencing has been used to reduce viral spread to off target sites. [86–90] One example using the Semliki Forest virus reported a reduced viral spread to the central

nervous system whilst maintaining glioma targeting *in vivo* through the introduction of neuron-specific micro-RNA (miRNA) sequences. [91] Another glioma specific OV was reported by Delwar *et al* in which HSV-1 was transcriptionally regulated using a specific survin promoter in place of the ICP4 gene leading to enhanced replication in gliomas when compared to normal neuronal cells *ex vivo*. [92]

Genetic modification has also been used to alter virus capsid surface and thereby directly alter cell tropism. [93, 94] Furthermore, such modification of capsid surface can also be coupled with chemical strategies, to enhance de-targeting of OV to non-target tissues and re-target them to both tumour tissues and their associated vasculature. Genetic modification of the oncolytic measles virus was performed to create a receptor specific, and hence infection specific, OV. The viral surface was modified to display single-chain antibody fragments against target receptors, including CD38 and epidermal growth factor receptor (EGFR). [95] Receptor mediated infection was observed both *in vitro* and *in vivo* on Chinese hamster ovary (CHO) cells transfected to express each of the target receptors, leading to anti-tumour activity *in vivo*. In another interesting approach, Kreppel *et al* [96] genetically modified the capsid of Ad5 to introduce cysteine residues into the HI-loop of the fiber protein. These cysteine residues were then conjugated via a bifunctional polymer to transferrin molecules while the rest of the capsid surface was modified with poly(ethyleneglycol) N-succinimidyl propionate (SPA-PEG). This resulted in an Ad vector which was uniquely selective for cells with transferrin receptors. A combined genetic and chemical modification was also used on Ad5 to replace its naturally occurring coagulation factor X (FX) shield, a change which was shown to reduce detection by NAbs and complement *in vitro*, and extend circulation time and hepatocyte infection *in vivo*. [97]

Choice of serotypes with low sero-prevalence in the human population (as with ColoAd1) is one approach to dampening blood stream neutralisation. Notably, the wild-type Newcastle disease virus (NDV) isolated from Russian migratory birds, which is non-pathonogentic in mammals, has been shown to selectively replicate in malignant cells. [15] NDV is unable to replicate in healthy cells due to their

functional interferon (IFN) response [98, 99] but replicates rapidly in cancer cells with ablated IFN response, thereby inducing cell death. NDV has proved effective in preclinical studies and Phase I and II clinical trials have been performed. [15, 100–102] In addition, some OV, such as VV, have their own "natural" methods to prevent detection whilst undergoing cell to cell infection. Once replication begins, VV generates two subspecies (as detailed in section 1.2.1). One of these subspecies, the extracellular enveloped virus incorporates proteins from the membrane of the cell it has infected and uses them to form an envelope, a process which has been shown to enable its avoidance of neutralising antibodies. [51]

1.3.1.2 Chemical Modification

Section 1.3.1.1 discussed some of the genetic modifications which have been used to enhance the delivery of OV. These strategies, although effective, can be expensive and complex, and can require new engineered and validated cell lines and harvesting procedures. This section provides details of some of the studies reported using theoretically simpler and less expensive chemical modification strategies to enhance the systemic delivery of OV.

1.3.1.2.1 Polymer stealthing viruses for enhanced blood stability

The bloodstream stability and tumour accumulation of OV can be improved using biocompatible polymers to shield the virus from antibody binding and interactions with other blood components. [11] Biocompatible polymers are used in a wide range of drug delivery systems. [103] Such polymers are very useful carriers as they have good blood compatibility and maintain structural integrity. Polymer coated therapeutic viruses were first reported in 1999. [104] Coating strategies most commonly utilise polymers, typically based on a PEG or poly[N-(2-hydroxypropyl) methacrylamide] (PHPMA) polymer backbone, to modify viruses covalently or non-covalently. Covalent methods have involved the use of mono-functional polymers with terminal amine reactive groups. These amine reactive groups react with viral capsid lysine residues creating either brush-like or complete polymer shields. [76, 96,

104–109] These modifications of the viral capsid can lead to a knockdown, or in some cases ablation, of viral infectivity, as the virus cell-binding mechanisms are covered.

Early examples of polymer coating were able to provide the therapeutic viruses with protection from the immune system whilst maintaining a sufficient level of infection. In cases where infection ability was reduced or ablated, bifunctional polymers were used with targeting ligands attached to produce a retargeted therapeutic virus. This will be discussed further in section 1.3.1.2.2.

Much of the work performed to characterise the impact of polymer coating on clearance, infection and blood stability of OV was performed on viruses based on Ad. PEGylation of Ad5 has been reported to reduce binding of neutralising antibodies (NAbs) both *in vitro* and *in vivo*. [109, 110] Notably, it was also shown that PEGylation reduced anti-Ad5 adaptive immune response induction in immune competent mice with a reduction in the number of cytotoxic T lymophocytes (CTLs) and anti-NAbs detected, a finding which has implications for re-dosing regimes. [110] Interestingly, it was also shown that the reactive group used for the PEGylation impacted the scale of the NAbs response against Ad5 that was generated, with the PEGylation using a methoxypolyethylene glycol tresylate reactive group producing the lowest titre of NAbs. These PEGylated Ad5 were still able to express transgenes, and although this ability was still inhibited after repeat dosing in murine models, [110] when sequential doses of Ad5 modified using different amine reactive linkers was used infectivity could be maintained. This raises the hypothesis that the NAbs produced were specific to the antigenic epitopes associated with the linker used. Heavy PEGylation of Ad5 was shown to reduce blood clearance rate 4-fold [111] and experiments followed to show that despite a reduction in Kupffer cell capture, PEGylation strategies did not reduce hepatic damage *in vivo*. [112] These studies were notable for an absence of full analysis of the clearance profile and biodistribution of the modified viruses.

Fisher *et al* compared the use of a multivalent hydrophilic polymer based on PHPMA to the use of PEG. [76] PHPMA was considered the preferred material for coating as it required a lower concentration of reactive esters for co-operative

binding than PEG. Using transmission electron microscopy, it was determined that the polymer coated Ad retained its gross morphology, and analysis of particle size using photon correlation spectroscopy showed a diameter increase of 23.1 nm. Infection of polymer coated adenovirus *in vitro* was abolished because the PHPMA coating blocked the regions of the adenovirus used for binding. [76] A further study showed that while viral infectivity is reduced when adenovirus is modified with PHPMA, hepatic uptake was also reduced by almost 60% in comparison to an uncoated adenovirus. [113] Overall hepatic toxicity was also decreased, the impact of which means higher doses of coated viral particles could be safely administered. [113] The polymer coated Ad had an increased circulation half-life (> 30 vs 5 minutes) as a result of blocking receptor-mediated clearance and infection pathways. [113] A study followed which took advantage of this increase in circulation time which showed that increased passive tumour accumulation was obtained for PHPMAylated Ad5. [114] When Kupffer cell inhibiting biophosphonate liposomes were preadministered followed by polymer coated Ad, acute inflammatory toxicities related to Ad treatment were prevented. [115] This vector was able to avoid rapid clearance but was incapable of infecting any cells, and so provided a platform onto which retargeting ligands could then be attached to provide specific cancer cell tropism (discussed further in section 1.3.1.2.2).

This approach did produce some impressive findings, but limitations included knockdown in infectivity and the lack of control over which epitopes were being modified. Studies utilising "bioresponsive" polymers (eg. polymers that were cleavable in acidic conditions) to shield Ad were investigated. [116, 117] After intratumoral injection, Carlisle *et al* [116] showed increased levels of infection with a bioresponsive PHPMA coating when compared with an irreversible PHPMA Ad5 coating. The bioresponsive coating also achieved an 8000-fold decrease in hepatic sequestration and a 50-fold increase in circulation time when compared with unmodified Ad5.

Non-covalent methods using cationic polymers (e.g. polyacrylates [118], branched polyamine copolymers [119] or polypeptides [120–123]) to coat viruses were first

reported in 1997 but achieved limited success due to their serum instability. [124] The modulation of complex surface charge using PEG or oligoethylene glycol blocks enabled the polymer coated viruses to overcome their instability in serum.

To date, none of these pre-clinically promising Ad modification approaches have progressed into the clinic. This might reflect insufficient consideration of the differences in immune status and clearance pathways between animal models and humans and difficulties in scaling these coating approaches to the quality standards required for clinical use.

Whilst there has been a wealth of research into the chemical modification of non-enveloped viruses, little has been reported regarding chemical modification of enveloped viruses such as HSV and VV. One example of chemical modification by Nosaki *et al* used layer by layer deposition of a linear polyethyleneimine hydrochloride (PEI) and negatively charged chondroitin sulfate to coat an oncolytic measles virus (MV). [125] Modification was shown to protect MV from NAbs *in vitro*. *In vivo*, pre-immunised mice bearing subcutaneous LL/2-CD46 tumours were treated intratumourally with MV or modified MV and enhanced cell lysis was observed for modified MV. Unfortunately testing following IV administration was not reported, and so the value of this approach to enhance its PK profile could not be determined.

Overcoming the challenges associated with systemic delivery of enveloped viruses has not however been completely overlooked. Studies have been performed into the use of cell based delivery systems for effective delivery of enveloped OVs and are discussed in reference [3]. An alternative method involving the enzymatic treatment of the oncolytic VV surface to remove its N-linked and simple O-linked glycans, namely a deglycosylated oncolytic VV, was able to reduce neutralisation by pre-existing antibodies, and reduce TLR2 activation and anti-VV NAbs production. This translated to an improvement in viral gene expression after 24 hours, which continued so that after 5 days a 5-fold increase was achieved, *in vivo* with the deglycosylated oncolytic VV when compared with unmodified VV. [126]

A final noteworthy approach is the application of molecules to dampen the anti-OV immune response. Evgin *et al* demonstrated that pre-treatment with

complement inhibiting peptide extended the pharmacokinetics and increased the activity of an oncolytic VV. [75] This study is an excellent demonstration of the barrier presented by complement. However, translation of this approach into a clinical context with patients in varying degrees of ill-health and immunosuppression due to their underlying disease and the impact of previous failed therapies, may be a complex process.

1.3.1.2.2 Active Retargeting of Oncolytic Viruses

Active retargeting strategies have been employed in the delivery of a host of different types of cancer therapeutics. In common with the retargeting by genetic modification of viral capsid proteins [94], these techniques take advantage of cell-surface proteins that are over expressed in tumours and uses ligands to target them. Large proteins (e.g. antibodies) as well as small peptides can be used as agents for active OV retargeting by decorating the surface of the virus which leads to increased tumour cell recognition and entry. [127]

A seminal report of the addition of targeting peptides to a PEG modified Ad2 in 1999 by Romanczuk *et al* [128] showed successful evasion of NAbs which led to a 4 to 5-fold increase in cancer cell infection *in vitro*. Fisher *et al* [76] showed that once successful detargeting of Ad5 using a PHPMA shield had been achieved, viral tropism could be redirected using fibroblast growth factor-2 (FGF2) or vascular endothelial growth factor-165 (VEGF165) to infect cancer cell lines with the corresponding receptors. As mentioned previously (section 1.3.1.1), controlled modification of capsid proteins could lead to enhanced efficacy for modified OVs and this was explored in a study by Campos and Barry. [129] It was suggested using Ad that retargeting through the attachment of ligands might only be effective when done through the site on the OV which is responsible for natural tropism; i.e. the fiber protein in the case of Ad. It has been shown previously *in vitro* that genetic retargeting of Modified Vaccinia virus Ankara (MVA), a heavily attenuated member of the poxvirus family, to baby hamster kidney (BHK) cells transfected to

become positive for the tumour-associated antigen mucin-1 (MUC1) was possible by replacing the p14 externally membrane associated protein (A27L gene) with p14 fusion molecules carrying a single-chain antibody targeting MUC1. [130]

Initial translation of these successful retargeting studies *in vivo* did not provide huge success. When modifying adenovirus Stevenson *et al* reported that despite seeing strong selective infection of PC-3 cells through a laminin-derived (SIKVAV) peptide *in vitro*, there was no observed increase in transgene expression *in vivo*. [108] Green *et al* reported similarly disappointing outcomes using an FGF2 ligand to retarget Ad and showed a decrease in tumour infection after IV administration compared to non-modified Ad *in vivo*, with the retargeted Ad having strong association with murine erythrocytes. [106] More positive results were seen by Morrison *et al* by targeting the EGFR, but these studies were performed using intraperitoneal administration. [107] Hence, although it is clear that polymer coating of Ad provides dramatic improvement in PK profile, the challenge of active retargeting by ligand inclusion has yet to show robust effects. It is also clear that the advantages of polymer coating evident in mice should be recapitulated in humans [131], although clinical testing has yet to be performed.

To date although genetic and enzymatic modification of VV surface has been described with varying degrees of success,[47, 126, 130, 132–134] these polymer coating approaches have not been attempted for VV which, in common with Ad5, suffers a range of bloodstream interactions which dramatically reduce its ability to disseminate efficiently and therefore its overall anti-tumour efficacy. [75]

1.3.1.2.3 Lipid Membrane and Lipid Anchors

Phospholipids are amphipathic molecules; one end is hydrophilic (polar) and the other is hydrophobic (non-polar). A double layer of phospholipids form the lipid bilayer with their hydrophobic ends meeting in the centre of the layer and their head groups in contact with aqueous environments. Under the right formulation conditions these bilayers can be encouraged to form spherical particle's known as liposomes.

The bilayer structure enables liposomes to maintain their structure and controls the amount of fluid leaving and entering their aqueous core. Cholesterol is a naturally occurring membrane component, consisting of only one hydroxyl group, and a large hydrophobic tail, which, given the correct conditions, can embed into a lipid bilayer. [135, 136] Lipid-polymer conjugates, such as Cholesterol-PEG, have been widely used to enhance the pharmacokinetics of therapeutic loaded liposomes. [136]

In Cholesterol-PEG conjugates the hydrophilic end (hydroxyl group) of a cholesterol group is linked to one end of PEG chains, which are also hydrophilic. The resulting structure is a long chain with one hydrophilic end made of PEG, and another hydrophobic end comprised of cholesterol. When a lipid-PEG solution and a solution containing biologics with lipid membranes are combined, the lipid groups, in order to remove themselves from the water, embed into the lipid bilayer while leaving the water-seeking polymer chain on the outside. This technique is commonly used in the PEGylation of "stealth" liposomes to increase their circulation time and can either occur at the point of bilayer formation or after, when bilayers are already formed. [137]

1.3.1.3 Flow Virometry for Virus Particle Detection

The use of a flow cytometer to analyse viral particles is called flow virometry [138]. Recent advances in the field of flow cytometry have resulted in the ability of microparticles (100-1000nm) to be detected. This is primarily possible due to the more powerful lasers, improved optics and photomultiplier tubes (PMTs) used in newer and adapted instruments. [139] A range of different single viral particles have been shown to be directly detected and their characteristics analysed using flow virometry. [140] Much like in standard flow cytometry analysis of cells, viruses are isolated and incubated with stains. In an early study utilising a FACSCalibur flow cytometer in a standard set-up it was shown that DNA viruses stained with a nucleic acid specific SYBR Green I could be detected above background fluorescence. [141] This study reported that side scatter (which traditionally provides information on cell granularity and internal structure) was not related to virus shape and size.

It was hypothesised that this was likely due to the viruses being smaller than the wavelength of the conventional laser light (488 nm) and hence the light scatter distribution would not have bearing to the structure of the viral particle. Gaudin *et al* reported the detection and sorting of an enveloped Junin virus stained with a YOYO-1 nucleic dye on a conventional FACSAria II Special Order cell sorter. [142] Junin virus particles which were sorted and imaged using TEM were shown to be between 60-150 nm in size. Additionally, and of relevance here, a previous report was able to successfully identify the VV virion using flow virometry. [139] A MoFloAstios EQ (Beckman) flow cytometer was used and virus samples were labelled with DiO/DiD labelling solutions. It was therefore hypothesised that flow virometry could be used to determine polymer coating of VV.

1.3.1.4 Tumour-associated antigen Mucin-1

Mucin-1 (MUC1) is a tumour-associated antigen over expression of which is often associated with cancers including those of the colon, breast, ovaries and pancreas. [143, 144] MUC1 is a transmembrane glycoprotein which consists of a unique N-terminal extracellular domain and a C-terminal intracellular domain. The N-terminal domain has a variable number of tandem repeats containing 20 amino acids. These amino acids are extensively modified by O-glycosylation. [145] In tumour cells it is expressed in a hypo glycosylated form over the entire cell surface, making it accessible to systemically administered antibodies. [143] The MUC1 cytoplasmic tail in the C-terminal domain has been shown to play an important functional role in cell proliferation and deregulation of apoptosis. [146, 147] Many antibodies against MUC1 have been developed. The antibody which was used in the work presented here (see Chapters 5 and 6) is a monoclonal antibody raised against the tandem repeat (HMFG2).

Over the past 30 years, MUC1 has gathered much interest as a therapeutic target for immunotherapy, due to the selectivity of its raised expression in cancer cells, resulting in over 100 clinical trials being initiated and reported. [148] The results of these trials have not shown clinical benefit great enough for approval of

general applications. VV has previously been modified to encode for the human MUC1 gene as part of a vaccination approach whereby a systemic anti-tumour response could be instigated, initiating an antibody response to tumoural MUC1. This modified VV was assessed in Phase 1 clinical trials and the treatment was shown to improve overall survival, however this was not due to anti-MUC1 antibody response. [149] Modified vaccinia ankara (MVA) expressing MUC1 administered in combination with chemotherapy and nivolumab was also tested in a Phase 2 clinical trial which did not reach its primary endpoint (improved overall response rate). Of importance here, MVA has been genetically modified to alter its tropism to MUC1 as a cancer cell surface target in *in vitro* studies. [130] This was achieved by replacing the externally membrane-associated protein p14 (A27L gene) with p14 fusion molecules carrying a single-chain antibody directed against MUC1, thereby resulting in the fusion protein carrying the single-chain antibody at the envelope of the MVA. This approach showed targeting success with the construct containing the single-chain antibody shown to bind to a MUC1 peptide and infect MUC1 expressing cells more efficiently *in vitro*. Specifically, MUC1 negative P815 and BHK cells were transfected with human MUC1 c-DNA to form MUC1 positive cell lines. Infection studies with MOI 0.1 showed that MUC1 targeted MVA detected on the cell surface of MUC1 positive cells by flow cytometry using an anti-MVA antibody had a higher infection capacity than unmodified MVA (79% vs 64%).

1.3.2 Improving Delivery within Solid Tumours

One of the cell death mechanisms utilised by OV is to infect and destroy cancer cells (oncolysis) via necrosis, releasing viral progeny after the cancer cells are killed. [150] These progeny OV are then responsible for cell-to-cell spread and infection of surrounding cells so that efficient cell death is possible from a small initial delivered dose. However, there are limitations to the viral spread into and throughout tumours. Tumour physiology poses a formidable barrier in cancer treatment as its heterogeneous morphology results in unpredictable and non-uniform drug distribution. [151] During the delivery phase OV do not typically have a

sufficiently long circulation half-life to benefit greatly from the enhanced permeability and retention (EPR) effect, meaning only a tiny percentage of the IV administered dose passively accumulates in tumours. As cancer treatment modalities continue to move away from conventional small drug molecules towards larger biologics the selective passive accumulation of drugs at tumour sites due to tumour's enhanced permeability will have less and less impact. The true scale of the benefit gained from the EPR effect has caused much recent controversy [152, 153] and although it has been heavily relied on it has been shown to be unable to enhance delivery of a range of anti-cancer therapeutics (including small molecule drugs, antibodies and OVs) over distances of more than around 50 µm from the vasculature. [116, 154–156] This means a small amount of virus can infect and spread near the blood vessels which supply a tumour, but the majority of the tumour remains untreated. In response, research has been directed towards developing mechanically activated transport mechanisms to aid the penetration of OV and hence increase the anti-cancer activity of viruses.

1.3.2.1 Modification of Intratumoural Physiology

Whilst the challenge of poor bloodstream stability and rapid clearance may be best addressed by trying to alter the OV vectors (by genetic or chemical means or both). The challenge of poor penetration into and throughout target tumours may be best addressed by trying to alter the tumour environment.

1.3.2.1.1 Vascular Normalisation

Angiogenesis, the development of new blood vessels, is crucial for healthy human growth. [157] In healthy adults, angiogenesis is a heavily regulated process, triggered by specific molecular and mechanical stimuli. Many diseases are characterised by the uncontrolled formation of new blood vessels, including solid tumours. Induction of new vessel formation is stimulated by hypoxia and a huge range of other molecular features within the tumour; angiogenesis is relentless. [158–160] The result is a microvascular network which is able to produce a rich blood supply, but which is

very abnormal and disorganised. Indeed, some areas of the tumour have excessive blood flow whilst others have next to no perfusion. [158, 161–163]

Vascular endothelial growth factor (VEGF) is the driving force behind tumour angiogenesis and a host of investigations using inhibitors of the VEGF receptor as monotherapies to ameliorate VEGF activity have been performed. Although these studies provided strong preclinical data [164], clinical results have been less encouraging. In response more sophisticated combination regimens have been developed, with the concept of vascular normalisation being applied. [165] Vascular normalisation uses antiangiogenic drugs to prune some vessels and transform the abnormal vessel structure into a more normal state. [157]

Specifically, anti-VEGF/VEGFR therapy has been associated with successfully reducing vessel density, vessel maturation and, in some cases, re-organisation of the basement membrane. [166–168] With these structural changes to the vasculature, normalisation of the vessel function also occurs. A reduction in vessel permeability brought about by therapy against the VEGF-VEGFR pathways leads to a reduction in intratumoural interstatic fluid pressure. This re-establishes a pressure gradient across the vasculature and improves perfusion which enables improved drug penetration in tumours. [167–169] Such vascular modulation has generated interest in the field of small molecule delivery, but to date has been under-researched for OV delivery.

Recently it was shown in vivo that oncolytic VV targeted tumour associated blood vessels in pancreatic neuroendocrine tumours in RIP-Tag2 transgenic mice, which led to vascular pruning and resulted viral leakage occurring for a longer time in tumours. Of interest, this affect was not inhibited by VEGFR2 inhibition. [170] An in vivo study by Kurozumi *et al* showed that intratumoural (IT) administration of the OV hrR3 (a derivative of the HSV-1) had anti-angiogenic effects resulting in significantly greater vascular leakage when compared with PBS treatment in mice with intracranial D74/HveC glioma cell tumours. [171] This was investigated by imaging of resected brain tumour sections from treated mice, injected with Texas Red-dextran five minutes before cull. The addition of an angiogenic inhibitor, cRGD

peptide, treatment prior to OV IT administration to reduce vascular permeability was also investigated. Mice were treated with either cRGD or PBS three days after intracranial cell implantation, and were then randomised and treated with OV seven days after implantation. The resected brain tumour sections showed significantly reduced vascular density when treated with cRGD over those treated with PBS. The effect of the reduction of perfused functional vessels was then supported by the reduction in the number of tumour blood vessels seen using immunostaining with anti-CD31, an antibody specific for endothelial cells. [171] Furthermore, it was shown that pretreatment with cRGD reduced microvessel density and prevented rapid viral clearance from the tissue, which led to significantly increased survival of mice pretreated with cRGD and then given intratumoural OV therapy. [171]

Following this report that hrR3 has anti-angiogenic properties itself, the same observation was reported by Breitbach *et al* who showed in humans that VV disrupts tumour associated vasculature after IV administration. The selective infection of tumour associated endothelial cells caused reduced perfusion and increased hypoxia in the tumour as early as five days after treatment. [172] This was further reported by Hou *et al* who observed that re-vascularisation after treatment with VV was delayed until after it was cleared in murine models. [173] It is doubtful whether such events could ever be controlled sufficiently to enable vascular normalisation created by a first dose OV to enhance subsequently delivered chemotherapy. Indeed, the concept of vascular normalisation to enhance subsequently IV dosed OV, may be flawed, as work with liposomes suggests that any gains provided by re-establishment of tumour perfusion are negated by decreased passage of particulates through vasculature that has regained structural integrity and lost EPR. [156] However, studies using tumour necrosis factor alpha (TNF-α) have shown that this modifier of vascular permeability may well provide a good route to enhanced tumour uptake of OV when used in a perfused limb context. [174, 175] The differences in the timescales and modes of action between anti-VEGF based and TNF-α based perfusion modulation may explain the opposing impact they have when combined with OV, although safe systemic use of TNF-α remains a challenge. Of note, a

study by Arulanandam *et al* reported that delivery and spread of IV administered oncolytic VV was inhibited when VEGF signalling was supressed in vivo, further questioning whether combined sequential vascular normalisation treatment followed by OV infection is suitable. [176]

1.3.2.1.2 Altering the Internal Pressure Gradient

Studies have been performed to address whether actively altering the pressure gradient across a tumour can enhance transvascular OV transport. One impressive and important study by Miller *et al* [177] looked at the interaction of blood pressure on blood flow and tumour perfusion in multiple myeloma tumour models. This study compared mice in which the mean arterial pressure (MAP) was manipulated to either increase or decrease the intratumoural perfusion pressure. They showed that physical exercise could be used as a method to increase the mouse MAP, 160 mm Hg, and inhalation of 5% Isoflurane would decrease the mouse MAP, 50 mm Hg. Vesicular stomatitis virus (VSV) was then delivered systemically to mice bearing myeloma tumours. [177] Miller *et al* showed using SPECT/CT imaging that there was significantly increased density of VSV intratumoural infection on days 1 and 2 post treatment in the exercise group. Tumours harvested on day 1 post treatment showed around a 100-fold increase in VSV present in the exercise group over those present in the 5% Isoflurane group. This increased infection resulted in significantly higher survival in the exercise (high MAP) group when compared to the 5% Isoflurane (low MAP) group. Crucially, the survival in the 5% Isoflurane group was not statistically significant compared to the saline control group. [177] It has also been noted that the findings in this study, showing the impact of anaesthesia on intratumoural pressure and hence perfusion in murine models, provides strong evidence for the need for standardized animal handling and anaesthesia protocols. [178] It has been suggested that difference in these practices could be a reason why there has been variability in delivery and efficacy of similar therapeutics used in different facilities.

1.3.2.2 Ultrasound

Ultrasound (US) has been utilised for many years in the biomedical imaging field and within this application has a well-defined safety profile. [179] At higher intensities, US can also be used for therapeutic purposes such as thermal ablation of tissue, lithotripsy, enhanced drug delivery, temporary opening of the blood brain barrier and triggered drug release. [180]

A significant benefit of ultrasound as a therapeutic mechanism is that it can be highly focussed (from outside the body) to target small, well defined regions of tissue that are located at depth in the body. The focussing of US to within a few cubic millimeters provides pinpoint accurate external stimulus, especially when used to create cavitation events.

1.3.2.2.1 Acoustic Cavitation

The positive and negative peaks in pressure created by an US wave interact with gas bubbles in its path. These may be naturally entrained bubbles or bubbles provided by injection of micro or nano bubble formulations. [181] During the alternating rarefactional and compressional cycles of the US wave, the bubble may expand and collapse, oscillating repeatedly. [181] This is commonly referred to as 'non-inertial' cavitation. However, if the pressure is sufficient, the bubble will expand and then collapse violently under the inertia of the surrounding media resulting in the bubble breaking into smaller bubbles. This is known as inertial cavitation. During cavitation events, there are two mechanisms which increase blood flow; acoustic streaming and microstreaming. [182] The streaming mechanisms and shock waves that are generated by cavitation have the potential for use in enhancing drug delivery to tumours. [183]

Microstreaming and acoustic radiation forces are the overarching forces which enable increased penetration of therapeutic agents deep into solid tumours and can facilitate the delivery of OV from the bloodstream. [179]

Microstreaming is a term describing the transfer of momentum from a pulsating bubble to the surrounding fluid resulting in motion within the fluid during cavitation.

Bubbles which have been acoustically excited, either oscillating stably or collapsing transiently, have the potential to cause the surrounding fluid to move. The fluid motion generated produces streaming patterns around the oscillating bubble. [184] This movement in the fluid then results in momentum being passed on to surrounding structures, and enables transport of these structures out of the vasculature. Acoustic radiation force is the driving force experienced by an object, such as an OV, in an acoustic field occurring as a result of a pressure gradient across a volume. [182, 185]

Cavitation events (both inertial and non-inertial) can be detected using an ultrasonic transducer and examined by the acoustic emission that they produce (discussed further in section 1.3.2.2.3). Non-inertial cavitation predominantly produces harmonic acoustic emissions which are associated with the non-linear oscillations of bubbles themselves. Conversely, inertial cavitation, which is associated with violent bubble collapse, produces broadband acoustic emissions which are due to the formation of shockwaves. [186]

1.3.2.2.2 Ultrasound Mediated Cavitation for Enhanced Drug Delivery

The earliest report of enhanced delivery of OV using US was in 2006. [187] Adenoviral vectors were incubated in the presence or absence of microbubbles before being incubated with human plasma and exposed to 2.5 MHz of US at 535 kPa continuously for 1 minute in the presence of DU-145 and H23 cells. Ad-GFP-Microbubble formulations showed a strong fluorescence signal when infection took place with US exposure when compared with the same formulation in the absence of US exposure. [187]

An early hallmark study was reported in 2010 when enhanced delivery of oncolytic adenovirus microbubble constructs (Ad-MB) was seen in the US treated tumour in one of two bilateral tumours in the same mouse. [188] A further study also showed that in two xenograft mice models, enhanced delivery in one tumour led to growth reduction in the other tumour. This could suggest that increased tumour infection in one tumour led to systemic abscopal anti-tumour effects, however,

it is noted that a lack of an adequate control for just IV injected Ad-MB limits the conclusions that could be made. [188]

Increased OV delivery into and improved dissemination throughout tumours was shown using a polymer stealthed Ad and US-inducted cavitation. [116] Ad was "stealthed" with a PHPMA polymer, showing a 50-fold increase in circulation half-life in murine models bearing human ZR-75-1 xenograft tumours (see section 1.3.1.2.1). To noninvasively increase extravasation of the circulating polymer-coated Ad into the tumour, it was co-injected with gas microbubbles and the tumour was exposed to 0.5 MHz focused US at peak rarefactional pressure of 1.2 MPa, triggering inertial cavitation which was then monitored remotely in real-time. [116] The combination of polymer stealthing and US induced cavitation resulted in a significant increase in tumour infection, measured by bioluminescence, of over 30-fold ($p=0.03$). [116] Not only was an increase in tumour infection seen, but dissemination into the tumours away from the blood vessels was also improved, with cell death seen hundreds of microns from blood vessels, compared to tens of microns without US.

Microbubbles are destroyed in the process of undergoing inertial cavitation meaning that the cavitation events provided are rather short-lived, and repeat microbubble administration is required if cavitation levels sufficient to provide enhanced delivery are to be achieved. [189] Kwan *et al* have addressed this limitation with the development of a nanoscale sonosensitive particle (SSP) which is capable of sustaining inertial cavitation for several minutes [189], substantially longer than the cavitation time observed with microbubbles.

A study by Myers *et al* saw this nanoscale cavitation technology applied in vivo to vaccinia virus (VV) delivery. [190] It was reported that when a combined IV injection of SSPs and VV expressing luciferase were administered in CD1 nude mice bearing xenograft HepG2 or SKOV-3 tumours and exposed to focused US there was a substantial (1000-10000-fold) increase in infectivity. This increase of infectivity correlated with number of VV genomes recovered from the tumours as assessed by qPCR at cull. Furthermore, this study looked into the comparison of a commercially available US contrast agent, SonoVue® (SV), and showed significantly

improved infection using SSP ($p < 0.05$). The use of therapeutic US for enhanced delivery of OV therefore offers a potential solution to the reported limited tumour extravasation and intratumoural viral spread.

1.3.2.2.3 Monitoring Cavitation Events

Cavitation events produce acoustic emissions and so monitoring of cavitation utilises the ability to detect and inspect the frequency spectra of these emissions to determine the levels of non-inertial and inertial cavitation occurring during a treatment. [191] Cavitation activity is detected via transducers which are listening passively. Inertial cavitation events are short in the time domain and broadband in the frequency domain, whereas non-inertial cavitation events are associated with subharmonic, harmonic and ultraharmonic emissions. Acoustic signals can be analysed for the harmonic and broadband signals present, and therefore the non-inertial and inertial cavitation can be quantified.

In this work, acoustic emissions are detected on linear arrays which have a bandwidth of 5 - 11 MHz. Thus recorded signals are already partially filtered. To further clean the recorded signals, a digital bandpass filter of 5 - 11 MHz and a digital comb filter (applied at integer multiples of the fundamental frequency) are used, thereby leaving only the broadband signal (representative of inertial cavitation) for analysis. It is noted that with SSP cavitation nuclei, only inertial cavitation is produced, however the same filtering process is applied to cavitation activity which is detected.

Passive acoustic mapping (PAM) is a technique that can be used to monitor cavitation events spatially in real-time and could be used to monitor treatments. [192] A linear array placed within a HIFU transducer transverse to its axis is used to detect cavitation events. [193] In PAM, the differences in time of arrival of acoustic emissions to the different elements within the linear array are used to resolve the source location and as a result generates a spatial map of cavitation activity. [194]

1.4 Implications for Current Work

This field has heavy interest from researchers globally and there is extensive literature on previous investigations and results. Clinical trial analysis has shown VV to be hindered by bloodstream neutralisation after IV administration and in repeat dosing. Sufficient dissemination throughout tumours has also contributed to low infection levels after systemic injection. Techniques to enhance the bloodstream stabilisation of non-enveloped viruses such as the oncolytic adenovirus have included chemically attaching polymers such as PEG and PHPMA directly to the viral capsid leading to improved bloodstream stability and pharmacokinetics *in vivo*. Furthermore, the addition of targeting ligands to the polymer coating was able to re-instate the infectivity achieved by the polymer coated adenovirus. PEG polymers synthesised with hydrophobic groups on one end (i.e. PEG-Cholesterol and PEG-DSPE) have been used previously in abundance to increase the circulation kinetics of drugs and drug carriers (i.e. liposomes). The use of ultrasound in combination with cavitation nuclei has been shown to improve the intratumoural viral load (and hence the infection levels achieved) of oncolytic viruses after both intratumoural and intravenous administration pre-clinically.

1.4.1 Research Questions

During my review of this literature, I have determined the following questions which are yet to be looked at and which I aim to answer in this thesis:

1. Can ultrasound mediated cavitation enhance the delivery and infection of oncolytic vaccinia virus in a xenograft murine model *in vivo* after intratumoural injection?

2. Can a polymer synthesised with a cholesterol group at one end be used to coat the enveloped oncolytic vaccinia virus and under what conditions is this most effective?

3. What is the impact of polymer coating an enveloped oncolytic vaccinia virus on infection levels of human cancer cell lines *in vitro* in the presence and absence of human serum and in a xenograft murine model *in vivo*?

4. Can targeting ligands be attached to the polymer coating of an oncolytic vaccinia virus and enable binding to a new cell surface target?

5. What is the impact of a retargeted polymer coating on the infection levels achieved *in vitro* in the presence and absence of human serum and in a xenograft murine model *in vivo*?

6. What is the effect of polymer coating (with and without targeting ligands) the oncolytic vaccinia virus on its circulation kinetics in murine models?

7. Can ultrasound mediated cavitation using a dual transducer setup with high resolution monitoring enhance the delivery, infection and tumour control of oncolytic vaccinia virus in a CAPAN-2 xenograft murine model after intravenous injection?

Chapter 2

Methods and materials

2.1 Chemicals and Equipment

2.1.1 Polymers

Polymers used for coating of VV in this research were:

- Poly(ethylene glycol) of length 8 kDa conjugated at one end to a cholesterol group (O-methyl-O'-[N-(cholesterylsuccinyl) aminoethyl]poly(ethylene glycol) 8 KDa, named here as Chol-PEG(8K)) and structure shown in Figure 2.1 (synthesised by Victor Ramos).

- Poly(ethylene glycol) of length 10 kDa with a cholesterol group conjugated to one end and a fluorescein conjugated to the other end, (O-(fluorescein-5-yl-thioureidoethyl)-O'-[N-(cholesterylsuccinyl)aminoethyl]poly(ethylene glycol) 10 KDa), named here as Chol-PEG(10K)-FITC) (Nanocs, PG2-CSFC-10k).

- Poly(ethylene glycol) of length 10 kDa with a cholesterol group conjugated to one end and an N-Hydroxysuccinimide (NHS) group conjugated to the other end (O-(succinimidyl carbonate)-O'-[N-(cholesterylsuccinyl)aminoethyl]poly(ethylene glycol) 10KDa), named here as Chol-PEG(10K)-NHS) (synthesised as reported in section 2.3.1 and purchased from Creative PEGWorks, PLS-9985).

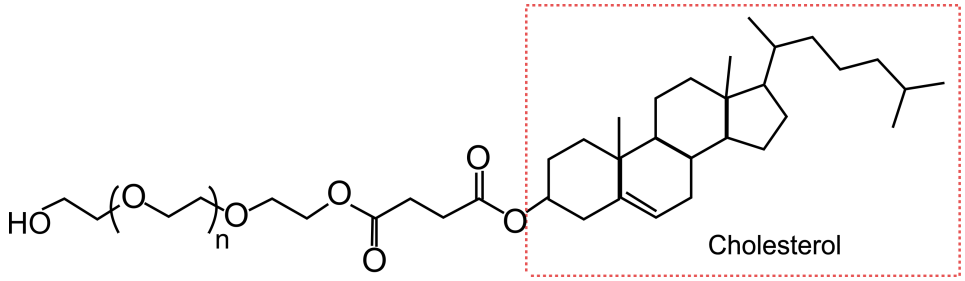


Figure 2.1: Poly(ethylene glycol)-Cholesterol (PEG-Chol) structure, Molecular mass 8000-10000 g mol^{-1}

2.1.2 Blood Work, DNA extraction and qPCR

Human blood was collected using Sodium Heparin Vacutainers (VS368480, Bunzl Healthcare). DNA extraction was performed using the Genelute mammalian DNA extraction kit (G1N-350, Sigma-Aldrich). qPCR was performed using Forward Primer (TGACTACGTTGTTATGAGTGCTTGGTA), Reverse Primer (AGATCATCGTATGGAGAGTCGTAAGAT) and Probe (5'-[6FAM]ATCAAAATACAAGACGTCGCTTTTAGCAGCTAAAAGAA[TAM]) (Sigma-Aldrich UK), qPCRBIO Probe Mix Hi-ROX (P820.22-05, PCR Biosystems Ltd), and a StepOne System (ThermoFisher) qPCR machine were used.

2.1.3 In Vitro studies

The following products were purchased and used according to the manufacturer's instructions.

The cell lines and their corresponding growth media which were used in this research were:

- A549 cells (European Collection of Cell Cultures), Dulbecco's Modified Eagle's medium (DMEMX1) (D5546, Sigma-aldrich, UK) and 10% Fetal Bovine Serum (FBS; Life Technologies, UK)

- DLD cells (European Collection of Cell Cultures), Dulbecco's Modified Eagle's medium (DMEMX1) (D5546, Sigma-aldrich, UK) and 10% Fetal Bovine Serum (FBS; Life Technologies, UK)

- CAPAN-2 cells (American Type Culture Collection), McCoy's 5A (M4892, Sigma-aldrich, UK) and 10% Fetal Bovine Serum (FBS; Life Technologies, UK)

Phosphate-buffered saline (P5493-1L, Sigma-aldrich, UK), Trypsin (ThermoFisher, UK) and Trypan Blue (ThermoFisher, UK) were used for cell culture and counting. Reporter Lysis Buffer 5X (E3971, Promega, UK) and Luciferase Assay System (E1501, Promega, UK) were used in the Luciferin assays. CellTiter 96® Aqueous One Solution Cell Proliferation Assay (G3582, Promega, UK) was used in MTS Assays. Both luciferase and MTS assays were analysed using a FLUOstar Omega (BMG Labtech, UK) plate reader. 4-20% pre-cast polyacrylamide gel, 4X Laemmli Sample Buffer (BioRad, 1610747), 2-mercaptoethanol (BME, Sigma, M6250), tris-glycine-sodium dodecyl sulfate (TGS) running buffer (BioRad 1610375), barium chloride (Sigma-Aldrich, 342920), iodine solution (Sigma-Aldrich, 38084), Coomassie Brilliant Blue R Dye (Sigma-Aldrich, B7920) and CL-XPosure™ Film (34088, Fisher Scientific) were used in SDS-PAGE and western blot analysis. YOYO-1 (Y3601, Thermo-Fisher), YOYO-3 (Y3606, Thermo-Fisher), anti-vaccinia rabbit monoclonal antibody (Abcam, ab35219), anti-mouse IgG-AF647 (Invitrogen, A-21235), anti-rabbit-APC (R&D Systems, F0111) were used in flow virometry experiments.

2.1.4 Vaccinia Viruses

Vaccinia viruses (VV) used in the work reported here was kindly supplied by Transgene SA, France. The plaque forming unit (pfu) to viral genome (VG) ratio was determined by Transgene SA for all viruses to be 1 pfu: 50 VG. The unit of pfu is used throughout to describe the concentration and dose of VV used. The unit of VG is used to describe values of VV obtained by QPCR.

All viruses were stored in 10-50 µL aliquots at the concentration stated at −80 °C. The oncolytic VV used here was Copenhagen strain attenuated recombinant vaccinia virus (VV) has a deletion of the thymidine kinase and ribonucleotide reductase genes (VVTK-I4L-). It encodes either GFP (VV-GFP) or luciferase (VV-luc) under the control of the p11K7.5 promoter. [195] This double deleted vaccinia virus is

highly attenuated in normal cells, yet it displays tumour-selective replication and cell kill. [195] VV has an 8 hour replication cycle. [50]
1) "VV-GFP": VVTK-I4L-/GFP, stock concentration 2.5x10^9 pfu/mL
2) "VV-luc": VVTK-I4L-/luc, stock concentration 1.7x10^9 pfu/mL

2.1.5 In Vivo studies

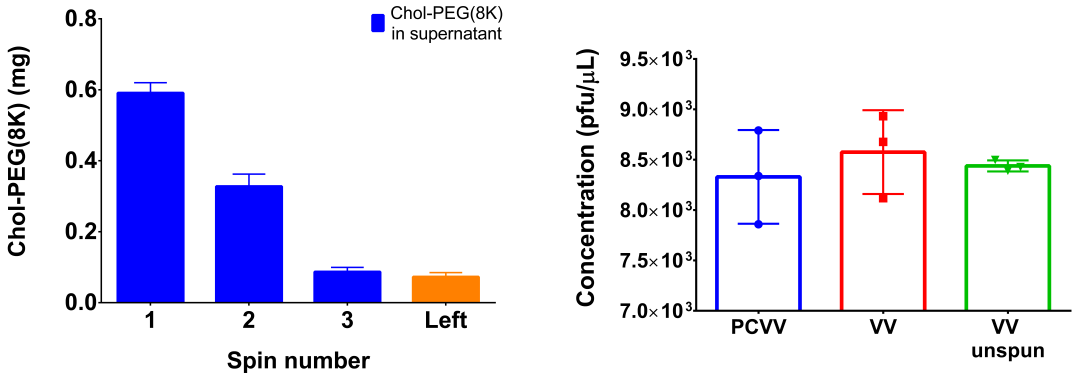
Sonosensitive particles (SSPs) were used as the cavitation agent in in vivo work and were supplied by Oxsonics Ltd. For imaging 100 µL Pierce™ D-Luciferin, Monopotassium Salt (ThermoFisher Scientific, 88294) was used at 15.8 mg/mL in PBS by intraperitoneal injection. Imaging was performed using an in vivo imaging system (IVIS Lumina, Caliper Life Sciences).

2.2 Polymer Coating VV

Polymer stock solutions were made fresh before they were mixed with VV. For coating, a 2X concentrated stock solution of Chol-PEG(8K) was made up in PBS before being added 1:1 with virus solution. For instance, for coating at a polymer concentration of 10 mg ml^{-1}, a 20 mg ml^{-1} stock solution was formed by mixing the dry polymer in DPBS thoroughly using a vortex to ensure a homogeneity. 10 mg ml^{-1} was the maximum coating concentration used. An initial study looked at the temperature of formation. In this study the VV and polymer mixture was incubated at either 4 °C or 37 °C for an hour. All formation after this initial test used 37 °C as the temperature during formation, allowing the lipid layer of the virion to become more fluid (section 1.3.1.2.3) and amenable to the cholesterol on the polymer embedding.

2.2.1 Purification of coated VV

VV was coated (section 2.2) in high excess of polymer. Most studies were performed using a washed polymer coated sample, where the coated VV was separated from the excess PEG-Chol. The polymer and VV mixture was diluted 1:10 in DPBS, centrifuged at 22,000g for 10 minutes to form a viral pellet and the supernatant was



(a) (b)

Figure 2.2: VV and PCVV samples were made at a concentration of 8x10^3 pfu/µL and with a Chol-PEG(8K) concentration of 10 mg ml^{-1}. The removal of Chol-PEG(8K) from PCVV was performed by pelleting 100 µL samples at 22,000g for 10 minutes to form a viral pellet and then removing 90 µL of the supernatant. The pellet was then resuspended in DPBS to a total volume of 100 µL. This was repeated a total of 3 times. The concentration of the virus samples after washing was determined by qPCR after DNA extraction. (a) The Chol-PEG(8K) in each supernatant (blue) was determined using a cholesterol assay. The remaining Chol-PEG(8K) in the retentate was also determined (orange). In an unwashed 100 µL PCVV sample there was 1 mg Chol-PEG(8K). (b) The concentration of PCVV (blue) and VV (red) were determined by qPCR after washing was performed to determine the amount of sample lost when compared with an unwashed sample of VV (green).

removed (90 µL of a total 100 µL volume). The process was repeated 3 times and the final pellet was resuspended in PBS. A cholesterol assay (Cambridge Bioscience, STA-390) was performed as per the manufacturers instruction using Chol-PEG(8K) standards between 0.1 and 1 mg ml^{-1} to determine the amount of Chol-PEG(8K) in the supernatant of each wash (supernatants were diluted 1/10 for the assay). This showed that most (0.6 mg) of the free Chol-PEG(8K) incubated with VV to form PCVV was removed in the first wash (shown in Figure 2.2a). It was important to know how much VV or PCVV was lost during purification and so DNA extraction and quantitative polymerase chain reaction (qPCR) was performed as described in section 2.7 to determine viral concentrations after washing. An example of this is shown in Figure 2.2b which demonstrated how the concentration of VV and PCVV were affected by this washing technique. Virus solutions were then resuspended at a final concentration as necessary for the specific assay performed.

2.3 Retargeting VV

2.3.1 Cholesterol-PEG-NHS synthesis

Cholesterol-PEG (8kDa) with a carboxylic acid group (Chol-PEG-COOH) was previously synthesised by Megan Grundy and Professor Victor Ramos. The structure of the Chol-PEG-COOH used and the steps taken to produce Chol-PEG-NHS can be seen in Figure 5.4.

In the study reported in section 5.2.2.1 of this thesis 100 mg of stock Chol-PEG-COOH was dissolved in 1250 µL acetonitrile (ACN, 271004, Sigma-Aldrich) in a glass vile and then 125 µL 150 mM dicyclohexylcarbodiimide (DCC, 633267, Sigma-Aldrich) and 125 µL 2000 mM N-Hydroxysuccinimide (NHS, 130672, Sigma-Aldrich) were added. The solution was left at 4 °C for 6 hours during which a dicyclohexyurea (DCU) precipitate formed and was filtered out. The solution was then purified by precipitation in cold di-ethyl ether (296082, Sigma-Aldrich). The reaction mixture (1.5 mL) was added dropwise to cold diethyl ether (11mL) inside a Supelco PSE tube with 2 PE frit filters and kept on dry ice for 15 minutes. The ether was subsequently filtered out of the tube. This process was repeated until no more DCU precipitate formed when the precipitate was resuspended in ACN. The precipitate was then blown dry under N_2 gas, and dried completely in vacuo. The identity of the product was determined by H-NMR analysis which was performed with the help of Dr Luca Bau.

2.3.1.1 Testing the efficiency of conversion of COOH to NHS esters on Chol-PEG-NHS

The efficiency of the COOH conversion to NHS was determined using a TNBS assay. A standard curve of NHS acetate (S0878, TCI Chemicals) in dimethylformamide (DMF, 227056, Sigma-Aldrich) with top standard of 0.75 mM in 0.15 mM steps to a bottom standard of 0.15 mM. Chol-PEG-NHS samples were made up to a concentration of 1.24 mM in DMF. 100 µL of 1.66 mM ethanolamine solution in DMF was added to 100 µL each standard and Chol-PEG-NHS sample and incubated

on a mixing plate for 15 minutes at RT. The final concentration of ethanolamine was 0.83 mM and NHS was 0.6225 mM. 50 µL of each sample or standard in ethanolamine was added to individual eppendorfs containing 950 µL Borate buffer (0.2 M boric acid, pH 9.2). 0.4% 2,4,6-trinitrobenzenesulfonic acid (TNBS, P2297, Sigma-Aldrich) was prepared in ddH_2O and 50 µL was added to each eppendorf containing a sample or standard. The samples and standards were incubated at 55 °C with the TNBS and borate buffer on a shaking plate for 15 minutes. Tubes were then cooled before 100 µL of each sample or standard was added in triplicate to a clear 96-well plate. Absorbance spectra of the plate was measured on a plate reader (FLUOstar Omega, BMG Labtech). A decrease in the TNBS-Ethanolamine signal was indicative of a reaction between the NHS and the ethanolamine.

2.3.2 Cholesterol-PEG(10K)-NHS reaction with amine groups of IgG or anti-MUC1 antibody

A polymer with a PEG backbone conjugated to a cholesterol group on one end, and an NHS group on the other end (Chol-PEG(10K)-NHS) was used to form IgG-polymer and aMUC1-polymer conjugates (as detailed in section 2.1.1). The NHS group was reacted with primary amine groups on the IgG (R&D Systems, MAB002) or aMUC1 antibody (Abcam Ltd, ab245693) to form an amide bond. This is depicted in the schematic in Figure 7. The reaction took place at polymer concentrations of 330 µM, 132 µM and 6.67 µM with an antibody concentration of 6.67 µM in a 100 mM borate buffer (pH of 8.3). [196] The polymer-antibody mixture was left to incubate for 60 minutes, as it was determined by sequential HPLC runs over a 160 minute time period that the reaction reached completion within 45 minutes at these conditions. The reaction was quenched with 0.5M Tris-HCl and finally buffer exchanged into PBS using an Amicon Pro Purification System and a 30 kDa filter (Millipore, ACS503012). Successful attachment was then verified using high performance liquid chromatography (HPLC) and sodium dodecyl sulfate polyacrylamide gel electrophoresis (SDS-PAGE).

2.3.2.1 HPLC analysis of PEGylated anti-MUC1

Samples were analysed by reverse phase HPLC with an Agilent 1290 Infinity II with a quarternary pump (G7104A) and a diode array detector (G7117B) on a MAbPac™ RP column (2.1x100mm, 4 nm particle size, 1500 A pore size). Chromatographic separation was accomplished with a mobile phase comprised of 0.1% trifluoroacetic acid in water (A) and 0.1% trifluoroacetic acid in acetonitrile (B), with an isocratic hold at 10% B for 4 minutes followed by a linear gradient from 10 to 90% B over 24 min at a flow rate of 0.35 mL/min and column temperature of 80 °C, an injection volume of 8 µL and UV-Vis detection at 210 and 280 nm.

2.3.2.2 SDS-PAGE

Samples were mixed with Laemmli buffer (BioRad, 1610747), or reduced in 10 % 2-mercaptotheanol (BME, Sigma, M6250) in Laemmli buffer, at a volume to volume ratio of three parts sample to one part buffer and then run on a 4-20% precast gel polyacrylamide gel (BioRad, 4561096). Reduced samples were heated at 95°C for 5 minutes. 10 µL of each sample was loaded into the gel and run at 160 V for 40 minutes in 1X tris-glycine-sodium dodecyl sulfate (TGS) running buffer (BioRad, 1610732). Precision Plus Protein™ Kaleidoscope™ Prestained Protein Standard (Bio-Rad, 1610375) was loaded to well number 1 for molecular weight (MW) analysis. The presence of PEG was determined by incubating the gels in a barium iodide stain. 5% barium chloride in 1M HCl was added to a 0.1N iodine solution at a 5:2 ratio. [197] The presence of protein was determined by incubating the gels in Coomassie Blue stain (0.05 g Coomassie Brilliant Blue R Dye (Sigma, B7920), 45 mL methanol, 10 mL acetic acid and 45 mL water) for 2 hours and then destaining overnight in a solution of 50% methanol, 10% acetic acid and 40% water.

2.3.3 ELISA analysis of PEGylated aMUC1

2.3.3.1 Ability for Chol-PEG-aMUC1 to bind target

The MUC1 core peptide GVTSAPDTRPAPGSTA (Cambridge Bioscience, ANA60600-1) was diluted to a concentration of 10 µg/mL in 0.05 M pH 9.6 bicarbonate buffer

(Sigma-Aldrich, C3041-50), and 100 µL of this solution was added per well to a 96-well PierceTM Maleic Anhydride activated plate (Life Technologies, 15110). Plates were incubated at 4°C overnight.

The following morning plates were then left at RT for 30 minutes before wells were then washed using a PBS and 0.05% Tween-20 buffer and blocked using 10% FBS in PBS (X3). Unmodified and modified aMUC1 samples were serially diluted to produce a range of antibody concentrations from 0.05 to 6.67 nM. 50 µL of each concentration was added to wells in duplicate for the unmodified and modified anti-MUC1 samples and incubated for 90 minutes at RT. Wells were emptied and washed as above using a PBS and 0.05% Tween-20 buffer (X5). Anti-Rabbit HRP-conjugated antibody (Abcam, ab205718) was diluted 1: 5000 in 10% FBS and 100 µL was then added to each well and incubated for 1 hour. Plates were then washed as above and then each well was incubated with 100 µL TMB substrate (Thermofisher, 34029). Development was stopped by addition of 100 µL of 0.5 M sulphuric acid. Absorbance was read at 450 nm using a plate reader (FLUOstar Omega, BMG Labtech).

2.3.3.2 Characterising Chol-PEG-aMUC1 by assaying for presence of PEG

The MUC1 core peptide was immobilised as described in section 2.3.3.1. Unmodified and modified (1:20) aMUC1 samples were serially diluted to produce a range of antibody concentrations from 7.8 to 1000 ng/mL. 50 µL of each concentration was added to wells in duplicate for the unmodified and modified aMUC1 samples and incubated for 90 minutes at RT. Wells were emptied and washed as above using a PBS and 0.05% Tween-20 buffer (X5). Anti-PEG IgM raised in rabbit (abcam, ab133471) was then diluted 10 µL/mL in 10% FBS and 100 µL was then added to each well and incubated for 1 hour at RT. Wells were emptied and washed as above using a PBS and 0.05% Tween-20 buffer (X3). Anti-rabbit IgM HRP (abcam, ab97195) was diluted 1:10,000 in 10% FBS and 100 µL was then added to each well and incubated for 1 hour at RT. Plates were then washed as above and then each well was incubated with 100 µL TMB substrate (Thermofisher, 34029). Development

was stopped by addition of 100 µL of 0.5 M sulphuric acid. Absorbance was read at 450 nm using a plate reader (FLUOstar Omega, BMG Labtech).

2.3.4 aMUC1-PCVV, IgG-PCVV and MUC1-aMUC1-PCVV formation

Chol-PEG-aMUC1 and Chol-PEG-IgG conjugates were formed as described in 2.3.2 and resuspended to a 20 mg/mL coating concentration. Samples of aMUC1-PCVV which were blocked with MUC1 peptide (MUC1-aMUC1-PCVV) were made by incubating Chol-PEG-aMUC1 with MUC1 core peptide GVTSAPDTRPAPGSTA (Cambridge Bioscience, ANA60600-1) at 5 times mass excess compared to the level of aMUC1 antibody present. Incubation was performed overnight at 4 °C before the Chol-PEG-aMUC1+MUC1 was then incubated with VV. 20 mg/mL antibody-polymer conjugate solutions were then added at 1:1 volume:volume to $1x10^6$ pfu/µL solutions and left at 37 °C for one hour before purification as described in 2.2.1 was performed.

2.3.5 qPCR of aMUC1-PCVV bound to immobilised MUC1 target peptide

The MUC1 core peptide was immobilised on a Pierce maleic anhydride activated 96-well plate (Life technologies, 15110) and blocked as described in section 2.3.3.1. The final wash step and an additional 10 minute rinse before samples were added to the plate was done with PBS (no Tween-20), to avoid disruption of the VV envelope. VV and a range of aMUC1 coating concentrations (0.1, 1 and 10 mg/mL) of aMUC1-PCVV were tested and samples were made up as described in section 2.3.4. For the 0.1 and 1 mg/mL concentration aMUC1-PCVV samples, extra Chol-PEG with no aMUC1 was added to make the total concentration of polymer (whether with aMUC1 antibody or without) that was incubated with VV during coating equal to 10 mg/mL in all three groups, in order to test the effect of the surface density of antibody independently from the surface density of the polymer coating. $7x10^4$ pfu were added to each well in a final volume of 100 µL. Plates were then incubated for 3 hours on a shaker plate at room temperature. Samples were then removed

from the plate and 3 washes in PBS were performed with the final wash left for 10 minutes. 10 µL of proteinase K and 100 µL of cell lysis buffer from GenElute™ Mammalian Genomic DNA Miniprep Kit Protocol (Sigma Aldrich, G1N350) were then added to each well and left for 30 mins on a shaker plate. The contents of each well was then transferred into Eppendorf tubes, vortexed and incubated at 55 °C for 10 minutes for DNA extraction, and qPCR was performed as in reference [190].

2.4 Flow virometry

2.4.1 Using YOYO-1 nucleic stain to identify a VV FSC/SSC population

YOYO-1 has previously been used to stain a highly attenuated version of the VV family, Modified Vaccinia Ankara (MVA) and so it was hypothesised that this may translate to successful staining of VV. [198] Gaudin *et al* also reported the detection and sorting of an enveloped Junin virus stained with a YOYO-1 nucleic dye on a conventional FACSAria II Special Order cell sorter. [142]

The samples were stained for aMUC1 using a goat anti-mouse Alexa Fluor 647 secondary antibody (Invitrogen, A-21235). VV populations were determined using a YOYO-1 nucleic acid stain (Thermo Fisher, Y3601), YOYO-3 nucleic acid stain (Thermo Fisher, Y3606) and an anti-VV antibody (Abcam, ab35219).

VV samples were diluted to 2.6x10^4 pfu/µL and added in equal volumes to a 2 µM YOYO-1 or YOYO-3 solution, resulting in a staining concentration of 1.3x10^4 pfu/µL and 1 µM YOYO-1 or YOYO-3. The sample was left at room temperature for 20 minutes before being centrifuged at 22,000g for 15 mins. Pellets were rinsed three times in PBS by centrifugation at 22,000g for 15 mins and then resuspended at a final volume of 500 µL. Samples were kept on ice before used in experiments.

Preparation and washing of modified VV was performed as described in section 2.2 and 2.3.4, with VV incubated for an hour in excess aMUC1-PEG-Chol (10 mg/mL) solutions and washed vigorously. Flow virometry was performed at a final concentrations of 5.26 x10^3 pfu µL^{-1} or 3.4 x10^4 pfu as defined at the time of experiment.

2.4.2 Confirmation of Chol-PEG coating VV on BD FACS Calibur

To determine whether coating of VV in the conditions reported was successful, flow virometry of VV coated with a fluorescently tagged Chol-PEG(10K)-FITC (FPC) was performed. VV virions further modified to PCVV were coated and purified as detailed in section 2.2, and resuspended at a final concentration of 5.26 x10^3 pfu μL^{-1} or 3.4 x10^4 pfu μL^{-1} as specified depending on the experiment. A "high" flowrate was selected and a volume of 50 µL was flowed through for each sample.

2.4.3 Confirmation of Chol-PEG and Chol-PEG-aMUC1 coating VV on Attune NxT

Virus preparation and purification was performed as described in section 2.3.4, with VV incubated for an hour in excess Chol-PEG (10 mg/mL) and Chol-PEG-aMUC1 (10 mg/mL) solutions and washed vigorously. The samples were stained for aMUC1 using a goat anti-mouse Alexa Fluor 647 secondary antibody (Invitrogen, A-21235). VV populations were determined using a YOYO-3 nucleic acid stain (Thermo Fisher, Y3606) and an anti-VV antibody (Abcam, ab35219). Flow virometry was performed at a final concentration 1.27x10^3 pfu/µL. An Attune™ NxT cytometer (Invitrogen) was adapted to record forward and side scatter through the violet channel using the Attune™ NxT No-Wash No-Lyse Filter Kit (Thermo Fisher, 100022776). Analysis was performed using FlowJo v10.6.1 software.

2.5 In Vitro Cell Work

Cell work was carried out in a class II microbiological safety cabinet. The medium used for DLD (DMEM X1 with 10% FCS), A549 (DMEM X1 with 10% FCS)or CAPAN-2 (McCoy's 5A with 10% FCS) cell growth, the DPBS and the trypsin were purchased from Sigma-Aldrich and ThermoFisher respectively. These solutions were stored as chilled or frozen aliquots and were preheated to 37 °C before use.

2.5.1 Cell culture

DLD, A549 or CAPAN-2 cells were incubated in cell culture flasks at 37° C in 5% CO_2. Cells were split once they reached 90% (DLD and A549) or 75% (CAPAN-2) confluence. Old growth media was removed from the flasks and a wash was performed with 10 mL of DPBS. 3 mL of trypsin was then added to the flask and left at room temperature (A549 or DLD) for 5 minutes or or 37 °C for 10 minutes (CAPAN-2). Cells were checked under a microscope to see if they had detached from the surface of the flask and were rounded. If the cells were sufficiently detached, the trypsin was then neutralised with 13 mL of the cell growth media by flushing it over the surface of the flask several times until the media was well mixed and, hence, any remaining trypsin was neutralised. The cell and media mixture was transferred to a conical tube and then centrifuged at $181g$ for 5 minutes. After the cells were centrifuged, the media was removed and replaced with 10 mL of fresh growth media. The cells were then split into a new flask with fresh growth media in a 1:12 ratio (A549 or DLD) and 1:4 ratio (CAPAN-2) or counted and used for infection experiments or subcutaneous implanting.

A Neubauer chamber was used to determine the concentration of cells suspended in a solution. 100 µL of DPBS, 50 µL Trypan Blue and 50 µL of the cell solution being counted were combined and added to the Neubauer haemocytometer. Cells were counted under the microscope.

2.5.2 Adherent Cell Culture assays

A549, DLD or CAPAN-2 cells were plated in a tissue-culture 96-well plate at a concentration of 10^4 or 10^5 (VV-GFP, flow cytometry) cells in 100 µL DMEM per well. They were incubated overnight at 37°C to allow for cell-adherence. VV encoding luciferase (VV-luc) or VV encoding green fluorescent protein (VV-GFP) were stored at −80°C, were diluted to a concentration of between 0.1 - 100 pfu per cell for infection studies. Concentrations used in specific experiments are specified where the results are reported. Plates were incubated between 24 and 72 hours at 37°C and 5% CO_2. Initial studies used pooled human serum (11556345, TCS

Bioscience) to challenge VV infection. In later studies, fresh human plasma from a donor who had been exposed to vaccinia virus via childhood smallpox vaccination was used to challenge VV infection. Both pooled human serum and fresh human plasma were stored in aliquots at −80 °C. Aliquots were defrosted for use on the day of experiments. Pooled human serum and fresh human plasma were added to infection media to form final concentrations of between 0.5 - 25%.

2.5.3 Suspension Cell Culture Assays

CAPAN-2 cells were harvested and counted as described in section 2.5.1 and diluted to 2 x10^5 cells/mL in McCoy's 5A growth medium. Virus solutions were made up as described in section 2.2 using VV encoding luciferase (detailed in section 1). VV and modified VV samples were added to cells to a final 0.1 multiplicity of infection (MOI) and 1 x10^5 cell/mL. In studies using human plasma (from a donor with known prior exposure to VV due to smallpox vaccination), the plasma underwent one freeze-thaw cycle before use and was added in solution to cells at the same time as the VV and modified VV samples. Solutions were incubated at 37°C on a rotor wheel for 2 hours to allow for viral infection. Cells were then pelleted and resuspended in fresh medium at a concentration of 1 x10^5 cells/mL. Each sample was added to wells on a tissue-culture 96-well plate at a concentration of 10^4 cells in 100 µL McCoy's 5A growth medium per well. Cells were then incubated overnight at 37°C before infection was assessed using a luciferase assay as described in section 2.5.4. A Quick Start Bradford protein assay (Bio-Rad, 5000201) was used to determine protein content in wells and adjust luminescence values for any differences.

2.5.4 Lysing Cells and Luciferin Assay

To quantify the level of infection achieved by the VV in the A549 cells, a luciferase assay was performed. When cells are successfully infected, the luciferase enzyme is produced. When the luciferin (substrate to luciferase) is added to the lysed infected cells, it interacts with the luciferase thereby catalysing a reaction in which a photon is produced. Therefore, by adding the luciferin in excess, the number

of photons produced can be determined and, hence, the amount of infection that has occurred can be quantified.

After infection, the cells were lysed so as to release any luciferase present inside the cells. This was done using a lysis buffer diluted 5 times in ddH_2O. First, the media from each well was removed, and 100 µL of the lysis buffer solution was added. The plate was then sealed and placed in the −80°C freezer for a complete freeze-thaw cycle. When the plate completely thawed at RTP, 25 µL of each well was then transferred to the corresponding well on an opaque white 96 well plate. 25 µL of luciferin was then added to the wells. Luciferin was added in excess of the luciferase produced in each well to ensure that the number of photons detected during the assay was not limited by the amount of substrate present. A FLUOstar Omega was used to measure the amount of luminescence produced.

2.5.5 MTS Assay

Cell-viability was quantified using CellTiter 96® Aqueous One Solution Cell Proliferation Assay. 24 - 72 hours post-infection, media was removed from each well and 100 µL of DPBS supplemented with 20 µL of MTS assay reagent (CellTiter 96® Aqueous One Solution Reagent) was added. Plates were then incubated for up to 1 hour at 37°C and 5% CO_2. Absorbance was measured every 5 minutes in a plate reader (FLUOstar Omega) at 490 nm until absorbance values exceeded 1.

2.5.6 Fluorescent Microscopy

Adherent cell culture infection studies with VV-GFP were performed on A549, DLD and CAPAN-2 cells are detailed in section 2.5.2. 24 hours after infection media was added to cells and left to incubate, brightfield and fluorescent microscopy was performed. This enabled differences in morphology and the levels of GFP fluorescence and hence VV-GFP infection levels of cells to be determined. Cells were imaged using an inverted Nikon Ti Eclipse fluorescent microscope (Nikon Instruments, Melville, NY, USA), with CoolLED pE Excitation system (CoolLED, UK). 4x magnification was used with FITC and brightfield filters. No adjustments to

brightfield images were made post capture. Fluorescent images were post processed by setting black to transparent and white to green. Brightfield and fluorescence images taken of the same view are presented as overlays.

2.5.7 Flow Cytometry

2.5.7.1 Determining infection of cells with VV-GFP

Adherent cell culture infection studies with VV-GFP were performed on A549 and CAPAN-2 cells (10^5 cells per well) as detailed in section 2.5.2. Infection media was added to cells and left to incubate at 37 °C for 24 hours. Infection media was then removed from wells and wells were washed with 100 µL PBS. PBS was then removed from each well and placed into a corresponding eppendorf for that well. 50 µL 1x trypsin was then added to each well. Cells were incubated at 37 °C for 5-10 minutes until cells were rounded and detached from the well surface. 150 µL of growth media was added to wells and the well contents was transferred to the corresponding eppendorf. 100 µL growth media was flushed over each well surface and added to the corresponding eppendorf to ensure all cells had been recovered. Eppendorfs were then centrifuged and cells were washed x3 in PBS before being resuspended in 200 µL PBS. Cells were analysed using an Attune NxT Flow Cytometer (Invitrogen). 2,000 events were acquired for each sample. FlowJo v10.5 data analysis software was used to process the data recorded.

2.5.7.2 Determining cellular MUC1 expression of A549 and CAPAN-2 cells

CAPAN-2 or A549 cells were recovered from cell culture flasks, washed and counted as described in section 2.5.1. They were resuspended in growth media at a concentration of $1x10^6$ cells/mL and left at 37 °C for 45 minutes so as to allow for surface proteins to recover from trypsin exposure. After 45 minutes, cells were removed and pelleted by centrifugation (181g, 5 minutes) and resuspended in cold PBS + 1% BSA. Cells were then counted and split into eppendorfs (n=3) of total volume 600 µL. Eppendorfs were then centrifuged to form a cell pellet and resuspended in 600 µL aMUC1 antibody raised in mouse (HMFG2 clone, Merck

Millipore, MABC1613) was diluted in PBS + 1% BSA to a final concentration of 1 µg/mL. Cells were incubated at 4 °C for 1 hour. After incubation cells were centrifuged, supernatant was removed and cells were washed 3x with cold PBS + 1% BSA. After washing fluorescently tagged anti-mouse secondary antibody raised in goat (A-21237, ThermoFisher Scientific) was added to the cells at a final concentration of 2 µg/mL in PBS + 1% BSA. Samples were incubated at 4 °C for 1 hour and cells were washed 3x with cold PBS + 1% BSA and analysed using an Attune NxT Flow Cytometer. 22,000 events were acquired for each sample. FlowJo v10.5 data analysis software was used to process the data recorded.

2.6 In Vitro Blood Work

2.6.1 Evaluation of the impact of PCVV on Antibody Binding when compared to VV

Anti-VV antibody binding was determined using flow virometry. VV and PCVV (formulated as described in section 2.2) were made up to a concentration of 3.4x10^4 pfu/µL. They were then incubated with an anti-VV antibody (Abcam, ab35219) at a 1:50 virus to antibody ratio for 40 minutes at 4°C. Samples were washed and pelleted as described in section 2.2.1. They were then incubated with an anti-rabbit antibody conjugated to APC (R&D Systems, F0111) at a concentration of 10 µL per 1x10^6 pfu for a further 30 minutes at room temperature. Samples were then washed and resuspended at a concentration 3.4x10^4 pfu/µL in a total volume of 250 µL. A BD FACSCalibur Flow Cytometer was used and analysis was performed using FlowJo v10.6.1 software. VV populations were gated in FSC/SSC so as to exclude events that were present in PBS control samples.

2.6.2 Human Blood Component Separation

Human blood was taken by venipuncture into Vacutainers coated with sodium heparin anticoagulant. Separated blood fractions were obtained by centrifugation at 2000g for 5 minutes. This allowed the plasma and erythrocyte fractions to be isolated from 8 mL of whole blood.

In distribution studies, 8 mL blood was incubated with 8.5 x10^6 pfu of VV or (unwashed) PCVV at 37°C for 15 minutes. Sodium Heparin vacutainers were inverted every 3 minutes to ensure thorough mixing during incubation and were then centrifuged for 5 minutes at 2000*g*. Plasma fractions were then used in infection studies. Genome quantity of VV/PCVV in plasma and erythrocytes were analyzed by quantitative polymerase chain reaction (qPCR) (section 2.7).

2.7 DNA Extraction and Quantitative Polymerase Chain Reaction (qPCR)

All 200 µL samples tested for VV genome content were first digested using proteinase-K and DNA extracted using the GenElute™ Mammalian Genomic DNA Miniprep Kit Protocol (Sigma Aldrich, G1N350). QPCR was performed by sampling 5 µL of extracted sample. Reactions were carried out in a total volume of 25 µL in qPCRBIO Probe Mix containing primers and probes at concentrations of 1.0 and 0.1 µM, respectively. Thermocycling parameters were optimised as 2 min at 95°C, followed by 40 cycles of 95°C (5 s) and 65°C (30 s). Data is presented either as plaque forming units (pfu) or as % recovered virus, to correct for recovery variation.

2.8 In Vivo Studies

UK Home Office guidelines and the UKCCCR Guidelines for the Welfare of Animals in Experimental Neoplasia were followed. All experiments were performed under a Home office approved project licence by experimenters holding Home Office personal licences. Weights of the mice were tracked and tumour growth was monitored by measurements with callipers. Tumour volumes were calculated as half the product of three dimensions: i.e. (l x w x h)/2).

2.8.1 Assessment of the use of US mediated cavitation to enhance the infection intensity and spread after IT administration

2.8.1.1 Subcutaneous tumour inoculation: DLD bilateral xenografts

DLD cells were cultured and counted as described in section 2.5. Cells were resuspended in DPBS at a concentration of 1x10^4 cells/L. Female CD-1 nude mice (Charles River laboratories) were anaesthetised with 2-3% isoflurane in O_2 enhanced air prior to injection. Two 100 µL subcutaneous injections were performed on either flank.

Treatment began when the tumours had reached sizes of approximately 150 mm^3.

2.8.1.2 Injection and treatment: IT administered VV-GFP infection of DLD bilateral xenografts

Mice were anaesthetised with 2-3% isoflurane in O_2 enhanced air and then loaded onto the mouse holder. Following anaesthesia, cannulas were inserted directly into tumours and secured with tissues adhesive (3M Vetbond). Mice were loaded into a heated waterbath. 5 µl of 25 mg/mL SSPs was mixed with 10 µl of VV-GFP (1.25×10^7 pfu), and was injected into each of the two tumours via a cannula. The cannula was flushed with 10 µL 5% glucose and then left in for the duration of treatment. The tumour receiving US was then exposed for 5 minutes.

2.8.1.3 IVIS Imaging: IT administered VV-GFP infection of DLD bilateral xenografts

24 hrs and 6 days after treatment, fluorescence was measured in tumours after treatment with VV-GFP using an in vivo imaging system (IVIS Lumina, Caliper Life Sciences). Mice were anaesthetised with 2-3% isoflurane in O_2 enhanced air. Images were taken with 1s exposure and emission filters set to GFP (465 nm) and auto fluorescence (430 nm) at each time point. Images were analysed on Living Image software and Image Math was performed to remove auto fluorescence (B) from GFP signal (A) using the following equation:

A – B*K where K = background ROI_A / background ROI_B

ROIs were drawn around tumours on the resultant image and the average radiant efficiency was measured. The area of infection was defined as the area of around fluorescence over a minimum threshold for radiant efficiency. That area was then calculated as a percentage of the total tumour area drawn around in the IVIS images. Here the minimum threshold of radiant efficiency was 7.35×10^8 [p/s/cm^2/sr] / [µW/cm^2].

2.8.2 Assessment of the use of US mediated cavitation to enhance the infection intensity and spread of pre-seeded VV infection

2.8.2.1 Subcutaneous tumour inoculation: CAPAN-2 unilateral xenografts

CAPAN-2 cells were cultured and counted as described in section 2.5. Cells were resuspended in DPBS at a concentration of 1×10^4 cells/µL. BALB-C nude mice were anaesthetised with 2-3% isoflurane in O_2 enhanced air prior to injection. 100 µL subcutaneous injections were performed on one flank to form unilateral subcutaneous xenografts.

Treatment began when the tumours had reached sizes of between approximately ˜45-140 mm^3.

2.8.2.2 Injection and treatment: IT administered VV-GFP infection of CAPAN-2 unilateral xenografts

Intervention 1:

40 mice bearing unilateral CAPAN-2 xenografts were divided into two groups: +US and -US. Mice were anaesthetised with 2-3% isoflurane in O_2 enhanced air and then loaded onto the mouse holder. Following anaesthesia, cannulas were inserted directly into tumours and secured with tissues adhesive (3M Vetbond). Mice were loaded into a heated waterbath. 5 µL of 0.05 mg SSPs suspended in 5% glucose was mixed with 10 µL of VV-GFP (5.0×10^6 pfu), and was injected into tumours via a cannula. The cannula was flushed with 10 µL 5% glucose and left in tumours for the duration of treatment. Half the tumours received US and were exposed for 5 minutes as described in section 2.8.7.

Intervention 2:

Mice were split into 4 groups with 10 mice in each (int 1/ int 2): US/US, US/no US, no US/US and no US/no US. Mice were anaesthetised with 2-3% isoflurane in O_2 enhanced air and then loaded onto the mouse holder. Following anaesthesia, cannulas were inserted into tail veins and secured with tissues adhesive (3M Vetbond). Mice were loaded into a heated waterbath. 50 µL of 1.1 mg SSPs suspended in 5% glucose was administered IV the tail vein via a cannula. The cannula was flushed with 50 µL 5% glucose and then left in the tail vein for the duration of treatment. The tumours receiving US were exposed for 5 minutes as described in section 2.8.7.

2.8.2.3 IVIS Imaging and tissue processing: IT administered VV-GFP infection of CAPAN-2 xenografts

On days 1, 2, 7, 9 and 14 after treatment, IVIS imaging was performed to assess the GFP fluorescence in tumours as described in section 2.8.1.3.

On day 14 mice were culled and tumours were recovered. Tumours were first imaged using the IVIS imager and then homogenised to a concentration of 50 mg/mL in PBS. 200 µL of tumour homogenate was DNA extracted and VV viral genomes were quantified using qPCR as detailed in 2.7.

2.8.3 CAPAN-2 tumourigenicity

CAPAN-2 cells were cultured as described in section 2.5 and single flank tumour inoculation of female BALB-C nude mice (Charles River Laboratories) was performed as described in section 2.8.1. Tumour and welfare monitoring were performed as described in section 2.8.1.

2.8.3.1 Western blot analysis to determine MUC1 expression in CAPAN-2 human xenograft

Recovered CAPAN-2 human xenografts were diluted and homogenised to a concentration of 40 mg/mL in 1X cell culture lysis buffer (E1531, Promega) supplemented with protease inhibitor cocktail (ab65621, Abcam). Tumour lysates were diluted and loaded into wells at a mass of 20 µg or 200 µg. Precision Plus Protein™

Kaleidoscope™ Prestained Protein Standards (1610375, Bio-Rad) were used to determine the molecular weight of proteins. Separation occurred in non-reducing conditions using SDS-PAGE as in section 2.3.2.2. Separated proteins were then transferred over night at 30V to a 0.2 µm pore size nitrocellulose membrane (162-0213, BioRad, UK). The transfer buffer was made up of Tris-Glycine-SDS running buffer with the addition of 20% methanol. Transfer occurred at 4 °C. After transfer was complete, the membrane was removed and blocked for 1 hour in a 10% FBS in DPBS (14190094, Life Technologies, UK). The membrane was rinsed once in DPBS and incubated with aMUC1 (HMFG2) raised in rabbit (ab245693, Abcam) at 0.1 µg/mL in DPBS and 10% blocking buffer for 1 hour. The membrane was then washed 3 times with a wash buffer consisting of DPBS and 0.05% Tween-20 (161-0781, BioRad, UK). The membrane was then incubated with an anti-rabbit IgG Horseradish Peroxidase (HRP)-conjugated antibody raised in goat (ab205718, Abcam, UK) diluted 1:20,000 from stock in DPBS and 10% blocking buffer. After incubation for 1 hour, the membrane was washed 5 times with washing buffer. Immobilon Western HRP Substrate (WBKLS0500, Merck Millipore, USA) was used to detect chemiluminescent signal. HRP substrate was prepared by mixing equal volumes of luminol reagent and peroxide solution. The HRP substrate (3 mL) was then added to each membrane and incubated for 1 minute. Excess solution was removed and the membrane was covered in plastic wrap. The membranes were then exposed to X-ray film (CL-XPosure™ Film, 34088, ThermoFisher, UK) for approximately 1 second in a dark room. Films were developed using an Agfa CP 1000 film processor.

2.8.3.2 DCE MRI

DCE-MRI was performed with the help of Sheena Wallington.

DCE-MRI was performed as in reference[199] using a respiratory gated 3D spoiled gradient echo scan with 30 µL of a Gd-contrast agent (Omniscan, GE Healthcare) infused via a tail vein cannula over 5 s. [200] MRI was performed using a 7.0 T 210 mm horizontal bore VNMRS preclinical imaging system equipped

with 120 mm bore gradient insert (Varian Inc, CA) and a 32 mm ID quadrature birdcage coil (Rapid Biomedical GmbH, Germany).

2.8.4 Pharmacokinetic studies

2.8.4.1 Pharmacokinetic study: VV and unwashed PCVV

This pharmacokinetic (PK) study (described in Chapter 4) was undertaken with the help of Megan Grundy and those described elsewhere were not.

CD1 nude mice were used and pre-innoculated with a subcutaneous injection of HEPG2 cells.

2.8.4.1.1 Injection and treatment Viral samples were made up on the day of treatment as detailed in section 2.2. PCVV was not purified from free polymer. The injectates were made up to a concentration of 2 x10^4 pfu μL^{-1} in a volume of 100 µL for each mouse. Injectates were kept on ice until used. These virus samples were not purified from free polymer as it was thought that the potential impact of free polymer would not be a significant factor in 1.5 mL of moving mouse blood.

Mice were anaesthetised with 2-3% isoflurane in O_2 enhanced air. PCVV groups were injected first to ensure there were no acute adverse effects from the Chol-PEG and VV mix. Mice were placed in a warming box for recovery and observed for any signs of distress.

2.8.4.2 Pharmacokinetic studies: VV, PCVV and aMUC1-PCVV

Female BALB-C nude mice were inoculated with a subcutaneous injection of 10^6 CAPAN-2 cells (cultured as in section 2.5.1) suspended in a total volume 100 µL of PBS. Dosing was performed when tumours reached a size of 50-150 mm^3.

2.8.4.2.1 Injection and treatment

Virus samples were made up on the day of treatment as detailed in sections 2.2 and2.3.4. The injectates were made up to a concentration of 2 x10^4 pfu μL^{-1} or 1 x10^5 pfu μL^{-1} in a volume of 100 µL for each mouse. These virus samples were purified from free polymer as described in section 2.2.1. Injectates were kept on ice until used.

Mice were anaesthetised with 2-3% isoflurane in O_2 enhanced air. aMUC1-PCVV groups were injected first to ensure there were no acute adverse effects from the aMUC1-PEG-Chol and VV mix. Mice were placed in a warming box for recovery and observed for any signs of distress.

2.8.4.3 Blood Collection and Sample processing

20 µL blood samples were taken from the tail vein at times indicated for each experiment and mixed into an eppendorf containing 180 µL PBS. Mice were sacrificed by cervical dislocation after the final bleed. Livers and tumours were resected and stored on ice.

Blood samples, tumours, livers and injectates were processed and measured for the quantity of VV genomes present. All samples and injectates were DNA extracted using the GenElute™ Mammalian Genomic DNA Miniprep Kit Protocol (Sigma Aldrich, G1N350) and qPCR was done as detailed in section 2.7. Standard curves made up in mouse blood had a top standard of 5 x10^5 pfu and decreased on a 1:10 scale to a lowest standard of 0.5 pfu in 5 µL.

2.8.5 In Vivo Model for Delivery of VV, PCVV, aMUC1-PCVV and IgG-PCVV

Female BALB-C nude mice were inoculated with a subcutaneous injection on both flanks of 10^6 CAPAN-2 cells (cultured as in section 2.5.1) suspended in a total volume 100 µL of PBS. Dosing was performed when tumours reached a size of ˜45-180 mm^3.

2.8.5.1 Injection and treatment

Virus samples were made up on the day of treatment as detailed in sections 2.2 and 2.3.4. The injectates were made up to a concentration of 2 x10^4 pfu μL^{-1} in a volume of 100 µL for each mouse. Injectates were kept on ice until used, with QPCR used to ensure equivalent pfu levels in different samples.

Mice were anaesthetised with 2-3% isoflurane in O_2 enhanced air and then loaded onto the mouse holder. Following anaesthesia, cannulas were inserted into

tail veins and secured with tissue adhesive (3M Vetbond). Mice were submerged up to the neck in a heated waterbath.

50 µL of 1.1 mg SSPs suspended in 5% glucose was administered IV via the tail vein cannula. The cannula was flushed with 50 µL 5% glucose and then left in the tail vein for the duration of treatment. One of the bilateral tumours was exposed to US for 5 minutes as described in section 2.8.7.

2.8.6 In Vivo Model for Tumour Volume Change of VV, aMUC1-PCVV and Glucose +/- US

Female BALB-C nude mice were inoculated with a subcutaneous injection on one flank of 10^6 CAPAN-2 cells (cultured as in section 2.5.1) suspended in a total volume 100 µL of PBS. Dosing was performed when tumours reached a size of 100 mm^3. Injection and treatment were the same as detailed in section 2.8.5.1.

2.8.7 Ultrasound Treatment of Tumours

Figure 3.1 depicts the set-up used to expose tumour-bearing mice to ultrasound. The water tank was degassed and heated to 37 °C. Two perpendicular HIFU transducers were confocally aligned. The HIFU transducers had a fundamental frequency of 0.5 MHz (H-107C-033 and H-107C-034, Sonics Concepts, USA) and were single element spherically focused. The focal length was 63 mm. HIFU transducers had rectangular cutouts (45 x 18 mm) which allowed for two L11-5v 128-element linear arrays with 6.25 MHz centre frequency, 5-11 MHz bandwidth and 38 mm aperture (Verasonics Inc.) to be mounted within and aligned with the HIFU transducers. Cavitation events were detected and mapped by these arrays. Custom made software in MATLab (written by Dr. Christian Coviello, Dr Calum Crake, and Seán Finn) was used to control a signal generator (33250A, Agilent), which output to a 55 dB power amplifier (1040L, Electronics and Innovation). The power amplifier output then passed through an impedance matching network (Sonic Concepts) to the HIFU transducers. A high-voltage probe and oscilloscope was used to measure the voltage at the output from the RF power amplifier. Transmit and

receive signals were synchronised using an output trigger pulse from the Verasonics system (Vantage 256 Channel, Verasonics Inc). A driving frequency of 0.5 MHz, pulse repetition frequency (PRF) of 0.5 Hz, and duty cycle (DC) of 5% (50,000 cycles per burst) were used. Peak rarefactional focal pressure (PRFP) was varied between 1.5-2 MPa unless otherwise stated. B-mode imaging was used to ensure correct targeting with HIFU to tumours.

Resulting cavitation signals were detected and recorded passively and mapped onto B-mode images using a custom Passive Acoustic Mapping (PAM) algorithm. This enabled the magnitude and spatial extent of cavitation activity in real time.

2.8.8 IVIS Imaging and tissue processing: VV-luc infection of CAPAN-2 xenografts

At multiple time points after mice were treated with luciferase expressing VV (VV-luc) IVIS imaging was performed to assess the luminescence in tumours. Mice were anaesthetised with 2-3% isoflurane in O_2 enhanced air and then were injected intraperitoneally with 100 µL of 15.8 mg/mL luciferin (15225733, ThermoFisher). The dose was split between two injections of 50 µL on each side of the abdomen of the mouse being imaged. 5 minutes after luciferin administration, the mice were imaged at 1s, 10s and 30s exposure.

On the final day of treatment mice were culled and tumours were recovered. Tumours were homogenised to a concentration of 75 mg/mL in PBS. 200 µL of tumour homogenate was DNA extracted and VV viral genomes were quantified using qPCR as detailed in 2.7.

Chapter 3

Investigating the use of US-mediated cavitation to enhance the dissemination of VV-GFP after intratumoural administration

---

3.1 Introduction

The two clinically approved oncolytic viruses are the oncolytic adenovirus *H101* (China State Food and Drug Administration) and oncolytic herpes simplex virus *Imlygic* (USA FDA) that have been approved for intratumoural (IT) administration only. In the clinical trials for VV which are discussed in detail in section 1.2.1, IT administration was the preferred method used in the majority of trials. Despite the limitations of IT administration (discussed in section 1.3), there are established benefits, in particular for easy to reach tumours such as melanoma lesions. Primarily, IT delivery circumvents the challenges of blood stream interactions and tumour uptake which are encountered following IV administration. However, once at the tumour site, the unique tumour physiology and microenvironment present barriers to infection and spread regardless of the administration route.

Poor dissemination of oncolytic viruses into and throughout tumours causing pockets of infection close to tumour vasculature within large areas of uninfected tumour sites have been reported. [77, 201] In particular, Carlisle *et al* reported that after IV administration of polymer coated Ad, infection was heavily associated

with tumour vasculature and was limited to tumour cells within 100 µm of the vasculature. [116, 127] Many attempts have been made to overcome these challenges including some successes with anti-angiogenic treatments aimed at normalising the heterogeneous vasculature and moderating the pressure gradients within the tumour as detailed in section 1.3.2.1. Focused ultrasound (US) mediated cavitation has also been shown to improve the dissemination of oncolytic viruses within tumours. Of interest here, Bazan-Peregrino *et al* reported that using SonoVue as a cavitation agent and focused US increased the distribution and transgene expression of a non-replicating oncolytic adenovirus (Ad) after intratumoural injection. [202]

Hence it was hypothesised that the increase in biodistribution using US mediated cavitation seen for Ad could be used to produce more homogeneous distribution of VV after IT administration. It has also been observed that OV infection is often confined to hotspots within the tumour, resulting in areas of highly infected cells and large areas completely void of infection, despite tumour cells being viable. [77] Hence, even well established initial foci of infection may be prevented from spreading further. [201] It was therefore postulated that the use of US mediated cavitation might also be able to spread pre-seeded infection within tumours. This could potentially enable repeated non-invasive US treatments to aid the efficacy of virotherapy treatments without the need for re-dosing with the OV and thereby reduce the number of virus dosings required.

The aims of this chapter are summarised as:

1) Assess whether US mediated cavitation could enhanced dissemination and infectivity of VV after IT administration in DLD or CAPAN-2 xenograft models

2) Assess the differences between cavitation activity achieved with sonosensitive particle (SSP) cavitation nuclei delivered IT at 0.05 mg and IV 1.1 mg in a CAPAN-2 xenograft model

3) Assess whether US mediated cavitation could enhanced infectivity and spread of pre-seeded VV-GFP infection in CAPAN-2 xenografts

In order to assess these aims two *in vivo* experiments were conducted:

- Experiment 1 looked at the ability of US mediated cavitation to enhance the intratumoural infection levels and spread after IT administration of VV and SSPs in DLD xenograft tumours.

- Experiment 2 determined whether US mediation cavitation could enhance the intratumoural infection levels and spread after IT administration of VV and SSPs in CAPAN-2 xenograft tumours. A second intervention of US mediation cavitation using IV administration of SSPs was used to assess its ability to spread the infection of pre-seeded infection foci within tumours.

3.2 Results: Experiment 1- Bilateral DLD xenograft model with IT administered VV-GFP

3.2.1 Experiment 1: Experimental Design

A bilateral DLD xenograft model was used to determine whether focused US administered in combination with a SSP cavitation nuclei could enhance the dissemination of VV-GFP throughout DLD xenografts and therefore increase the intensity or area of infection. Female CD1 nude mice were implanted with subcutaneous xenograft DLD tumours (described in section 2.8.1) and were treated when they reached a volume of between 140 - 440 mm^3 in size. Bilateral tumours were assigned to treatment groups so that the means of US and non-US treated tumours were approximately equal. This bilateral tumour model was previously used to demonstrate the improved delivery to tumours treated with US + cavitation nuclei as opposed to no US control after IT administration of a non-replicating oncolytic adenovirus (Ad5) constitutively expressing GFP. [202] The schematic of the dual transducer setup can be seen in Figure 3.1 and the US parameters are displayed in Table 3.2. The study design details are in Table 3.1.

The schematic depicts two HIFU transducers (with centre frequencies of 0.5 MHz) mounted perpendicular to each other and aligned confocally. Each transducer had a rectangular cut out into which a linear transducer array was mounted. Real-time passive acoustic map (PAM) of cavitation events that occurred within the

Xenograft model	**Administration route**	**Cavitation nuclei**
Bilateral, DLD	IT	0.125 mg SSPs
	Treatment	**Average tumour volume (mm^3)**
Group 1	$1.25x10^7$ pfu VV + SSP - US (n=5)	226
Group 2	$1.25x10^7$ pfu VV + SSP + US (n=5)	223

Table 3.1: Experimental design details of experiment 1: infection of IT administered VV with SSPs with or without US.

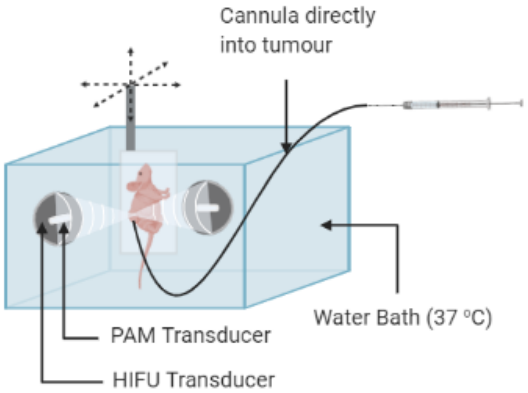


Figure 3.1: Schematic of in vivo US setup. Mice were place in a 37 °C water bath to facilitate coupling of US. The two HIFU transducers were aligned to the tumour using B-Mode images obtained from the linear arrays. Resulting cavitation signals were detected with Passive Acoustic Mapping (PAM) transducers. Whole tumours were "painted" during the treatment using a 3D movement unit. VV was pre-mixed with SSP cavitation nuclei before being administered IT into both tumours through a cannula inserted directly into the tumour.

tumour were obtained using the US arrays, allowing for both real-time treatment monitoring and post treatment analysis of cavitation activity. Cavitation data acquired by the arrays was processed using custom generated MatLab code written by Dr Christian Coviello, Dr Calum Crake and Seán Finn (Oxsonics Ltd.). The bistatic configuration of transducers used here enabled greater PAM resolution in the axial direction allowing more accurate localisation of cavitation activity. [192]

CD-1 nude mice bearing unilateral DLD xenografts were anaesthetised, their tumours were cannulated and positioned on a custom holder submerged in the heated waterbath up to the neck. The two HIFU transducers that were used to

Frequency (MHz)	PRF (Hz)	DC (%)	Cycles/Burst	PRFP (MPa)
0.5	0.5	5	50 000	1.5

Table 3.2: Parameters for in vivo US treatment of mice dosed with SSPs plus VV and administered IT.

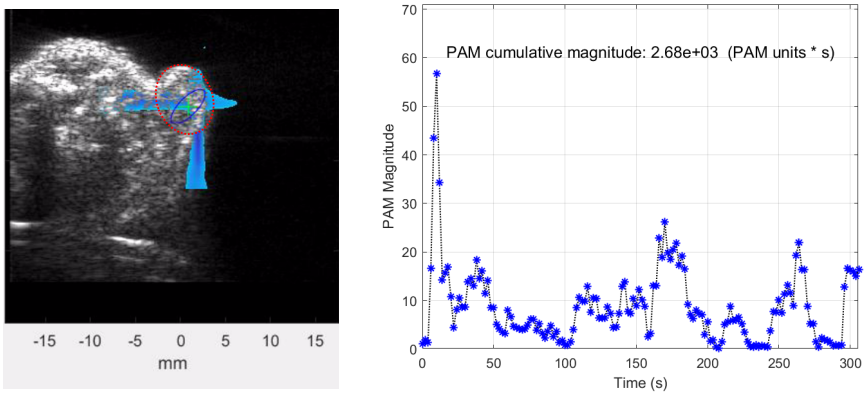
treat one of their tumours (randomly assigned) were positioned using the US arrays for B-mode imaging. The injectate was made up of premixed 1.25 x10^7 pfu VV with 0.125 mg of SSP. The tumour not receiving US was injected first. US treatment was started and then the tumour receiving US was injected. A detailed description of US treatment can be found in section 2.8.7.

At the beginning of the treatment, the US focus was positioned at the largest part of the tumour. After the injection, the mouse was moved incrementally in 3 dimensions enabling the US focus to treat the entire tumour. The Peak Rarefactional Pressure (PRFP) was kept constant during the treatment. PAM magnitude was monitored for all US treated tumours. All 5 tumours treated with US showed prolonged PAM Magnitude values of 0-40 (au) over the entire treatment. At the end of the treatment the tumour regions were examined for signs of bruising, and mice were monitored as they recovered from the anaesthetic. Tumour volume was monitored post treatment and GFP fluorescence was then measured in the tumours using an IVIS imager.

3.2.2 Experiment 1: Acoustic Feedback

B-mode imaging with co-registered PAM (Figure 3.2a) was used to spatially map cavitation events providing real-time feedback of acoustic cavitation during US treatment of tumours. The feedback during treatment gave the location and strength of cavitation events which occurred and the pixel with the maximum energy was extracted for each frame, denoted PAM Magnitude, and plotted against time (Figure 3.2b). The PAM Magnitude plots displayed here are the same images obtained during experiments.

These plots depict in a clear manner a snap-shot of the maximum cavitation events occurring over time and allow the uniformity of the treatment to be



(a) (b)

Figure 3.2: Acoustic data acquired during US treatment of DLD tumour-bearing mice with IT administered VV and SSPs. (a) B-mode imaging with co-registered PAM for mouse 5. (b) The PAM Magnitude trace for mouse 5. Cumulative PAM Magnitude (integral of the PAM Magnitude over time) is printed at the top of the image. 'mm' represents the distance from the focal point in mm, the dark blue ellipse represents the focal region of the intersecting US and the tumour boundary is denoted by the red dotted line. PAM Magnitude is in au.

determined for each mouse. From these PAM Magnitude plots, metrics can be quantified to determine the amount of cavitation that occurred during treatment. One of these metrics is the cumulative PAM magnitude which takes the PAM derived energy calculated for each pulse, determined as the magnitude of the pixel with the highest PAM energy, and sums those magnitudes over time. For the mice treated here, the cumulative PAM magnitudes were calculated to be between 2.26 x10^3 - 3.55 x10^3 au.

Immediately after treatment tumours were assessed for damage within the exposed tumour area and no visible damage could be seen within or on the skin of any of the 5 tumours that received US.

3.2.3 Experiment 1: Assessment of US mediated cavitation with VV on tumour infection levels

Mice were monitored for infection (fluorescence imaging for GFP) for 6 days post treatment. GFP imaging using an *in vivo* imaging system (IVIS) was performed on days 1 and 6 post treatment to enable the infection levels over time to be determined (Figure 3.3a). Regions of interest (ROI) were drawn around tumours

and the average radiant efficiency within the ROI was recorded (Figure 3.3a). This is detailed further in section 2.8.1.3.

The average radiant efficiency is a measure of the number of photons (p) per second recorded from within the ROI divided by the area (cm^2) of the ROI per steradian (sr) and then normalised against the incident excitation power ($\mu W/cm^2$) (to give units: [p/s/cm^2/sr] / [μW /cm^2]). On day 1, the average radiant efficiency recorded in the tumours was low (Figure 3.3b) and only two tumours, mouse 3 (+ US) ($5.9x10^8$ [p/s/cm^2/sr] / [$\mu W/cm^2$]) and mouse 5 (-US) ($2.4x10^6$ [p/s/cm^2/sr] / [$\mu W/cm^2$]), displayed an average radiant efficiency value of above background. By day 6, all tumours displayed much higher average radiant efficiency values (Figure 3.3a and b). 3 of the 5 treated mice showed average radiant efficiency values to be higher in +US tumours than -US tumours. Differences between the average radiant efficiency for tumours +US ($1.2x10^8$+/-$2.6x10^8$) and -US ($4.8x10^5$+/-$1.1x10^6$) were analysed using a two-tailed t-test on day 6 and were found to not be statistically significant ($p>0.05$).

The threshold radiant efficiency displayed in Figure 3.3a was set to $7.35x10^8$ [p/s/cm^2/sr] / [$\mu W/cm^2$]. This threshold was determined based on a value which reduced the background fluorescence to non-visible on the images. The fluorescence images were then exported and the area of infection within the tumours was then determined using particle analysis on Image J. The area of infection was then calculated as the per cent (%) of the total tumour area and the results are displayed in Figure 3.3c. There was an increased % area of tumour infected with VV in all +US tumours when compared with their respective -US tumours. There was a 2-fold difference in the % area of tumour infected with VV for the +US (64% +/- 15) when compared with -US (34% +/- 14) groups ($p=0.0253$). This increased infection area could potentially be due to greater homogenous dissemination of VV throughout tumours at the time of dosing. It was also noted that within the infection areas, (Figure 3.3) the number of infection foci in the + US tumours was higher with a 4.2 +/- 2 mean number of foci compared to -US tumours which had a 1.6 +/- 0.5 mean number of foci ($p=0.0329$, paired two-tailed t-test).

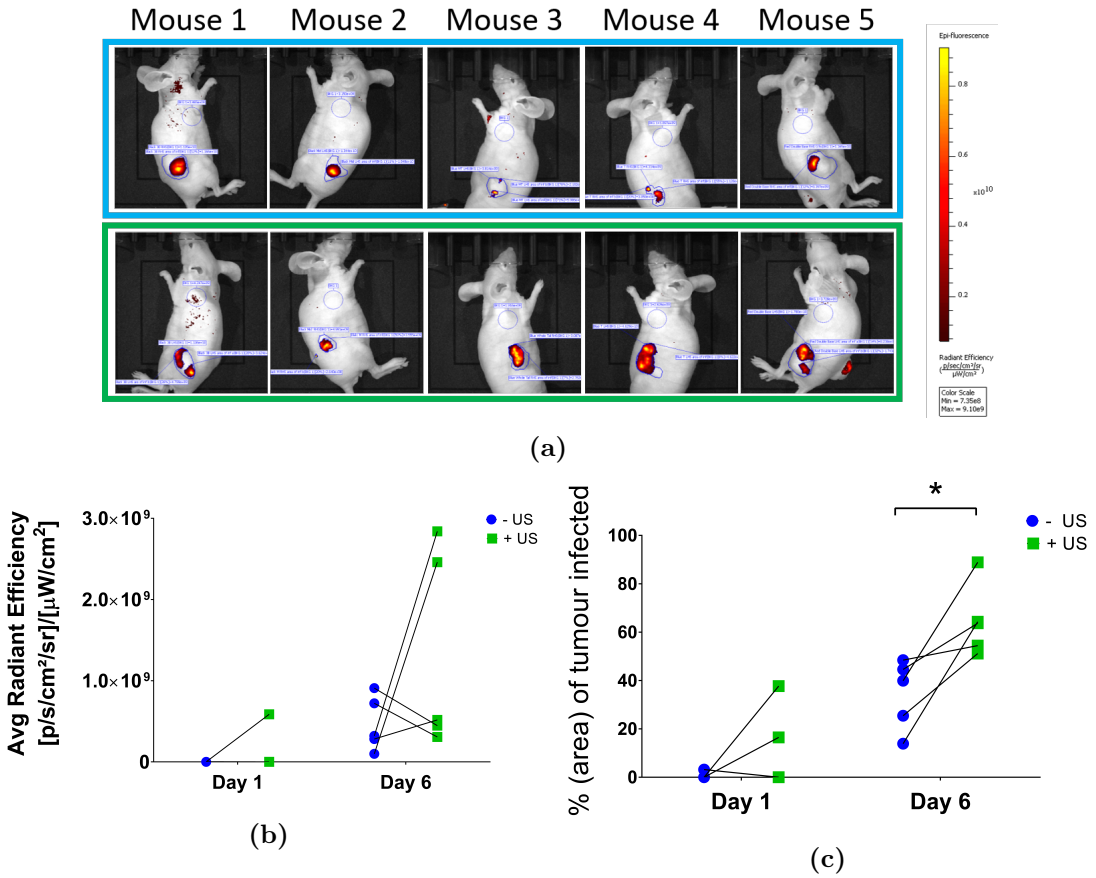


Figure 3.3: GFP fluorescence quantification after treatment with SSPs (0.125 mg) and 1.25x10^7 pfu VV without US (blue box, blue dots) or with US (green box, green squares). SSPs were co-injected IT with VV into CD-1 nude mice bearing bilateral DLD xenograft tumours. One tumour was exposed to US for 5 minutes. (a) The average radiant efficiency was recorded from regions of interest (ROIs) drawn around tumours on images as depicted in day 6 images. IVIS images were taken under the following conditions: exposure 1s, excitation filter 465, emission filter GFP. Blue box indicates the tumours not exposed to US (-US) and the green box indicates the tumours that are exposed to US (US+). (b) Individual values for the average radiant efficiency of tumours -US (blue dots) and +US (green squares) are displayed with black lines connecting tumours from the same mouse. (c) Individual values for the % area of infection in tumours -US (blue dots) and +US (green squares) are displayed with black lines connecting tumours from the same mouse. Statistical significance was determined using two-tailed paired t-test comparing each tumour to its internal control on the same mouse, at each time point. Statistically significant differences are displayed using * = $p<0.05$. n=5

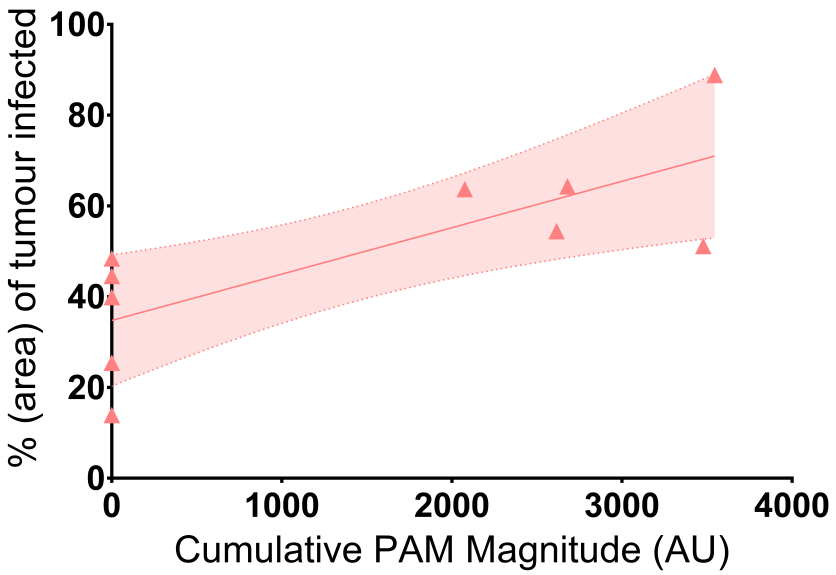


Figure 3.4: DLD xenograft percentage area of infection (day 6) as a function of cumulative PAM magnitude. Points show data from individual tumours (n=10) against cumulative PAM magnitude with linear regression. The shaded regions represent the 95% confidence interval of the linear regression.

3.2.4 Experiment 1: Relationship between PAM and delivery of VV-GFP (DLD xenograft model)

The increase in the % area of tumours that was infected was shown to be ˜2-fold higher for +US tumours when compared with -US tumours on day 6 post treatment (p=0.0253). Following this finding, a relationship between the quantity of cavitation activity recorded and the % area of infection was probed. Cumulative PAM magnitude was plotted against % area of infection for each tumour to determine whether a relationship between the cumulative PAM magnitude recorded at the time of therapy could be a predictor for the dissemination of VV infection with the tumours (Figure 3.4). Tumours that were not exposed to US were given a cumulative PAM magnitude of 0, as they did not receive any cavitation.

A linear regression was applied and gave a reasonable fit (R^2=0.6) producing the equation $Y = 0.00889 * X + 34.8$. The linear relationship between cumulative PAM magnitude and % area of tumour infected was determined to be significant (F test, p=0.0382) suggesting that the impact of cavitation activity did result in increased % area of tumour infection.

3.3 Results: Experiment 2- Unilateral CAPAN-2 xenograft model with IT administration and pre-seeded VV infection foci

3.3.1 Experiment 2: Experimental Design

To further assess the impact of focused US on enhancing the dissemination of VV after IT injection in another cancer cell line, a study using a unilateral CAPAN-2 xenograft model was performed. Tumours were treated at volumes between 45-180 mm^3. This study had two interventions as depicted in Figure 3.5 and the experimental design details are in Table 3.3.

In Intervention 1, VV-GFP ($5x10^6$ pfu) and SSP (0.05 mg) were administered IT before half of the tumours received US (n=20) and half of the tumours did not (n=20). The VV-GFP and SSP doses were reduced in this study (both 2.5 times lower) when compared to the previous DLD xenograft model for two reasons: the mean tumour volumes were markedly lower for the CAPAN-2 xenografts at treatment (80 mm^3 +/- 33) than the DLD xenografts (250 mm^3 +/- 102) and the impact of increased infection area was to be measured over a 14 day period as opposed to a 6 day period. Therefore it was thought that choosing a lower dose of VV-GFP would be more appropriate to seed infection in these smaller tumours and a reduced dose of SSPs would prevent any damage due to the smaller tumour size. In Intervention 2 (7 days after Intervention 1), 1.1 mg SSP in 5% glucose were IV injected to each mouse and half the mice which received US on Intervention 1 and half of the mice which did not were exposed to US (Figure 3.5). This created four groups: (1) US d1 then US d7 (2) US d1 then no US d7 (3) no US d1 then US d7 (4) no US d1 then no US d7, these were denoted US/US, US/no US, no US/US and no US/no US, respectively.

BALB-C nude mice bearing unilateral CAPAN-2 xenografts were anaesthetised, their tumours were cannulated and they were positioned on a custom holder submerged in a waterbath up to the neck. The two HIFU transducer setup and conditions used were the same as those described in section 3.3.1 and displayed in

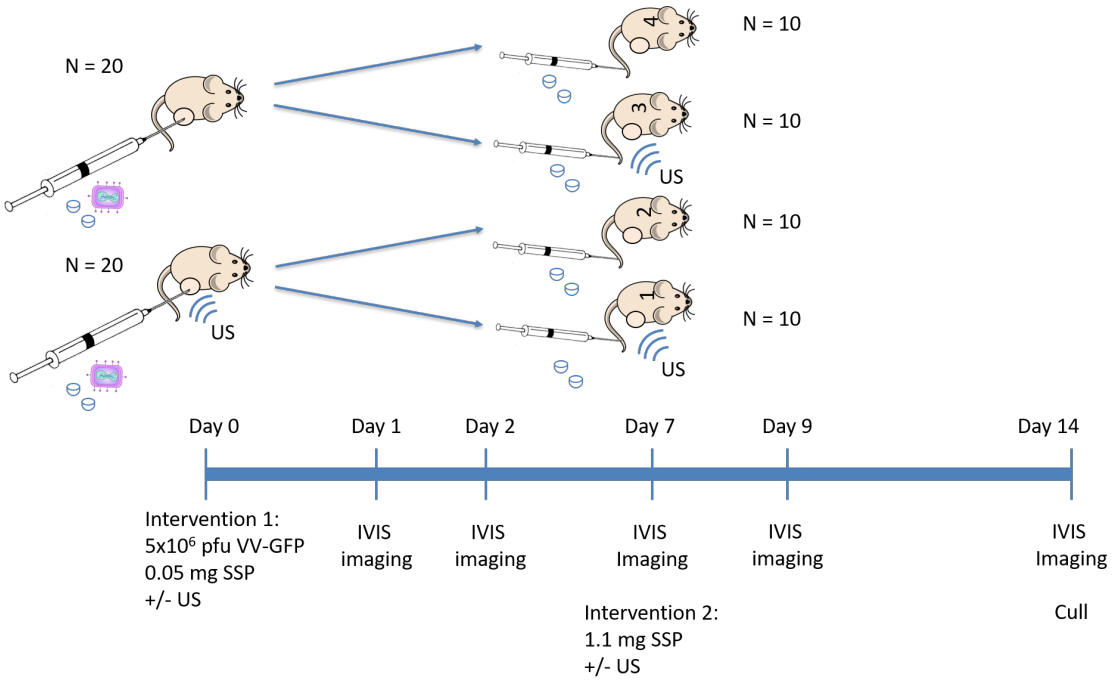


Figure 3.5: Schematic to describe the experimental design. Intervention 1 is depicted by the top two rows. Mice with unilateral CAPAN-2 tumours were anaesthetised and IT injected via a cannula directly into the tumours with a pre-mixed $5x10^6$ pfu VV-GFP and 0.05 mg SSP solution. Half of the mice then had their tumours exposed to US (n=20) and the other half did not (n=20). At Intervention 2, bottom row, mice were IV administered SSPs at a higher dose were either exposed to US or not exposed (i.e no VV-GFP was administered) creating 4 groups: no US/ no US, no US/ US, US/ no US, US/ US. (n=10)

Xenograft model	Unilateral, CAPAN-2		
Intervention	**1**	**2**	**Average tumour volume**
Administration route	IT	IV	
Cavitation nuclei	0.05 mg SSPs	1.1 mg SSPs	
US/ US (n=10)	$5x10^6$ pfu VV + SSP + US	SSP + US	83 mm^3
US/ no US (n=10)	$5x10^6$ pfu VV + SSP	SSP	81 mm^3
no US/ US (n=10)	$5x10^6$ pfu VV + SSP + US	SSP + US	84 mm^3
no US/ no US (n=10)	$5x10^6$ pfu VV + SSP	SSP	77 mm^3

Table 3.3: Experimental design details of experiment 2: infection of IT administered VV with SSPs with or without US.

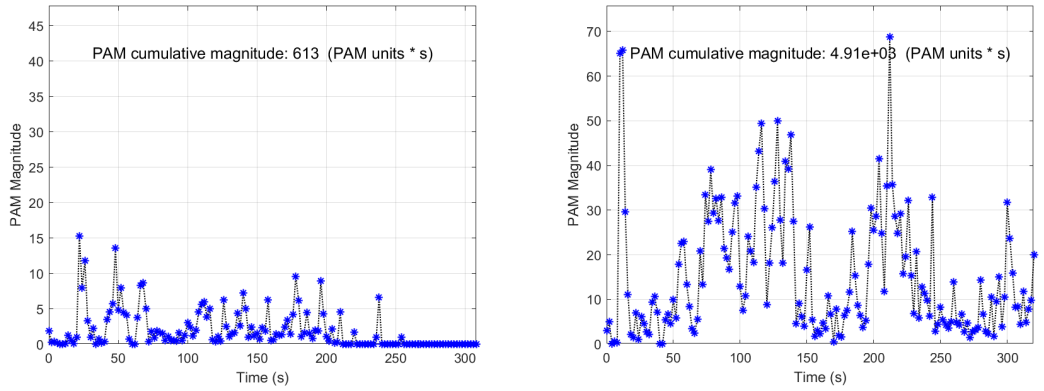
Figure 3.5 and Table 3.2. At the end of both treatments the tumour regions were assessed for signs of bruising and the mice were monitored as they recovered from anaesthetic. Tumour volume was monitored post treatment and GFP fluorescence was measured in tumours using an IVIS imager on days 1, 2, 7, 9 and 14 post treatment. On day 14 mice were culled and tumours were recovered for viral genome (VG) quantification.

3.3.2 Experiment 2: Acoustic Feedback

B-mode imaging with co-registered PAM as described previously in section 3.2.2 was used to determine cavitation activity for each treatment. The feedback seen during treatment gave the location and strength of cavitation events, which occurred and the pixel with the maximum energy was extracted for each frame, denoted PAM Magnitude (AU), and plotted against time (Figure 3.6a). These maps gave a clear indication at the time of treatment of areas of high cavitation activity and areas of low cavitation activity. It was hypothesised that differences in areas of high and low cavitation activity seen within a tumour are due to heterogeneous vascularity, IT pressure and drainage. [177]

For Intervention 1, after SSPs were administered IT, the PAM Magnitude plots obtained during exposures showed varied profiles between tumours with cumulative PAM magnitude (described in section 3.2.2) ranging between 4.5 x10^2 - 4.9x10^3 au. A representative image for a “low” (mouse 394) cavitation profile and a “high” cavitation profile (mouse 386) are displayed in Figures 3.6a and 3.6b.

Post treatment, the PAM data which was recorded during exposures can be reprocessed and another metric for cavitation activity called “cavitation dose” can be determined. Cavitation dose is described in a recently published paper to be a more sophisticated quantification that takes into account the total PAM derived energy of each pulse (as opposed to just the maximum pixel) and also considers the volume of the tumours. [203] It is calculated by integrating the PAM derived power received by the tumour, over the volume measured and time (the duration of the treatment). This gives the total electrical energy that the tumour received which



(a) **(b)**

Figure 3.6: Acoustic data acquired during US treatment of CAPAN-2 tumour-bearing mice with 5x10^6 pfu VV-GFP and 0.05 mg SSPs administered IT over a 5 minute treatment period. The value for the cumulative PAM Magnitude (integral of the PAM Magnitude over time) is printed at the top of the image. (a) Low cavitation profile (mouse 394) (b). High cavitation profile (mouse 386).

is then normalised by the volume of the tumour and thereby gives an estimate of the average energy experienced by the tumour tissue. [203] The cavitation doses reported here were produced with the help of Cameron Smith.

Both metrics for cavitation were calculated for tumours treated at Intervention 1 and 2 in this experiment and the values are displayed in Figures 3.7a and 3.7b. In Intervention 1, 0.05 mg SSPs were administered IT. The cumulative PAM Magnitude values ranged between 4.5 x10^2 - 4.9x10^3 au (Figure 3.7a, orange) and the cavitation dose (Figure 3.7b, orange) ranged between 0.3 nJ (VV) and 9.9 nJ. The large range in both metrics, even for the cavitation dose which takes into account tumour volume, suggests that cavitation activity after IT delivery in this CAPAN-2 xenograft model varies significantly between tumours. In Intervention 2, 1.1 mg SSPs were administered in 5% glucose IV. The cumulative PAM Magnitude values ranged between 9.2 x10^2 - 4.6x10^3 au (Figure 3.7a, purple) and the cavitation dose ranged between 0.5 nJ (VV) and 5.8 nJ (Figure 3.7b, orange). The range in both metrics decreased in the second intervention, especially for the cavitation doses. Differences between cavitation activity recorded in Intervention 1 (IT) and Intervention 2 (IV) were assessed using a two-tailed t-test and were deemed

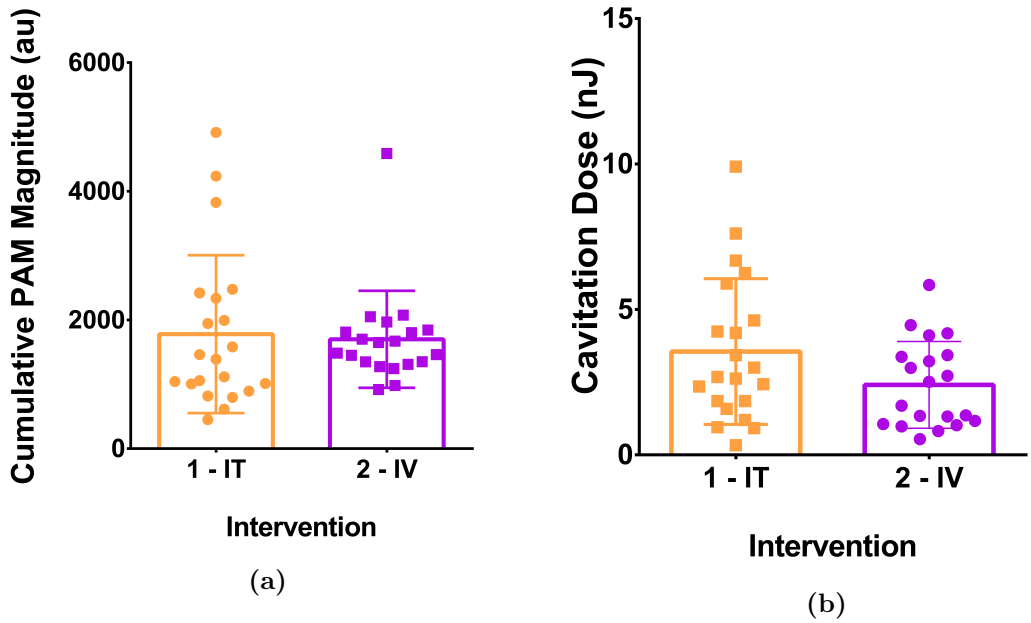
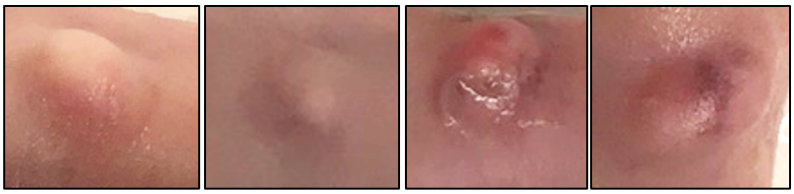


Figure 3.7: Acoustic data was acquired during US treatment of CAPAN-2 tumour-bearing mice with 5x10^6 pfu VV-GFP and 0.05 mg SSPs administered IT (orange) in intervention one and then 1.1 mg SSPs IV (purple). US exposure lasted 5 minutes. Subsequently two metrics were determined to quantify acoustic activity (a) Cumulative PAM Magnitude (au) (b) Cavitation dose (nano-Joules (nJ)). The bar represents the mean value and values for individual tumours are over laid. Error bars represent SD. Differences between groups were assessed using a two-tailed unpaired t-test. No differences between groups were deemed statistically significant.

to not be statistically significant for either cumulative PAM magnitude values (p=0.802) or cavitation dose (0.0851).

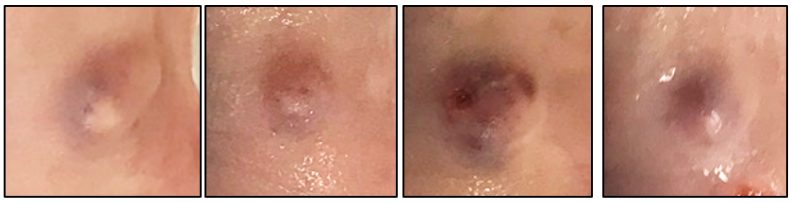
After treatments, tumours were assessed for damage. In Intervention 1, bruising was seen in 10 of the 20 mice. The majority of the bruising observed was on the skin surface or within the tumour capsule. When comparing the mice which displayed bruising with their cumulative PAM magnitude values, all mice with a cumulative PAM magnitude of 1900 or a cavitation dose of 4.2 nJ and above displayed signs of bruising. The two tumours with the highest cumulative PAM magnitudes each displayed the most marked bruising. A selection of representative images of the bruising seen alongside their the cumulative PAM magnitude values is displayed in Figure 3.8. Damage was monitored and all visible signs of bruising had gone by day 3.

In Intervention 2, bruising was seen to varying degrees in all 20 of the mice. The degree to which the bruising occurred did appear to be linked to the cavitation



Mouse number	356	394	384	386
Cumulative PAM Magnitude (au)	1013	613	2476	4914
Cavitation dose (nJ)	0.95	1.2	6.3	9.9

Figure 3.8: Intervention 1: Damage was observed on 10/20 CAPAN-2 xenografts exposed to high cumulative PAM magnitude values and cavitation doses of US. A representative selection of images taken immediately after treatment for mice with increasing cavitation doses (left to right increasing). The mouse number, cumulative PAM magnitude values and cavitation dose are displayed below the images.



Mouse number	436	448	359	427
Cumulative PAM Magnitude (au)	918	980	1844	1310
Cavitation dose (nJ)	0.54	0.8	3.0	4.11

Figure 3.9: Intervention 2: Damage was observed on all CAPAN-2 xenografts exposed to US after the IV administration of SSPs. A representative selection of images taken immediately after treatment for mice with increasing cavitation doses (left to right increasing). The mouse number and cumulative PAM magnitude values are displayed below the images.

activity quantified (Figure 3.9). When compared with Intervention 1, the cavitation activity threshold at which damage was caused was substantially lower in Intervention 2. This suggests that pre-infection with VV-GFP prior US mediated cavitation treatment may impact the amount of damage seen in the tumours.

3.3.3 Experiment 2: Assessment of US mediated cavitation with VV and pre-seeded VV infection on tumour infection levels

Mice were monitored for infection intensity and spread using GFP fluorescence imaging. Fluorescent imaging was performed using an *in vivo* imaging system (IVIS) on days 1, 2, 7, 9 and 14 post Intervention 1. Intervention 2 was performed after the imaging on day 7. IVIS imaging and processing was performed as described previously in section 3.2.3.

3.3.3.1 Intervention 1

Intervention 1 aimed to determine the impact which US exposure to tumours would have on tumour infection levels and infection area after VV-GFP ($5x10^6$ pfu) and SSPs (0.05 mg) were administered IT. IVIS images from day 1, 2 and 7 post treatment are displayed in Figure 3.10a. ROIs were drawn around tumours and the mean average radiant efficiency was determined for each time point (Figure 3.10b). A minimum radiant efficiency threshold of $2.2x10^6$ [p/s/cm^2/sr] / [µW/cm^2] was set for each time point, to remove background fluorescence, and then the images were exported and particle analysis on ImageJ was performed to determine the area of infection (Figure 3.10c).

On day 1 post treatment, GFP fluorescence was measured above background in all tumours (Figure 3.10b). This was in contrast to what was seen on day 1 for the larger DLD xenografts (section 3.2.3, Figure 3.3), where infection was only recorded for 3 out of 10 tumours. The mean average radiant efficiency was higher for the -US mice ($8.9x10^8$ [p/s/cm^2/sr] / [µW/cm^2] +/- $1.0x10^9$) than for the +US ($3.1x10^8$ [p/s/cm^2/sr] / [µW/cm^2] +/- $4.4x10^8$) (p=0.0285).

The % area of infection for each mouse was determined as described in section 2.8.1.3. The mean values for no US tumours (44% +/- 8) were higher than the US tumours (19% +/- 7) as assessed by a two-tailed t-test (p=0.0302). For the tumours not exposed to US, 12 of the 20 had a % area of infection greater than 0%. Once again this was in contrast to what was seen in on day 1 for the larger

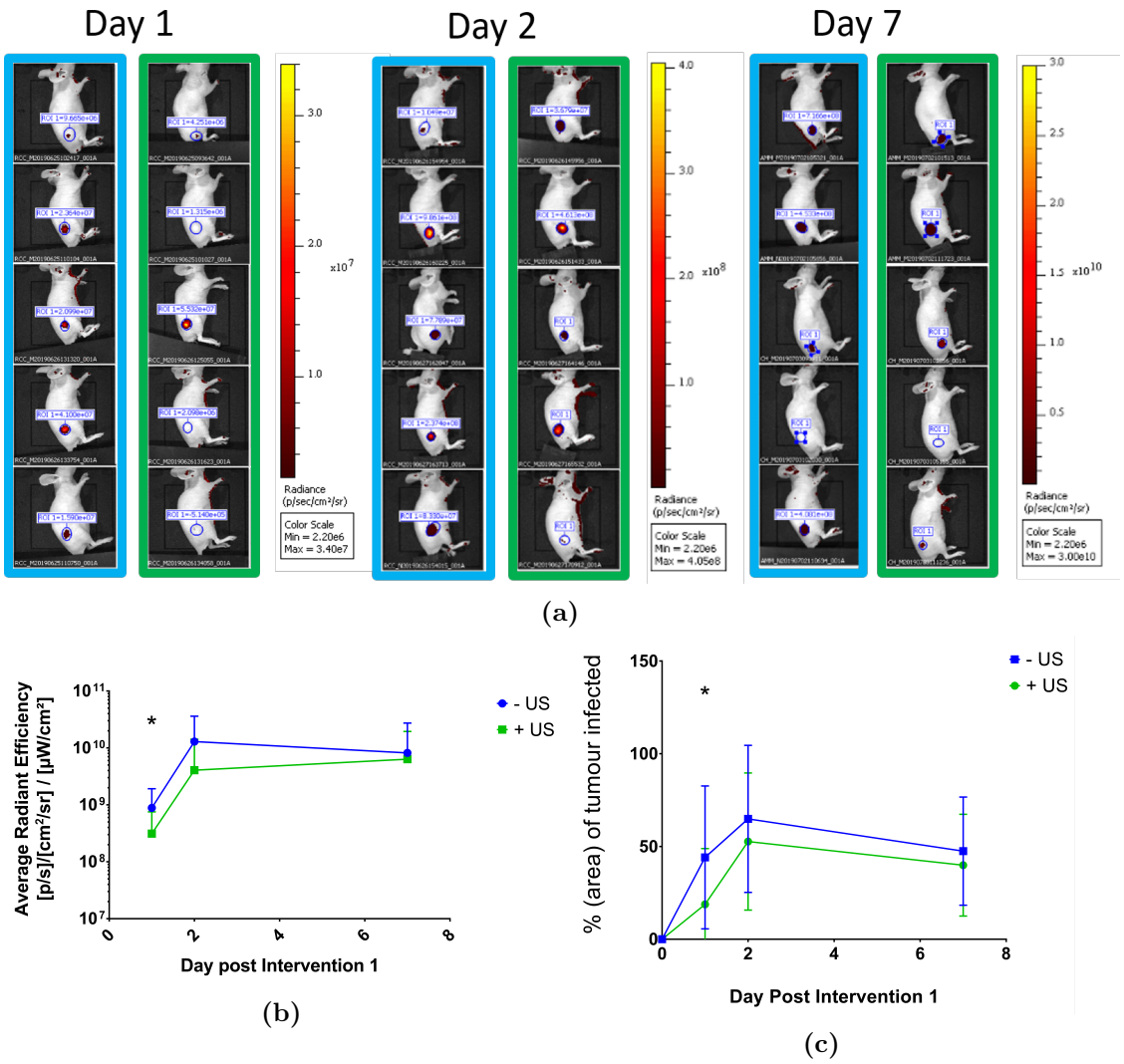


Figure 3.10: IVIS imaging was performed on mice bearing CAPAN-2 tumours after IT administration of 5x10^6 pfu VV-GFP and 0.05 mg SSPs on days 1, 2 and 7 after treatment at Intervention 1. Tumours were either exposed to US (+US, green) or not (-US, blue). (a) Representative images for each time point are shown. Individual values for the average radiant efficiency were determined for each mouse by drawing ROIs around each tumour. (b) The mean average radiant efficiency was calculated for each group +US (green) or -US (blue). Points represent the mean average radiant efficiency. Error bars represent SD. n=20 (b) Area of infection was determined by setting the minimum threshold radiance to 2.2x10^6 p/s/cm^2/sr, n=20. Differences between groups were assessed using unpaired two-tailed t-tests at each time point. *=$p<0.05$

DLD xenograft study (section 3.2.3) where only one of the non-US treated tumours and two of the US tumours had a % area of infection greater than 0%.

By day 2, the mean average radiant efficiency measured in both the -US (1.3x10^{10} [p/s/cm^2/sr] / [µW/cm^2] +/- 2.3x10^{10}) and +US (4.1x10^9 [p/s/cm^2/sr] / [µW/cm^2]

+/- 1.0x10^{10}) treated tumours surpassed the average radiant efficiency values reported in the DLD xenograft study (Figure 3.10b). This suggests that even with a smaller dose of 5x10^6 pfu VV-GFP has a higher infection efficiency after IT administration in these smaller CAPAN-2 xenografts than the 1.25x10^7 pfu VV-GFP in the larger DLD xenografts. Differences between +US and -US groups were assessed by a two tailed t-test and determined not to be statistically significant (p=0.123). The mean % area of infection was determined for no US (65% +/- 9) and US groups (53 % +/- 8) and differences as assessed by unpaired two-tailed t-test were found to be non-statistically significant (p=0.333) (Figure 3.10c). The discrepancy between the lack of significance seen here when compare with the DLD xenografts is likely due to the substantial difference in xenograft volumes, with the CAPAN-2 xenografts having an average volume of ˜80 mm^3 compared with the DLD xenografts having an average volume of ˜230 mm^3.

Intervention 2 aimed to determine the impact of US mediated cavitation on pre-seeded infection, and thus determining the levels of infection in tumours prior to Intervention 2 treatment was important. By day 7, the mean average radiant efficiency of -US had reduced from day 2 ((1.3x10^{10} [p/s/cm^2/sr] / [µW/cm^2] +/- 2.3x10^{10}) to (8.2 x10^9 [p/s/cm^2/sr] / [µW/cm^2] +/- 1.9x10^{10})) whereas the mean average radiant efficiency for the +US group had increased from day 2 ((4.1x10^9 [p/s/cm^2/sr] / [µW/cm^2] +/- 1.0x10^{10}) to (6.3 x10^9 [p/s/cm^2/sr] / [µW/cm^2] +/- 1.3x10^{10})) (Figure 3.10b). Differences between -US and +US were assessed by unpaired two-tailed t-test and determined not to be statistically significant (p=0.724). The large variability in the average radiant efficiency values recorded for mice within each treatment group resulted in standard deviations greater than the means, despite n=20. The lack of reproducibility within treatment groups reported here speaks to the challenges that IT administration faces in successful clinical translation. The % area of infection values on day 7 were lower for both no US (47% +/- 7) and US (40% +/- 6) exposed tumours than they were on day 2 and differences between them were non-statistically significant (p=0.417).

Given that there was some level of infection recorded in tumours for all mice, they were all included in Intervention 2.

3.3.3.2 Intervention 2

In Intervention 2 mice were split again into no US and US tumours as described in section 3.3.1 to form 4 treatment groups: (1) US/ US (2) US/ no US (3) no US/ US (4) no US/ no US.

First the impact of US or no US on the infection levels and spread of infection regardless of whether the mice received US or no US at Intervention 1 was determined, i.e. groups 1 and 3 were compared to 2 and 4. IVIS imaging to determine GFP fluorescence was performed on day 9 (2 days post Intervention 2) and 14 (7 days after Intervention 2) as previously described (section 2.8.1.3).

There was a substantial decrease in the mean average radiant efficiency recorded on day 9 compared with day 7 for both -US ($1.8x10^8$ [p/s/cm^2/sr] / [µW/cm^2] +/- $1.3x10^8$, 60-fold decrease) and +US ($1.0x10^8$ [p/s/cm^2/sr] / [µW/cm^2] +/- $8.3x10^7$, 20-fold decrease) tumours (Figure 3.11). The difference between the means at day 9 was assessed using an unpaired two-tailed t-test and found the mean average radiant efficiency for -US to be statistically higher than +US (p=0.0298). This suggests that receiving US at Intervention 2 did impact detrimentally on pre-infected foci and therefore the average radiant efficiency recorded two days after exposure. The mean % area of the tumour which was infected was also lower for both -US (23% +/- 26) and +US (13% +/- 16) at day 9 when compared with the % area of tumour infected on day 7. Differences between the mean % area infected recorded for -US and +US at day 9 were found to not be statistically significant (p=0.130).

By day 14, the mean average radiant efficiency for -US tumours had decreased to $1.3x10^8$ [p/s/cm^2/sr] / [µW/cm^2] +/- $7.5x10^7$ and +US tumours had increased to $1.86x10^8$[p/s/cm^2/sr] / [µW/cm^2] +/- $1.1x10^8$. Differences between the +US and -US mean average radiant efficiency were assessed by two-tailed t-test and found to not be statistically significant (p=0.0778). The mean % area of tumour infected followed a similar pattern: with the -US tumours showing similar values at

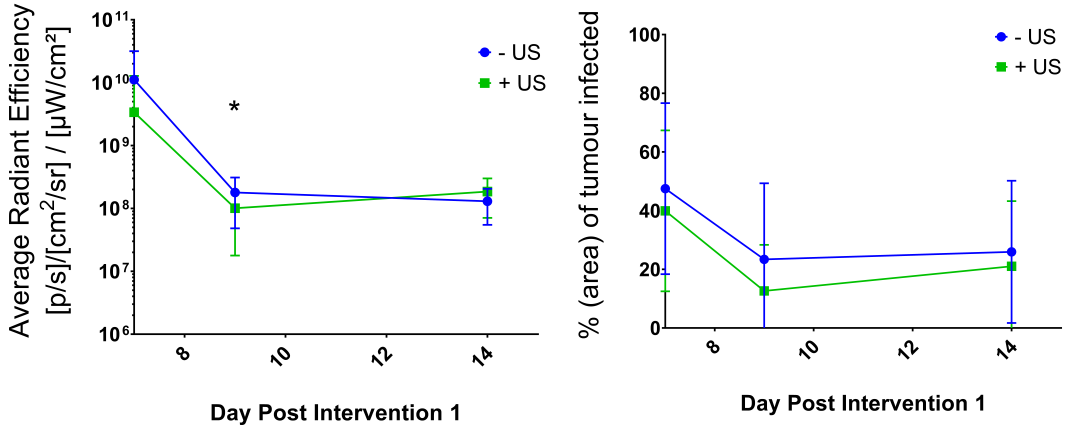


Figure 3.11: IVIS imaging was performed on mice bearing CAPAN-2 tumours on days 2 and 7 after treatment at Intervention 2. During Intervention 2 IV administration of 1.1 mg SSPs in 5% glucose was performed and tumours were either exposed to US (US+, green) or not (US-, blue). (a) Individual values for the average radiant efficiency were determined for each mouse by drawing ROIs around each tumour. Points represent the mean average radiant efficiency. Error bars represent SD. n=20 (b) Area of infection was determined by setting the minimum threshold radiance 2.2x10^8 p/s/cm^2/sr to remove background fluorescence. n=20

day 9 to those at day 14 (23% +/- 26 and 26% +/- 24, p=0.0420) and the +US tumours showing an increase between day 9 and 14 (13% +/- 16 and 21% +/- 22, p=0.0088), differences between days 9 and 14 within treatment groups were assessed using a paired two-tailed t-test. On day 14, differences between the no US and US treatment groups were assessed by an unpaired two-tailed t-test were found to be non-statistically significant (p=0.519).

To probe whether the treatment received during Intervention 1 did in fact impact the results obtained after the second intervention, average radiant efficiency results from Intervention 2 were split into the 4 groups (1) US/ US (yellow) (2) US/ no US (green) (3) no US/ US (red) (4) no US/ no US (purple). IVIS images taken on day 9 and day 14 are displayed in these four groups in (Figures 3.12 and 3.13) respectively. These images show clearly that the infection levels in the US/US group were impacted the most by US exposure at Intervention 2 with only 2 tumours out of 10 showing infection about the minimum threshold at day 9. All other groups (US/ no US, No US/ US and no US/ no US) appeared to be impacted to a similar

Figure 3.12: IVIS imaging was performed on mice bearing CAPAN-2 tumours on day 2 after Intervention 2 (day 9 after Intervention 1). During Intervention 2, 1.1 mg SSPs in 5% glucose was administered IV to tumours which were subsequently exposed to US or not. Taking into account the treatment that was performed in the first intervention, this gave 4 groups: US/ US (red) (2) US/ no US (green) (3) no US/ US (yellow) (4) no US/ no US (purple). A minimum threshold radiance of $2.2x10^8$ p/s/cm^2/sr was set to remove background fluorescence.

extent with only 2 or 3 tumours failing to display infection above the minimum threshold in each group. This analysis suggested that for tumours exposed to US at the second intervention there was a difference on day 9 based on whether the tumours were exposed to US at Intervention 1.

Inspection of the tumours for mice on day 14 (Figure 3.13) showed that for US/US mice infection levels had recovered with 8 out 10 tumours showing infection above background. The no US/ no US group had reduced to only 5 out of 10 tumours that showed infection levels above background. This suggested that for the mice which received US at Intervention 1, the exposure to US at Intervention 2 reduced infection levels 2 days post treatment at Intervention 2. However, by day 14 levels these infection levels had recovered and indeed surpassed the number of tumours showing infection in the no US group.

The average radiant efficiency and % area tumour infected data from across both Intervention 1 and 2 is displayed in Figure 3.14a and b.

As anticipated from the IVIS images in Figure 3.12, on day 9 the mean average radiant efficiency for US/US ($6.0x10^7$ [p/s/cm^2/sr] / [µW/cm^2] +/- $4.7x10^7$) was the lowest out of all groups. A one-way ANOVA followed by Tukey's test for multiple comparisions was used to assess differences between means of each group and found that US/US treated mice had statistically significantly lower mean average radiant efficiency level than no US/ no US ($2.2x10^8$ [p/s/cm^2/sr] / [µW/cm^2] +/- $1.8x10^8$) treated mice (p=0.0160). The % area of tumours infected also showed this knockdown with US/US treated tumours showing a mean % infected area of just 1% +/- 2. A dramatic reduction as no US/ no US, no US/ US and US/ no US all showed approximately equivalent mean % area of tumour (24%+/-30, 20% +/- 22 and 23% +/- 15). Differences between all four groups on day 9 were assessed using a one-way ANOVA and differences between means were found to be statistically significant (p=0.0458). However, post hoc Tukeys test for multiple comparisons found that differences between individual groups were non-statistically significant (p>0.05) although for no US/ no US vs US/US p=0.0641.

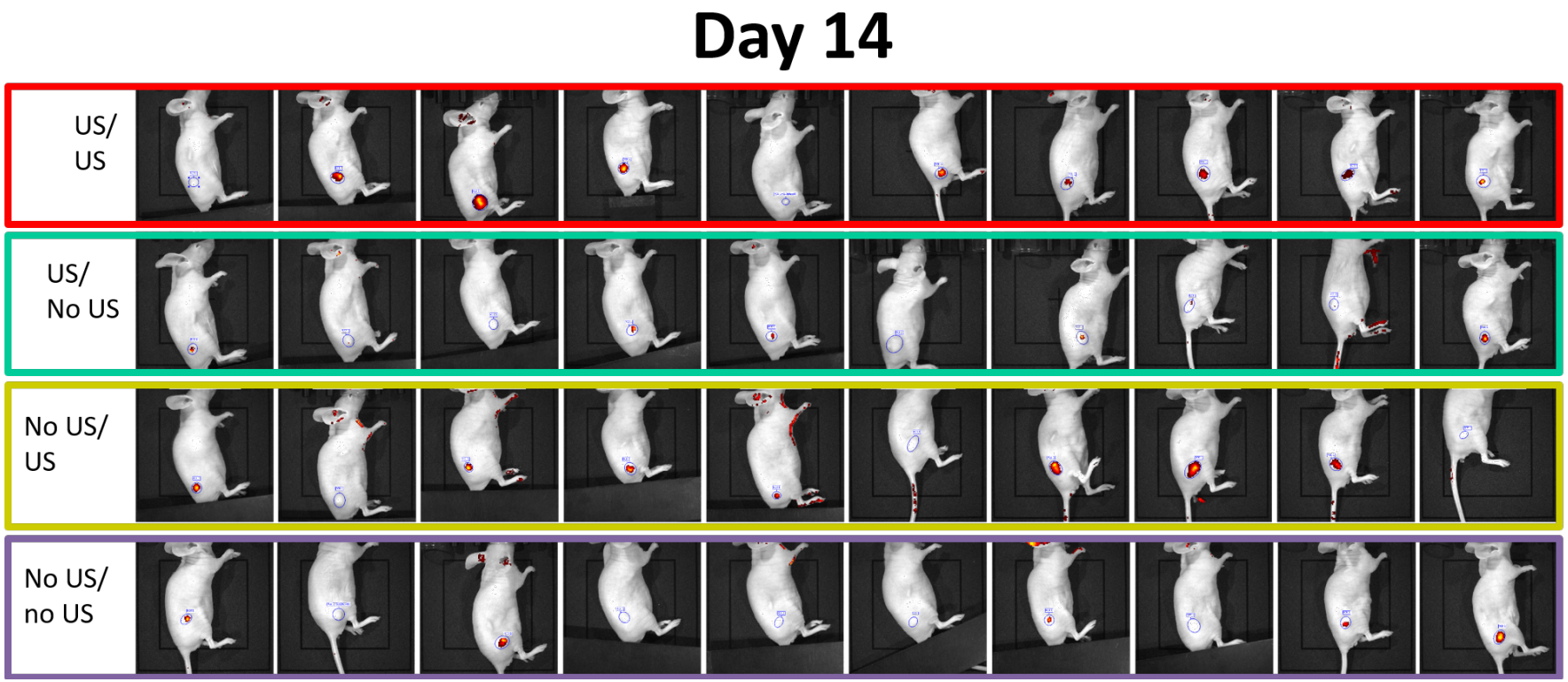


Figure 3.13: IVIS imaging was performed on mice bearing CAPAN-2 tumours on day 7 after treatment at Intervention 2 (day 14 after Intervention 1). During Intervention 2, 1.1 mg SSPs in 5% glucose was administered IV to tumours which were subsequently exposed to US or not. Taking into account the treatment that was performed in the first intervention, this formed 4 groups: US/ US (red) (2) US/ no US (green) (3) no US/ US (yellow) (4) no US/ no US (purple). A minimum threshold radiance of $2.2\text{x}10^8$ p/s/cm^2/sr was set to remove background fluorescence.

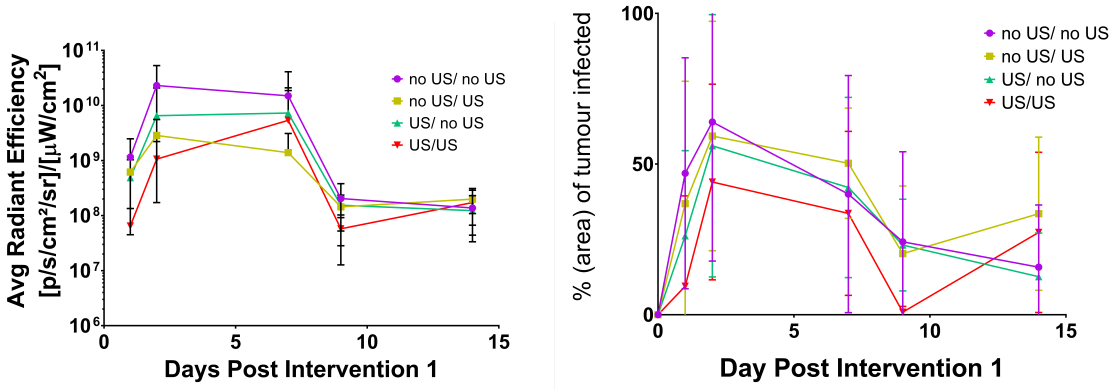


Figure 3.14: IVIS imaging was performed on mice bearing CAPAN-2 tumours on days 1, 2, 7, 9 and 14 after treatment at Intervention 1. At Intervention 1 (day 0) 5x10^6 pfu VV-GFP and 0.05 mg SSPs were IT administered before half of the mice received focused US and half did not. During Intervention 2 (day 7) IV administration of 1.1 mg SSPs in 5% glucose was performed and tumours were either exposed to US or not. This formed 4 groups: (1) US/ US (red) (2) US/ no US (blue) (3) no US/ US (yellow) (4) no US/ no US (purple). (a) Individual values for the average radiant efficiency were determined for each mouse by drawing ROIs around each tumour. Points represent the mean average radiant efficiency. Error bars represent SD. n=20 (b) Area of infection was determined by setting the minimum threshold radiance 2.2x10^8 p/s/cm^2/sr to remove background fluorescence. n=10

On day 14, the mean average radiant efficiency had increased 3-fold for US/US (1.9x10^8 [p/s/cm^2/sr] / [µW/cm^2] +/- 1.3x10^8, p=0.0142) whereas no US/ no US had a 1.5-fold decrease in mean average radiant efficiency (1.5x10^8 [p/s/cm^2/sr] / [µW/cm^2] +/- 9.0x10^7) from values recorded on day 9. No US/ US also showed an increase in mean average radiant efficiency (2.0x10^8 [p/s/cm^2/sr] / [µW/cm^2] +/- 9.0x10^7) and US/ no US showed a small decrease in average radiant efficiency (1.3x10^8[p/s/cm^2/sr] / [µW/cm^2] +/- 4.9x10^7) from day 9. This result suggested that groups which received US at Intervention 2 were increasing in infection levels between day 9 and day 14 when compared to mice that did not receive US, however differences between mean average radiant efficiency values were assessed and found to non-statistically significant (one-way ANOVA, p>0.05). The % area of tumour infected showed a similar pattern to that observed for the mean average radiant efficiency: both groups which received US at Intervention 2 had increased % area tumour infected at day 14 when compared to day 9 and both groups which did not receive US at day 7 showed a decreased in infected area between day 9 and

14 (US/US = from 0.85% +/- 1.9 to 27% +/- 27, no US/ US= from 20% +/- 22 to 34% +/- 25, US/ no US= from 13% +/- 15 to 13 % +/- 14 and no US/ no US= from 24 % +/- 30 to 16% +/- 21). The change in area is visualised clearly for all mice in Figure 3.15. For each group the number of mice with increasing % area tumour infected can be seen between day 7-14. In both no US/no US (purple) and US/no US (green) groups, the % area tumour infected increased from day 9 to 14 in only 1 mouse. This was in contrast to no US/US (yellow) that showed an increase in the % area tumour infected from day 9 to 14 in 5 out 10 mice and US/US (red) that showed an increase in the % area tumour infected from day 9-14 in 7 out of 10 mice. Of note, no US/ no US had the highest number of mice (5/10) that had a % area tumour infection of 0%.

3.3.3.3 Ex vivo assessment of excised tumours

On day 14 mice were sacrificed and tumours were excised. IVIS imaging of excised tumours was performed to assess the GFP fluorescence. For technical issues, only 5 mice from each group were able to be robustly measured for GFP signal post cull.

For this analysis it was determined most appropriate to report the total radiant efficiency for each tumour which had been normalised by the volume measured for each tumour after recovery (Figure 3.16a). The mean total radiant efficiency/ mm^3 tumour ([(p/s) / $\mu W/cm^2$]/mm^3) was highest for the US/US group ($7.3x10^7$ [(p/s) / $\mu W/cm^2$]/mm^3 +/- $3.2x10^7$) when compared with no US/ no US ($2.0x10^7$ [(p/s) / $\mu W/cm^2$]/mm^3 +/- $1.7x10^7$, p= 0.0053) and US/ no US (($2.6x10^7$ [(p/s) / $\mu W/cm^2$]/mm^3 +/- $1.2x10^7$), p=0.0128). Differences between the mean total radiant efficiency/ mm^3 tumour for the US/US group and the no US/US group (($3.7x10^7$ [(p/s) / $\mu W/cm^2$]/mm^3 +/- $1.7x10^7$), p=0.0645) were assessed and found to be non-statistically significant.

Finally, qPCR analysis was performed on DNA extracted from all 10 tumour homogenates (50 mg/mL) in each treatment group (as detailed in section 2.7) and the results are displayed in Figure 3.16b. Differences between mean VG/ g tumour assessed using a one-way ANOVA were shown to not be statistically significant.

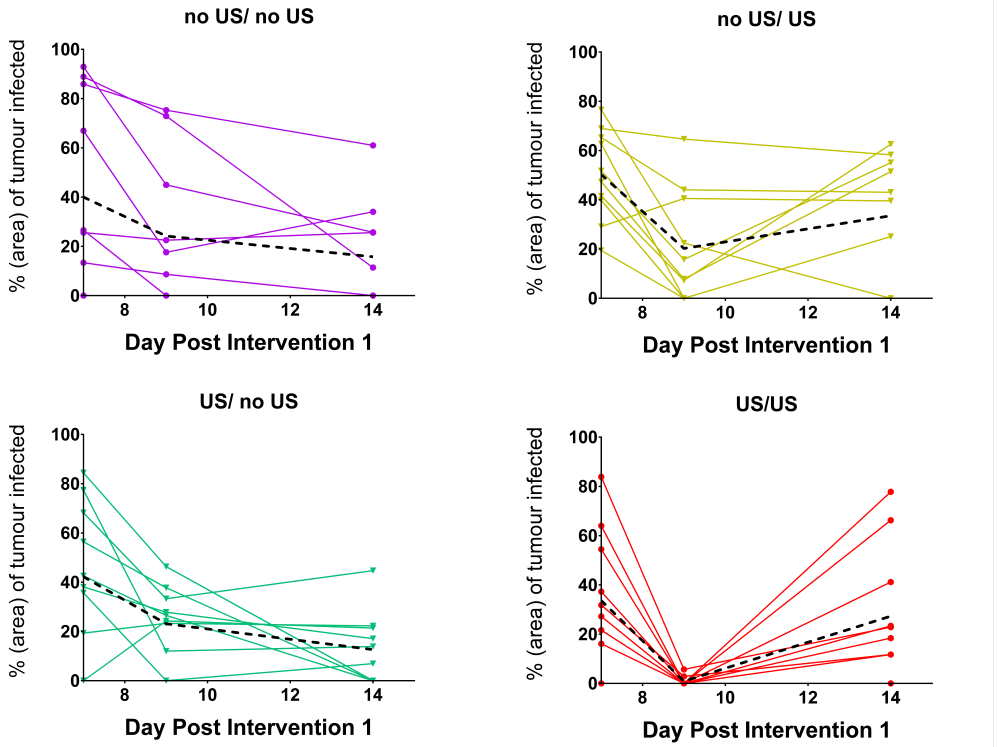
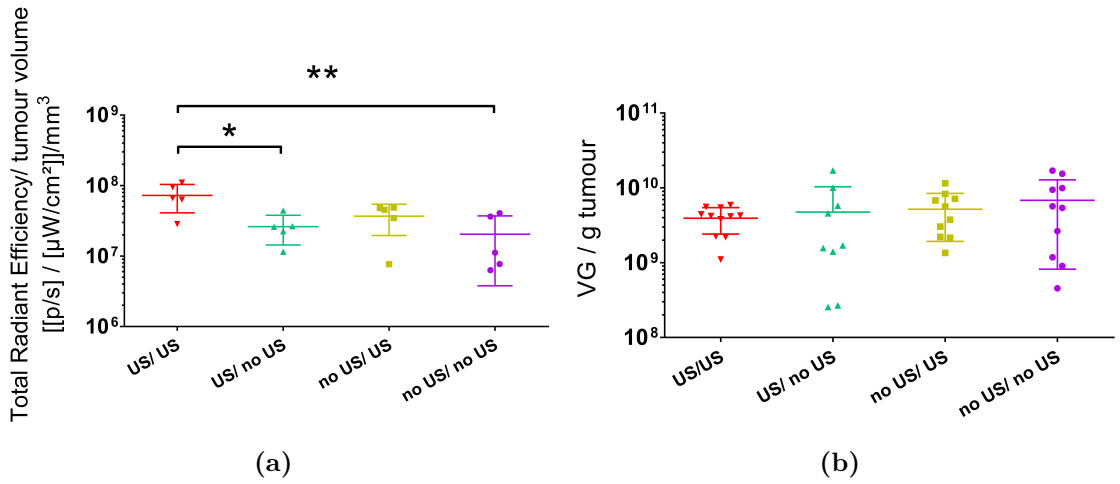


Figure 3.15: Area of infection was determined by setting the minimum threshold radiance 2.2x10^8 p/s/cm^2/sr to remove background fluorescence on days 7, 9 and 14 after treatment at Intervention 1. During Intervention 2 (day 7) IV administration of 1.1 mg SSPs in 5% glucose was performed and tumours were either exposed to US or not. This formed 4 groups: (1) US/ US (red) (2) US/ no US (blue) (3) no US/ US (yellow) (4) no US/ no US (purple). Individual values for the % area tumour infected at each time point and data for individual mice is presented. The mean % area tumour infected is overlayed as a black dashed line for each group. n=10

There was large variability in the viral genome (VG) content/ g tumour within groups and it was observed that this variability was reduced in both the US/US (3.9x10^9 SD = +/- 1.5x10^9) and no US/US (5.2x10^9 SD = +/- 3.3x10^9) groups when compared with no US/ no US (6.8x10^9 SD = +/- 6.0x10^9) and US/ no US (4.7x10^9 SD = +/- 5.6x10^9). This suggests that receiving US at Intervention 2 could potentially result in less variability within treatment groups.



(a) (b)

Figure 3.16: Assessment of excised tumours *ex vivo* on day 14 after treatment at Intervention 1. At Intervention 1 (day 0) 5x10^6 pfu VV-GFP and 0.05 mg SSPs were IT administered before half of the mice received focused US and half did not. During Intervention 2 (day 7) IV administration of 1.1 mg SSPs in 5% glucose was performed and tumours were either exposed to US or not. This formed 4 groups: (1) US/ US (red) (2) US/ no US (blue) (3) no US/ US (yellow) (4) no US/ no US (purple). (a) Individual values for the total radiant efficiency per volume tumour for individual mice is presented. Horizontal lines represent mean and error bars represent SD. n=5 (b) qPCR for the viral genome (VG) content per g tumour. Horizontal lines represent mean and error bars represent SD. n=10 Differences between means were assessed by one-way ANOVA and where appropriate post-hoc Tukey's test for multiple comparisons was used.

3.4 Discussion

The first clinical trial utilising VV in cancer treatment was by Mastragelo *et al* in 1999, where VV encoding GM-CSF was administered IT in patients with cutaneous melanoma. [27] The next report of JX-594 (Pexa-Vec) use in clinical trials was in 2005 where a dose escalation study found a MTD of 1x10^9 pfu/dose after IT administration. [28] Since, there have been 9 studies which have investigated JX-594 that used IT as the administration route of choice. IT administration of JX-594 has shown success in Phase II clinical trials, with the report by Hoe *et al* in 2013 being the first to show improved median survival linked to the administered dose. [68] Hence, it was hypothesised in this chapter that improving the homogeneity of VV dissemination after IT administration, greater efficacy could be achieved.

It was first reported by Bazan-Peregrino *et al* that US mediated cavitation (SonoVue cavitation nuclei, 500 kPa, 90% DC, 10 Hz for 20s) could be used to

enhance the level of GFP expression and its distribution within tumours exposed to US after IT administration $2x10^9$ pfu of a non-replicating Ad. [202] SSPs were used in the experiments reported here (1.5 MPa, 5% DC, 0.5 Hz) and due to their extended cavitation profile over time when compared to SonoVue under these conditions [190], a 5 minute treatment window was chosen. The hypothesis that US mediated cavitation may be able to improve the diffusion of viral infection within tumours was further investigated to determine the outcome on pre-seeded infection foci in xenograft tumours. The micro-environment of tumours coupled with the large size of vaccinia make diffusion and penetration particularly challenging. [204] Indeed, previous reports by Miller *et al* investigated the evolution of intratumoural VSV infection from individual infection centres over time. [77] It was reported that in a notable number of cases the infection focus would increase between 24 hours and 48 hours, but then diminish by the 72-hour time-point, despite the presence of large regions of viable tumour. This highlights the injection heterogeneity profiles between tumours and the potential need for an external mechanism to help infection foci break out of their isolated regions. Therefore the application of a second intervention of US to spread infection from pre-seed infection foci was also investigated. The main findings in this chapter are:

1. In a bilateral DLD xenograft model (140-440 mm^3) $1.25x10^7$ pfu VV-GFP was pre-mixed with 0.125 mg SSPs before IT administration to both tumours. One tumour was then exposed to focused US for each mouse. It was shown that 24 hours after treatment levels of GFP production were low for both +US and -US tumours. By day 6 post treatment, the average radiant efficiency was higher in 3/5 tumours exposed to US when compared to the control bilateral no US tumour in the same mouse. The % area of tumour infected above a 7.35 $x10^8$ $p/s/cm^2/sr$ / µW $/cm^2$ threshold was higher in all 5 +US tumours (mean of 64%) when compared to the -US control tumours (mean of 34%, p=0.0025). This suggested that by day 6, a greater spread of infection was seen for VV-GFP +US when compared with VV-GFP -US under these conditions. It was previously reported by Fend *et al* that IT administration of $1x10^7$ pfu dose of VV-FCU1, (deleted for thymidine

kinase (TK) and ribonucleotide reductase (RR) genes that expressed the fusion suicide gene FCU1), to renal carcinoma xenografts, gave a virus production (by plaque assay) peak on day 2 which was persistent until day 14 post injection. [205] Therefore, increased transgene expression and infection area reported here between day 1 and day 6 could be due to enhanced dissemination throughout the tumour at the time of treatment as a result of US exposure, hence resulting in more spread out infection detected on day 6.

2. Analysis of PAM recorded during treatments showed a cumulative PAM magnitude of $2.3\text{x}10^3$-$3.6\text{x}10^3$ au. Damage was assessed for the 5 tumours receiving US in this cumulative PAM cavitation range and no bruising was seen in any tumour. Tumours that were not exposed to US were given a cumulative PAM magnitude of 0. Due to the increased % area tumour infected for +US tumours compared with -US tumours, a correlation between cumulative PAM magnitude and % area of tumour infected was probed. A linear regression was applied and produced a reasonable fit for the limited number of data points analysed. The equation produced was $Y = 0.00889X + 36.8$ and suggested that for every 1000 Cumulative PAM Magnitude dose received, the % area tumour infected increased by ˜9%. Due to the non-uniform spread of cumulative PAM magnitude obtained in this study, an experiment which had a wider range of cumulative PAM magnitude values would perhaps resolve a more robust relationship between the cumulative PAM magnitude and % area tumour infected.

3. In a second study, a unilateral CAPAN-2 xenograft model (45- 180 mm^3) was used. The first aim of the study was to determine whether the same impact on increased % area of tumour infected could be achieved as was seen in the larger bilateral DLD xenograft model. The second aim of the study was to assess the impact of a second US mediated cavitation intervention on enhancing the spread and intensity of pre-seeded VV-GFP infection. SSPs were used as the cavitation nuclei and a reduced dose of 0.05 mg was administered IT (intervention 1) compared with 1.1 mg IV (intervention 2). The cavitation activity was compared for these two doses in their respective administration routes. It was shown that both cumulative

PAM magnitude and cavitation dose metrics gave a picture of cavitation activity. The cavitation dose reduced the extent that the three highest cumulative PAM magnitude values were above the standard deviation by taking into account the spatial distribution and total tumour volume of the tumours. Both metrics showed that cavitation activity recorded after IT administration gave a large range of values. The mean cumulative PAM magnitude and cavitation doses measured following IT or IV administration were found to not be statistically significantly different (two-tailed t-test, $p>0.05$).

In contrast to the 5 tumours that received US in the DLD xenograft study, half of the tumours which received US at intervention 1 (0.05 mg SSP, IT administration) showed signs of bruising which were related to the dose of cavitation that they received. It is thought that this could be due to differences in the vasculature or differences in xenograft sizes (the CAPAN-2 xenografts being smaller in this study compared with the larger DLD xenografts).

After intervention 2 (1.1 mg SSP, IV administration) despite the range of cumulative PAM magnitude being approximately similar to that at intervention 1, bruising was seen on the skin and/or inside the tumour capsule for all mice that received US. This suggests that pre infected tumours with VV-GFP make tumours more susceptible to bruising regardless of the cavitation dose they received. This could be in-line with reports in the literature which describe VV infection of tumour endothelial cells and disruption of tumour vasculature in mice as early as 5 days post treatment. [172, 176, 206]

4. After intervention 1, IVIS imaging was performed to determine and compare infection levels and % area of tumour infected for mice that received US (+US) to those that did not (-US). A reduced dose ($5x10^6$ pfu) was used for the CAPAN-2 xenografts when compared with the DLD xenograft study due to the difference in tumour size. The high levels of average radiant efficiency for both +US and -US at day 1 post treatment (which was in contrast to the low levels seen in the DLD xenografts at day 1) suggested that the 2.5-fold reduction in dose was not sufficient to produce a comparable infection regime between the two models. On day 1 the

mean average radiant efficiency was higher for -US tumours ($8.9x10^8$ [p/s/cm^2/sr] / [µW/cm^2] +/- $1.0x10^9$) compared with +US tumours ($3.1x10^8$ [p/s/cm^2/sr] / [µW/cm^2] +/- $4.4x10^8$). This also resulted in a higher % area of tumours infected in -US tumour when compared with +US tumours. By day 6, differences between mean average radiant efficiency and % area of tumours infected were found to not be statistically significant. These results suggest that in this smaller volume unilateral CAPAN-2 xenograft model, VV in tumours that received US performed worse than those that did not initially (day 1), but their infection levels and area of infection caught up to the same levels evident in -US tumours by day 2.

5. All mice showed infection within tumours on the day of intervention 2 (day 7) and were sorted into treatment groups so that the mean tumour volume was approximately the same for each group. When not taking into account the treatment at intervention 1 which seeded the VV-GFP infection (i.e whether US or no US was received at intervention 1), it was noted that both infection levels and % area of tumour infected were reduced on day 9 when compared to those recorded on before intervention 2 on day 7. The average radiant efficiency levels and % area of tumour infected reduced slightly for -US mice and increased markedly for +US mice by day 14.

When taking treatment at intervention 1 into account, four treatment groups are compared no US/no US, no US/US, US/no US and US/US (n=10). The US/US group was most impacted by the second intervention, with both average radiant efficiency values and % area of tumour infected reducing on day 9 when compared with the other 3 treatment groups which remained approximately equal. This was clearly depicted in the IVIS images on day 9 in which only 2 tumours in the US/US treatment group had any visible infection on day 9 (compared with 7-8 tumours in other treatment groups). By day 14 however, the infection levels seen in the US/US group had made a recovery and both treatment groups which had received US at intervention 2 had increased average radiant efficiency and % area of tumour infected when compared with no US/no US and US/no US treatment groups, which both showed decreases compared with day 9. This suggests that

US potentially had a delayed impact on enhancing the infection levels seen on pre-seeded VV-GFP infection. It would have been of interest to continue this study on to a further time point to determine whether re-intervention with US did result in a longer propagation of infection when compared with no US. This would require a more open ended experimental design with adaptive imaging days so as not to exceed licence restrictions before later time points are reached. It is apparent that an infection plateau is often reached in oncolytic virus treatments (IT or IV) before complete tumour removal is achieved. Any approach that offers a means of improving spread from established foci may be very impactful.

This is especially pertinent when redosing with virus may be hampered by raised anti-virus immunity resulting from the first dose or, indeed, when a consequence of infection is alteration to the function of the vasculature [3, 22, 75, 172, 176]. Unfortunately due to restrictions in the license under which this *in vivo* work was performed, the number of imaging sessions in the work reported in this thesis is limited to 5.

6. *Ex vivo* analysis of the tumours showed that there was an US mediated difference between the levels of fluorescence recorded in tumours at the time of cull. Values were normalised by respective tumour volume and were analysed. This showed that on day 14 (day of cull) there was a significantly higher mean total radiant efficiency per mm^3 tumour for US/US when compared with no US/no US (4-fold, $p<0.01$) and US/no US (3-fold, $p<0.05$) treatment groups. qPCR analysis did not however show a difference in VG content in the tumours. This was in line with reports by Bazan-Peregrino *et al* who also showed increased transgene expression with no increase in VG content, and suggested that the increased spread provided had not translated into increased replication at this time-point. [202]

3.5 Summary and Conclusions

In summary it was shown here that US mediated cavitation using SSPs as the cavitation nuclei was able to enhance VV's area of infection in large DLD xenograft tumours. Cavitation activity was measured as cumulative PAM magnitude for this

study and a reasonable linear relationship was probed which suggested that for every 1000 cumulative PAM magnitude a tumour received, the % area of infection increased by 9%. This enhancement in VV infection spread due to US mediated cavitation was not reproduced in a smaller volume CAPAN-2 xenograft tumour model where a higher average radiant efficiency was reported for -US tumours 24 hours post treatment. This is in contrast to Bazan-Peregrino *et al* who reported increased fluorescence in ZR75.1 tumours exposed to US 24 hours after treatment, differences that are the likely consequence of the different tumour cell lines used, different infection pathways of VV and Ad5 and the difference in acoustic parameters used. [202] Bazan-Peregrino *et al* utilised parameters which resulted in non-inertial cavitation where as the parameters and cavitation nuclei (SSPs) used in the experiments within this thesis resulted in only inertial cavitation. Indeed, SSPs have been shown to only produce inertial cavitation. [207] SSPs have been shown to have an elongated cavitation profile when compared to SV which resulted in enhanced delivery of VV after IV administration *in vivo*. [190] The choice to use SSPs as the cavitation nuclei was based upon this finding by Myers *et al*, and the ultrasound parameters consequentially were chosen to be those which resulted in elongated detectable inertial cavitation. It is noted however that the resulting inertial cavitation produced could result in high levels of damage after IT administration and hence may explain the reduction of transgene expression observed in the +US groups. Future experiments utilising US parameters and cavitation nuclei which produce non-inertial cavitation may show an increase in the area of infection in tumours exposed to US and align more closely with the results reported by Bazan-Peregrino *et al*. [202] By day 6 fluorescence levels reported between -US and +US tumours were approximately equal and mice were further divided into groups for a second intervention of IV administered SSPs or IV administered SSPs + US. Mice that had received US during intervention 1, had the greatest reduction in infection (average radiant efficiency and area of infection) 48 hours post treatment if re-exposed to US at intervention 2 (US/US). Mice that did not receive US at intervention 2 (US/no US and no US/no US) showed a steady

decline in average radiant efficiency and area of infection at both 48 hours and 7 days post intervention 2. This was in contrast to both of the groups which did receive US at intervention 2 (US/US and no US/US) which both showed a mean increase in both average radiant efficiency and % area of infection on day 7 post intervention 2 when compared to 48 hours post intervention 2. Limitations on the number of IVIS imaging sessions prevented this study from continuing to later imaging time-points which could have shed light on whether this increasing infection was a continuing trend that may have provided a solution to the infection plateau. [208]

The following is therefore concluded for Chapter 3:

- A correlation between the cavitation dose received by DLD xenograft tumours after IT administration of VV + SSPs and the % area of tumour infected was determined, suggesting that the inertial cavitation received by tumours resulted in enhanced delivery and dissemination of VV after IT administration.
- However, no correlation was shown between cavitation dose received by CAPAN-2 xenograft tumours after IT administration of VV + SSPs and the % area of tumour infected in a larger powered study. These results suggest that there is no benefit in delivery and dissemination seen when US mediated inertial cavitation is applied to CAPAN-2 xenograft tumours after IT administration.
- A re-intervention with US mediated inertial cavitation after SSPs were administered IV on CAPAN-2 xenograft tumours did not result in enhanced infection levels and spread of pre-seeded VV infection foci within the 7 days of monitoring post intervention. There was a suggestion that the impact of re-intervention with cavitation was beginning to have a positive impact on the % area of infection by the final day of tumour monitoring, however further experiments would need to be performed to assess this robustly.

Chapter 4

Polymer Coating for Enhanced Blood Stability of Oncolytic VV

4.1 Introduction

The pharmacokinetics of drug and gene delivery systems can be made more favourable by providing a protective surface layer of polymer, such as poly(ethylene glycol) (PEG) or polyhydroxypropylmethacrylamide (PHPMA), to prevent opsonisation and antibody binding. This is an approach which has been successfully deployed in the formulation of blood-stable liposomal drug carrier systems. The standard method for adding PEG to drug delivery systems containing lipid bilayers is to incorporate a low percentage (5-10 %) of phospholipid-PEG molecules into the synthesis mix during formulation (premixed). This is a simple approach which has been successfully deployed in the formulation of agents such as Doxil, widely considered to be the first FDA approved 'nanomedicine'. [209] Another less commonly applied method involves adding lipid-PEG molecules after liposome formulation (post insertion) which often done by co-incubation of lipid-PEG polymers with liposomes for 1 hour at 40 °C. [210] As discussed in section 1.2.1, vaccinia virus (VV) is an enveloped virus with huge potential as a cancer therapeutic but is limited clinically by rapid opsonisation and clearance from the bloodstream, making it a good candidate for protection using PEGylation. As VV is manufactured using vats of infected cells, incorporation of phospholipid-PEG at the point of

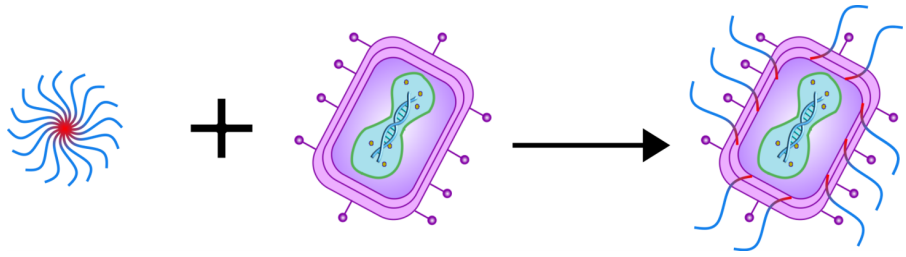


Figure 4.1: Schematic drawing depicting the PEG-Chol and VV integration process. PEG-Chol polymer chains form micelles in solution with the hydrophobic head inside. Cholesterol (red) embeds into the lipid bilayer of VV (purple) leaving PEG (blue) brushes outside the virion.

'formulation' is not feasible. In response, a strategy whereby polymer coating could be achieved by incubating isolated and purified VV with poly(ethylene glycol)-cholesterol (PEG-cholesterol), was devised and tested here. Specifically, when a PEG-cholesterol solution and a solution containing lipid membranes are combined, the hydrophobicity of the cholesterol groups can lead to their insertion into the lipid bilayer leaving the hydrophilic PEG polymer chain protruding from the surface. This cholesterol-embedding technique has been used to PEGylate "stealth" liposomes to increase their circulation time. [135–137] Hence, as VV is encased in a lipid bilayer it was hypothesised that PEGylation of VV, using a cholesterol anchor, could be a novel and simple way of increasing its circulation time. It was hoped that as with stealth liposomes, when many PEG chains embed in the lipid layer of the VV virion, a protective polymer brush coating would be formed (as depicted in Figure 4.1).

Lipid bilayer fluidity allows for diffusion of its constituents. The fluidity of the lipid bilayer is affected by temperature and is described as its phase behaviour. [211] At a given temperature, the lipid bilayer can exist in either a liquid or solid phase. The temperature at which a phase change occurs depends on the length of the lipid tails and the degree of unsaturated lipids present in the layer. The higher the temperature of the lipid bilayer, the more fluid it will be. The addition of a cholesterol group to a liposomal lipid bilayer makes it less fluid and decreases the ease of particle diffusion within the monolayer. [212] This is ideal for polymer coating of VV, as it means once the cholesterol groups have embedded into the lipid bilayer at 37 °C, they are less likely to be separated during circulation in the body. [135, 136, 213]

The polymer coated-VV (PCVV) is expected to have an increased circulation time when compared to that of VV alone, as the polymer coating should decrease the immune system mediated clearance. This may allow higher levels of still infectious virus to reach its tumour targets post IV injection as was reported by Fisher *et al* in studies using a polymer-coated adenovirus in preclinical models. [114] However, it is expected that as with these previous adenovirus polymer coating studies [76, 109, 111–114, 116, 117], that there will be an overall knock-down (decrease) of VV infection as a result of polymer coating concealing cell binding and entry mechanisms. Hence, PCVV may circulate and accumulate more effectively but may be less able to bind to and infect target cells compared to non-modified VV. Such knock-down could result from polymer chains blocking regions on the virus virion which are usually used to enter and infect cells. The aim for the PCVV is that, despite this potential infectivity knock-down, the level of infection will stabilise in the presence of blood components *in vitro*. If polymer coating strategies can be shown to be effective, addition of ligands to achieve specific retargeting and restoration of infection can be investigated (see section 1.3.1.2.2). Such 'retargeting' strategies have previously proven viable in studies using other viruses, but to date such effects have not been shown for VV. [114]

The aims of this chapter are:

1) Assess the optimum conditions required for successful polymer coating via a lipid anchor into the lipid bilayer envelope of VV.

2) Determine the impact of polymer coating on VV stability in blood components and anti-VV antibody binding.

3) Assess the impact of polymer coating on the circulation kinetics of VV in a tumour bearing murine model.

4.2 Results: Polymer Coating

There were a few important factors to consider when selecting polymers for use in the coating of VV. Biocompatibility is a crucial consideration for any agent that will be injected into the bloodstream. Biocompatible polymers are ones

which will not cause adverse effects in the body and are commonly used to aid the acceptance of foreign objects in medical use. One family of biocompatible polymers commonly used in drug delivery are Poly(ethylene glycol) (PEG) polymers which will be discussed here. [11, 214–217]

PEG is a polyether compound which can be used for many purposes. A large amount of research, at a variety of stages, is being performed using PEG for different medical purposes. PEG is hydrophilic and soluble in a range of solvents including water and PBS. Its high solubility makes PEG suitable for many purposes, including polymer coating, as desired in these experiments. [218] The two PEG molecules used in this chapter, one of length 8 kDa and another of length 10 kDa, were both linked at one end to a cholesterol group. The structure can be seen in section 2.1.1, Figure 2.1.

4.2.1 Determining optimum PEG-Cholesterol embedding conditions

First, Cholesterol-PEG(8K) (Chol-PEG(8K)) coated VV (PCVV) formulated as per the protocol described in section 2.2 with increasing concentrations of Chol-PEG(8K) at room temperature pressure (RTP) was investigated (Figure 4.2a). If embedding of Chol-PEG(8K) occurred, a knockdown in virus infectivity as the concentration of Chol-PEG(8K) increased from 1 to 10 mg mL^{-1} was expected, as this would suggest a concealment of the cell binding mechanisms of VV. However, it was observed in this study (performed as described in section 2.5.2) that PCVV constructs formed by incubation with Chol-PEG(8K) at RTP showed no significant incremental decrease of A549 cell infection when compared to VV alone as the concentration of Chol-PEG(8K) increased. The only statistically significant ($p<0.01$) knock-down in infection was between 1 mg mL^{-1} and 10 mg mL^{-1} coatings where a 4-fold decrease in A549 cell infection, as determined by luciferase assay, was observed. The lack of any meaningful drop in virus activity as measured by luciferase production by infected cells suggested that there was poor polymer integration into the lipid bilayer of VV when co-incubation was performed at RTP. When PCVV constructs formulated by co-incubation with polymer at RTP were tested in infection studies performed

in the presence of 5% pooled human serum, there was a large knockdown in A549 cell infection for all groups with the largest knockdown seen in the uncoated VV group (approximately 860-fold). As displayed in Figure 4.2.1c, the level of infection knockdown for PCVV formulated at all three concentrations was less than the naked VV. In these early infection experiments, free polymer was not removed from virus samples before addition to cells. Therefore, this suggested that the presence of polymer, either embedded or free in solution, was interacting with the human plasma thereby reducing the neutralisation effect seen in the absence of polymer coating.

Taking into account the relationship between bilayer fluidity and temperature (section 4.1) experiments were repeated with VV incubation with Chol-PEG(8K) (PCVV formation) taking place at 37 °C. Cell infection studies with these constructs showed a substantial knockdown in infection as the concentration of Chol-PEG(8K) increased. This is in accordance with what would be predicted with a well-integrated polymer coating of VV, Figure 4.2.1d. [113] There was no significant change in infection between uncoated VV and VV co-incubated at 37 °C with 1 mg mL^{-1} Chol-PEG(8K), suggesting that at low concentrations the polymer was either unable to embed successfully into the VV membrane under such formation conditions, or that the polymer coating had little effect on the infectivity of VV. This was further supported by the results of an infection study performed with 5% pooled human serum (PHS) (figure 4.2e) in which the PCVV formed from pre-incubation at 37 °C with 1 mg mL^{-1} Chol-PEG(8K) showed no greater infection when compared to that of naked VV. The infection level observed with VV pre-incubated with a 2.5 mg mL^{-1} Chol-PEG(8K) solution in the absence of human serum was 3-fold lower than uncoated VV ($p<0.0001$). However, this level of infection was maintained in the presence of 5% PHS (Figure 4.2f). For PCVV formed from pre-incubation at 37 °C with 10 mg mL^{-1} Chol-PEG(8K) the infection level in 5% PHS was approximately 2-fold higher than that it was in 0% PHS. This showed that PCVV formed from incubation with both 2.5 mg mL^{-1} and 10 mg mL^{-1} Chol-PEG(8K) solutions at 37 °C, showed a knockdown of infection compared to VV but that the presence of PHS in the infection media had minimal impact on its effectiveness.

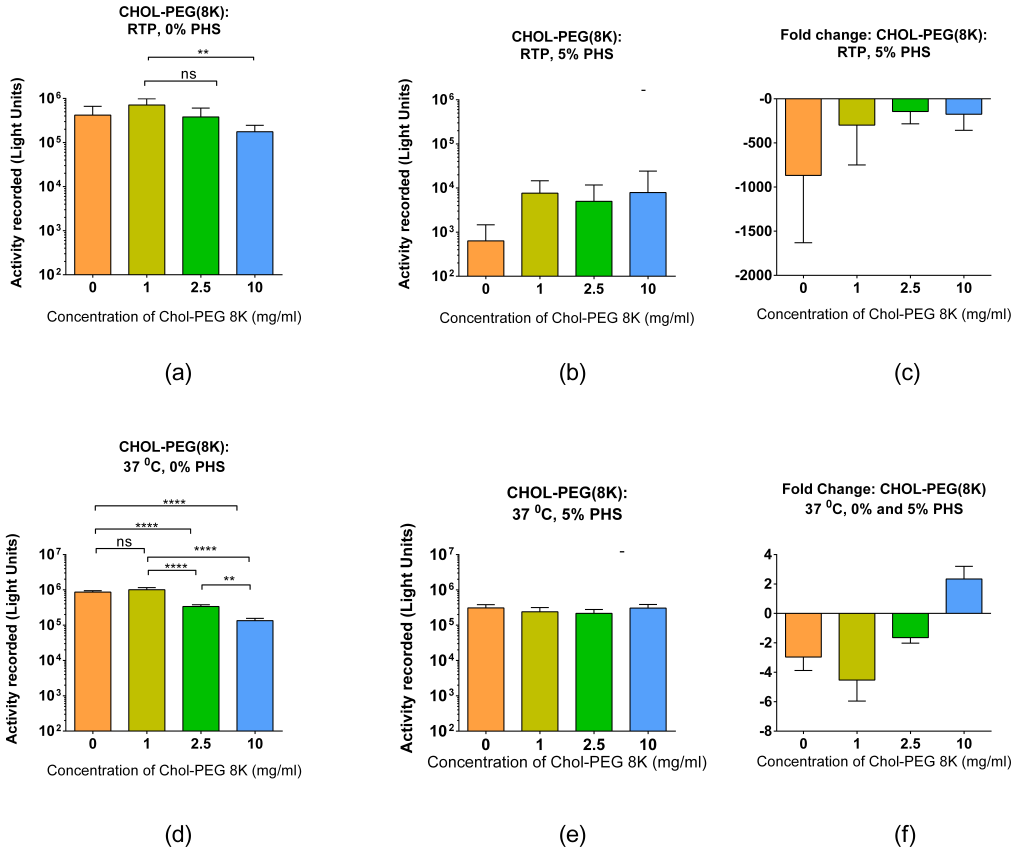


Figure 4.2: Comparing the ability for different PEG(8K)-Chol coating concentrations of VV formed at RTP or 37 °C to infect A549 (10,000 cells per well) over 24 hours. The PCVV formed at different concentrations was left to combine for 1 hour. PCVV samples were not purified from free polymer in this study. One-way ANOVA analysis followed by Tukey's test for multiple comparisons was performed on the data to determine whether the results between groups were significant. (a) Infection after formation at RTP. (b) Formation at RTP with infection in 5% pooled human serum (PHS). (c) Fold change in infection level (fold-decrease) between 0% PHS (a) and 5% PHS (b). (d) Infection after formation at 37 °C. (e) Formation at 37 °C and infection in 5% PHS. (f) Fold change in infection level (fold-decrease or increase) between 0% PHS (d) and 5% PHS (e). n=6, ANOVA key: ns = -, $p > 0.05$, * = $p < 0.05$, ** = $p < 0.01$, *** = $p < 0.001$, **** = $p < 0.0001$. Error bars represent standard deviation.

This hypothesis was investigated in more detail by infecting A549 cells with 0.1 pfu/cell of naked VV (Figure 4.3a) or 0.1 pfu/cell of PCVV formed by pre-incubation with 10 mg mL^{-1} Chol-PEG(8K) at 37 °C in the presence of a wider range of PHS to a maximum of 25% (Figure 4.3b). As expected from literature, the infectivity of naked VV on A549 cells was significantly reduced as the concentration of human serum increased from 0-25%, reaching a knockdown of 150-fold and over in the presence of 12.5% human serum and above (Figure 4.3a). This provided assurance that human plasma would provide a neutralisation effect on the naked VV in these conditions. As with naked VV, the infectivity of PCVV on A549 cells was also impacted by the presence of human plasma in a concentration dependent manner, however whereas VV suffered a knockdown in infectivity of 950-fold in 25% PHS for PCVV the greatest knockdown observed at 25% human plasma was 40-fold (see Figure 4.3).

Comparing infection levels achieved by VV and PCVV in the same concentration of PHS (5% (red), 12.5% (green) and 25% (purple)) showed that PCVV achieved higher levels of infection, 16, 40 and 25-fold greater respectively, at all three concentrations of PHS. This suggested that a coating formed from pre-incubation of VV with 10 mg mL^{-1} Chol-PEG(8K) could stabilize VV infectivity when compared to naked VV in the presence of high concentrations of PHS.

It is worth noting that these initial studies were performed without purifying free polymer from any formulated PCVV. Therefore making a determination of whether polymer coating was achieved based on a knockdown in infectivity was viewed with caution as the possibility that free polymer could somehow impact over-all infection levels, could not be excluded. Therefore further studies to confirm the formation and purity of PCVV using flow virometry were performed.

4.2.2 Confirming coating with Flow Virometry

To confirm PEG(8K)-Chol coating of VV, a fluorescently labelled PEG-Chol chain was substituted for PEG(8K)-Chol, and the VV particles incubated with the fluorescent PEG-Chol (according to standard protocol see section 2.2) were analysed using either a FACS Calibur or Attune NxT ™ Cytometer adapted as described in

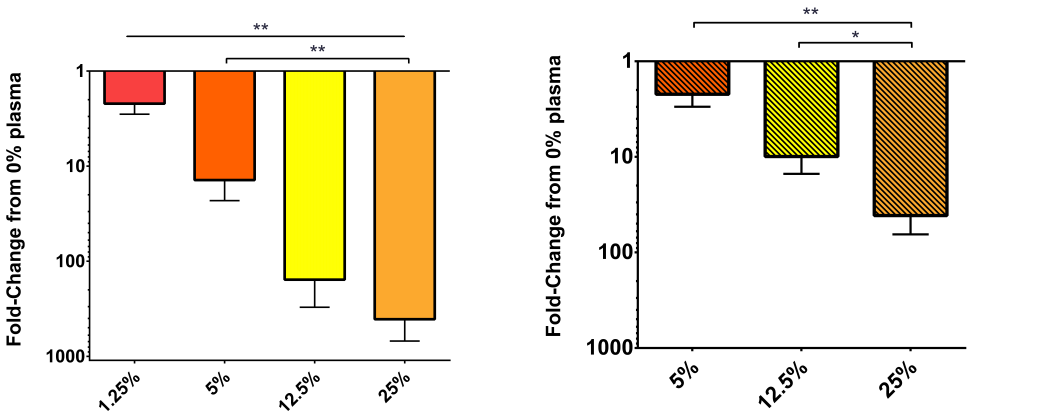


Figure 4.3: Infection of A549 cells achieved after 24 hours with 0.1 pfu/cell of either (a) naked VV or (b) 10 mg mL^{-1} Chol-pEG(8K) 37 °C coated VV (stripes) in increasing amounts of Pooled Human Serum. The fold-change (fold-decrease) of luminescence recorded between 0% at each concentration is displayed. Error bars represent SD. ANOVA analysis was performed on the data to determine whether the results between groups were significant. n = 5, ANOVA key: ns = p> 0.05, ** = p < 0.01

section 2.4.3. As discussed in detail in section 1.3.1.3, the use of a flow cytometer to analyse viral particles is called flow virometry. [138] A previous report was able to successfully identify the VV using flow virometry [139], and so it was hypothesised that this technique could be used to demonstrate successful coating of VV.

Initial tests to determine the settings required to resolve uncoated ('un-stained') and fluorescently coated ('stained') VV populations on the BD FACSCalibur Cytometer were performed. With dimensions in the 350 nm range, VV is at the limits of what can be detected using flow cytometry and so some assurance that a DNA containing particle was detected was needed. For this reason, in initial studies a YOYO-1 nucleic stain was used to provide a 'ground truth' and probe whether VV could be reliably identified in forward scatter (FSC), a measure of size and/or side scatter (SSC), a measure of granularity. Solutions of PBS, VV and VV + YOYO-1 were analysed and the results are shown in Figure 4.4.

The population that was observed for VV was in line with what is reported in the literature; VV was identifiable in SSC, but not in FSC. [138, 139] As YOYO-1 is a green fluorescent nucleic acid stain, any fluorescent particles detected in the

FL-1 channel should correspond to stained VV particles. The histogram for FL1 of the VV no YOYO-1 and VV-YOYO-1 sample (both ungated) are shown in Figures 4.4d and 4.4e respectively.

There was a large number of events recorded in both samples (VV: 101625 and VV-YOYO-1: 51855). A gate for YOYO-1 positive staining (YOYO1+) was set as displayed in Figure 4.4d using the unstained VV no YOYO-1 sample (shown in green on the graphic). Positive YOYO-1 fluorescence was set as being the level of fluorescence in FL1 greater than 98% of the events in the control VV no YOYO-1 sample. In the VV-YOYO-1 sample (Figure 4.4e), a small (1256 events) but highly fluorescent (FL1) peak was observed within the YOYO1+ gate that wasn't observed in the VV no YOYO-1 sample. The small size of this peak gave way to two hypotheses: first, that at the high voltages required to detect the VV particles a large amount of background "noise" events were detected as well as real "VV-YOYO-1" events and second, that the staining efficiency of YOYO-1 on VV was low. To determine whether this was a detection issue or staining issue, gating was used to remove some of the background events. Background events were defined as events which were observed in the PBS sample. Therefore a broad gate based on FSC vs SSC was set so as to exclude the background events observed in the PBS sample as depicted in Figure 4.4f.

Histograms comparing the green fluorescence (FL1) of VV (shown in green) and VV-YOYO-1 (shown in purple) under the FSC vs SSC gating strategy are displayed in Figure 4.4g. As expected, for both VV and VV-YOYO-1 the gating strategy reduced the overall number of events to 11211 (32% of total) and 1118 (2% of total) respectively. However, this reduction in events alone didn't clarify whether this was actually removing "noise" events while preserving VV events and so it was probed whether this gate was able to retain the positive peak seen in the VV-YOYO1 events. The same YOYO1+ gate was applied to the FL1 histograms (shown in Figure 4.4g). The small (1068 events) highly fluorescent peak seen in the VV-YOYO-1 sample Figure 4.4e was still present (purple) with a median FL1 fluorescence (MFI) of 636 and the "noise" events (large peak with very low FL1

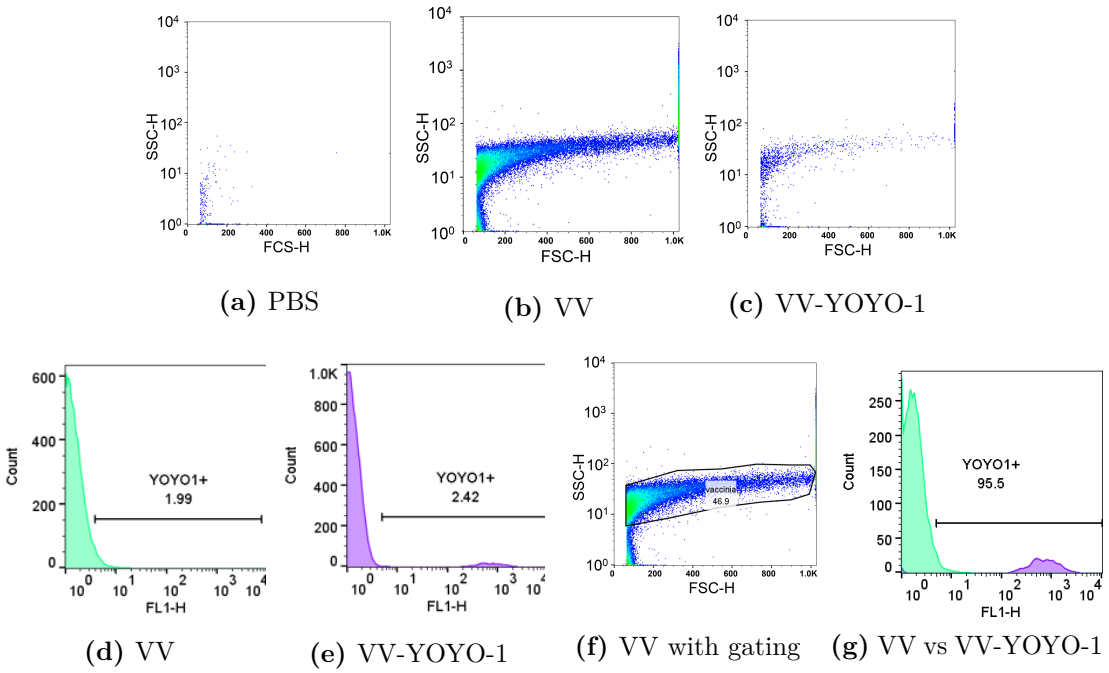
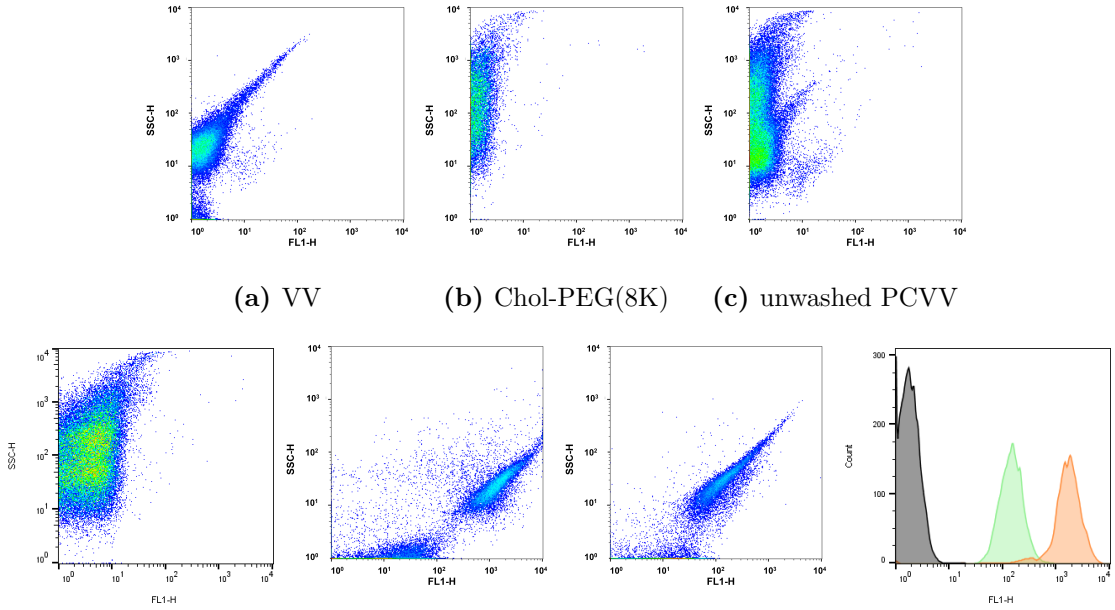


Figure 4.4: Identifying VV population using nucleic acid staining with YOYO-1. Solutions were at a concentration of 5.26 x10^3 pfu µl^{-1}. (a)-(c) FSC vs SSC for PBS, VV, VV-YOYO-1 respectively. The events counted were 102960, 101625 and 51855 respectively. (d) Gating for VV. (e)& (f) FL1 histograms for VV and VV-YOYO-1 respectively (without gating applied). It was observed that, though small, only the VV-YOYO-1 showed an above-background peak in FL1. (g) Histogram in FL1 overlaying data from panels (e) and (f) after the gating strategy was applied. Green coloured peak on the histogram is VV (count 11211) and purple coloured peak on the histogram is VV-YOYO-1 (count 1068).

in 4.4e) were substantially reduced in the FL1 channel. This suggested that the FSC/SSC gate used for VV did manage to reduce noise events while maintaining VV (as identified by nucleic acid stain).

It is noted that the subpopulation of VV-YOYO-1 which displayed "positive" staining (as measured by MFI in FL1) is smaller than the sub-population of unstained VV gated for using the FSC/SSC gate. This is thought to be due to the fact that the initial total number of events recorded in the VV-YOYO-1 sample was lower. This difference in total events recorded led to a substantial difference in the total number of events that was included in the FSC/SSC gate when comparing the VV and VV-YOYO-1 samples. Hence any direct comparison of the number of events within the FL1 region cannot be made as this would need to assume that the number of events detected within the gate were comparable. As the median FL1 fluorescence



(a) VV **(b)** Chol-PEG(8K) **(c)** unwashed PCVV

(d) FITC-PEG-Chol **(e)** FITC-PCVV **(f)** FITC-PEG + VV **(g)** Histogram, Fl-1

Figure 4.5: Determining VV coating using FITC-PEG(10K)-Chol. (a)-(f) SSC vs FL-1 plots of VV, Chol-PEG(8K), PCVV (unwashed), FITC-PEG(10K)-Chol, FITC-PCVV (FITC-PCVV) (washed) and FITC-PEG + VV (washed). Both FITC-PCVV and FITC-PEG + VV display a shift in the FL1 axis compared with VV alone. (g) Histogram displaying the FL-1 fluorescence of gated VV populations in VV (grey), FITC-PEG + VV (green) and FITC-PCVV (orange). The event counts were VV: 10341, FITC-PEG + VV: 5829 and FITC-PCVV: 5446.

in the VV-YOYO-1 sample was substantially higher than that of the VV sample, it was concluded that successful identification of a VV population was possible but that if the staining efficiency was low, then further analysis on this positively stained population could be a conservative subsection of the total VV population.

Subsequently, experiments were performed to determine the feasibility of using flow virometry to analyse coating of VV with a fluorescently labelled Chol-PEG. 10 mg mL^{-1} FITC-PEG(10K)-Chol was pre-incubated with VV (see section 2.2) coating. Samples were then washed as described in section 2.2.1. Flow virometry was used to analyse and compare samples of FITC-PEG(10K)-Chol-VV (FITC-PCVV), with controls of VV alone, PEG(8K)-Chol alone (to account for the possibility of detecting Chol-PEG micelles), PCVV (unwashed), FITC-PEG(10K)-Chol alone, and FITC-PEG (i.e no cholesterol) + VV. The results are shown in Figure 4.5.

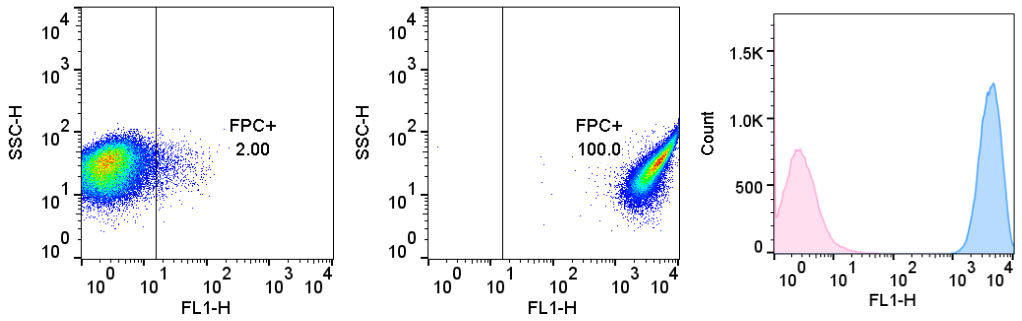
The unwashed PCVV sample (Figure 4.5c) had a large amount of background

scattering when compared with VV (Figure 4.5a) which is likely due to the abundance of free PEG in the solution, as the same scattering can also be seen in the samples of Chol-PEG(8K) alone and FITC-PEG(10K)-Chol alone (Figures 4.5b and 4.5d respectively). This large background scattering was reduced in the washed FITC-PCVV sample (Figure 4.5e), thus confirming the washing procedure (see Chapter 2 section 2.2.1) achieved robust purification of FITC-PCVV from free, un-integrated, FITC-PEG(10K)-Chol.

Gating for VV population in FSC vs SSC was performed on samples as depicted in Figure 4.4f. Comparing the FL-1 histograms for gated populations in VV, FITC-PCVV and PEG-FITC + VV samples (Figure 4.5g), distinct median fluorescent intensities were observed for each sample. Unmodified VV had a negligible fluorescence (MFI value of 1.64) in FL-1. Comparatively, within the same gated VV population, the FITC-PCVV sample had a MFI of 1625, suggesting that despite the multitude of washes, the FITC-PEG(10K)-Chol was successfully embedded in the VV membrane and the VV population was highly fluorescent.

To ensure that the cholesterol group was the element of the FITC-PEG(10K)-Chol chain which was embedding into the VV membrane and not the FITC group, a PEG-FITC +VV control was analysed. The VV population of PEG-FITC + VV sample had a MFI of 144 which was >10-fold lower than the MFI of FITC-PCVV. The populations of FITC-PCVV and PEG-FITC + VV gated for VV contained a similar number of events, 5446 and 5829 respectively. This indicates that although there was a small amount of PEG-FITC sticking to VV membranes, the level of interaction was substantially lower than that seen with FITC-PEG(10K)-Chol. This demonstrated successful coating of VV by FITC-PEG(10K)-Chol, even after washing, via the proposed mechanism of cholesterol embedding in the VV lipid membrane.

Once evidence of cholesterol embedding as a mechanism of coating was shown, robust validation of the coating method using multiple replicates (n=4) was performed with an increased viral sample concentration of 3.4 x10^4 pfu µl^{-1}, as shown in Figure 4.6. VV populations in all samples were gated by FSC vs SSC as described



(a) VV **(b)** FITC-PCVV **(c)** Histogram, FL-1

Figure 4.6: Confirming VV coating using FITC-PEG(10K)-Chol and BD FACS Calibur cytometer. Samples were first gated using the FSC/SSC gate shown previously in Figure 4.4f to exclude particles detected in control samples. (a) & (b) SSC vs FL-1 plots of VV and FITC-PCVV (FITC-PCVV). FITC-PCVV displays a shift in the FL1 axis compared with VV alone. An FPC+ gate was set via the unstained VV population to include 2% of recorded events. Anything with a FL1 fluorescence above this gate was considered to be positively stained. (c) Histogram displaying the FL-1 fluorescence of gated VV populations of VV (pink) and FITC-PCVV (blue). The event counts were of samples displayed in this histogram are VV: 36082 and FITC-PCVV: 37744. Data shown is representative of n=4 replicates.

previously (Figure 4.4f), and fluorescence of a FITC-PEG(10K)-Chol polymer was again used to confirm polymer coating when analysed with flow virometry.

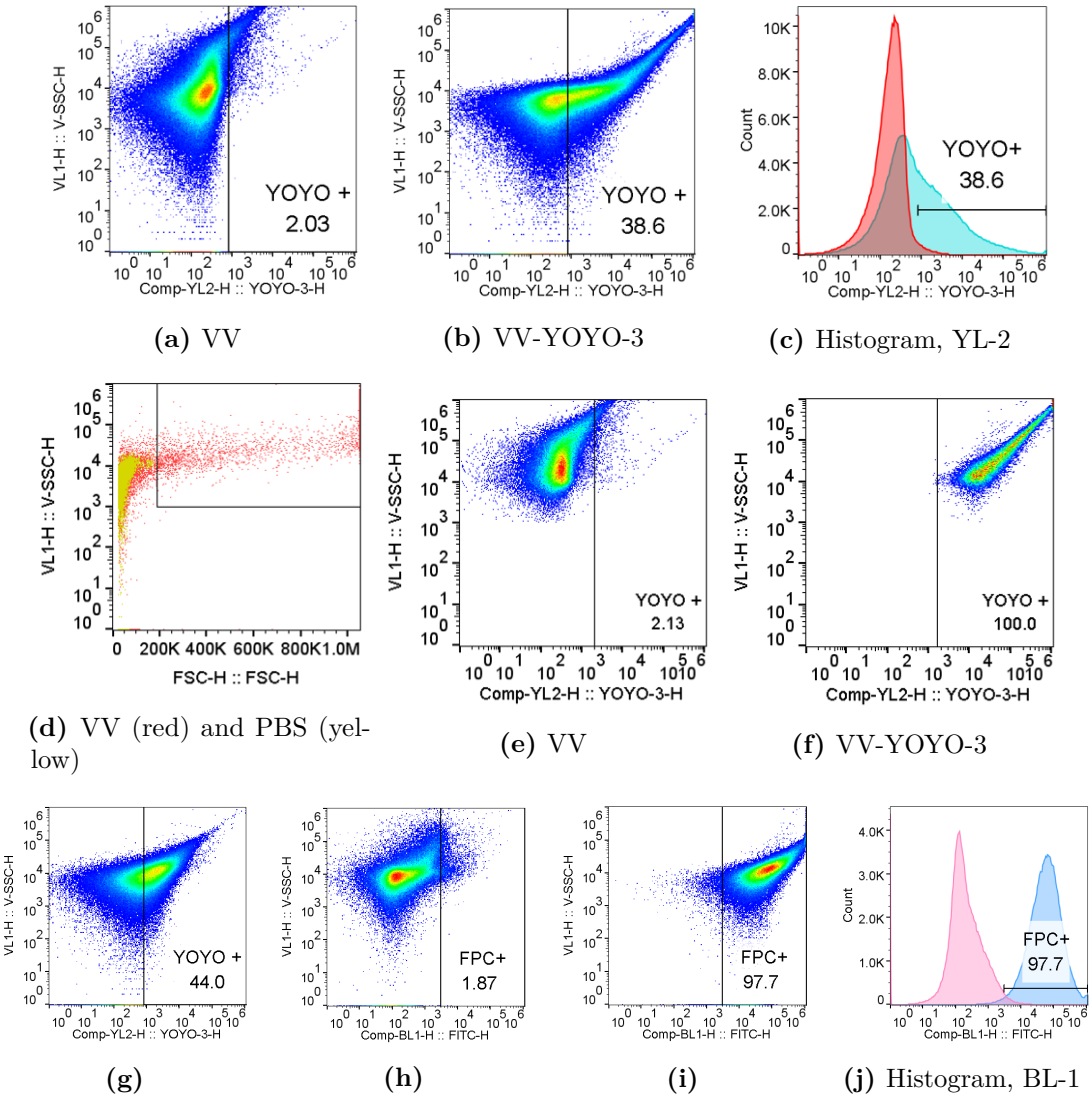
A gate for FITC positive staining (FPC+) was set as displayed in Figure 4.6a using the unstained VV sample. Positive FITC fluorescence was set as being the level of fluorescence in FL1 greater than 98% of the events in the control VV sample. In these experiments (Figure 4.6), strong FITC signal was obtained in the FITC-PCVV samples with a mean, across n=4 replicates, of 99.9% of events showing positive FITC staining (FPC+) and over a 1000-fold increase in the mean MFI (FL-1) when compared with unmodified VV. This suggests that, within the VV gated population, all of the recorded events in all four of the FITC-PCVV samples displayed FITC staining to a substantial extent. Therefore, these results and those of the previous experiment (Figure 4.5g), provided evidence of the successful production of a polymer coated VV using a cholesterol anchor.

VV detection via a nucleic acid stain and coating with a fluorescently labelled polymer was then investigated using an Attune NxT^{TM} flow cytometer (Invitrogen) which was adapted to detect side scatter through a violet laser (V-SSC) (as described

in section 2.4). This allowed clearer resolution of VV particles while allowing for detection of both a YOYO-3 nucleic acid stain (Yellow Laser-2, YL-2) and a FITC-PEG-Chol (Blue Laser-1, BL-1) in order to identify a polymer coated vaccinia population using fluorescence.

Initial tests to determine the settings required for identification of a YOYO-3 stained VV on the Attune NxT Cytometer were undertaken. Solutions of VV, VV-YOYO-3 and PBS were analysed and the results shown in Figures 4.7a to 4.7c. Similarly to results obtained using the BD FACSCalibur, the population that was observed for VV in FSC vs V-SSC plots was in line with what is reported in the literature; VV was identifiable in SSC but not in FSC. [138, 139] Therefore plots are shown comparing the V-SSC and YOYO-3 fluorescence. As seen in Figure 4.7c, a YOYO-3 stained VV population was successfully identified. YOYO-3 is an orange fluorescent nucleic acid stain which only fluoresces when it is bound to DNA, and hence, any fluorescent particles detected in the YL2 (561-620/15) channel should correspond to stained VV particles. A gate for YOYO-3 positive staining (YOYO+) was set as displayed in Figure 4.7c using the unstained VV control sample (shown in red on the graphic). Positive YOYO-3 fluorescence was set as being the level of fluorescence in YL-2 greater than 98% of the events in the control VV sample. Figure 4.7b shows that 38.6% of the events detected stained positively for YOYO-3 in the VV-YOYO-3 sample.

It was therefore concluded that in these conditions, successful identification of the YOYO-3-stained VV population was possible and hence by gating for positive YOYO-3 staining, a VV population could be identified with certainty. As these populations were not gated in FSC/SSC before YOYO+ gating was performed, it is hypothesised that a number of the 61.4% unstained events are events due to background noise. To determine the staining efficiency of YOYO-3 as a VV nucleic stain, these background events would need to be removed by FSC/SSC gating first. When FSC/SSC gating was performed as in Figure 4.7d to remove events that were present in PBS alone samples, the events counts reduced to 9.4×10^4 for unstained VV and 2.7×10^4 for VV-YOYO-3. 100 % of the events maintained after



(a) VV **(b)** VV-YOYO-3 **(c)** Histogram, YL-2

(d) VV (red) and PBS (yellow) **(e)** VV **(f)** VV-YOYO-3

(g) **(h)** **(i)** **(j)** Histogram, BL-1

Figure 4.7: Identifying VV population using Flow Virometry with a nucleic acid stain (YOYO-3) and confirmation of coating with a FITC-PEG-Cholesterol polymer within this YOYO-3 population. Solutions were at a concentration of $5.26x10^3$ pfu/ µL. Violet-SSC (V-SSC) vs YL2-H for VV (panel a) and VV+YOYO (panel b) respectively. The events counted were $3.55x10^5$ and $4.31x10^5$ respectively. (c) Histogram in YL2-H, red coloured peak on the histogram is VV and blue coloured peak on the histogram is YOYO + VV. (d) Overlay of PBS and VV to determine V-SSC / FSC gate. (e&f) V-SSC/FSC subpopulation of VV (e) and VV-YOYO3 (f) gated for YOYO-3. (g) V-SSC vs YL2-H for FITC-PCVV-YOYO-3 ungated. (h, i) V-SSC vs Blue Laser-1 (BL-1) plots of VV-YOYO-3 (panel h) and FITC-PCVV-YOYO-3 (panel i), from a YOYO-3 gated VV population (as shown in (g)). The events counted were $1.66x10^5$ and $1.74x10^5$ respectively. (j) Histogram displaying the FITC fluorescence of gated VV (pink, MFI= 165) and FPC (blue, MFI= $5.63x10^4$) populations.

FSC/SSC gating in the VV-YOYO3 sample were stained positively for YOYO-3 (displayed in Figures 4.7e and 4.7f).

An investigation to characterise coating of VV with a fluorescent PEG-Chol (FPC) on a YOYO-3 gated VV population was undertaken. 10 mg mL^{-1} FITC-PEG(10K)-Chol (FPC) was preincubated with VV to form a YOYO-3 stained coated VV which was then washed as described in section 2.2. Flow virometry was used to analyse and compare samples of FITC-PEG(10K)-Chol-VV-YOYO-3 (FITC-PCVV-YOYO-3) and VV-YOYO-3. The results are shown in Figure 4.7. The recorded events were gated for VV using YOYO-3 fluorescence and viral FITC fluorescence was used to confirm the polymer coating using the BL1 channel (488-530/30). Virus particles with a fluorescence higher than the control sample (VV-YOYO-3) were considered coated with a FITC-PEG(10K)-Chol (FPC positive) and were gated for. The percentage of events that were within this gate were quantified and denoted 'FPC+'.

Comparing the BL1 histograms for VV and FITC-PCVV (Figure 4.7j), distinct median fluorescent intensities were observed for each sample. Non-modified VV had a very low fluorescence with MFI (BL1) of 165 when compared with the FITC-PCVV sample which had a MFI of $5.63x10^4$, suggesting that despite many washes, the FITC-PEG(10K)-Chol was successfully embedded in the VV membrane and the VV population (97.7% positive) was highly fluorescent.

4.3 Results: Interaction of VV and PCVV with Human Blood Components

Section 4.2 demonstrated formation of a polymer coated VV which was able to successfully infect cells in the presence of 5% pooled human serum (Figure 4.2). While these results suggest potential for enhanced *in vivo* performance of PCVV, further investigations were needed to study the effect of whole blood from a donor previously exposed to VV by vaccination as a child, as this model would more accurately recapitulate the barriers to clinical use of VV [131]. Further

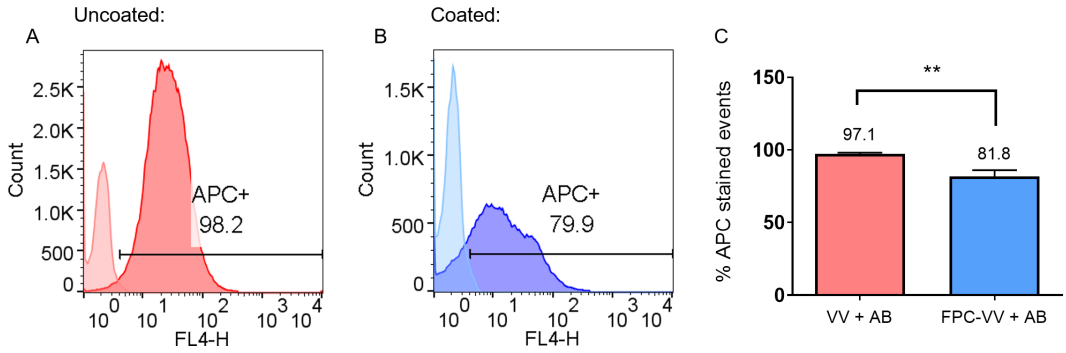


Figure 4.8: Comparing the binding of a neutralising anti-vaccinia antibody to coated and uncoated VV samples using Flow Virometry and an anti-vaccinia primary antibody raised in rabbit (aVV) and anti-rabbit secondary antibody labelled with fluorophore APC, which is detected in the FL4 channel. (a) A representative histogram of the VV + aVV group. Naked VV (red) showed 98.2% of events stained positively for APC. (b) A representative histogram of the PCVV + aVV group. PCVV (blue) showed 79.9% of events stained positively for APC. (c) Graph displaying the mean percentage of APC stained events. Antibody binding was significantly lower for PCVV (blue) than for naked VV (pink) as determined using a two tailed unpaired t-test, p = 0.0038, n=3, key: ** = p<0.01

investigations into PCVV's interaction with neutralising antibodies and fresh whole blood were performed.

4.3.1 Impact of PEG-Cholesterol Coating on VV Binding of Neutralising Antibodies

One way to extend the bloodstream circulation half-life of VV following IV injection is to reduce the binding of neutralising anti-VV antibodies (aVV), which are present in a large proportion of the population (80% vaccine coverage was achieved in many countries by 1969). [219] Therefore, studies were performed to determine the efficacy of coating VV in reducing antibody binding and thereby potentially increasing circulation half-life.

The binding of a neutralising antibody (aVV) to unmodified VV and PCVV particles, formed and stained as described in section 2.4.3 and 2.4.3 respectively, was investigated.

Virus particles were incubated for 40 minutes with aVV antibody (which had been raised in rabbit) (abcam, ab35219) at a virus to antibody ratio of 1:50. Binding was detected through conjugation with an anti-rabbit IgG secondary antibody

conjugated to APC fluorophore and flow virometry. Viral particle fluorescence was used to quantify the antibody binding via flow virometry. Samples were first gated for a VV population as described in section 2.6.1. Figure 4.8a and b show representative histograms of VV (red) and PCVV (blue) antibody binding respectively. Virus particles with a fluorescence higher than the control sample (VV alone) were considered APC positive and were gated for. The percentage of events that were within this gate were quantified and denoted 'APC+'. The mean percentage of events stained for APC of three samples was taken and the result shown in Figure 4.8c. There was substantially and significantly higher aVV binding of VV, with a mean of 97.1 +/- 1.0% events bound with aVV when compared with a mean binding of 81.8 +/- 4.3% PCVV events ($p = 0.0038$). The mean MFI (FL4 channel) for the VV gated population of each sample was calculated to be 20.8 (+/- 3.8) for VV and 11.6 (+/- 1.4) for PCVV. These data suggest that the intensity of aVV binding was almost double that of the PCVV.

4.3.2 Distribution Of VV and PCVV In Human Blood Components

To better understand the possible effects of polymer coating on VV's circulation kinetics and infectivity, it was important to determine any difference in the distribution of VV and PCVV in whole blood. Whole blood samples were collected in sodium heparin vacutainers from a healthy volunteer who had been exposed to the virus by vaccination as a child. Samples were then mixed with either VV or PCVV for 15 minutes as described in section 2.6. Separation into erythrocyte and plasma blood components then followed (samples were centrifuged at $2000g$ for 5 minutes) and VV genome (VG) quantification was performed using qPCR (see methods in section 2.7). Standards for VV and PCVV were made up in human plasma and erythrocytes. The results (Figure 4.9) showed that 71% of the initially added copies of VV was recovered, while only 34% of the PCVV copies were recovered. Based on the raw concentration obtained from qPCR analysis, there was significantly more VV association with erythrocytes than PCVV (a difference of 4.83×10^7 +/-

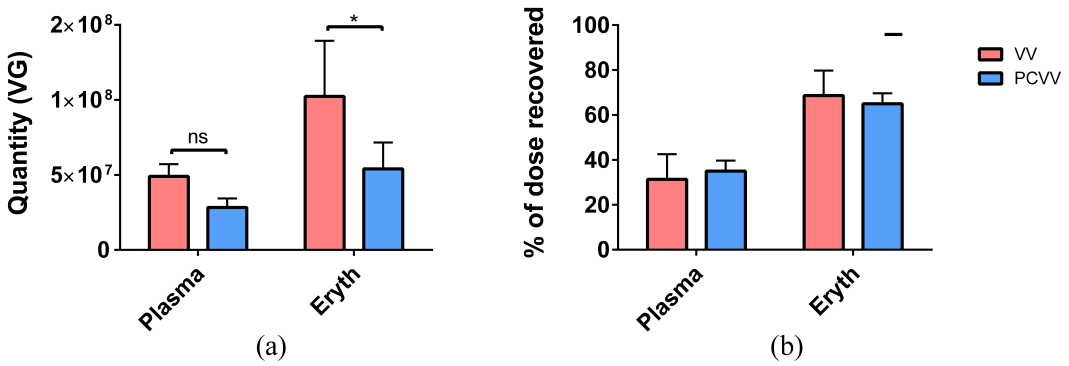


Figure 4.9: Distribution of VV and PCVV in whole blood fractions collected and separated in Sodium Heparin Vacutainers. (a) Number of VG in blood fraction containing Plasma and Erythrocytes. The mean overall recovery of VV was 1.5 x 10^8 VG and PCVV was 8.5 x 10^8 VG. (b) Percentage of recovered dose in Plasma and Erythrocytes. The number of pfu recovered in each section were divided by the total number of pfu recovered for each sample and the averages for each group are displayed here. After correcting for the difference of recovery, there was no significance in the dose % recovery for PCVV and VV both in the erythrocytes and plasma.
n=4, ANOVA key: ns = p> 0.05, * = p < 0.05, - = ns on any group

3.1x10^4 VG). Due to the difference in total recovery, a more fair comparison of genome content in each blood component was done using the percentage of the dose recovered for each sample. When the quantity of VV and PCVV was calculated as a percentage of the total dose recovered, there was no significant difference between the level of VV or PCVV association to either erythrocytes or plasma.

4.3.3 Investigating the stability of VV and PCVV in Human Plasma

The interaction of VV and PCVV in the plasma is of great interest as this is where the majority of neutralization occurs (section 1.3.1). This section describes the *in vitro* studies performed to compare the stability (and hence ability to infect A549 cancer cells) of VV and PCVV in the presence of fresh human plasma (as opposed to pooled human serum) from a donor who had been pre-exposed to VV during childhood vaccination. PCVV samples were washed as described in section 2.2.1 in all experiments.

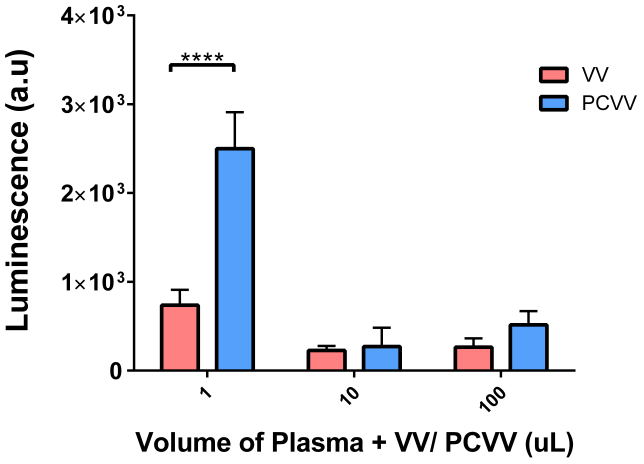
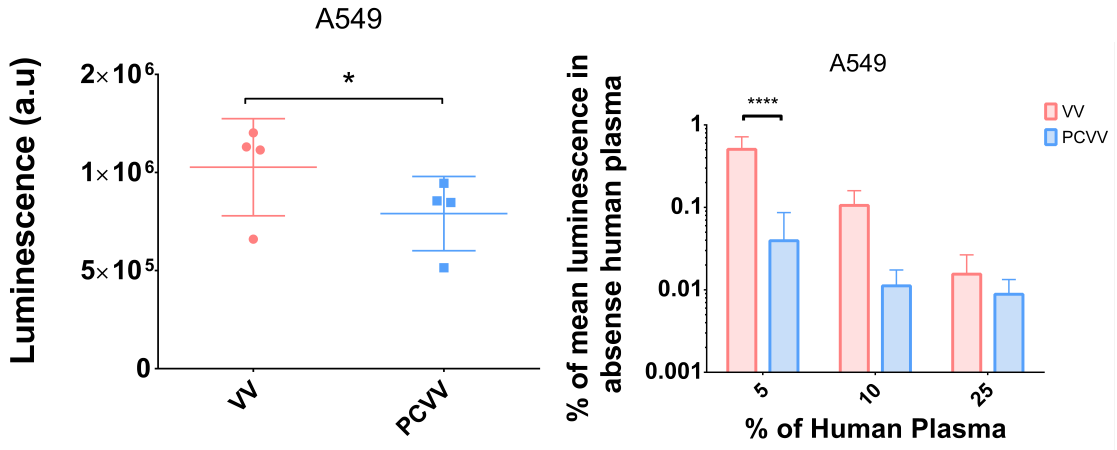


Figure 4.10: Infection levels after 24 hours of A549 cells incubated with increasing volumes of plasma from whole blood which was pre-mixed with VV (pink) and PCVV (blue) for 15 minutes. There is a significant difference in the levels of infection observed after incubation with 1 µL of plasma infected with PCVV vs VV. n=4, ANOVA key: **** = $p < 0.0001$. Error bars represent standard deviation.

First, the effect of pre-incubation with whole blood on the infectivity of VV and PCVV in A549 cells was investigated. To simulate the conditions of VV circulation in the body, the virus samples were incubated for 15 minutes at 37 °C in whole blood collected in CPT vacutainers coated with sodium heparin and then separated into their blood fractions as described in section 2.6.2. The plasma fractions were then used in infectivity studies with A549 cells whereby the levels of cell infection by virus were measured 24 hours after infection.

The effect of increasing the concentration of pre-infected plasma per well on infection levels after 24 hours is shown in Figure 4.10. Concentrations of VV and PCVV in the infected plasma samples were determined by QPCR and found to be 88 pfu μL^{-1} and 98 pfu μL^{-1} respectively.

At 1 µL plasma/well (0.5% total well volume, approximately 0.01 pfu/cell) there was a substantial (almost 3-fold) and significant ($p<0.0001$) increase in infection (as measured by luciferase production) for cells incubated with PCVV in plasma compared to those incubated with naked VV in plasma. At both 10 and 100 µL plasma/well (5% & 50% total well volume, and 0.1 pfu/cell & 1 pfu/cell respectively), the levels of infection were greatly decreased for both VV and PCVV.



(a) (b)

Figure 4.11: Infection levels of A549 cells after 24 hours of infection by 0.1 pfu/cell doses of VV and washed PCVV in increasing concentration of human plasma. (a) Infection levels of VV and PCVV infected A549 cells in the absence of human plasma. (b) Infection levels in the presence of 5%, 10% and 25% fresh human plasma as assessed by expression of the luciferase reporter gene as a percentage of the infection levels in 0% fresh human plasma. n=4, Two-way ANOVA with post hoc sidaks test for multiple comparison. ANOVA key: ns = p> 0.05, * = p < 0.05, **** = p < 0.0001. Error bars represent standard deviations.

There are several factors impacting on the luciferase output of such experiments. Firstly, plasma alone can cause cell death (due to the impact of complement proteins or anticoagulants). Such cell death leaves fewer cells available for infection and ultimately less luciferase expression. Secondly, the oncolytic life cycle of the virus means high levels of infection can kill cells and mask the level of luciferase produced and detected. Finally, there is the output of interest, whereby higher levels of infection give higher levels of expression. In order to unpick these factors and determine what was causing the decrease in infection as the volume of infected plasma increased, a study with a fixed concentration 0.1 pfu/cell of VV and PCVV in an increasing concentration of human plasma was performed with concordant MTS analysis for cell viability. PCVV was formed and purified as describe in section 2.2.1.

Increasing concentrations of human plasma (5%, 10% and 25%) were incubated with A549 cells and infections at 0.1 pfu/cell of VV or PCVV performed. In the absence of human plasma (Figure 4.11a, 0%) a small but statistically significant decrease in infectivity between VV (mean luminescence of 1.03 x10^6 +/- 2.5 x10^5) and washed PCVV (7.91 x10^5 +/- 1.89 x10^5) was observed. Therefore it was determined

that even after washing away excess polymer, PCVV still showed a knockdown in infectivity when compared to that of naked VV. Infection of A549 cells by VV or PCVV in the presence of human plasma was determined by luciferase assay for each plasma concentration and is recorded as the percentage of luciferase expression recorded in the absence of human plamsa (0%). VV showed higher infection levels of 0.5 (+/- 0.1)% when compared with PCVV 0.04 (+/- 0.02) % ($p<0.0001$) in the presence of 5% fresh human plasma (Figure 4.11b). No significant differences were found between infection levels at higher concentrations of fresh human plasma.

To determine whether this ablation of infection was due to cell death by the plasma alone or due to neutralisation of the virus an MTS assay was performed on A549 cells infected under the same protocol as for the infectivity luciferase assay (Figure 4.11). In the absence of human serum (Figure 4.12, 0%), the percentage of viable cells in the PCVV samples and the VV samples were not statistically different. The MTS assay showed that cell death increased as the percentage of human plasma increased from 0 to 25%. This increase in cell death was greater for PCVV in particular at both 5% (VV 95% and PCVV 78%, $p<0.01$) and 10% (VV 80% and PCVV 65%, $p<0.01$) which could indicate more oncolysis. Hence, it is possible the luciferase levels reported in Figure 4.11b for PCVV in 5, 10 and 25 % plasma could be an underestimate for the levels of infection achieved. It was determined that making conclusions on the difference in infectivity for the 10% and 25% human plasma groups would not be possible given the significant impact on cell viability recorded at these plasma concentrations.

The infection study with 0.1 pfu/cell VV or PCVV was repeated in a DLD cancer cell line. This study was to determine whether the same knockdown in infectivity was seen between VV and PCVV in the absence of human plasma in a DLD cancer cell line. The impact of the fresh human plasma on the infection levels (luciferase assay) achieved in DLD cells in increasing concentrations over a lower range (2.5%, 5% and 10%) of human plasma was also ascertained. As shown previously, in the absence of human plasma a significant ($p<0.01$) knockdown in infection of DLD cells was seen between VV (mean luminescence of 6.15 $x10^5$ +/-

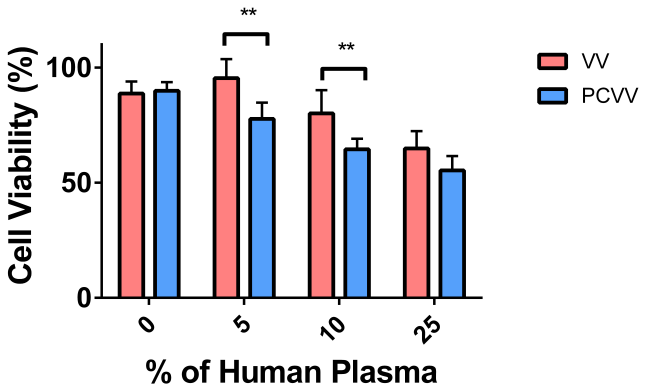


Figure 4.12: Viability of A549 cells after 24 hours of infection by 0.1 pfu/cell doses of VV and washed PCVV in 0%, 5%, 10% and 25% human plasma. n=4, Two-way ANOVA with post hoc sidaks test for multiple comparison. ANOVA key: ns = p> 0.05, * = p < 0.05, ** = p < 0.01. Error bars represent standard deviations.

6.02 x10^4) and washed PCVV (4.12 x10^5 +/- 4.05 x10^4) (Figure 4.13a). For DLD cells incubated with increasing concentrations of human plasma (Figure 4.13b), the same reduced infectivity was seen across the range of human plasma concentrations as was reported for A549 cells. In the presence of 2.5% human plasma, 0.09 (+/- 0.06) % of luminescence reported in the absence of human plasma was seen with cells infected with VV. Comparatively, PCVV had 0.03 (+/- 0.003) % (p<0.0001). There was no significant difference found between luminescence values observed for VV and PCVV infected cells in the presence of 5% and 10% of human plasma.

To further investigate the impact of human plasma concentration on cell viability and infection, a VV encoded with a green fluorescent protein reporter gene (VV-GFP) was used instead of VV-luc, and infection (as determined by GFP production in infected cells) was detected using fluorescent microscopy. This enabled cell viability to be observed by brightfield microscopy, while at the same time that fluorescence levels in viable cells could be determined. DLD cells were infected with 0.1 pfu/cell of VV or washed PCVV and were incubated in either 0, 5 or 10% human plasma. After 24 hours cells were imaged using brightfield and fluorescence microscopy (FITC filter). Wells were imaged under brightfield to determine cell viability, while fluorescence microscopy was used to detect cells successfully infected with VV-GFP (Figure 4.14). With both VV and PCVV in the absence of human

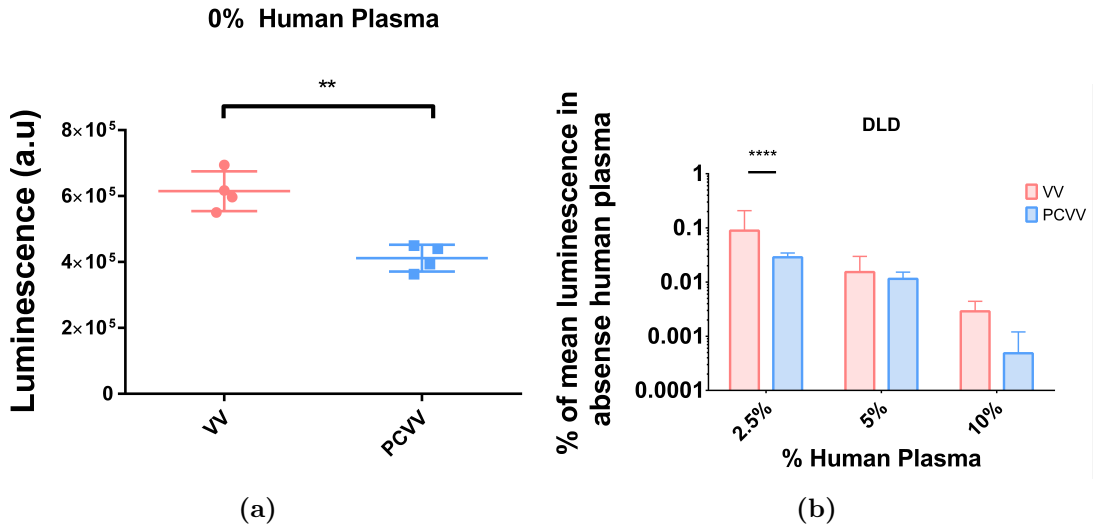
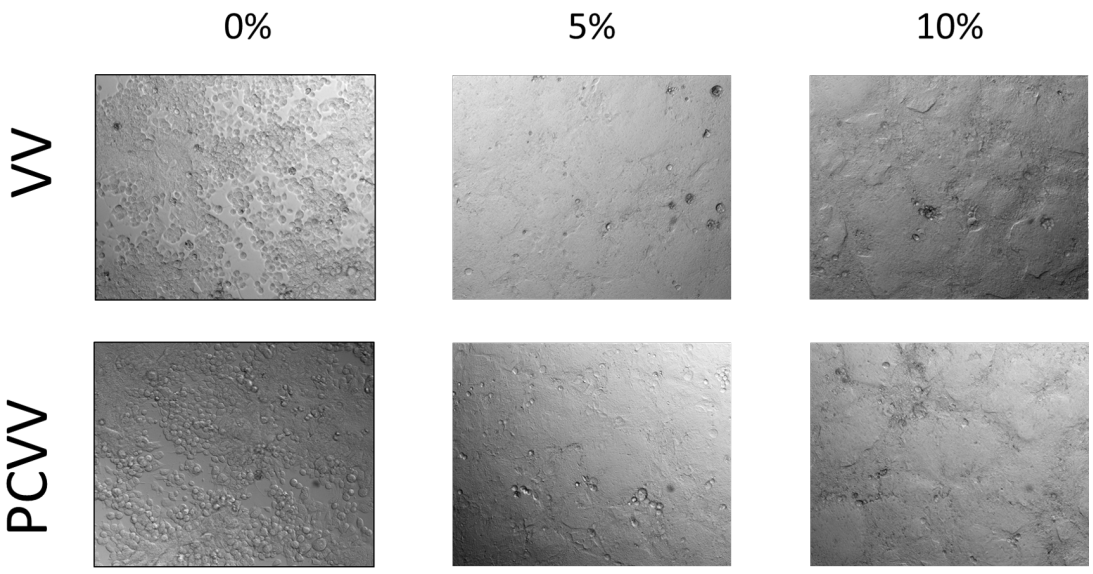


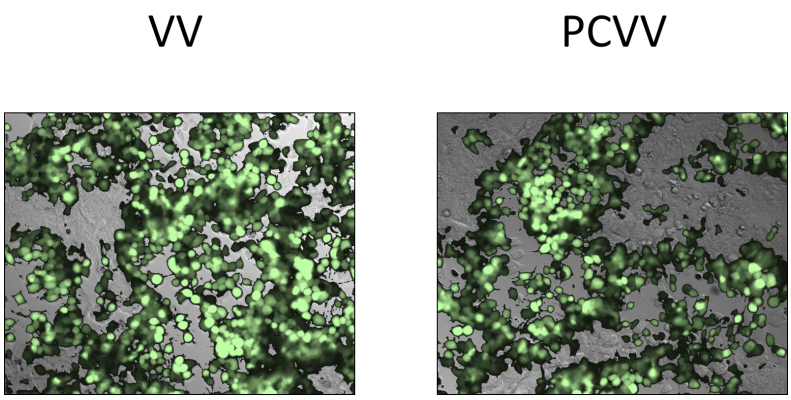
Figure 4.13: Infection levels DLD cells after 24 hours of infection by 0.1 pfu/cell doses of VV and washed PCVV in increasing concentrations (2.5%, 5% and 10%) of human plasma. (a)Infection levels of VV or washed PCVV infected DLD cells in the absence of human plasma. (b) Infection levels of VV or washed PCVV in the presence of 0%, 5%, 10% and 25% human plasma as assessed by expression of the luciferase reporter gene. n=4, (a) unpaired two sided t-test and (b) Two-way ANOVA with post hoc sidaks test for multiple comparison. ANOVA key: ns = p> 0.05, * = p < 0.05, ** = p < 0.01. Error bars represent standard deviations.

plasma, cell infection was clearly visible in brightfield with evident cell rounding seen (Figure 4.14 0%). Cell rounding was greatly reduced to just a few cells in each view for both VV and PCVV in 5% and 10% plasma (Figure 4.14 5% and 10%), suggesting that many fewer cells were infected. From brightfield microscopy it was determined that cell viability was impacted in all cells incubated with 5% and 10% human plasma as large amounts of cell debris was observed.

When GFP levels were studied it was apparent that in the absence of human plasma, wells incubated with VV showed more widespread infection and higher intensity of fluorescence signal than those incubated with PCVV (Figure 4.14b). This was in line with the knockdown in infectivity upon coating that had been observed with VV-luc (Figure 4.11a). For wells incubated with 5% and 10% human plasma, no fluorescence was observed for either VV or PCVV. As GFP is only produced during VV-GFP replication within infected cells, this suggests that there was no cell infection in any of the samples incubated with VV or PCVV in the



(a) Brightfield



(b) Fluorescence

Figure 4.14: Brightfield and fluorescence microscopy of DLD cells infected with 0.1 pfu/cell of VV or washed PCVV encoded with a GFP reporter gene incubated with 0%, 5% or 10% human plasma. After 24 hours wells were imaged with brightfield and fluorescence microscopy. (a) Brightfield images of representative wells. (b) Images of overlaying brightfield and fluorescent (FITC, green) images for wells infected with VV or PCVV in the absence of human plasma. Images were processed to set black to transparent on fluorescence images and white was re-coloured to green. A representative set of images are shown here. n=5

presence of 5% and 10% human plasma.

Hence, combining what was seen with the MTS assay results in A549 cells and the observations seen in microscopy of DLD cells using VV-GFP, it was determined that the ablation of infection signal was likely due to both cell viability loss as a result of incubation in human plasma, and neutralisation of VV and PCVV. It was therefore determined that both VV and PCVV were impacted by neutralisation of fresh human plasma containing anti-VV antibodies, but the precise degree of this inhibition was difficult to assess due to the confounding factors of cell death caused by plasma components and oncolysis. There was however a suggestion that the impact of plasma was reduced for PCVV, and that losses in infectivity due to coating could be recouped somewhat in highly neutralising environments.

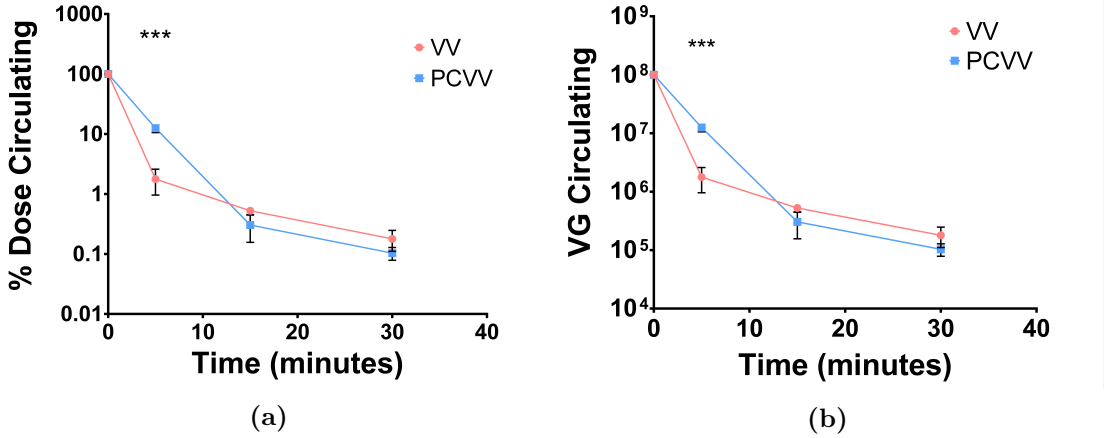
4.4 Results: Investigating the impact of polymer coating on circulation kinetics in murine models

A pharmacokinetic (PK) study was performed to determine the circulation kinetics of VV and PCVV in CD1 nude mice bearing HEPG2 xenograft tumours. Blood samples (20 µL) were taken at time points 5, 15 and 30 minutes after infection. VV and PCVV samples were made up as described in section 2.8.4.1. Notably free polymer was not purified from PCVV in this study, as it was felt the potential impact of free polymer would not be as significant a factor in 1.5 mL of moving mouse blood as it may have been in the 100 µL of a stationary *in vitro* 96 well plate experiment. The results are displayed in Figure 4.15, both as the percentage of the dose injected (panel a) and the raw quantities of viral genome (VG) circulating as determined by qPCR (panel b).

Figure 4.15a showed a highly significant ($p < 0.0001$) increase in the percentage of injected dose of PCVV (13% +/- 2) circulating in the mice at 5 minutes post-injection compared to VV (2% +/- 1). By 15 minutes, the levels of VV and PCVV detected in circulation were similarly negligible. The experiment was ended at 30 minutes and qPCR analysis on the recovered livers and tumours from this time

point showed that over 99% of the injected dose was recovered in the liver for both groups, with no detectable level of VV or PCVV in any tumour (data not shown). From Figure 4.15bb this translates to a substantial and highly significant reduction in VG circulating at 5 minutes for VV (56-fold) compared with PCVV (8-fold). The half-life of PCVV was determined to be 1.67 minutes [95% CI:1.57 to 1.76] compare with the half-life of VV which was determined to be 0.8154 [95% CI: 0.74 to 0.92]. Area under the curve (AUC) analysis showed that this difference in VG circulating between VV and PCVV lead to an increase of the virus exposure for PCVV ($2.30x10^8$ VG min/mL) when compared with VV ($1.78x10^8$ VG min/mL).

These results provide evidence that the PEG(8K)-Chol coating of VV provides increased blood stream stability resulting in an increased concentration of PCVV circulating when compared with VV at early time-points post IV injection. This increased stability, however, did not increase PCVV tumour accumulation. Although it is important to note that the tumours used in this study were potentially too small to be effectively vascularized and that even a 5-fold increase in circulating concentration is unlikely to provide sufficient increase to allow for an 'EPR effect' to occur. Indeed the true scale and nature of the EPR effect has been recently questioned [220, 221] but even at its most marked it would be expected to take 24-48 hours to show an effect.



(a) (b)

Figure 4.15: Pharmacokinetic study comparing the circulation time of VV and PCVV in tumour bearing CD1 nude mice. 2 x10^6 pfu were injected into each mouse. The amount of VV present was determined by qPCR of blood samples obtained. (a) Circulating VV or PCVV at 5, 15 and 30 minutes in tumour bearing mice. The number of genomes obtained in each sample is shown as a percentage of 2 x10^6 pfu. (b) Circulating VV or PCVV at 5, 15 and 30 minutes shown as quantity from QPCR.
n= 3 ANOVA key: ns = p> 0.05, * = p < 0.05, ** = p < 0.01, *** = p < 0.001

4.5 Discussion

In this chapter, a novel approach to improve the anti-cancer utility of VV was undertaken. Specifically it was hypothesised that if the VV could be protected from interactions with plasma it would be able to circulate more effectively following IV injection. Such protective coating may potentially lead to increased tumour delivery due to improved passive accumulation, but would certainly provide a platform for the addition of tumour specific targeting ligand to the coat and the subsequent combination with ultrasound mediated cavitation delivery mechanisms, as reported with adenovirus. [116] The investigations detailed in this chapter have looked at three main areas; polymer coating methods of VV, whole blood stability of PCVV *in vitro* and circulation kinetics of PCVV *in vivo*.

Initially, polymer coating was validated through a series of infection studies in A549 cells in the presence and absence of pooled human serum, and was subsequently more robustly profiled using flow virometry with FITC labelled Chol-PEG. Once successful coating of PCVV was confirmed, a series of experiments determining the construct's stability in whole blood were completed. First PCVV was incubated

for 15 minutes in whole blood to simulate circulation time in the body. The whole blood was separated and qPCR analysis on the plasma and erythrocyte fractions to determine distribution was performed. Some of the VV or PCVV loaded plasma separated from the whole blood was used in an infection study in A549 cells. Studies were then undertaken to characterise the effect of increasing plasma concentration with a fixed concentration of VV and PCVV on cell infectivity and kill. Finally, the circulation kinetics of PCVV and VV were compared in a HEPG2 xenograft bearing murine model.

The main findings of the work presented in this chapter are outlined here:

1. Integration of the polymers into the lipid membrane of VV virions agreed with theory relating to lipid phase changes and meant integration would occur preferentially at a temperature of 37°C compared to 21°C, due to the lipid bilayer being more fluid at this higher temperature. This was observed in experiments where Chol-PEG(8K) had little effect on reducing or maintaining VV's (0.1 pfu/cell) infection ability in absence or presence of pooled human serum respectively when formed at 21°C. However following incubation of VV with Chol-PEG(8K) at 37°C, protection against immune neutralization was observed; there was a maintenance of infection capacity or even a 100-fold increase in infection level, in the presence of up to 25% pooled human serum (section 4.2.1).

2. It was observed that when VV was preincubated with a high concentration of Chol-PEG(8K), (10 mg mL^{-1}), this led to an increase in infection of A549 cells in the presence of pooled human serum compared to that seen in the absence of pooled human serum. Due to the increased infectivity shown for VV pre-incubated with 10 mg/mL Chol-PEG(8K) in the presence of PHS, this incubation concentration was used for formulation of PCVV in further studies.

3. Flow virometry using two different flow cytometers (BD FACS Calibur and an adapted Invitrogen Attune NxT) allowed the detection of a VV population (as detected by nucleic stains YOYO-1 and YOYO-3) which could be resolved in SSC but not FSC, in line with what has previously been reported by Tang *et al* and Arakelyan *et al.* [138, 139] This method was then utilised to resolve VV

incubated with a fluorescently labelled PEG(10K)-Chol chain in order to provide a more robust method of confirming VV coating, and enabled validation of the washing and purification of PCVV. Although polymer coating of adenovirus and adeno-associated virus has previously been reported, this is the first compelling evidence demonstrating effective coating of a vaccinia virus.

4. Neutralising anti-VV antibody binding was assessed by flow virometry and shown to be reduced for PCVV when compared to VV. The percentage of the VV gated population stained for anti-VV antibodies was lower for PCVV (81.8%) when compared with naked VV (97.1%). This is the first direct demonstration that chemical modification of the surface of VV can alter the ability of antibodies to bind to its surface. Of note in VV immunized patients, which make up a large proportion of today's cancer population, it has been reported that a prominent mechanism of VV clearance is through neutralization by anti-VV antibodies which is mediated by complement. [75] Therefore, a reduction of antibody binding and avoidance of complement could result in an increased dose of VV achieving transfer into tumours after intravenous infusion in patients.

5. Despite differences in total recovered dose when Sodium Heparin Vacutainer were used to separate whole blood components, there was no difference between the distribution of VV and PCVV within plasma and erythroctye blood fractions as a percentage of that total recovered dose. Therefore, it can be concluded that there is no significant difference in the association of VV and PCVV with these two blood fractions, when incubated in whole human blood for 15 minutes before separation. This suggests that the improved protection against aVV antibody binding provided by polymer coating was not yet sufficient to impact the binding of VV to erythrocytes. It is noted that the impact of polymer coating on the binding and interaction of VV with leukocyte fractions of whole blood was not assessed in this thesis and therefore further experiments probing whether there are any differences in the interactions between VV or PCVV with leukocytes would be interesting future work.

In a previous study by Carlisle *et al* where adenovirus was stealthed with a N-(2-hydroxypropyl)methacrylamide copolymer (PHPMA) polymer, it was reported

that stealthing with PHPMA prevented binding of the CAR receptor which reduced erythrocyte binding when compared to unmodified adenovirus. [131] The differences seen with the adenovirus is potentially due to the specificity of the few well documented cell surface receptors that are required for adenovirus cell entry. Therefore, when successful detargeting of adenovirus occurred, binding of adenovirus to cells was almost entirely ablated. [109] Vaccinia viruses infect cells through a number of different membrane fusion pathways, of which four are known and documented. [222] This may make them more challenging to fully detarget and protect and therefore may explain why less impact on erythrocyte binding was seen. [222]

Evgin *et al* reported that when VV (JX-594) was incubated with whole human blood or plasma fractions from patients which had been exposed to VV through vaccination at childhood, virus neutralization (as determined by plaque assay) was approximately equal in whole blood and plasma. This suggests that loss of infectivity was primarily due to plasma components. [75]

6. When 15 minutes of preincubation with whole blood (to mimic the circulation time of VV in the body) was performed before the plasma fractions were separated and added to A549 cells, 1 µL of PCVV/plasma was substantially and significantly more infective than VV/plasma, Figure 4.10. The pfu/µL recovery in the plasma fraction after incubation with whole blood and fractionation (as detailed in section 4.3.2) was slightly higher for the PCVV (98 pfu/µL vs 88 pfu/µL) sample which may well account for the higher luminescence values seen here. The infectivity levels at higher percentages of mixed plasma decreased to background levels, suggesting that either cell death was occurring (as a result of high plasma concentrations, or high virus titre), or that the high concentration of plasma prevented cell infection from occurring. A further study looking at cell death with increasing concentrations of premixed plasma would help to clarify this.

7. Infection studies performed in A549 and DLD cells showed that there was a significant knockdown in cell infection when 0.1 pfu/cell of a washed PCVV was used compared with VV in the absence of human plasma. Although the knockdown

in infection was not as pronounced for PCVV reported here, this follows what has previously been reported for an oncolytic adenovirus coated with pHMA polymer. [76, 106, 107, 114] The difference in the extent of knockdown could be due to several factors including, as mentioned previously, the more complex and multi-mechanistic cell binding and entry of VV compared with oncolytic adenovirus. Using techniques such as surface deglycosylation of VV particle such as that reported by Rojas *et al* may help to further detarget the virus before polymer coating using the methods described here. [126] It is also possible that the process of covalently attaching the pHPMA polymer to the oncolytic adenovirus may also have further implications on cell infectivity when compared to the cholesterol anchor method utilised here. Finally, the pHPMA polymer is multivalent whereas Cholesterol-PEG is mono-functional and so the morphology of the Cholesterol-PEG coating for VV may not result in as extensive detargeting *in vitro*.

8. The viability of A549 cells, as determined by an MTS assay, incubated with 0.1 pfu/cell after 24 hours was greatly impacted by the presence of human plasma as its concentration increased from 5% to 25%. This reduction in overall viability was also observed through microscopy of DLD cells infected at the same MOI in 5% and 10% human plasma of DLD cells. Although difficult to make conclusions due to the impact of human plasma on cell viability itself, it was observed that the cell viability of A549 cells infected with 0.1 pfu/cell of washed PCVV compared with VV was lower in the presence 5%, 10% and 25% human plasma and therefore there may be more oncolysis occurring in PCVV infected cells in the presence of human plasma than in VV infected cells.

9. Analysis of VV and PCVV circulation kinetics in a murine model showed that approximately 6-fold more virus copies remained in circulation 5 minutes after injection of PCVV, as compared to 5 minutes after injection of naked VV. The immunocompromised CD1 nude mice used in this pharmacokinetic study lack T cells and a complete adaptive immune response to pathogens, but retain an innate immune response. Hence, the enhanced circulation seen here for PCVV suggests that PCVV is able to evade the innate immune response more efficiently than

naked VV. This includes evasion of the mono-nuclear phagocytic system and hence slows the sequestration of VV from the blood stream to the liver. In this murine model, it is shown that the naked VV dose reduces 56-fold within 5 minutes of dosing whereas that reduction was substantially and significantly ($p<0.05$) reduced for PCVV which only showed an 8-fold reduction in dose. When considering the increase in circulation time reported here it is important to acknowledge the key role the adaptive immune system (which is not present in this murine xenograft model) plays in VV clearance, including specifically the role which anti-VV antibodies play. [75] It was shown here that there is a reduction in aVV antibody binding for PCVV compared with VV but it may be that there would be a substantial impact of complement mediated binding of aVV antibodies in fresh human (aVV+) blood which may go some way to explain the enhanced blood stream stability seen here in an immunocompromised murine model, but the lack of effect seen in blood deposition in fresh human blood from a donor who had been pre-exposed to VV during childhood vaccination.

Of note, despite these studies showing improved circulation kinetics of a polymer coated VV, greater accumulation of VV or PCVV within xenograft tumours did not result. This may be due to the small size of these tumours or the short duration before cull and tumour rescue; a short 30 minute window is unlikely to allow effective detection of either VV or PCVV within that time frame. A more detailed look at tumoural viral load using imaging of a reporter gene over multiple days (to allow for virus replication) may help to unpick whether a difference in accumulation due to the enhanced circulation kinetics was achieved (see Chapter 6).

Future studies comparing PCVV and VV PK in immunocompetent xenograft free murine models after single and repeated doses (hence aVV+) would enable this enhancement to be tested further. Given the previously reported viremic threshold of VV after IV infusion in patients required for successful viral load to be detected in tumours [22] (see section 1.2.1), were this substantial increase in viral load at early time points reported here to persist in the presence of aVV antibodies, the impact on its efficacy in metastatic cancer treatment could be marked.

4.6 Summary and Conclusions

In summary, it was reported in this chapter that a polymer coated VV could be achieved via a cholesterol anchor and that it could be detected using flow virometry. The small but significant reduction in infection ability of both A549 and DLD cells in the absence of human plasma supported the flow virometry data showing that a PCVV was formed. The polymer coating's impact on blood stream stabilisation was varied: no difference was reported in the blood fractionation in fresh human blood samples (donor pre-exposed to VV during childhood vaccinations) but a reduction in the percentage of antibody binding from a neutralising anti-VV antibody was reported for PCVV and substantially enhanced circulation in an immunocompromised murine model was shown. Neutralisation assays showed that there was no difference in infection levels found in VV and PCVV samples at 5, 10 and 25% human plasma (pre-exposed to VV during childhood vaccination) concentration. Therefore it could be argued that the polymer coating showed protection in the presence of human plasma which allowed its infection level to meet those of naked VV. This indicates that there has been some positive impact on PCVV's bloodstream stability but that there is opportunity for a more dense coating which could potentially provide greater protection, though this may be at the detriment to the maintained infection levels reported here. The polymer coating does provide a platform onto which tumour specific targeting ligands could be loaded, which may improve tumour accumulation using targeting as shown previously for other polymer coated oncolytic viruses such as adenovirus. [115]

The following is therefore concluded for Chapter 4:

- VV was successfully coated via a cholesterol lipid anchor with a PEG polymer and this coating occurred most effectively when VV was incubated with Chol-PEG at 37 °C for 1 hour.
- The Chol-PEG coating resulted in up to a 20% reduction in binding of a neutralising aVV antibody. In vitro infection studies on A549 and DLD cell monolayers showed that there was a knockdown in infection levels in cells

infected with PCVV when compared to cells infected with VV. In the presence of up to 10% human plasma containing aVV antibodies however, the infection levels of PCVV remained constant across the increasing concentrations of plasma where as the infection levels of VV decreased as the concentration of plasma increased.

- The Chol-PEG coating resulted in enhanced circulation kinetics for PCVV compared with VV in the first 5 minutes post IV injection in tumour bearing nude mice. The polymer coating did not however result in an increase in early tumour accumulation despite an enhanced PK.

Chapter 5

Retargeting VV to tumours over expressing Mucin-1

5.1 Introduction

As discussed in Chapter 1, the need for an oncolytic VV with enhanced bloodstream stability is crucial if it is to be adopted for widespread clinical use. In Chapter 4 coating of oncolytic VV using a Cholesterol-PEG polymer to form PEG-Chol-VV (PCVV) was demonstrated, and the impact this coating had on enhancing bloodstream stability was shown both *in vitro* and *in vivo*, culminating in a 6-fold increase in PCVV circulating at 5 minutes in a murine model compared to naked VV. However, the increased bloodstream stability came at a price: PCVV's ability to infect A549 and DLD cancer cells was inhibited when compared to that of naked VV. This reduction in infectivity was not compensated for by an increase in tumour accumulation for PCVV compared to VV, despite its enhanced pharmacokinetics (PK). Therefore, in order to realise the potential benefits provided by polymer coating it was decided that additional enhanced tumour targeting could be investigated using the attachment of a ligand to restore infectivity *in vitro* and *in vivo*. As detailed in section 1.3.1.2.2, it has been previously demonstrated for other oncolytic viruses, in particular oncolytic adenovirus, that the attachment of ligands to the polymer coat of the virion could provide specific redirection of the virus tropism. [76, 106, 107] To date however, although genetic and enzymatic modification of VV surface has been described to enhance stability and re-direct

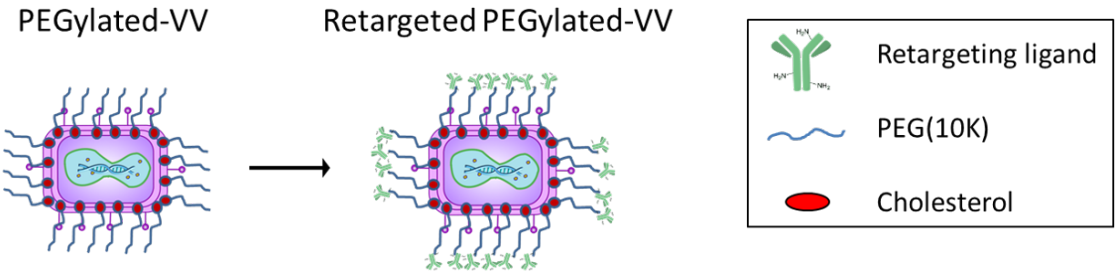


Figure 5.1: Schematic drawing depicting the PEG-Chol-VV and a retargeted PEG-Chol-VV with the addition of targeting ligands. Retargeting ligands (green) are conjugated to PEG-Cholesterol (blue-red) polymers which then embeds into the lipid bilayer of VV (purple) leaving ligand-PEG (green-blue) brushes outside the virion.

tropism [47, 126, 130, 132–134], to my knowledge, there have been no reports of attempts to chemically modify VV for enhanced protection and retargeting. The use of a Cholesterol-PEG polymer and an anti-mucin-1 (anti-MUC1) antibody (HMFG2 clone) to provide such coating and retargeting to the MUC1 tumour-associated antigen (details in section 1.3.1.4) as depicted in Figure 5.1 is investigated and described here. The aims of this chapter are:

1) Formulate a polymer coated and retargeted VV to tumour associated antigen (MUC1).

2) Assess the effect that the addition of aMUC1 targeting ligands to the polymer coating of VV has on its cancer cell infectivity and stability in human plasma.

3) Determine the impact of adding targeting ligands to the polymer coating of VV on the circulation kinetics and tumour accumulation in a tumour bearing murine model.

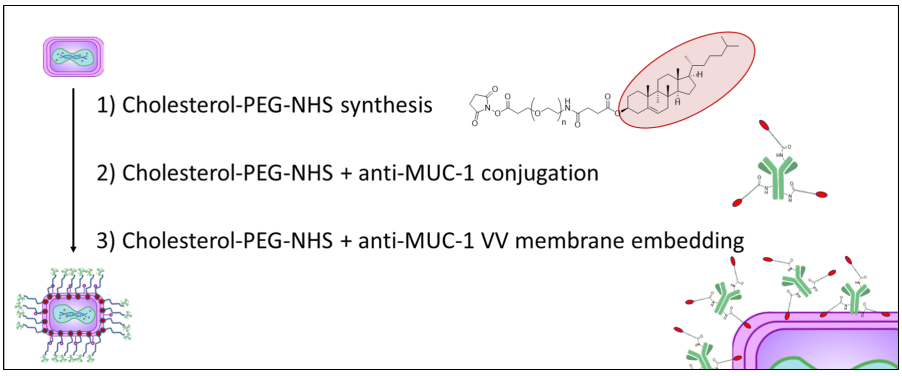


Figure 5.2: Schematic depicting the strategy by which polymer-aMUC1 conjugates were formed and added to VV to form a targeted, polymer coated VV.

5.2 Results: Formulation of an aMUC1 retargeted VV

The strategy to formulate an anti-MUC1 (aMUC1) retargeted VV (shown in Figure 5.2) was based upon the same method of polymer coating via embedding of a cholesterol group into the lipid membrane of oncolytic VV as described in chapter 4. The polymer used for the coating in the retargeted studies was conjugated with a cholesterol group on one end and an NHS group on the other end of a poly(ethylene)glycol (PEG) 10 kDa chain (Chol-PEG-NHS). This section details the conjugation process how cholesterol-PEG-aMUC1 (Chol-PEG-aMUC1) constructs were formed through reaction of the NHS group on the polymer with the amine groups on the anti-MUC1 antibody. Finally, embedding of the retargeting polymer in the VV was assessed using flow virometry.

5.2.1 Cholesterol-PEG-NHS synthesis

Prior to purchase of larger quantities of cholesterol-PEG-NHS, small pilot studies were performed to determine the feasibility of conjugating this linker to an antibody, in order to know which structure would produce a strong and stable amide link. Cholesterol-PEG (8kDa) with a carboxylic acid group (Chol-PEG-COOH) was previously synthesised by Megan Grundy and Professor Victor Ramos. The structure of the Chol-PEG-COOH used and the steps taken to produce Chol-PEG-NHS can be seen in Figure 5.4.

The structure of the product was determined by NMR analysis (not shown) and the efficiency of the COOH conversion to NHS was determined using a TNBS assay, Figure 5.3. This showed that there was 38% of PEG had NHS groups and this allowed for the concentrations of polymer used in future experiments to be chosen on the basis of the concentration of NHS groups.

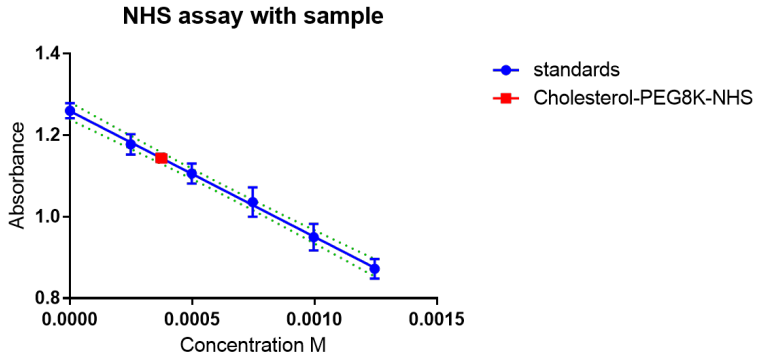


Figure 5.3: TNBS assay was performed to determine the percentage of Carboxylic acid converted to NHS.

5.2.2 Forming Cholesterol-PEG-NHS antibody conjugates

Antibody conjugates have gathered a lot of attention in literature over the past decade, predominantly due to the growth in popularity of using antibody-drug conjugates in clinical treatment. One of the most widely used techniques involves reacting lysine side chains on the antibody with an N-hydroxy-succinimide (NHS) ester to form an antibody conjugate through an amide link (Figure 5.5). This method of conjugation is widely used because of NHS's moderate reactivity to amines, with high selectivity towards aliphatic amines. It is also relatively easy to synthesise polymers with an NHS ester end-group, as discussed in section 5.2.1, and then further react them with lysine side chains on an antibody to create antibody-polymer conjugates.

5.2.2.1 IgG + Chol-PEG-NHS

Initially, conditions for successful conjugation were determined by conjugating a sample of rabbit IgG isotype (R&D Systems, MAB1050) with increasing concentrations of Chol-PEG-NHS polymer. The concentrations of polymer are described here as a ratio of polymer to antibody molar equivalents. To determine whether or not conjugation was successful, the antibody constructs were separated by SDS-PAGE and stained with barium iodine for PEG, and Coommassie for protein.

Incubation with barium iodide for 15 minutes followed by rinsing with pure water showed staining in lanes where the polymer had been loaded (Figure 5.6, right panel).

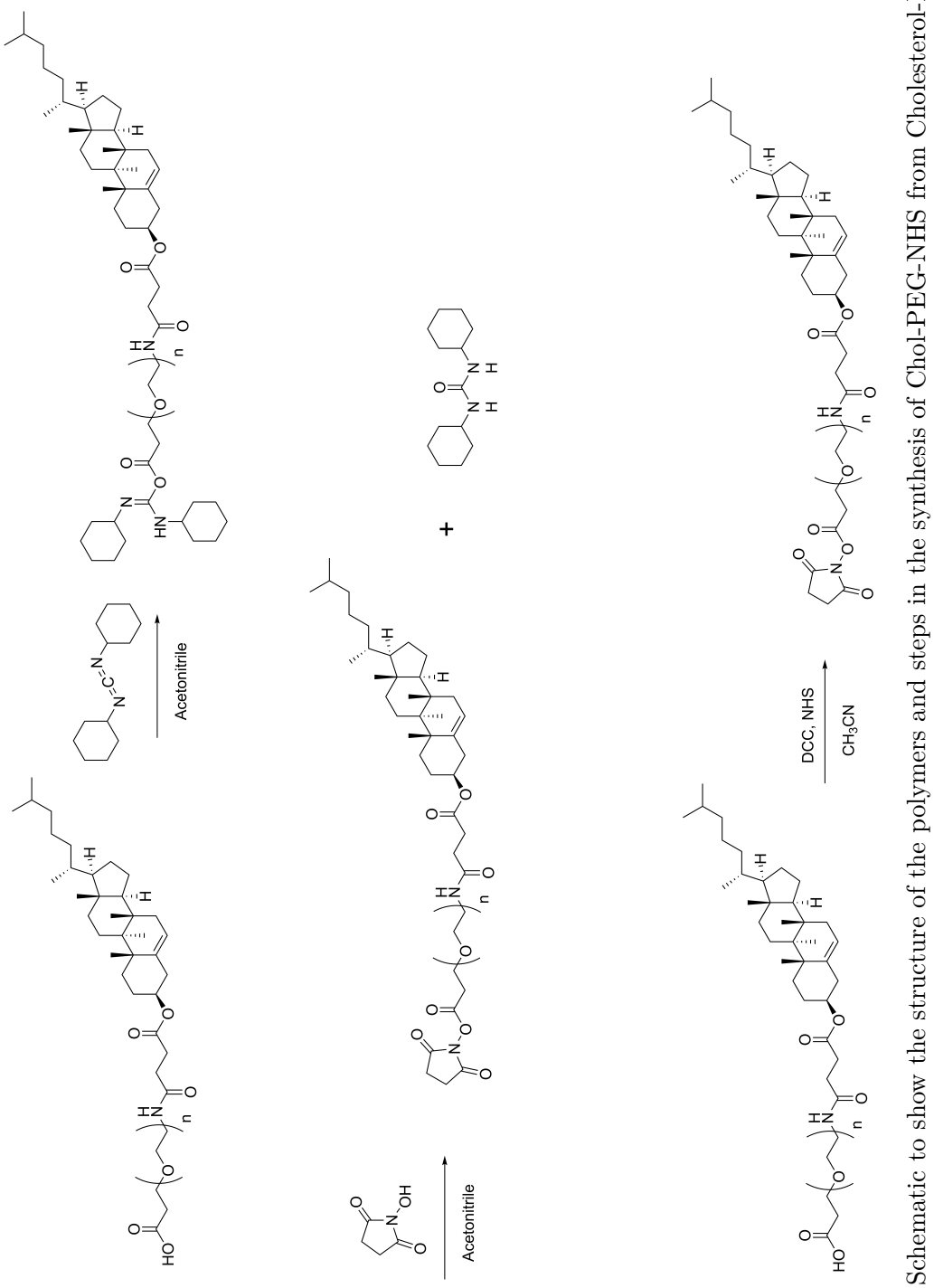


Figure 5.4: Schematic to show the structure of the polymers and steps in the synthesis of Chol-PEG-NHS from Cholesterol-PEG-COOH.

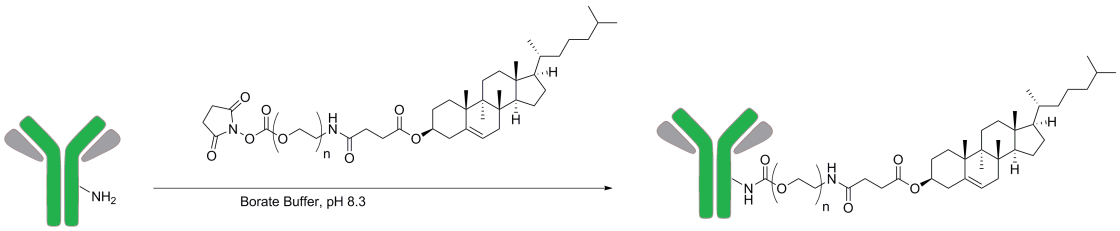


Figure 5.5: Schematic to show the antibody binding conditions of Chol-PEG-NHS.

The gel was then washed in pure water until the barium iodide stain had disappeared and incubated with a Coomassie stain until the gel formed a uniform blue colour. Subsequently the gel was de-stained and photographed (Figure 5.6, left panel).

The overlap of a Coomassie stain with a barium iodide stain indicates a PEGylated protein. [197] It has been shown previously that PEGylation affects the apparent molecular weight (MW) of proteins by adding to the MW, however, due to the interaction between the PEG molecule and SDS the relationship with MW is not linear. Therefore, whilst the image in Figure 5.6 may indicate that the IgG modified at a 1:20 antibody to polymer concentration ratio resulted in a shift from approximately 120 kDa to a population of between 150-250 kDa, this does not necessarily mean that 3 or more Chol-PEG-NHS were attached.

Coomassie staining showed that non-reduced IgG (lane 8) appeared as two bands, one thick band at MW of around 130 kDa and another fainter band at around 200 kDa. All three polymer modified IgG samples migrated in non-reducing conditions (lanes 5, 6, and 7) to produce bands with higher MW and broadened compared to the migration pattern of unmodified IgG (lane 8). As the concentration of polymer was increased from 10 to 50 times the antibody concentration, the shift in MW became greater and the broadening of the band decreased. The 1:10 modification conditions produced the most smearing in the non-reduced running conditions suggesting that there was a wide range of antibodies modified to different extents. As the ratio of polymer incubated with antibody increased (up to a ratio of 1:50), the population became more homogeneous with a highly modified antibody population with little to no overlap with the band of the unmodified IgG protein. Coomassie staining of the samples run in reducing conditions showed two distinct bands in

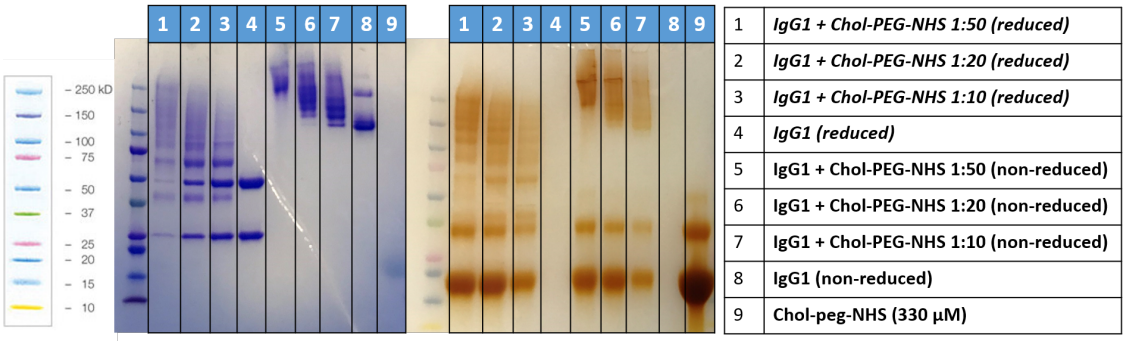


Figure 5.6: Conjugation of Cholesterol-PEG-NHS to rabbit IgG antibody. Characterization of PEGylated antibodies using SDS-PAGE with Coomassie (left) and barium iodide (right) staining. Samples run in reducing conditions are in lanes 1-4 and samples run in non-reducing conditions are in lanes 5-9. Conjugation levels were compared for Chol-PEG-NHS concentrations of 66.7 µM (Ab: polymer ratio 1:10), 132 µM (1:20) and 333 µM (1:50).

the unmodified sample (lane 4), a heavy chain band at 50 kDa and a light chain band at 25 kDa. As the molar ratio of Chol-PEG-NHS was increased, both the light and heavy chains displayed a shift to a higher MW and the intensity of the unmodified bands (i.e. the bands at 25 and 50 kDa) decreased. Smearing was also observed in all three modified samples run under reducing conditions.

Barium iodide PEG staining (right hand image) overlapped with protein staining in all modified samples run in both reduced (lanes 1 to 3) and non-reduced (lanes 5 to 7) conditions. Notably, the barium iodide staining indicated that, despite washing with centrifugal filtration (30 kDa filter), free un-conjugated polymer was still present in samples which were loaded onto the gel (see staining at 15kDa in all lanes except 4 and 8). It is hypothesised that the hydrophobic cholesterol group on the polymer leads to the formation of polymer micelles which are of similar size to the conjugated antibodies and are hence unable to be purified away using size exclusion methods.

In the reduced samples several distinct bands were observed after Coomassie staining of the polymer modified IgG samples, suggesting that modification of individual antibodies may have occurred to different extents. Further analysis was then performed using reverse phase UPLC to quantify the percentage of unmodified antibodies and antibodies modified to different extents in the samples.

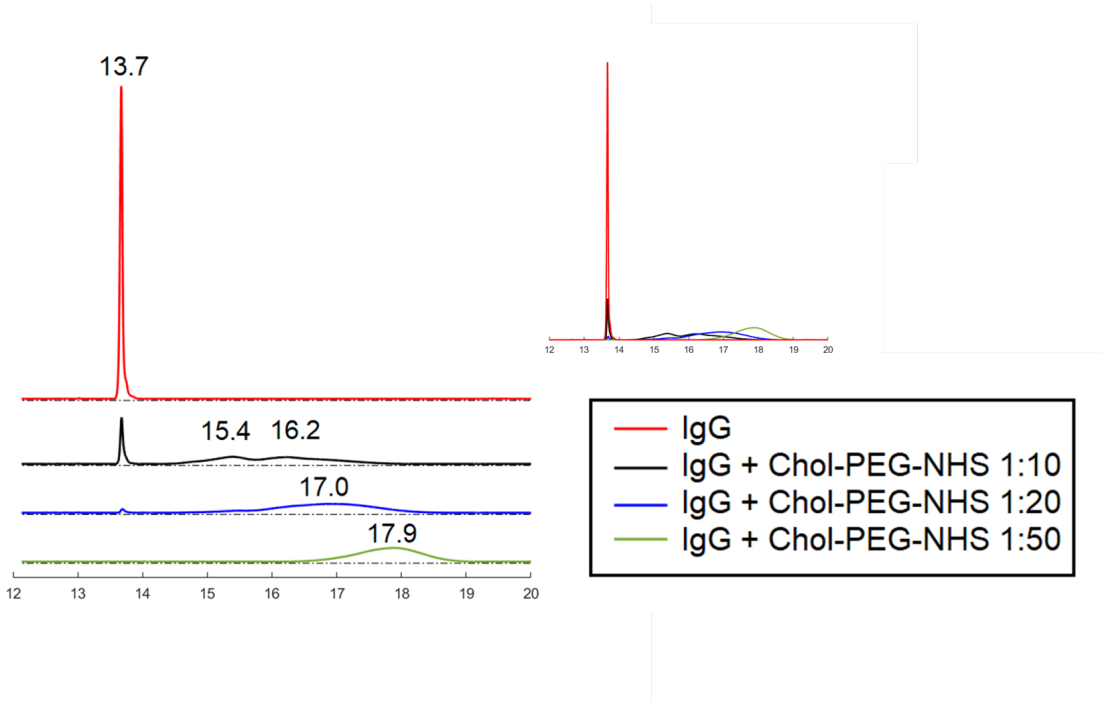


Figure 5.7: Conjugation of Cholesterol-PEG-NHS to rabbit IgG antibody. UPLC analysis of unmodified IgG (red) and IgG modified with 66.7 µM (black), 132 µM (blue) or 333 µM Chol-PEG-NHS (green). Chromatographs shown here were acquired at an absorbance of 210 nm and were baseline corrected. Modification extent was determined by looking at the percentage of the area under the curve at the "unmodified peak" and determining the area under the curve for peaks with a longer retention time.

Figure 5.7 shows traces of IgG antibodies modified as described in 2.3.2 in different concentrations of polymer. Polymer alone gave no detectable peaks in this range (data not shown). The red trace shows the profile for unmodified IgG and is characterised by a single peak at retention time of 13.7 minutes. The modified IgG (1:10, black trace) shows this unmodified peak reduce to 17.3% of the size of the original peak and two broad overlapping peaks (31.7% and 23.5%) with retention times of 15.4 and 16.2 minutes respectively were evident. Modified IgG at a 1:20 polymer concentration (blue) also shows a great reduction in the area under the "unmodified" peak at 13.7 minutes to 1.78% and the growth of a peak with retention time 17.0 minutes which accounted for 65.3% of the total area under the curve. Finally, the 1:50 modified IgG showed no detectable peak at the unmodified 13.7 mins retention time. There was a formation of a single broad peak with retention time 17.9 minutes. These traces suggest that as modification occurred

under increasingly higher polymer concentrations, the modification of each antibody occurred to a greater extent and this could be visualised by the reduction of the 13.7 minute peak detected in the unmodified IgG sample and the formation of broader peaks with longer retention times. These results confirmed that modification at pH 8.3 with a polymer concentration between 10 and 50 times that of the antibody was successful for an IgG isotype, and the that extent of modification was concentration dependent. Next, the question of whether modification at these same conditions was possible for an anti-Mucin-1 (aMUC1) antibody was addressed, this time with a commercially synthesised Chol-PEG-NHS (Creative PegWorks, PLS-9985).

5.2.2.2 aMUC1 + Chol-PEG-NHS

As with the IgG isotype, aMUC1 (Abcam Ltd, ab245693) was first conjugated to Chol-PEG-NHS as described in section 2.3.2 and SDS-PAGE and UPLC analysis were used to determine if conjugation was successful. Concentration ratios used for aMUC1 conjugation to Chol-PEG-NHS were chosen as 1:1 instead of 1:10 to see if conjugation could occur at this much lower polymer ratio, as this would favour good retention of target binding capacity. After separation by SDS-PAGE, unmodified and PEGylated aMUC1 antibodies conjugated at antibody:polymer ratios of 1:1, 1:20 and 1:50 were compared using a barium iodide stain for PEG (Figure 5.8, right panel) followed by a Coomassie protein stain (Figure 5.8, left panel).

The gels were treated as before in section 5.2.2.1. As before, an overlap of a Coomassie stain with a barium iodide stain was seen, suggesting successful PEGylation of the aMUC1 antibodies. Here we observed that non-reduced Coomassie stained PEGylated anti-MUC1 appeared as a smeared band (lanes 6-9) when compared to unmodified non-reduced aMUC1 (lane 10) which appeared as a band at 150 kDa. The degree of 'smearing' appeared to be dependent on the concentration of Chol-PEG-NHS used for conjugation. Observation of faint brown bands from PEG staining overlapping with Coomassie stain staining in lanes 2, 3, 6 and 7 indicated successful PEGylation of aMUC1 antibodies (relevant bands have been highlighted with red arrows). In the reduced samples several distinct bands were

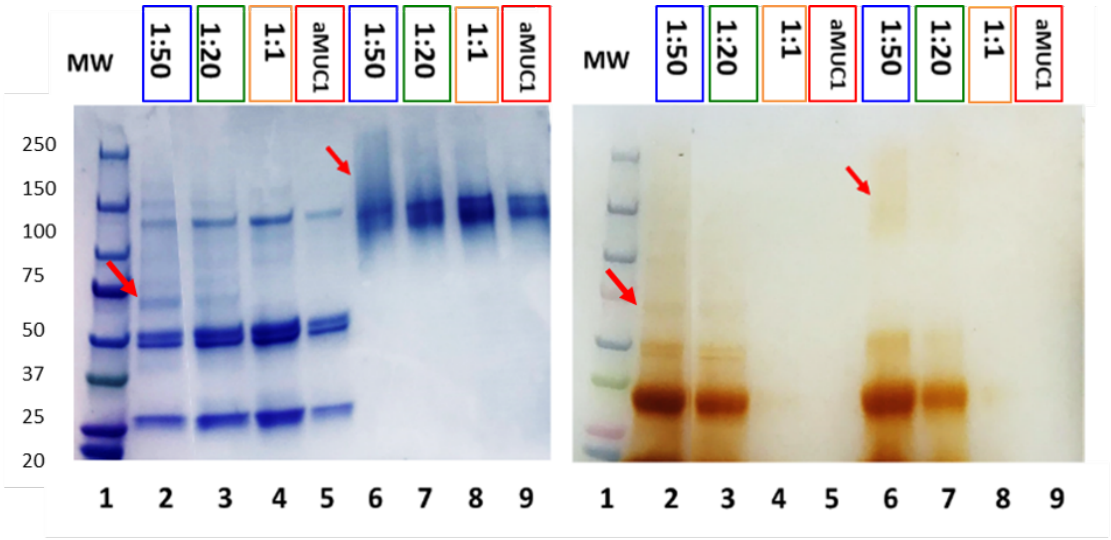


Figure 5.8: Conjugation of Cholesterol-PEG-NHS to aMUC1 antibody. Characterization of PEGylated antibodies using SDS-PAGE with Coomassie (left) and barium iodide (right) staining. Samples run in reducing conditions are in lanes 2-5 and samples run in non-reducing conditions are in lanes 6-9. Conjugation success was compared against unmodified aMUC1 (red) for Chol-PEG-NHS concentrations of 6.67 µM (Ab: polymer ratio 1:1, orange), 132 µM (1:20, green) and 333 µM (1:50, blue).

observed after Coomassie staining in the antibody to polymer 1:50 and 1:20 modified aMUC1 samples, suggesting that modification of individual antibodies may have occurred to different extents.

Due to the multitude of bands seen in the modified antibody lanes, further analysis using UPLC was undertaken to characterise PEGylation of the 1:20 and 1:50 modified samples. All samples were run in non-reducing conditions. Three traces are presented in Figure 5.9: unmodified aMUC1 (red) and aMUC1 modified with antibody to polymer ratios 1:20 (green) and 1:50 (blue).

Unmodified aMUC1 consists of two resolved peaks centred around retention times of 13.5 and 14.1 mins, these peaks are believed to correspond to differences in glycosylation of the heavy chain (as can be faintly seen in Figure 5.8 lanes 5 and 9). The modified aMUC1 samples also shows these peaks, however in both the 1:50 and 1:20 samples the area of these "unmodified" peaks was substantially reduced in size. This area decrease occurs in a concentration dependent fashion with aMUC1 modified at a 1:50 ratio with polymer having the smallest area, at just 25% of the area of the two peaks seen in the unmodified sample. The trace observed for the 1:1 aMUC1

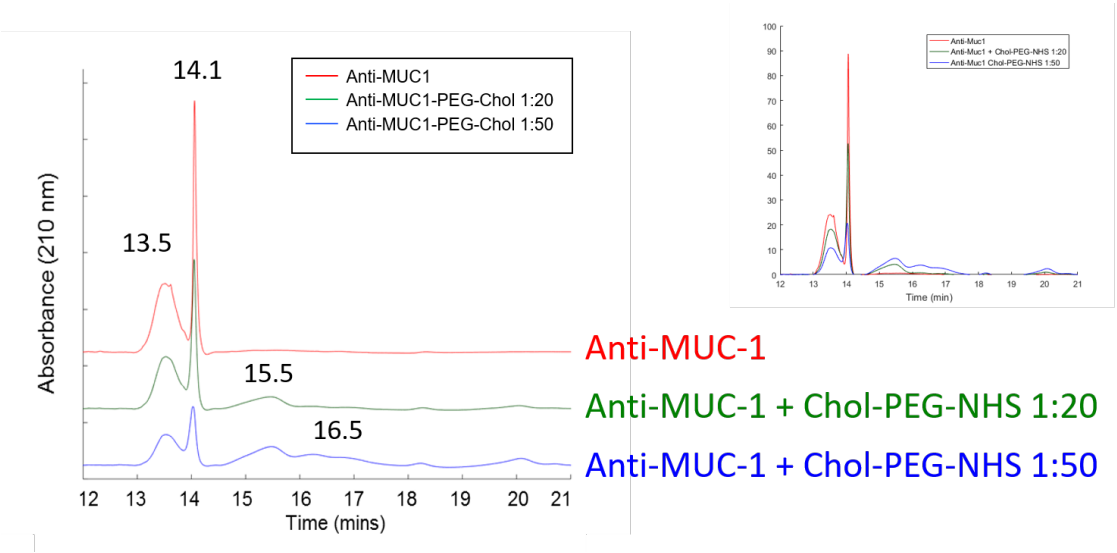


Figure 5.9: Conjugation of Cholesterol-PEG-NHS to aMUC1 antibody. UPLC analysis of unmodified aMUC1 (red) and aMUC1 modified with 132 µM (1:20, green) or 333 µM Chol-PEG-NHS (1:50, blue). Chromatographs shown here were acquired at an absorbance of 210 nm and were baseline corrected.

sample showed no difference to the unmodified aMUC1 trace with only two resolved peaks centred around retention times of 13.5 and 14.1 mins (data not shown).

Both the 1:20 and 1:50 modified aMUC1 traces have a broad third peak with a delayed retention time centred around 15.5 minutes. The area of the third peak is largest in the 1:50 modified antibody trace which suggests a larger proportion of moderately modified aMUC1 in this population. Furthermore, the presence of a fourth broad peak with retention time centred around 16.5 mins indicates the presence of a number of highly modified aMUC1. This indicates that PEGylation of a aMUC1 occurs more readily when conjugation is performed with a high concentration of Chol-PEG-NHS. The broad nature of the PEGylated aMUC1 peaks is assumed to be due to the nature of the conjugation technique allowing for modification of aMUC1 to varying degrees. The combination of the overlapping Coommassie and barium iodide stains and the UPLC analysis provides strong evidence of successful PEGylation of aMUC1. Stability of the Chol-PEG-aMUC1 antibody conjugate has been shown by UPLC for both 1:20 and 1:50 modified samples stored at 4°C to be at least three months.

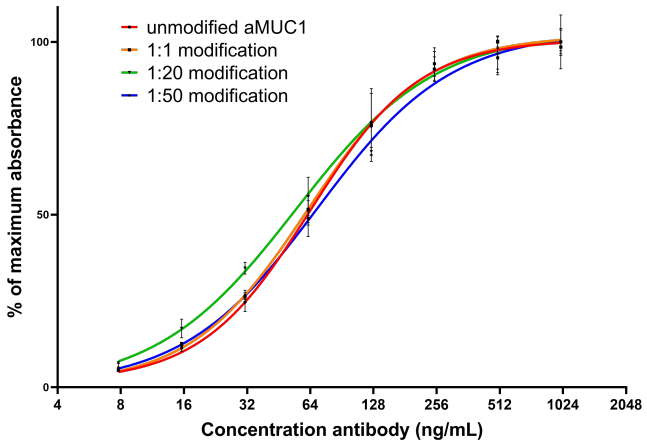


Figure 5.10: Conjugation of Cholesterol-PEG-NHS to aMUC1 antibody. Binding capability of aMUC1 (red) and aMUC1 incubated with 6.67 µM (1:1, orange), 132 µM (1:20, green) or 333 µM Chol-PEG-NHS (1:50, blue) using an ELISA.

Once aMUC1 was PEGylated, a conventional indirect ELISA was used to determine the ability of modified aMUC1 to bind its target antigen, a MUC1 core peptide. To achieve this, MUC1 core peptide was immobilised by adsorption onto a 96-well plate, and PEGylated aMUC1 (modified with Ab to polymer concentration ratios 1:1, 1:20 and 1:50) were compared with unmodified aMUC1. The binding curves are shown in Figure 5.10. All modified aMUC1 were shown to maintain their ability to bind to the MUC1 target, however it is noted that for the 1:50 modified anti-MUC1, the half-maximal saturation constant was almost 10% higher than that of the unmodified anti-MUC1 (69.9 ng/mL and 63.9 ng/mL respectively), indicating a decrease in functional affinity.

Incubation of anti-MUC1 with Chol-PEG-NHS at a 132 µM concentration (1:20) was shown to be effective at producing an aMUC1-PEG-Chol construct while maintaining a strong affinity for its target and hence this ratio was used for further VV modification.

Further validation that there was still Chol-PEG attached to the aMUC1 antibodies (which were bound to the immobilised MUC1 core peptide) was obtained using an indirect ELISA. This confirmed that the aMUC1 detected through the indirect ELISA was not simply remnant un-modified antibodies. Chol-PEG-aMUC1 antibodies were incubated in wells containing the immobilised MUC1 peptide.

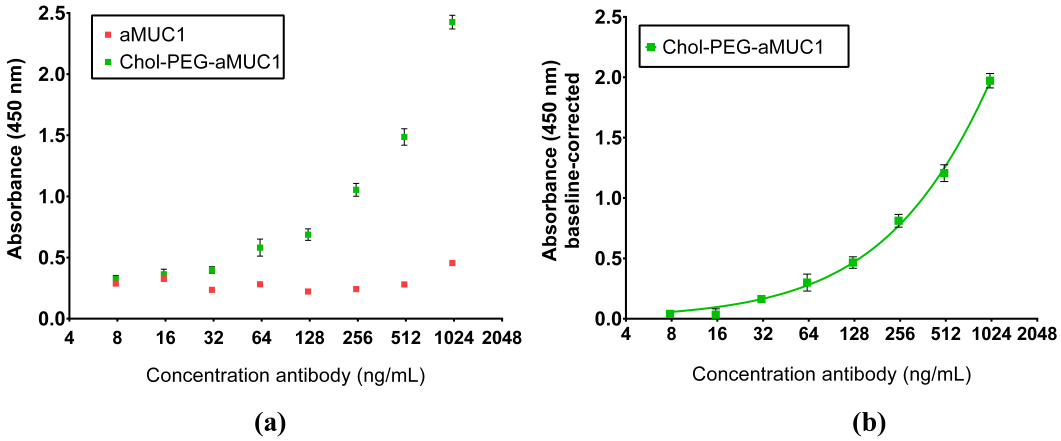


Figure 5.11: Characterising the Chol-PEG-aMUC1 binding to a MUC1 seeded ELISA plate by assaying for the presence of PEG using an anti-PEG antibody. Verification of Chol-PEG attachment in Chol-PEG-aMUC1 (conjugated at 1:20 antibody:polymer ratio) which is able to bind an immobilised MUC1 core peptide target. (a) PEG was detected using an anti-PEG antibody and the absorbance was recorded for samples of increasing concentrations of Chol-PEG-aMUC1 (green) and aMUC1 (red). (b) The background absorbance was determined by the aMUC1 trace in panel (a) and was removed from the absorbance recorded for each Chol-PEG-aMUC1 concentration. Mean absorbance for each concentration is reported and error bars represent SD. The curve represents non-linear regression using a one-site specific binding with Hill slope equation. n= 5

Rigorous washing was then performed before PEG was detected using a monoclonal anti-PEG IgM raised in rabbit (abcam, ab133471), followed by an anti-rabbit IgM HRP (abcam, ab97195) as described in full in section 2.3.3.2. The binding curves are shown in Figure 5.11a. For all concentrations of the unconjugated aMUC1 antibody, there was a small amount of non-specific background signal detected. For Chol-PEG-aMUC1 there was a clear concentration dependent increase in absorbance (450 nm) observed, indicating that the concentration of PEG was increasing with the concentration of Chol-PEG-aMUC1.

After baseline correcting to remove the non-specific binding signal, a one site specific binding with Hill slope non linear regression was fit to the data. This gave a good fit with an R^2=0.996. Without the use of a standard curve with known polymer concentrations, the specific concentration of polymer in each well can not be determined. The use of a standard curve in this type of ELISA is not possible because the Chol-PEG alone would not immobilise and hence its detection

would not be possible under these conditions. However, it is reassuring to see that the concentration of PEG detected in each well (post-washing) increases as the concentration of Chol-PEG-aMUC1 increases.

5.2.3 Attachment of aMUC1 retargeting ligand to VV via PEG-Cholesterol

To determine if embedding of the Chol-PEG-aMUC1 into the VV membrane was successful, flow virometry was used as described in section 2.4.3. Populations of VV were gated for using both a YOYO-3 nucleic acid stain and anti-VV staining. aMUC1-PEG-Chol-VV constructs were prepared using the same method used to prepare PCVV (section 2.2) and flow virometry was performed as described in section 2.4.3. Back gating enabled a VV population in FSC and V-SSC (side scatter using the violet laser) to be determined. The rabbit-raised aMUC1 antibody was stained using a secondary anti-rabbit antibody conjugated to Alexa Fluor^{TM} 647 (AF647) (Thermo Fisher Scientific, A27040) and MFI values were determined. Histograms for AF647 fluorescence of VV gated populations of VV, VV incubated with unmodified aMUC1 and VV incubated with Chol-PEG-aMUC1 samples are displayed in Figure 5.12.

AF647 staining was detected using the red laser 1 (RL1). A gate for AF647 positive staining was set using the unstained naked VV sample. As expected, unstained naked VV (red) had a very low MFI (RL1) of 1. Naked VV incubated with the AF647 secondary (Figure 5.12a) showed low levels of non-specific staining with 12.7% of VV-gated particles positively stained for AF647 and an MFI (RL1) 555. VV incubated with aMUC1 prior to staining (Figure 5.12b) had 28.4% positive staining and an MFI (RL1) of 916, showing that there is interaction between unmodified aMUC1 and VV. A 6-fold increase in MFI was observed for VV + Chol-PEG-aMUC1 (5432) compared with VV + aMUC1 (916). This suggests that despite multiple washing cycles, the Chol-PEG-aMUC1 was successfully embedded into the VV membrane (to give aMUC1-PCVV) and this could be detected using flow virometry.

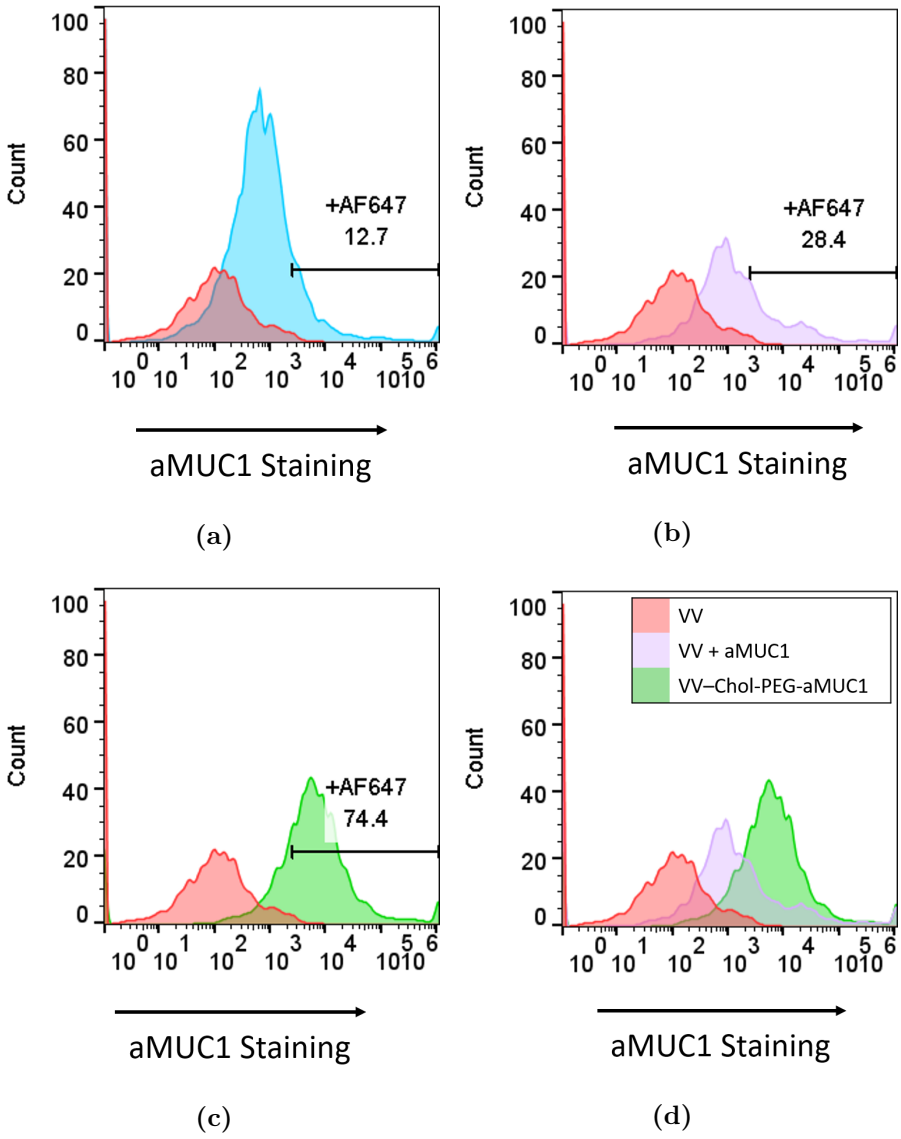


Figure 5.12: Determining of coating of VV using Chol-PEG-aMUC1 to form aMUC1-PCVV using flow virometry. Histogram in RL1-A to detect presence of aMUC1 by staining with anti-rabbit IgG-AF647. The percentage of events positively stained when compared to naked unstained VV (red) are displayed for (a) VV (blue), (b) VV preincubated with aMUC1 antibodies (purple) and (c) VV + Chol-PEG-aMUC1 (green). Solutions of VV , VV + aMUC1 and VV + Chol-PEG-aMUC1 were at a concentration of 1.27 x10^4 pfu/ µL. (d) An overlay of histograms in (b) and (c) against naked, unstained VV (red). The events counted were 3.09 x10^3, 1.98 x10^3 and 2.30 x10^3 respectively. Median fluorescence intensity (MFI) of AF647 for VV gated populations of VV, VV + aMUC1 and VV + Chol-PEG-aMUC1 were 1, 916 and 5432 respectively. Percentage of VV gated particles positively stained for AF647 were VV (2.13), VV + aMUC1 (28.4) and VV + Chol-PEG-aMUC1 (74.4).

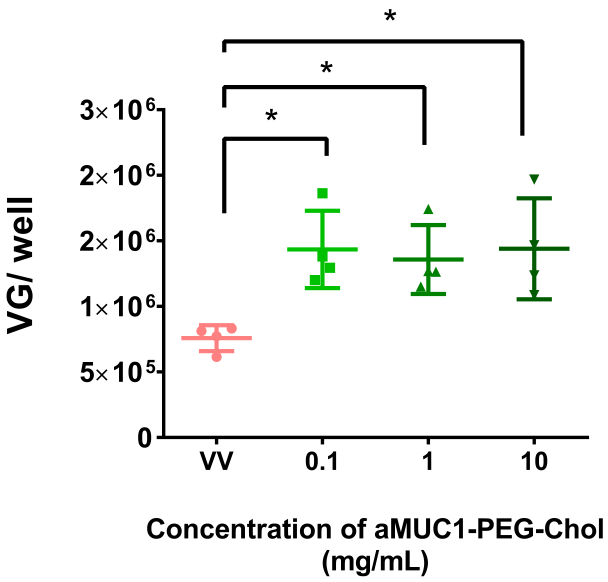


Figure 5.13: The ability of aMUC1-PCVV's ability to bind its MUC1 target was determined via incubation of 3.5 x10^6 VG the aMUC1-PCVV formed at aMUC1-PEG-Chol concentrations of 0 (red), 0.1, 1 and 10 mg/mL (shades of green) with an immobilised MUC1 peptide. After several washing cycles, DNA was extracted from samples which remained bound and QPCR was performed to determine the VG present. (n=4). Statistical significance was assessed with an ordinary one-way ANOVA followed by post-hoc Tukey's multiple comparisons test, * = $p < 0.05$

5.2.4 Determining ability for aMUC1-PCVV to bind MUC1 target

To further verify that an aMUC1-PCVV was produced and to determine its ability to bind to the MUC1 target, an assay was performed in which the number of VV and modified VV bound to an immobilised MUC1 peptide target were quantified using qPCR, as described in section 2.3.5. Naked VV and aMUC1-PCVV formed at different aMUC1 concentrations were added at 3.5 x10^6 VG/well and compared for their binding affinity to MUC1 peptide. The results are displayed in Figure 5.13. Non-specific binding of naked VV showed mean VG of 7.58 x10^5 VG (21.7% bound) in wells after washing. aMUC1-PCVV samples incubated with different Chol-PEG-aMUC1 antibody concentrations of 0.1, 1 and 10 mg/ml (i.e the Chol-PEG-aMUC1 was diluted in Chol-PEG to 0.1 and 1 mg/mL) all showed significantly higher binding with mean values of 1.43 x10^6 VG (41.0% bound), 1.36 x10^6 VG (38.8% bound) and 1.44 x10^6 VG (41.2% bound) respectively.

5.3 Results: Determining the impact of MUC1 retargeting of PCVV on virus infectivity in cancer cell lines *in vitro*

Once the ability of aMUC1-PCVV to bind the MUC1 peptide target was shown, aMUC1-PCVV's infection of cancer cells with high and low expression of MUC1 was investigated. Firstly, expression levels of MUC1 in 'high' and 'low' expressing cell lines were verified, then the infectivity of naked VV in these cells lines was determined, and finally the impact of retargeting on VV infectivity was examined.

5.3.1 Confirmation of aMUC1 antibody binding to high and low MUC1 expressing cell line

It has been shown in the literature that the human pancreatic cancer cell line CAPAN-2 has very high expression of MUC1 and that human lung cancer cell line A549 has lower expression of MUC1. Flow cytometry was performed to detect bound aMUC1 (HMFG2 clone) antibody (Merk Millipore, MABC1613) on the membrane of CAPAN-2 and A549 cell lines. Cells were incubated with aMUC1 antibody, then bound aMUC1 antibody was detected using a fluorescently conjugated secondary antibody, anti-mouse-AF647 (Thermofisher Scientific, A-21237).

As shown in Figure 5.14, aMUC1 antibodies bound at a high level with the CAPAN-2 cell line, which has been reported in literature as having high MUC1 expression. Within the singlet CAPAN-2 cell gated population, over 97% of events were highly positively stained for MUC1 (MFI (Fl4) 8.2 x10^3). By comparison, within the singlet A549 gated population, 29% of events were positively stained for MUC1 with a MFI (Fl4) fluorescence 119. Therefore it was determined that CAPAN-2 cells would be a good MUC1 positive cell line to characterise MUC1 retargeting of PCVV with. Furthermore, comparison with an A549 cell line with much lower expression of MUC1 would allow for investigation of VV infection through the MUC1 target.

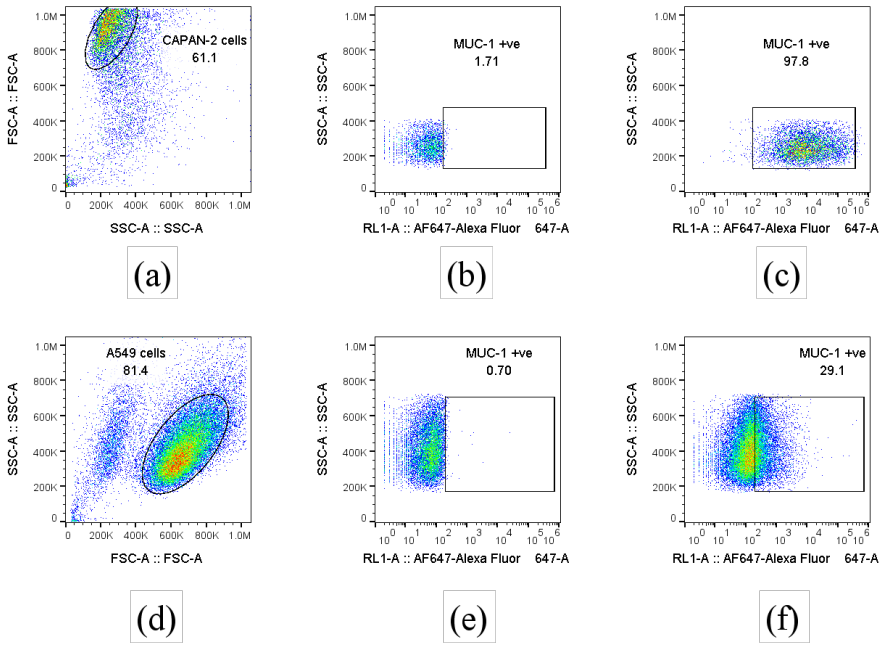
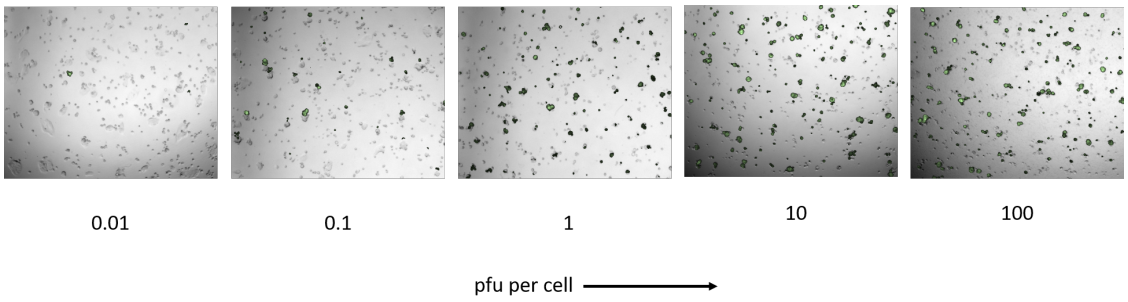


Figure 5.14: Determining the binding affinity of aMUC1 antibodies to a high (CAPAN-2) and low (A549) MUC1 expressing cell line. Flow cytometry was used to determine the binding affinity of aMUC1 antibodies to CAPAN-2 cells (top three panels) and A549 cells (bottom three panels). Cells were harvested and suspended at a $1x10^3$ cells per mL concentration and groups that were stained for MUC1 were incubated with a $1\,\mu g\ mL^{-1}$ concentration of aMUC1 antibody. Cells were then washed in PBS and aMUC1 binding was detected using an anti-mouse IgG AF647 secondary. (a) Gating for CAPAN-2 cell population. (b) Gating for positive MUC1 staining set by unstained CAPAN-2 cells and (c) CAPAN-2 cells stained for MUC1. (d) Gating for A549 cell population. (e) Gating for positive MUC1 staining set by unstained A549 cells and (f) A549 cells stained for MUC1.

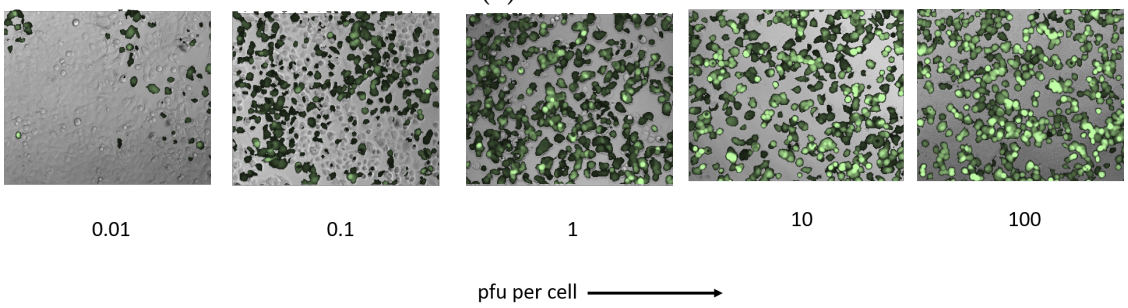
5.3.2 VV-GFP Infectivity of A549 and CAPAN-2 cells

To determine whether there was any difference in naked VV's ability to infect A549 and CAPAN-2 cells, a study was performed to determine how infection levels changed depending on the concentration of VV added to the cells. In these experiments VV encoding a green fluorescent protein (GFP) was used (VV-GFP) and GFP production assessed using fluorescent microscopy in order to determine levels of infection. This was further quantified using flow cytometry.

Cells were harvested and diluted to a concentration of 100 cells μL^{-1}. $100\,\mu L$ were added to wells to a 96 well plate and left to adhere over night before infection media containing increasing concentration of VV-GFP (0.01 - 100 pfu/cell) was added. Infection was left to occur over night before cells were imaged on a fluorescent



(a) CAPAN-2



(b) A549

Figure 5.15: Microscopy showing representative images of green fluorescence (green) overlaying brightfield and fluorescent (FITC) images for (a) CAPAN-2 cells and (b) A549 cells infected with increasing pfu/cell VV-GFP. Infection media was incubated with cells for 24 hours before imaging was performed. 4x magnification was used with FITC and brightfield filters. n=5

microscope. Representative images of wells infected at each pfu/cell concentration for CAPAN-2 and A549 are displayed in Figure 5.15a and b respectively. It is clearly depicted in the fluorescent overlays that VV-GFP was able to infect A549 cells to a far greater extent over 24 hours than CAPAN-2 cells. Both cell lines showed that, as expected, as the pfu/cell increased from 0.01 to 100 the number of infected cells increased from low infection density to a high infection density. In the A549 cell line, the actual fluorescence seen in infected cells at the higher pfu/cell concentrations (10 and 100) was much brighter than that seen in the lower pfu/cell concentrations. This same brightness effect was not as immediately apparent in the CAPAN-2 cells. This observed difference in infection ability may be driven by the difference in the morphology of the two cell lines as they become adherent; A549 grow in a very uniform single layer pattern whereas CAPAN-2 grow in clumps.

To further quantify this difference in infection, the cells were harvested, washed

and resuspended in a total volume of 200 µL PBS and run on a BD FACS Calibur flow cytometer. This allowed the number of infected cells (as determined by their GFP fluorescence) and the intensity of that fluorescence (extent of infection) to be quantified. Singlet cell populations were gated for as depicted in Figure 5.14 and a GFP-positive population was gated for by setting a GFP + gate as Fl1 fluorescence detected above that of a cells alone (negative) population. The percentage of infected CAPAN-2 cells was most closely fit with a hyperbola curve (R^2= 0.982) with a B_{max} of 52.3%. The percentage of infected A549 cells was most closey fit by a one site specific binding with hill slope equation (R^2= 0.996) with a B_{max} of 99.98%. The maximum percentage of infected cells (B_{max}) was reached at 10 pfu/cell for CAPAN-2 cells and 0.1 pfu/cell for A549 cells. This matched what was seen in the microscopy images with VV-GFP infection ability substantially higher in A549 cells than CAPAN-2 cells.

Within the GFP+ population of cells, the level of infection of cells was also much higher in the A549 cells with a maximum fold-difference of 5.5 in fluorescence intensity at 100 pfu/cell when compared to that in CAPAN-2 cells. From these studies it was determined that for infection of pre-seeded cells over 24 hours, a VV-GFP concentration of 1 pfu/cell would be optimum for CAPAN-2 cells and 0.1 pfu/cell for A549. This is because at these concentrations the percentage of GFP+ cells reaches its maximum and the mean fluorescence of infected cells is in the linear range of the infection profile, potentially allowing for a knockdown in and recovery of infectivity to be detected.

The marked difference in the MUC1 expression levels on the CAPAN-2 and A549 cells make these good candidates for “high” and “low” MUC1 expression cell lines to be used to determine the specificity of the MUC1 targeting. However, the differences in absolute infection levels obtained in CAPAN-2 when compared with A549 at the same MOI, as well as the difference in the morphology of the cell lines may confound the interpretation when testing target specificity of the viruses by comparing infection in these two cell lines. Therefore in the studies reported

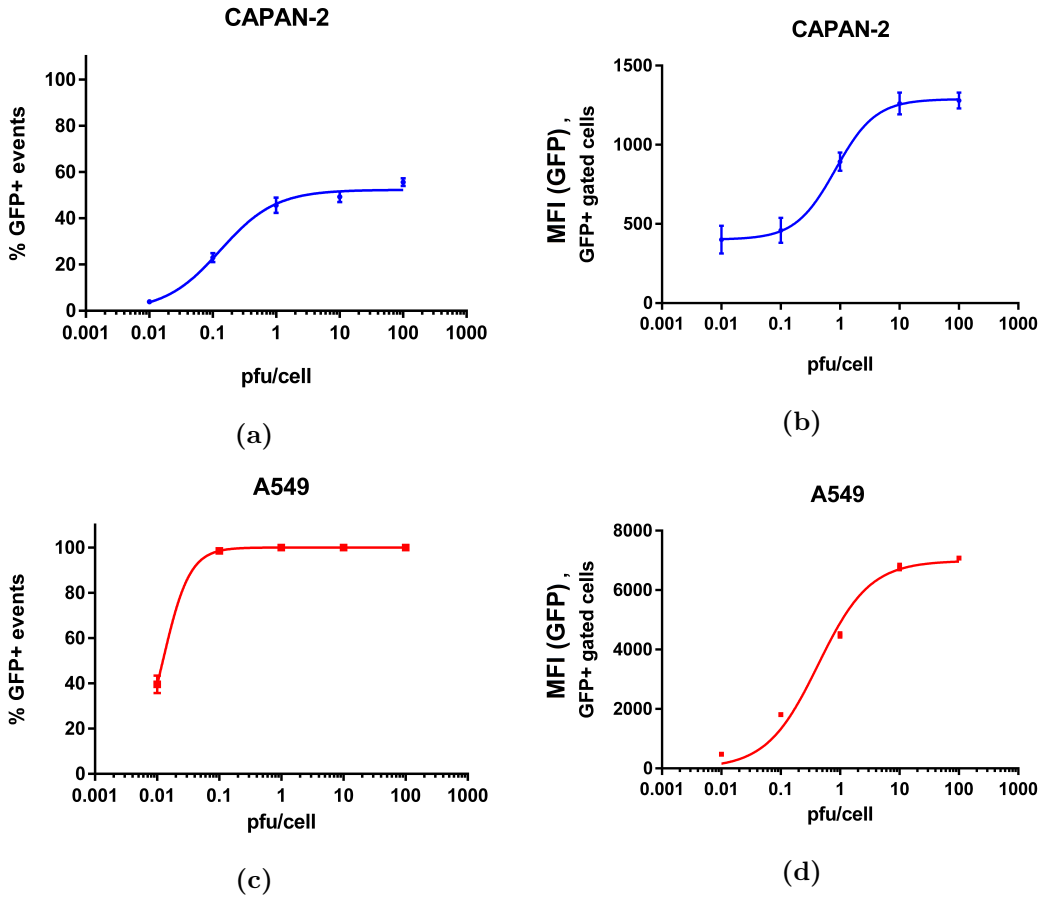


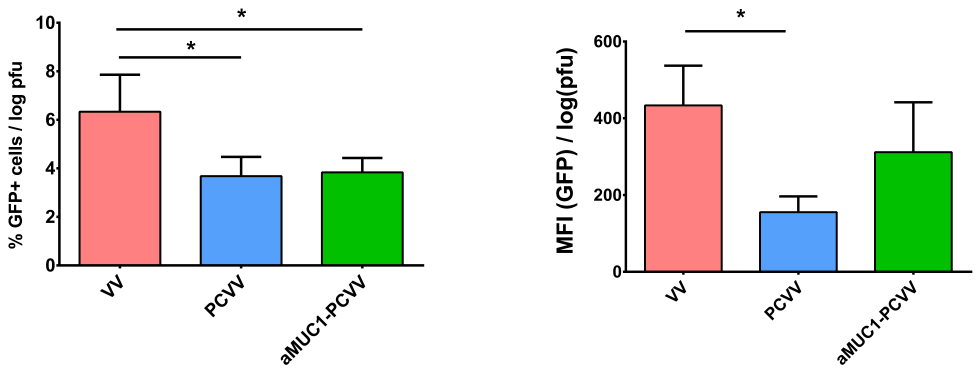
Figure 5.16: Infection of (a & b) CAPAN-2 (blue) and (c & d) A549 (red) cells with increasing pfu/cell of naked VV-GFP quantified using flow cytometry after 24 hours of infection. Cells were first gated for singlets and then populations of the cells were gated for as shown previously. The percentage of cells that were gated positively for green fluorescence was determined (GFP +, a & c) and the MFI (detected on FL1 channel) of that GFP+ population was then determined (b & d) for each cell line at different concentrations. Points represent the mean values. Error bars represent SD. n=5

in section 5.3.4 an IgG-PCVV and blocked aMUC1-PCVV controls were utilised instead of comparing a 'high' expression cell line to a 'low' expression cell line.

5.3.3 aMUC1 retargeting of VV-GFP in CAPAN-2 cells

CAPAN-2 cells were harvested and plated as described in section 2.5 and infected with VV, PCVV and aMUC1-PCVV made up and washed as described in section 2.2 and 2.2.1. Cells were harvested and resuspended in 500 µL PBS and then analysed using a BD FACS Calibur cytometer. The results are displayed in Figure 5.17.

In infection studies in A549 cells in Chapter 4 it was seen that polymer



(a) (b)

Figure 5.17: Infection of CAPAN-2 cells with VV, PCVV and aMUC1-PCVV at 1 pfu/cell (VV-GFP) analysed using flow cytometry after 24 hours of infection. Cells were first gated for singlets and then alive cells were gated for as shown previously. (a) The percentage of cells that were gated positively for green fluorescence was determined, GFP+. (b) The mean MFI (detected on FL1 channel) normalised by the log of pfu added per well as determined by QPCR. n=4, one-way ANOVA followed by Tukey's test for multiple comparisons. ANOVA key: * = p <0.05

coating VV-luc resulted in a knockdown in the level of infection achieved. It was hypothesised that this would be the same for VV-GFP in CAPAN-2 cells at 1 pfu/cell concentration. Flow cytometry determined that within the live cell population, a higher normalised percentage of cells were infected by VV (6.3 % /log(pfu/cell)) when compared with PCVV (3.7%/log(pfu/cell), $p<0.05$) and aMUC1-PCVV (3.8%/log(pfu/cell), $p<0.05$) as shown in Figure 5.17a. The levels of infection of the live cell population as determined by normalised MFI (GFP) showed that there was a statistically significant ($p<0.05$) 2.8-fold knockdown in normalised MFI between VV (433) and PCVV (155) (Figure 5.17b). The addition of aMUC1 antibodies to the polymer coating of VV-GFP, resulted in a 2-fold increase in the mean normalised MFI for aMUC1-PCVV (311) compared with PCVV (155). Variability between wells meant that this difference in infection between aMUC1-PCVV and PCVV was not statistically significant ($p>0.05$) when tested by one-way ANOVA followed by Tukey's test for multiple comparisons. These infection results suggest that although aMUC1-PCVV infected fewer cells than VV, the cells which were infected did achieve a high infection intensity, i.e. GFP per infected cell.

To try and reduce the variability between wells, two changes in the cell infection protocol were made before testing the difference of infection ability of VV, PCVV, aMUC1-PCVV and an IgG and block control in CAPAN-2 cell lines. First, cells were infected while in suspension and then transferred to a 96-well plate for incubation over night as opposed to pre-seeded onto a 96-well plate overnight before infection medium was added. Second, VV encoded with luciferase (VV-luc) was used instead of VV-GFP as it has a much larger dynamic range and hence would allow for difference in infection levels to be more precisely determined.

5.3.4 aMUC1 retargeting of VV-luc in high MUC1 expression cell line CAPAN-2

QPCR was performed on the washed samples of VV, PCVV, aMUC1-PCVV and IgG-PCVV before the infection and the concentrations were adjusted to be the same for each group. Initial tests were performed to determine the appropriate concentration of VV to add to cells in suspension to achieve high levels of infection without causing cell death over 24 hours. In these tests 0.1 pfu/cell was determined to be the best concentration.

CAPAN-2 cells were incubated in suspension and infected with VV, PCVV, aMUC1-PCVV or an isotype control IgG-PCVV. Virus samples were made up as described in section 2.3.4, added to CAPAN-2 cells in suspension at a concentration of 0.1 PFU/cell and incubated in rotation at 37°C for 2 hours. Infected cells were then spun down, resuspended in fresh media and added to a 96 well plate in replicates of 5. After 24 hours cells were lysed and analysed for luciferase expression. Luminescence values were adjusted for individual replicates by the well protein content of each replicate, as determined by advanced protein assay (APA), and are displayed in Figure 5.18.

Naked VV showed a high infection capacity at this 0.1 MOI in the CAPAN-2 cell line with a mean normalised luminescence of 1.7 x10^7 arbitrary units (a.u). PCVV showed a significant ($p<0.05$) 3-fold knockdown in infectivity with a normalised luminescence of 6.2 x10^6 a.u (Figure 6a). However, infectivity of VV was restored,

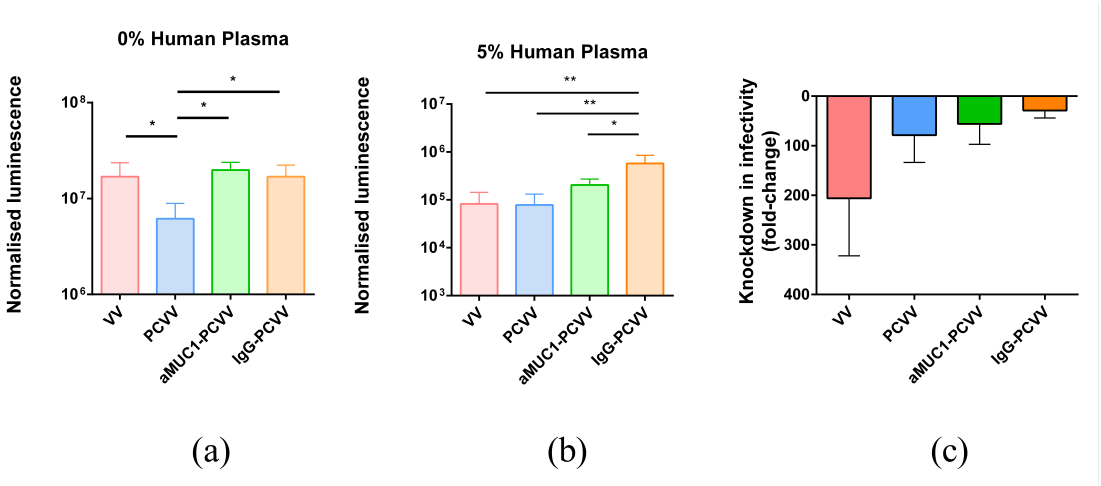


Figure 5.18: Infection of CAPAN-2 cells after 24 hours in the presence or absence of 5% human plasma positive for anti-VV antibodies. CAPAN-2 cells were suspended at a concentration of 10^5 cells/mL in infection media containing VV (pink), PCVV (blue), aMUC1-PCVV (green) or IgG-PCVV (orange) at a final concentration of 0.1 pfu/cell. (a) 0% Human Plasma. (b) 5% Human Plasma. (c) Knockdown in infectivity due to addition of 5% human plasma (data from a & b). Infection levels were determined by luciferase assay, adjusted by protein content of each replicate and reported as normalised luminescence.The bars represent the mean normalised luminescence for each group. Error bars represent SD, n=5. Statistical significance was assessed with an ordinary one-way ANOVA followed by post-hoc Tukey's multiple comparisons test, ** = $p < 0.01$, * = $p < 0.05$

and indeed increased above that of the naked VV, with aMUC1-PCVV with a mean normalised luminescence of 2.0 x10^7 a.u (Figure 5.18a). This was a significant ($p<0.05$) 3.2-fold increase in infectivity when compared to that of PCVV. To determine the specificity of the binding of the aMUC1 ligand to MUC1 target, a rabbit IgG isotype antibody modified with the same Chol-PEG-NHS polymer and using the same method as for the aMUC1 antibody (as described in section 2.3.2, Figure 5.19) was used to coat VV. The addition of an IgG antibody to the polymer coating also significantly restored infectivity when compared to PCVV with a normalised luminescence value of 1.5 x10^7 a.u (Figure 5.18a). Hence, it was determined that the presence of aMUC1 or IgG isotype control antibodies on the VV coating re-established infection of CAPAN-2 cells.

Infectivity of the viral constructs was further tested in the presence of human plasma which was positive for anti-VV antibodies (Figure 5.18b). The presence of 5% fresh human plasma greatly impacted the infectivity of all constructs in CAPAN-

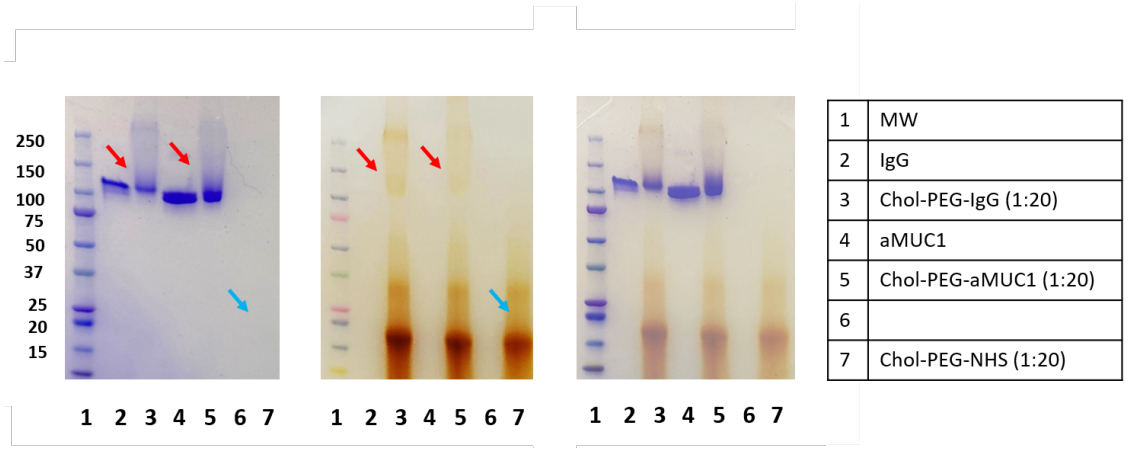


Figure 5.19: Conjugation of Cholesterol-PEG-NHS to aMUC1 or IgG antibody. Characterization of PEGylated antibodies using SDS-PAGE with Coomassie (left), barium iodide (middle) and an overlay of staining (right). All samples (lanes 2-7) were run in non-reducing conditions. Conjugation success was compared against unmodified aMUC1 and IgG for Chol-PEG-NHS concentrations of 132 µM (1:20).

2 cells. Of all four constructs, naked VV experienced the greatest reduction in its infectivity showing a 206-fold knockdown with a mean normalised luminescence of 8.2 x10^4 a.u in the presence of 5% human plasma. The modified viruses all showed lower knockdown in infectivity (PCVV= 79-fold, aMUC1-PCVV= 57-fold and IgG-PCVV= 29-fold), perhaps suggesting that the coatings provided some protection against human plasma (data from Figures 5.18a and b is displayed as fold-change in Figure 5.18c). IgG-PCVV infectivity was impacted the least by the presence of human plasma with a normalised luminescence of 5.7 x10^5 a.u, significantly higher than naked VV (1.4 x10^5 a.u), PCVV (7.8 x10^4 a.u) and aMUC1-PCVV (3.5 x10^5 a.u). Differences in normalised luminescence values between other groups were shown not to be significant ($p>0.05$).

Overall these results suggest that coating VV reduces the impact of human plasma on VV infection of CAPAN-2 cells. Furthermore, these results appear to potentially suggest that that this protection is enhanced by increasing the complexity of the coating by introducing protein ligands (i.e. statistically significant improvement for IgG antibodies ($p<0.01$)). Hence overall mean infectivity is higher to that of both the naked VV and PCVV with an aMUC1 antibody and statistically higher with an IgG antibody.

To explore the unexpected success of IgG-PCVV, differences in the Chol-PEG-NHS modification of aMUC1 and IgG antibodies (1:20) were determined by separation by SDS-PAGE followed by Coomassie and Barium Iodine PEG staining (Figure 5.19). Both antibodies showed clear overlap in Barium Iodine PEG staining and coomassie which suggested that both antibodies were modified. However, there were small differences potentially in the extent of the modification seen for the IgG and aMUC1 antibodies with the shift and smearing in MW of the aMUC1 antibodies being to a slightly greater extent than with the IgG. Therefore it was hypothesised that the impact on infection seen here could be a result of a difference in coating density or uniformity. For instance, if there was less polymer modification on each IgG antibody, then there may be more free polymer to embed into the lipid membrane and potentially a more dense coating. It was hence determined that further investigation into the impact and specificity of aMUC1 targeting was required. This could be done in two ways: finding a cancer cell line which was MUC1 negative or pre-incubating the retargeted VV constructs with a soluble MUC1 peptide to reduce the affinity to cell-bound MUC1. Given that it is difficult to find a cancer cell line which does not express MUC1 and the issues highlighted in previous comparisons to A549 cells (see section 5.3.2),[145] a MUC1 peptide (Cambridge Bioscience, ANA60600-1) was incubated with Chol-PEG-aMUC1 constructs in the aim of reducing affinity instead.

Chol-PEG-aMUC1 was either pre incubated with PBS or with 5 times the mass of aMUC1 antibodies of MUC1 peptide overnight at 4 °C (forming Chol-PEG-aMUC1-MUC1) before being tested in a conventional indirect ELISA to determine the impact on its binding to immobilised MUC1 core peptide. MUC1 core peptide was immobilised by adsorption onto a 96-well plate. Chol-PEG-aMUC1 or Chol-PEG-aMUC1-MUC1 were added to the plate at varying concentrations, and the binding curves are shown in Figure 5.20. Both Chol-PEG-aMUC1 and Chol-PEG-aMUC1-MUC1 were shown to bind to the MUC1 target, however the MUC1 blocked constructs showed a marked reduction in functional affinity, with a half-maximal saturation constant of 99.76 ng/mL compared with Chol-PEG-aMUC1's

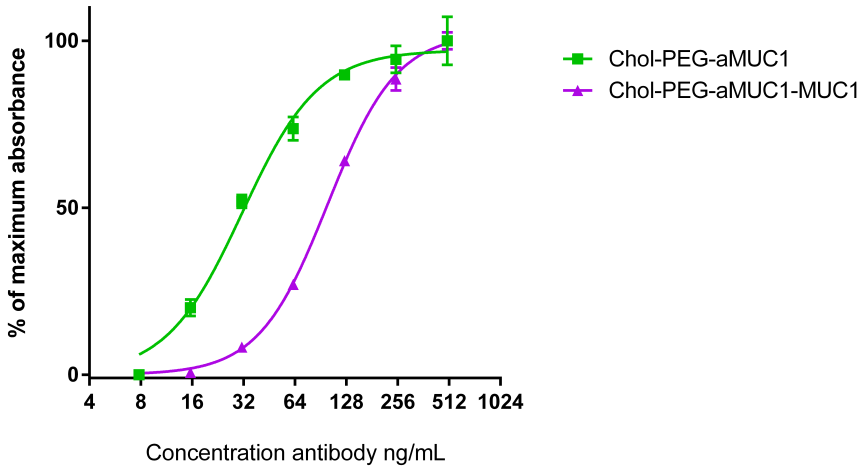


Figure 5.20: Conjugation of Cholesterol-PEG-NHS to aMUC1 antibody. Binding capability of Chol-PEG-aMUC1 (red) and Chol-PEG-aMUC1-MUC1 (green) using an ELISA.

31.5 ng/mL. Therefore it was determined that although there was still some ability for the construct to bind its target, Chol-PEG-aMUC1 binding affinity was impacted by preincubation with the MUC1 peptide core target to a marked extent.

The Chol-PEG-aMUC1-MUC1 was then incubated with VV and the subsequent "blocked" modified virus is referred to as MUC1-aMUC1-PCVV. Virus samples were formulated and washed as described in sections 2.2 and 2.3.4 and then incubated with CAPAN-2 cells in suspension for 2 hours in either the absence or presence of 2% human plasma. The concentration of human plasma was reduced in this study as the knockdown of infection in 5% human plasma concentrations was so substantial across all groups, it was not really possible to determine whether there was a difference in VV protection due to polymer coating or antibody-polymer coating.

In the absence of human plasma (Figure 5.21a), as seen previously, there was a small but significant ($p<0.05$) knockdown in infection (luminescence/ g of protein) for PCVV ($7.86x10^3$+/- $2.02x10^3$) when compared to naked VV ($1.52x10^4$+/- $2.82x10^3$) and with the addition of aMUC1 antibodies the infectivity of aMUC1-PCVV increased to approximately the same as that of VV ($1.40x10^4$+/- $4.9x10^3$). However, when the aMUC1 antibodies were blocked (MUC1-aMUC1), the mean

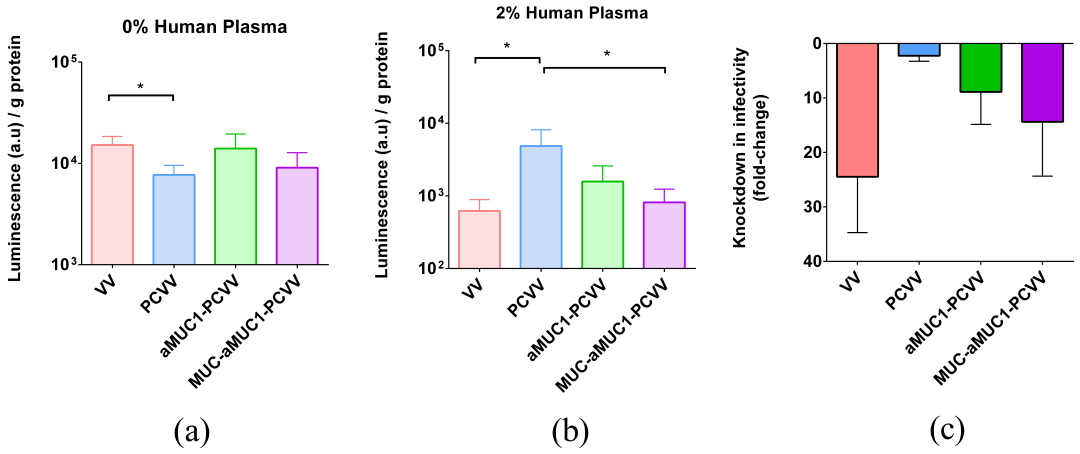


Figure 5.21: Infection of CAPAN-2 cells after 24 hours in the presence or absence of 2% human plasma positive for anti-VV antibodies. CAPAN-2 cells were suspended at a concentration of 10^5 cells/mL in infection media containing VV (pink), PCVV (blue), aMUC1-PCVV (green) or MUC1-aMUC1-PCVV (purple) at a final concentration of 0.1 pfu/cell. (a) 0% Human Plasma. (b) 2% Human Plasma. (c) Knockdown in infectivity due to addition of 2% human plasma (fold-change between data presented in a & b). Infection levels were determined by luciferase assay, adjusted by protein content of each replicate and reported as luminescence/ g protein. Bars represent the mean values for each group. Error bars represent SD, n=5. Statistical significance was assessed with an ordinary one-way ANOVA followed by post-hoc Tukey's multiple comparisons test, * = $p < 0.05$

infectivity was lower ($1.17x10^4$+/- $6.18x10^3$) however this difference was not found to be statistically significant.

In the presence of 2% human plasma (Figure 5.21b), the overall knockdown in infection when compared to previous studies in which 5% human plasma was used (Figure 5.18b) was substantially lower for all groups with the greatest mean knockdown seen in cells infected with naked VV with a fold-change of 24.5 +/- 10.25 (Figure 5.21c). Incubation with 2% human plasma had little impact on the infection levels seen with PCVV which showed a statistically significant ($p<0.05$) higher luminescence/g protein of $3.48x10^3$ +/- $1.16x10^3$ when compared with that of VV $6.22x10^2$ +/- $2.33x10^2$ and the lowest knockdown in infection with a fold-change of 2.25 +/- 1.01.

Both aMUC1-PCVV ($1.58x10^3$ +/- $9.01x10^2$) and MUC1-aMUC1-PCVV ($8.16x10^2$ +/- $3.68x10^2$ were impacted to a greater extent than PCVV by the addition of 2% plasma. The difference in infection with MUC1-aMUC1-PCVV when compared

to PCVV was found to be statistically significant ($p<0.05$). This suggests that in 2% human plasma, blocking the aMUC1 antibody on the coating of VV resulted in a lower infection than polymer coating with no retargeting antibody included. Incubating Chol-PEG-aMUC1 constructs with a MUC1 peptide to compete with cellular MUC1 binding of the aMUC1 targeting ligand resulted in an infection level similar to that of naked VV in the presence of 2% human plasma.

5.4 Results: Circulation kinetics of VV, PCVV and aMUC1-PCVV in murine models

PK studies were performed to determine the circulation kinetics of VV, PCVV and aMUC1-PCVV in murine models. Mice bearing CAPAN-2 xenograft tumours were treated once tumours reached volumes between 50 and 150 mm^3 as described in section 5.4. Two studies were performed, one in which mice were given a dose of $2x10^6$ pfu ($1\ x10^8$ Viral Genome (VG)) (Figure 5.22) and another at a $1x10^7$ pfu ($5\ x10^8$ VG) dose (Figure 5.23).

For the $2x10^6$ pfu dose (Figure 5.22a and b), the amount of VV genomes circulating in the mice at 5 minutes post-injection was statistically significantly increased (approximately 4-fold) for both PCVV ($5.7\ x10^6$ VG, $p = 0.0198$) and aMUC1-PCVV ($6.0\ x10^6$ VG, $p=0.0142$) compared to VV ($1.6\ x10^6$ VG). In a mouse, 5 minutes represents between 50 and 65 complete circulations of the blood. By 10 minutes, the levels of VG detected in circulation in mice treated with VV were very low and near the limits of detection. The limit of detection ($1.1x10^6$ VG) is represented by a black dashed line on Figure 5.22a and represents the line below which the actual quantity VG detected in the 5 µL eluted DNA qPCR sample was less than 5. This was also true for all three groups at 20 minutes.

The half life for both PCVV (1.23 mins) and aMUC1-PCVV (1.15 mins) were greater than VV (0.82 mins). This increase in half-life for both PCVV and aMUC1-PCVV suggested that there was increased drug exposure when compared with VV. Area under the curve (AUC_{0-20}) analysis with a baseline set at the limit of detection, confirmed this, showing that exposure was increased for both PCVV

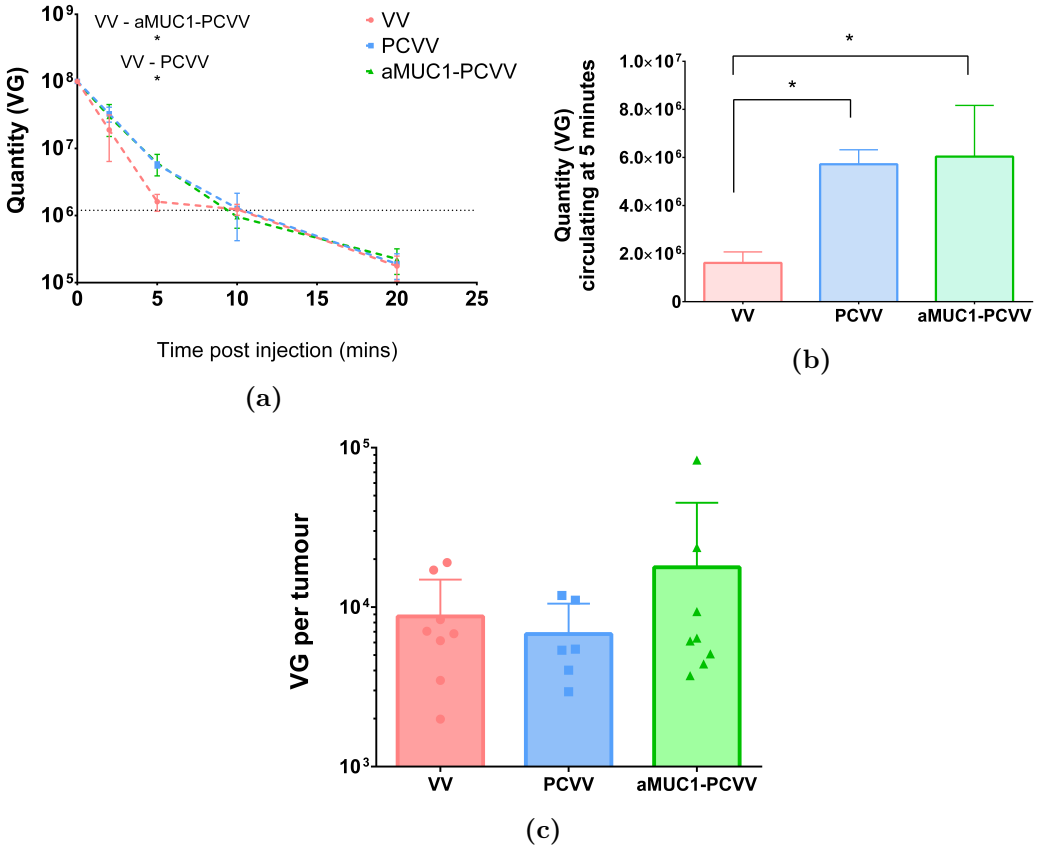


Figure 5.22: Pharmacokinetic (PK) studies showed polymer-coating and polymer coating with aMUC1 retargeting ligands enhances VV's circulation kinetics in mice bearing CAPAN-2 xenografts. (a) The mean quantity (viral genomes (VG)) of a 2 x10^6 pfu dose of VV, PCVV or aMUC1-PCVV circulating was determined by qPCR by taking bleeds from mice at either 2 and 10 mins (n=4) or 5 and 20 mins (n=4). Error bars represent SD. Ordinary one-way ANOVA was performed at 5 minutes with post-hoc Tukey's test for multiple comparisons. * = $p < 0.05$. (b) The mean quantity (VG) circulating at 5 minutes as determined by qPCR (n=4). Error bars represent SD. Ordinary one-way ANOVA was performed with post-hoc Tukey's test for multiple comparisons. * = $p < 0.05$. (c) Tumours were resected at 20 minutes for all mice. After homogenisation to 75 mg/mL, DNA was extracted and quantified by QPCR to determine accumulation after 20 minutes. Results are displayed for the mean VG/ tumour. Error bars represent SD (n=8) Statistical significance was assessed with an ordinary one-way ANOVA. No significance found for differences between any groups.

(AUC_{0-20} = 1.3 x10^8 VG min/mL) and aMUC1-PCVV (AUC_{0-20} =1.3 x10^8 VG min/mL) compared with VV (AUC_{0-20} = 1.0 x10^8 VG min/mL). The increase in the AUC for both PCVV and aMUC1-PCVV compared with VV suggests that over the 20 minute circulation time there is a marked increase in the amount of VV present for both of the coated VV when compared to the naked VV.

QPCR analysis on the recovered tumours showed very low passive accumulation after 20 minutes across all groups, Figure 5.22c. As discussed previously in Section 4.5, low levels of accumulation after 20 minutes are not surprising given the short window for passive dissemination. Therefore any meaningful viral accumulation at this early time point would suggest that delivery had been greatly improved. The mean quantities of VV genome copies recovered in tumours were $8.7x10^3$ (+/- $6.1x10^3$) VG/ tumour of naked VV, $6.8x10^3$ (+/- $3.7x10^3$) VG/ tumour of PCVV, and $1.8x10^4$ (+/- $2.7x10^4$) VG/ tumour of aMUC1-PCVV, however large variation within groups resulted in no statistically significant difference between groups. Of note, the two highest VG/ tumour values were in mice treated with aMUC1-PCVV. It is also suspected that given these low values, detection limits were encountered in determining the quantity of tumoural VV.

To overcome the low levels and potential detection limits encountered during quantification of intratumoural viral accumulation and to see whether this enhanced circulation time could also be observed at a higher dose, the PK study was repeated at a dose 5 times higher, i.e. 1 $x10^7$ pfu (Figure 5.23). There were no immediate adverse effects seen at this higher dose. There was a higher mean quantity of VG circulating for both PCVV (4.0 $x10^7$ VG) and aMUC1-PCVV (6.1 $x10^7$ VG, $p<0.05$) circulating at 5 minutes when compared with VV (2.1 $x10^7$ VG) (Figure 5.23b). The half life for both PCVV (1.39 mins) and aMUC1-PCVV (1.50 mins) were greater than VV (1.07 mins). Area under the curve (AUC_{0-20}) analysis was also performed on curves at this higher dose with the baseline set at the limit of detection. Once again this showed increased exposure of PCVV ($AUC_{0-20} = 9.6x10^8$ VG min/mL) and aMUC1-PCVV ($AUC_{0-20} = 1.1x10^9$ VG min/mL) compared with VV ($AUC_{0-20} = 9.1x10^8$ VG min/mL). This suggests that the positive impact on extending the circulation kinetics of VV was maintained even at a higher dose.

Tumour accumulation after 20 minutes was higher than that seen for the 2 $x10^6$pfu dose and detection limits were overcome (Figure 5.23c). The mean quantity of VV genome copies recovered in in tumours were 5.6 $x10^4$ (+/- $2.6x10^4$) VG/ tumour of naked VV, 1.5 $x10^4$ (+/- $1.3x10^4$) VG/ tumour of PCVV, and $4.0x10^4$

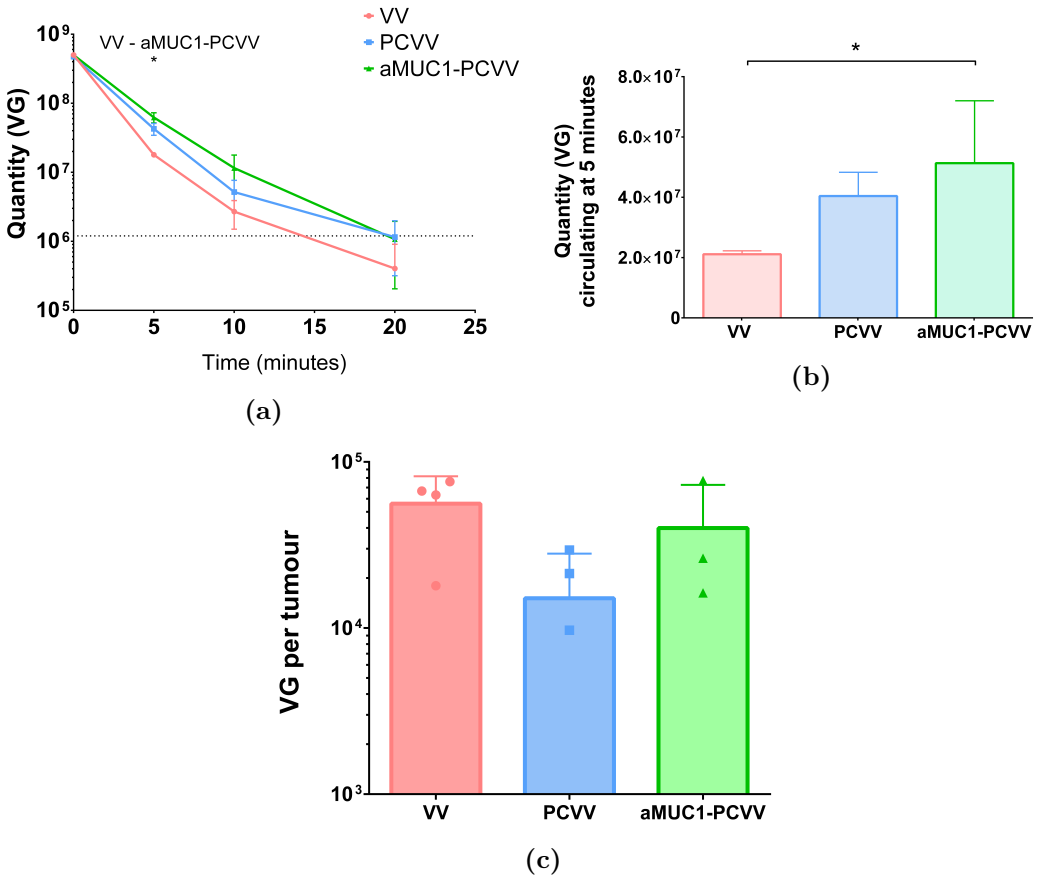


Figure 5.23: Pharmacokinetic (PK) studies showed polymer-coating and polymer coating with aMUC1 retargeting ligands enhances VV's circulation kinetics in mice bearing CAPAN-2 xenografts. (a) The quantity (VG) of a 1 x10^7 pfu dose of VV, PCVV or aMUC1-PCVV circulating was determined by qPCR by taking sequential bleeds from mice at 5, 10 mins and 20 mins (n=4). The mean quantity (VG) is displayed for each time point. Error bars represent SD. Ordinary one-way ANOVA was performed at 5 minutes with post-hoc Tukey's test for multiple comparisons. * = $p < 0.05$. (b) The mean quantity (VG) circulating at 5 minutes as determined by qPCR (n=4). Error bars represent SD. Ordinary one-way ANOVA was performed with post-hoc Tukey's test for multiple comparisons. * = $p < 0.05$. (c) Tumours were resected at 20 minutes for all mice. After homogenisation to 75 mg/mL, DNA was extracted and quantified by QPCR to determine accumulation after 20 minutes. Results are displayed are for the VG/ tumour. Error bars represent standard deviation (VV and PCVV n=4, aMUC1-PCVV n=3)

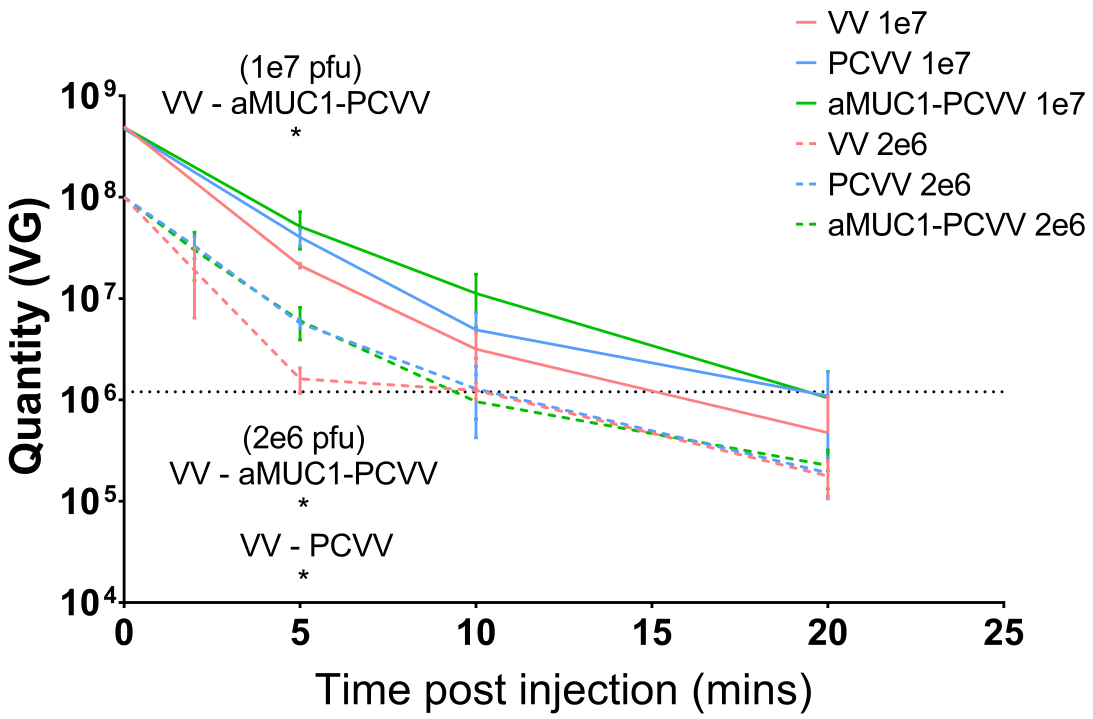


Figure 5.24: Overlay of pharmacokinetic (PK) studies at a high (1x10^7 pfu, solid lines) and low dose (2x10^6 pfu, dashed lines). The quantity (VG) of a 2x10^6 pfu or 1x10^7 pfu dose of VV, PCVV or aMUC1-PCVV circulating was determined by qPCR. In the 2x10^6 pfu dose PK, bleeds were taken from mice at either 2 and 10 mins (n=4) or 5 and 20 mins (n=4). In the 1x10^7 pfu dose PK, consecutive bleeds were taken at 5, 10 and 20 mins (n=4). Points represent mean VG quantity at each time point and error bars represent SD. Ordinary one-way ANOVA was performed with post-hoc Tukey's test for multiple comparisons. * = $p < 0.05$.

(+/- 3.3x10^4) VG/ tumour of aMUC1-PCVV. These differences between groups were not found to be statistically significant ($p>0.05$). Once again, the highest VG/tumour recovered from a tumour (7.7 x10^4 VG/ tumour) was observed in a mouse treated with aMUC1-PCVV. It would therefore be of merit to perform a study in which accumulation and its impact on infection over time was measured at a series of time points either by qPCR or imaging of a reporter gene. This may allow for greater separation between virus groups at early and late time points.

Comparing the PK for each viral sample observed at the high and low dose showed that a similar pattern can be seen at each dose (Figure 5.24). There is a difference however in the ratio between the amount circulating of the coated and naked virus at the lower dose and the higher dose. At the 2x10^6 pfu dose PCVV

and aMUC1-PCVV were around 4 times higher than that of VV. At the 1x10^7 pfu dose, this reduced to PCVV and aMUC1-PCVV being only approximately 2 and 2.5 times higher than naked VV respectively. It is hypothesised that this may be due to saturation of clearance mechanisms occurring for coated VV's at this dose. By performing the PK studies at two different doses, one 5 times higher than the other, it is possible to determine the linearity of the PKs and whether coating VV impacted the linearity. The relationship between drug exposure, represented by the area under the curve (AUC), and dose is as follows

$$AUC = \frac{1}{CL} * Dose$$

where CL is the clearance. As shown in the equation, if CL is constant, then any increase in dose results in an increase in exposure (AUC): the two are directly proportional and hence the PKs are linear. In the 2x10^6 pfu dose, the CL's determined for VV, PCVV and aMUC1-PCVV were 1, 0.77 and 0.77 respectively where the higher the clearance, the lower the drug exposure. In the 1x10^7 pfu dose, the CL's determined for VV, PCVV and aMUC1-PCVV were 0.55, 0.52 and 0.45 respectively. Therefore for these virus samples, the clearance was not constant and hence the PK's are non-linear i.e. the clearance changes with dose, and decreases as the concentration increases. This usually happens as the clearance mechanisms become saturated aka "saturated elimination" and could result in disproportionate increases in plasma VV concentration.

The most likely saturable clearance mechanism is removal by the reticuloendothelial system (RES), a mechanism previously shown to be involved in the clearance of other viruses. [116, 223] There is a possibility that increasing the plasma VV concentration would allow more opportunity for VV to flow through tumours and extravasate from the bloodstream into them.

5.5 Discussion

In this chapter, the protective and stabilising effect of including a Cholesterol-PEG polymer coating shown in Chapter 4 was built upon to determine whether the

inclusion of targeting ligands to a known tumour antigen (mucin-1) could improve the overall infectivity of a modified oncolytic vaccinia virus *in vitro* and *in vivo*. This technique of "detargeting" using polymer coating and then restoring infectivity has previously been shown to be effective *in vitro* for oncolytic adenovirus with a number of different tumour associated antigens as targets. [76, 96, 106, 107, 114, 224] The investigations in this chapter have included the production and characterisation of a stable anti-MUC1-PEG-Cholesterol antibody-polymer conjugate. Its use in coating a clinical grade oncolytic vaccinia virus to form an aMUC1-PCVV was verified using flow virometry and then tested for infectivity and plasma stability in a cell line highly expressing MUC1 *in vitro*. Finally, the circulation kinetics of the aMUC1-PCVV construct and passive tumour accumulation was investigated *in vivo*. The main findings are:

1. Synthesis of a Chol-PEG-NHS from a Chol-PEG-COOH was possible and initial studies showed that Chol-PEG-NHS formulated in the lab was able to form stable links with IgG and aMUC1 antibodies. IgG and aMUC1 antibodies were then combined with a commercial Chol-PEG-NHS and were shown by SDS-PAGE with protein and PEG staining and by altered retention times when separated by liquid chromatography to have successfully formed antibody polymer conjugates. The ability of Chol-PEG-aMUC1 to bind to a MUC1 peptide target, with increasing modification extents was determined using an ELISA. It was shown that as the concentration of polymer incubated with aMUC-1 antibody was increased, the ability of the antibody-polymer conjugate to bind the MUC1 peptide decreased with the greatest impact being a 10% increase in the half-maximal saturation constant at a 1:50 conjugation ratio. Hence it was determined that to avoid over modification, and hence impact on MUC1 binding, an aMUC1:Chol-PEG-NHS ratio of 1:20 would be optimal. Chol-PEG-aMUC1 that was able to bind the MUC1 core peptide target was also shown to still have PEG attached.

2. Flow Virometry using an adapted Invitrogen Attune NxT flow cytometer (as utilised in Chapter 4) enabled confirmation of the successful coating of an oncolytic VV population with the Chol-PEG-aMUC1 constructs by staining for

aMUC1 after washing. The inclusion of retargeting ligands has previously been shown for adenovirus, however, this is the first demonstration of effective coating with retargeting ligands of an enveloped vaccinia virus.

3. In order to show that after formation aMUC1-PCVV was still able to bind the MUC1 target, naked VV and aMUC1-PCVV formed at three different antibody concentrations on the polymer coating were compared for their ability to bind an immobilised MUC1 peptide target. There was a statistically significant ˜2-fold increase in VV DNA present in all three of the aMUC1-PCVV sample wells when compared to the naked VV wells after multiple rounds of washing. These results are in line with the first report of a genetically modified VV by Galmiche *et al* in which the envelope glycoprotein haemaglutinin was replaced by a fusion molecule carrying a single chain antibody directed against the tumour associated ErbB2 antigen. This proof-of-concept study showed that a retargeted VV was able to bind its target (soluble ErbB2) efficiently *in vitro*. [225]

4. CAPAN-2 was verified as a cancer cell line with high levels of MUC1 expression using flow cytometry. Initial tests using VV-GFP showed that infection of CAPAN-2 cells (as determined by cellular GFP fluorescence detected by flow cytometry) was reduced 2-fold for PCVV as compared to naked VV. It further showed that the addition of aMUC1 antibodies for retargeting could increase that level of infectivity (as determined by transgene expression), however this was determined not to be a statistically significant increase due to large variation within samples. This large variation was suspected to be due to difference in morphology of CAPAN-2 cells between different wells due to their propensity to clump during adhesion growth, with some wells containing far larger clumps of cells than others.

5. The infection conditions were changed so that CAPAN-2 cells were infected in suspension and therefore differences in cellular morphology between wells would not impact variability within samples as readily. A VV-luc was used instead of a VV-GFP to determine knockdown in infection due to the presence of human plasma as it has a much greater dynamic range. There was a high infection capacity at a 0.1 pfu/cell concentration. Differences in infectivity (as determined using a luciferase assay)

between naked VV and PCVV reiterated what was seen when infection occurred with VV-GFP: a 3-fold reduction ($p<0.05$) in infection (normalised luminescence) was observed with PCVV when compared with VV. The same pattern was also true for the aMUC1-PCVV which showed a 3.2-fold increase ($p<0.05$) in infection when compared with PCVV. In order to try and determine whether the MUC1 binding specifically of aMUC1-PCVV was responsible for restoring of infection, an IgG-PCVV control was formulated. As with the addition of aMUC1 antibodies, IgG-PCVV also showed a significantly ($p<0.05$) higher 2.4-fold infectivity than PCVV. This showed that, although to a lesser extent than the aMUC1 antibodies, the addition of IgG antibodies to the polymer coating was able to restore infection. As this restoration of infection, for both aMUC1 and IgG antibodies, could be due to physical differences in the VV coating i.e, potentially less uniform or less dense coating with the presence of 150 kDa proteins preventing efficient Chol-PEG embedding than in the PCVV samples, their stability was tested in the presence of 5% human plasma positive for anti-VV antibodies. All three polymer coated samples showed a reduced impact with the inclusion of human plasma when compared to naked VV which had a substantial (>200-fold) reduction in infectivity.

6. Differences observed between the conjugation of Chol-PEG-IgG and Chol-PEG-aMUC1 meant that it was more suitable to use a MUC1 peptide "blocked" aMUC1-PCVV (MUC1-aMUC1-PCVV) as a control for validation of specific MUC1 mediated binding to cells, thereby removing any effects that these differences in physical conjugation may have on overall infection levels. Incubation of Chol-PEG-aMUC1 constructs with the MUC1 peptide did reduce the mean infection levels achieved when compared to those of aMUC1-PCVV, however this difference in infection level was not found to be statistically significant. This perhaps indicated that the blocking of the aMUC1 antibodies was not efficient enough, although an ELISA showed a marked reduction in binding affinity for a Chol-PEG-aMUC1-MUC1 when compared to Chol-PEG-aMUC1. However, because the Chol-PEG-aMUC1 was blocked before embedding, it was then subject to multiple rounds of washing during which some of the peptide may have been removed. Therefore a more

robust method of blocking could have been to add the peptide into the cell culture medium at the point of infection, rather than preincubation with the polymer before embedding into the VV.

In a study by Paul *et al*, MVA (an attenuated strain of VV) was genetically modified to produce a single chain fragment of the aMUC1 antibody (SM3 clone). They were able to show a statistically significantly higher percentage (˜2-fold increase) of infected BHK-21 cells (Baby hamster kidney cell) transfected with MUC1 (79 (+/-5)%) when compared with control BHK-21 cells (39 (+/-2) %) at MOI 0.1. No significant difference was found in the % infected cells for unmodified MVA and modified MVA in the BHK (negative for MUC1) cells. Infected cells were identified by staining with a fluorescently conjugated anti-MVA antibody and then detection with flow cytometry. Given that MVA's high attenuation prevents it from replicating, the intensity of infection (i.e. infection per cell) was not reported. This was in contrast to the studies reported here where a VV-GFP was used in combination with flow cytometry to determine differences in infection levels between VV, PCVV and aMUC1-PCVV in CAPAN-2 cells (high in MUC1). Here, it was shown that 2-fold less cells were infected with aMUC1-PCVV (12% GFP+, $p<0.05$) compared with VV (24% GFP+). There was, however, no statistically significant difference ($p=0.33$) in the mean MFI for VV and aMUC1-PCVV suggesting that the intensity of infection in the aMUC1-PCVV infected CAPAN-2 cells was higher.

Another report used a biotin-avidin viral coating to conjugate biotinylated antibodies the surface of VV vectors. [226] This is more in line with the chemical modification techniques used here as the membrane was physically blocked through the antibody conjugation much like the use of the polymer here. Purow *et al* reported that the antibody coating resulted in reduced infection in control cells when compared to an unmodified VV and preserved infectivity for target cells (a transduced cell line). [226]

The oncolytic VV utilised in these studies is an attenuated recombinant vaccinia virus (VV) which is derived from the Copenhagen strain, encodes luciferase and has a deletion of the thymidine kinase and ribonucleotide reductase genes. This double

deleted vaccinia virus is highly attenuated in normal cells, yet display tumour-selective replication and cell kill. [195] Therefore it was important that cancer cells were used in infection studies as opposed to a transduced non cancer cell line such as the cells used in Paul *et al.* [130] Given that MUC1 is reported to be over expressed in most human cancer cells, an IgG control antibody and MUC1 peptide were used to try and show target specificity of aMUC1-PCVV here. Both these previous reports used a transduced cell line to show target specificity and hence suggest that it would be of merit to further assess the specificity of the MUC1 target binding of aMUC1-PCVV by silencing a low MUC1 expressing cancer cell line to create a truly MUC1 negative cancer cell line.

Fisher *et al* previously reported the efficient detargeting of oncolytic adenovirus (Ad) using a covalently conjugated pHPMA (16.5 kDa) polymer (PC-Ad) demonstrating an ablation in the percentage of A549 cells infected with a YOYO-1 stained PC-Ad when compared with unmodified YOYO-1 stained Ad as detected using flow cytometry. [76] The transgene expression (GFP) was also shown to have 10-fold reduction for PC-Ad compared with Ad. This is inline with what was reported here, however the reduction in transgene expression (luc) was to a lesser extent (3-fold) suggesting that Chol-PEG coating was not as efficient as detargeting VV and pHPMA coating was at detargeting Ad. This was discussed further in Chapter 4 section 4.5. Fisher *et al* then showed that the addition of FGF targeting ligands to the pHPMA coating was possible and enabled infection of A9 cells (positive for FGF expression) which Ad is not typically able to infect. Target specificity was shown in these murine A9 cells (positive for FGF expression) by preincubating the cells with soluble FGF to block the FGF receptor on the cells before they were washed and incubated with the retargeted Ad. This led to infection being reduced to the same level as that of the unmodified Ad. In the studies reported here, the Chol-PEG-aMUC1 constructs were preincubated with MUC1 peptide in an attempt to block the aMUC1 binding regions before aMUC1-PCVV formation and infection of CAPAN-2 cells. Due to the intensive washing cycles aMUC1-PCVV underwent prior to being added to CAPAN-2 cells,

the method of blocking may be less effective than the incubation of aMUC1-PCVV with MUC1 peptide or the inclusion of MUC1 peptide in the infection media at the point of infection. This may explain the low impact reported here on infection for the "blocked" aMUC1-PCVV with the MUC1 peptide.

The Paul *et al*, Purow *et al* or Fisher *et al* studies did not investigate the impact that their respective genetic and chemical retargeting of VV or Ad had on its ability to evade neutralisation, blood component stability or PK.

7. Analysis of VV, PCVV and aMUC1-PCVV circulation kinetics after systemic administration of a $2x10^6$ pfu dose in CAPAN-2 xenograft bearing BALB-C nude mice showed that approximately 4-fold more virus copies remained in circulation 5 minutes after injection of washed PCVV ($p<0.05$) and aMUC1-PCVV ($p<0.05$), as compared to 5 minutes after injection of naked VV. Area under the curve analysis showed that the exposure increased as a result of this reduced rate of clearance for both PCVV and aMUC1-PCVV when compared to that of VV. As with the PK study reported in Chapter 4, the immunocompromised BALB-C nude mice used in this pharmacokinetic study lack T cells and an adaptive immune response to pathogens but retain an innate immune response. Hence, the enhanced circulation seen here for both PCVV and aMUC1-PCVV suggests, as discussed in Chapter 4, that PCVV and aMUC1-PCVV is probably able to evade the innate immune response and RES more effectively than naked VV. It was hypothesised that the addition of an aMUC1 targeting ligand would increase tumour accumulation, however, with the exception of two mice in the aMUC1-PCVV group, the tumoural viral loads detected were extremely low across all groups.

In a study previously reported by Green *et al* the impact of pHPMA coating on Ad showed that differences in the PK between PC-Ad and unmodified Ad were greatest at 30 minutes where 10-fold more of the dose was circulating in all doses of PC-Ad when compared with unmodified Ad. The sequestration of unmodified VV from circulation reported here was much faster than that of unmodified Ad: VV showed barely detectable levels even in the higher dose by 20 minutes for VV, PCVV and aMUC1-PCVV. Therefore extent of improvement in circulating

dose at the 5 minute time point for VV is of importance. The extent of the improvement in quantity of circulating dose being 5-fold for the studies reported for PCVV here, when compared with PC-Ad being ˜10-fold, is in the line with the extent of infection ablation being lower for PCVV when compared with PC-Ad in *in vitro* infection studies.

8. Pharmacokinetic analysis of VV, PCVV and aMUC1-PCVV in the same CAPAN-2 xenograft bearing BALB-C nude mouse model at a 5-times higher ($1x10^7$ pfu) dose confirmed that the enhanced circulation kinetics seen for the lower dose translated to the higher dose. The mean amount of virus circulating at 5 minutes was higher for both PCVV (2.4-fold) and aMUC1-PCVV (3.5-fold, $p<0.05$) when compared with naked VV. An increase in overall exposure was determined for both PCVV and aMUC1-PCVV compared to VV.

At this higher dose, the tumoural viral loads detected by qPCR were approximately 10 fold higher across all groups suggesting that detection limits were overcome. There was no statistically significant difference between mean tumoural viral loads detected for any of the groups. It was noted that as with the $2x10^6$ pfu dose, the highest viral load was in an aMUC1-PCVV administered tumour. As discussed in Chapter 4, the lack of difference seen in tumour accumulation at 20 minutes between all doses may be due to the short time to allow for effective replication leading to easy detection and a more detailed look at tumoural viral load using imaging of a reporter gene over multiple days may help to unpick whether there are differences in accumulation (see Chapter 6).

9. Comparing the PK studies at both doses allowed the non-linearity of the VV, PCVV and aMUC1-PCVV PKs to be determined. Clearance was found not to be constant between doses and so it is likely that for all samples at the higher dose, clearance mechanisms were saturated. The enhanced PK achieved by PCVV and aMUC1-PCVV when compared to VV within the first 5 minutes of treatment in this murine model could translate to tangible benefits clinically. In a mouse, there are approximately 11-13 full circulations of blood each minute whereas in a human there are approximately 3 full circulations of blood every minute. Therefore, in a

VV naive patient, the results presented here could correspond to a 5-fold increase in viral titre in the first 25 minutes post infusion. In a study by Breitbach *et al* there was approximately a 10-fold decrease in genome concentration detected after the first 30 minutes following IV infusion in doses between $1x10^6$ - $3x10^7$ pfu/kg. [22] Polymer coating could reduce this to only a 2-fold knockdown in the first 30 minutes. On day 10 post-injection, biopsies of tumours showed that only tumours from patients treated with doses over $1.5x10^7$ pfu/kg were positive for VV. If PCVV or aMUC1-PCVV was to be used this may result in tumoural accumulation from a ~$3x10^6$ pfu/kg dose instead.

5.6 Summary and Conclusions

In summary, it was reported in this chapter that addition of an aMUC1 antibody to polymer coated VV could be achieved and that it could be detected and verified using flow virometry. In a CAPAN-2 cell line which greatly overexpressed MUC1, the presence of the aMUC1 antibody was able to restore infection levels *in vitro* lost due to polymer coating. This restoration of infection level was also seen with the addition of an IgG antibody, suggesting that this restoration was not MUC1 target specific. It was hypothesised that perhaps the presence of an antibody impacted the coating density. A blocked aMUC1-PCVV did show reduced mean infection levels when compared to that of aMUC1-PCVV but large differences within the blocked virus sample meant that this difference was found to not be statistically significant. All of the coated samples showed enhanced protection in the presence of plasma (from a donor pre-exposed to VV through childhood smallpox vaccinia) when compared to naked VV. In the presence of 2% plasma both the PCVV and aMUC1-PCVV showed the lowest impact with the least knockdown in infection observed. PCVV showed substantially higher infection levels ($p<0.05$) than both VV and MUC1-aMUC1-PCVV in 2% plasma. In 5% plasma, infection levels were impacted to a greater extent than at 2% with naked VV showing a 200-fold knockdown in 5% and a 24-fold knockdown in 2%. The aMUC1-PCVV and IgG-PCVV samples ($p<0.05$) had higher mean infection levels than PCVV and VV suggesting that at

higher concentrations of plasma the presence of an antibody on the coating lead to enhanced stability. PK studies showed that circulation kinetics were improved for PCVV and aMUC1-PCVV at two different doses, $2x10^6$ pfu and $1x10^7$ pfu, leading to longer circulation half lives and resulting increased overall exposure of tumours to virus. The clearance rates were determined to be dose dependent for VV, PCVV and aMUC1-PCVV. The increased exposure did not result in increased accumulation at 20 minutes, however this is considered unlikely at such an early time point. Given the complexity of the tumour microenvironment, especially for a xenograft such as CAPAN-2 which has a dense stroma, in order to realise the benefit of this enhanced PK, combination strategies, such as those described in section 1.3.2.1, may need to be utilised. These could include pretreatment with anti-angiogenic drugs for vascular normalisation [171] or the use of non-invasive techniques such as focused ultrasound in combination with cavitation nuclei [116, 190, 202].

The following is therefore concluded for Chapter 5:

- The addition of aMUC1 antibodies onto the polymer coating of VV via a cholesterol anchor to form aMUC1-PCVV was shown via flow virometry.
- In a high MUC1 expressing CAPAN-2 cancer cell line, monolayer experiments showed that, inline with the results in Chapter 4, PCVV had a knockdown in infection when compared to VV. aMUC1-PCVV infected cells showed restored levels of infection to those observed in VV infected cells.
- aMUC1-PCVV showed the same enhanced circulation kinetics as PCVV when compared with VV in *in vivo* PK studies at two different doses. However, this enhanced circulation and the presence of aMUC1 tumour targetting antibodies did not result in detectable enhanced tumour accumulation 20 minutes after IV injection as was hypothesised.

Chapter 6

In vivo assessment of cavitation-mediated delivery of VV, PCVV and aMUC1-PCVV

6.1 Introduction

VV has a number of inbuilt defences which help it evade host immune detection and which make it desirable as a candidate for IV administered oncolytic virotherapy as discussed in section 1.2.1. [53, 227] Once tumour cells have been infected, rapid viral replication cycles allow for infection propagation and dissemination to nearby cells. However, certain characteristics of solid tumours restrict the efficacy achieved by some novel biologic anti-cancer treatments. This is predominantly due to limitations during the delivery phase, i.e. low accumulation within tumour sites and non-uniform distribution of the virus which does manage to accumulate. Three key tumour characteristics serve to limit delivery by impairing convective flow in the tumour, namely irregular tumour vasculature, dense extracellular matrix structure, and high interstitial fluid pressure. [151]

As discussed in detail in Chapters 1 and 3, the majority of clinical trials involving oncolytic VV have been restricted to IT administration, despite the benefits that could be gained from IV administration. [3, 4] Externally applied ultrasound coupled with IV administered cavitation nuclei has been previously shown to improve the delivery of both oncolytic adenovirus [116] and oncolytic

VV [190] *in vivo*. In this chapter, the delivery of VV, PCVV and aMUC1-PCVV using US and cavitation nuclei is assessed.

In Chapter 5, the successful addition of a mucin-1 targeting ligand (aMUC1 antibody) to the polymer coating of oncolytic VV was shown and the infection capability of VV, PCVV and aMUC1-PCVV in CAPAN-2 cells was determined. Both the polymer coating and the retargeted polymer coating of VV showed enhanced circulation kinetics *in vivo*. However, the tumour accumulation at 20 minutes was assessed and no immediate enhancement in tumour accumulation was observed for PCVV or aMUC1-PCVV compared to VV, despite their enhanced PK. This finding is in accordance with studies on passive tumour accumulation in animal models, which suggest a raised circulating dose is needed over periods of 24-48 hours before enhancement is seen. [228] The best way to realise the advantage of the raised 5 minute circulating dose of PCVV or aMUC1-PCVV is therefore to apply a mechanical stimulus to the tumour directly after dosing. This principle has been previously applied to adenovirus [116] and liposomes [180]. Therefore, this chapter explores the hypothesis that application of focused ultrasound to tumours during the initial 5 minutes after dosing can lead to greater extravasation from the blood stream and hence even greater dissemination within tumours. The aims of this chapter are as follows:

1) Assess how the use of focused ultrasound (US) coupled with IV administered cavitation nuclei will impact tumour delivery in a bilateral tumour model for a virus with enhanced pharmacokinetics such as PCVV and aMUC1-PCVV.

2) Assess tumour growth following IV delivery of VV, PCVV and aMUC1-PCVV coupled with either passive accumulation, or US-enhanced delivery.

In order to assess these aims four *in vivo* experiments were conducted:

- Experiment 1 looked at the viability of the CAPAN-2 xenograft tumour model for use in the delivery and tumour growth studes studies reported here.
- Experiment 2 validated the dose to be used in the delivery and tumour growth studies.

- Experiment 3 assessed the impact that US in combination with SSP cavitation nuclei would have on the delivery of VV, PCVV, aMUC1-PCVV and IgG-PCVV.
- Experiment 4 determined the impact that US in combination with SSP cavitation nuclei would have on tumour growth following IV administration of VV or aMUC1-PCVV.

Myers *et al* compared the infection levels achieved at 48 hours post treatment in excised HepG2 xenografts treated with VV and one of two different types of cavitation nuclei: SonoVue (SV) or Sono-Sensitive Particles (SSPs). Assessment was achieved by analyzing luciferase levels after a 10 minute US exposure time covering different parts of the xenograft tumours. [190] This study provided compelling evidence that VV co-injected with SSPs followed by US exposure was able to substantially and statistically significantly enhance infection in HepG2 xenografts when compared with VV alone.

However, VV's neutralisation and clearance profile in human blood may hinder its translation into clinical use as a systemically delivered agent. This is evidenced by the predominant route of administration currently used in clinical trials being restricted to IT injection (detailed in section 1.2.1).

The single transducer setup used in the studies of Myers *et al* only allowed for low resolution therapeutic ultrasound monitoring with Passive Acoustic Mapping (PAM). A dual-transducer set-up has been shown to provide a higher resolution real-time treatment monitoring system, providing more detailed feedback on treatment to the operator, a feature which will aid clinical adoption. In addition, a coated and retargeted VV designed with consideration to the challenge presented by the human bloodstream may result in increased levels of infectivity. Therefore it is hypothesised that utilising a dual-transducer setup (as seen in Figure 6.5) combined with polymer coated VV with or without retargeting ligands would result in a more uniform and efficacious treatment that will be more likely to translate successfully into patients.

6.2 Results: Experiment 1- Assessment of suitability of CAPAN-2 xenograft model for ultrasound mediated cavitation studies

The CAPAN-2 cell line is a human pancreatic ductal adenocarcinoma derived cell line, which has a well-validated high level of MUC1 expression, making it a good potential target for a MUC1 targeted therapeutic. However, as many xenografts grow in a highly unpredictable and avascular way, making delivery impossible regardless of enhancement of PK or the application of cavitation, it was first important to profile the growth rate and perfusion of CAPAN-2 tumours. It is also possible that in adapting to grow as a xenograft the cells alter their receptor expression profile and so it was important to confirm MUC1 expression in tumour lysate.

Studies were performed to verify the tumourigenicity of CAPAN-2 xenografts in BALB-C nude female mice by regular measurement with calipers. The perfusion of tumours at different stages of growth was determined using Direct Contrast Enhanced magnetic resonance imaging (DCE)-MRI. Furthermore, the MUC1 expression in recovered tumours was confirmed with a western blot.

6.2.1 Experiment 1: DCE-MRI Imaging to assess perfusion

DCE imaging is a method which is commonly used for determining the tissue blood flow (commonly referred to as perfusion) in the body through IV injection of an appropriate contrast agent. This can be performed using an MRI, CT or US imaging modality.

In an MRI machine, the strong magnetic field forces protons in the body to align with it. A radiofrequency electromagnetic field is then pulsed through the patient which stimulates protons and spins them out of alignment. Energy is released from the protons as they realign after the radiofrequency field is turned off and this is detected by MRI sensors. Gadolinium (Gd) contrast agents such as the one used here (Gd-contrast agent (Omniscan, GE Healthcare)) increase the speed at which the protons realign, causing a brighter image to be obtained. Hence, by injecting

a Gd contrast agent during a series of MRI scans, brighter sections of images are produced where the contrast agent has diffused and darker sections of images remain where it is yet to diffuse. In this study, contrast agent is injected during the repeated acquisition of images and the single enhancement kinetics in the tissues (tissue enhancement kinetics) are determined. [229] Two phenomena occur simultaneously which are involved in tissue enhancement kinetics. The first is perfusion in the microcirulatory network and the second is the accumulation and clearance from the interstitium due to capillary leakage. By mapping of the accumulation rate of Gd in patients, the blood flow within different tissues can be assessed and compared.

Here DCE-MRI imaging was utilised to assess tumour blood flow in CAPAN-2 xenograft tumours at different stages of growth. This enabled the identification of a window of tumour volume in which treatment would not be hindered by a lack of perfusion within the tumour either due to lack of fully developed vascularilty or due to development of a necrotic core.

DCE-MRI imaging was performed consecutively on mice on days 33, 39 and 50 post subcutaneous inoculation with $1x10^6$ CAPAN-2 cells in PBS as described in section 2.8.3.2. Five mice were inoculated and four of the tumours showed persistent growth over the study, the fifth mouse was sacrificed when it was clear that the tumour would not grow larger than 20 mm^3. This allowed perfusion to be determined in xenograft tumours at different stages of growth. Gd MRI contrast agent (Omniscan, GE Healthcare) was infused into the blood stream and a sequence of 50 images was taken. The positive enhancement was traced at 5 points throughout the tumours and graphs depicting the MRI signal recorded for each mouse are displayed in Figure 6.1. The five points were chosen to reflect regions which may present different levels of perfusion: from the edge of the tumour capsule and moving towards the centre of the tumour.

At day 33 (imaging day 1) mice 1, 2, 3 and 5 showed similar perfusion profiles: the red trace at the rim of the tumour shows it to be the most perfused area of the tumour with the MRI signal still increasing at the end of the sequence. Lower levels of perfusion were observed at all other points in the tumours. Mouse 4 showed

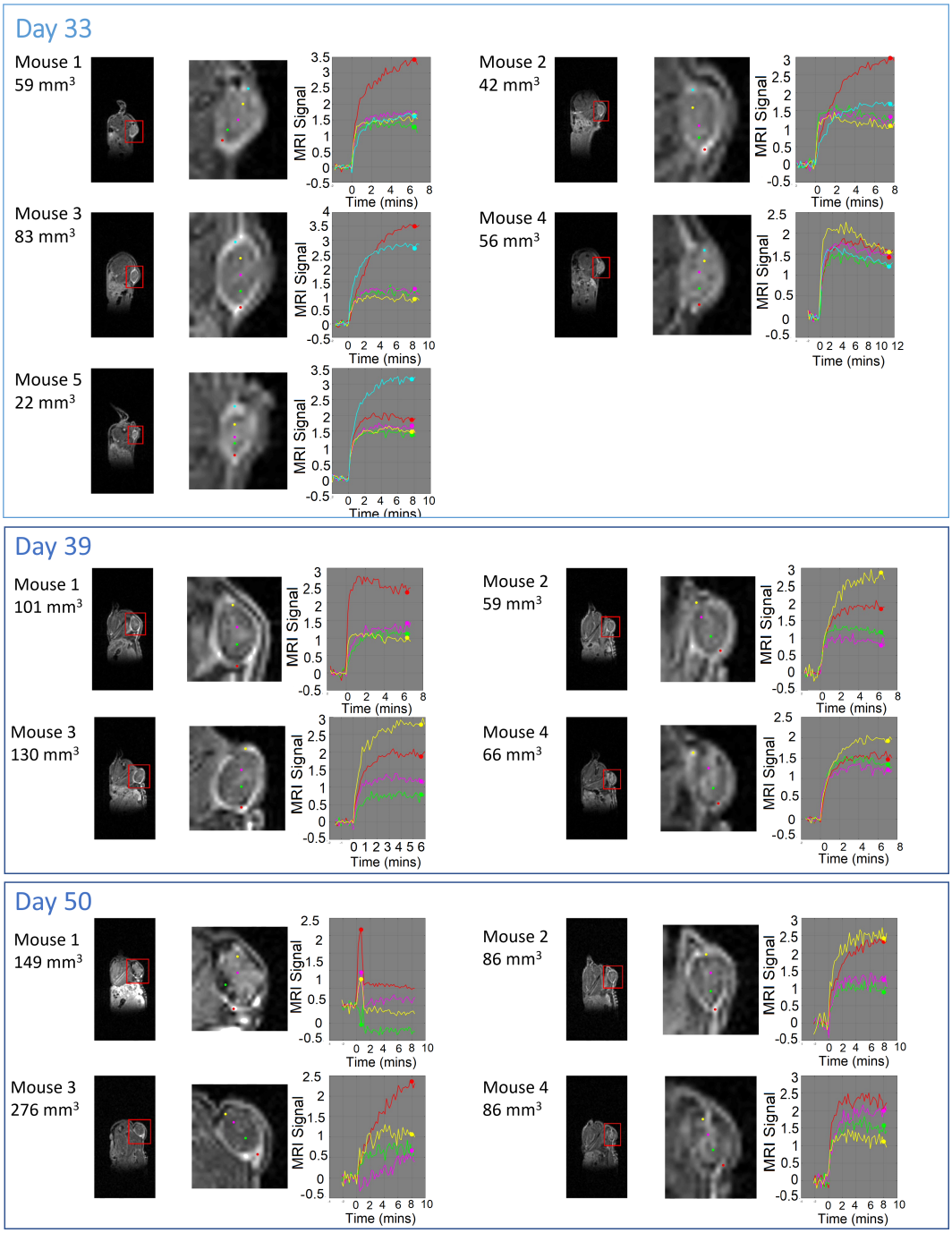


Figure 6.1: Final image in sequence after infusion of positive contrast enhancement of all mice at each imaging day. At day 33 all 5 mice that were inoculated were imaged. By day 39 it was clear that the xenograft for mouse 5 was not showing persistent growth as the volume remained at approximately 20 mm^3. For each mouse there are three images: (1) the plane of the mouse at which the images were taken, red box indicates tumour (2) the tumour with the coloured points at which the perfusion was traced in real time and (3) the traces of the MRI signal corresponding to each of the coloured points highlighted in (2). Tumour volumes recorded on the day of imaging are displayed beneath the mouse number.

a different profile to the other mice, with a more uniform perfusion throughout the tumour and a maximum MRI signal that was substantially lower, including that recorded in the rim of the tumour. Mouse 4's traces were decreasing after the maximum MRI signal was reached at about 3 minutes, suggesting that contrast agent flow out of the tumour was faster than was evident in the other mice. At day 33 there seemed to be little correlation between the perfusion profile recorded and the mouse tumour volumes, which ranged between 22 and 83 mm^3.

By day 39 (imaging day 7), four of the five tumours had continued growing and so were revaluated by DCE-MRI. The volume of the CAPAN-2 xenograft on mouse 5 had not increased and so this mouse was sacrificed. Tumour volumes for the four xenografts were between 59 and 130 mm^3. Mice 2 and 3 displayed very similar, heterogeneous, perfusion profiles despite xenograft 3 having over double the volume of xenograft 2. The highest perfusion levels were in the rim of the tumour (yellow and red lines) and the lowest perfusion levels in the centre (green and magenta lines). Despite an increase in volume to 101 mm^3, the xenograft on mouse 1 had a very similar perfusion profile to that recorded at Day 33. Mouse 4 continued to display the most uniform perfusion throughout the tumour, however the MRI signal at the periphery did stabilise once the maximum signal was met, suggesting that blood flow out of the tumour was occurring at a slower rate than it was on Day 33.

On day 50 (imaging day 18) there was a malfunction with the MRI imaging for mouse 1 and the maximum contrast enhancement was saturated causing the MRI signal recording to bleach and stop. Therefore, it is possible to see that there was perfusion, but any further analysis is not possible. There was a marked tumour volume increase for mouse 3 (276 mm^3), suggesting that tumour growth rapidly increases once a volume of 130 mm^3 was recorded. It is however highlighted that this is an n=1 study and so an assessment of this using a greater number of tumours should be performed to robustly examine this. The perfusion profile changed substantially and by day 50 showed signs of poor perfusion at the core points (purple and green) in the tumours with traces consistent with the contrast agent leaking out of the outer vessels and diffusing slowly into the (possibly necrotic)

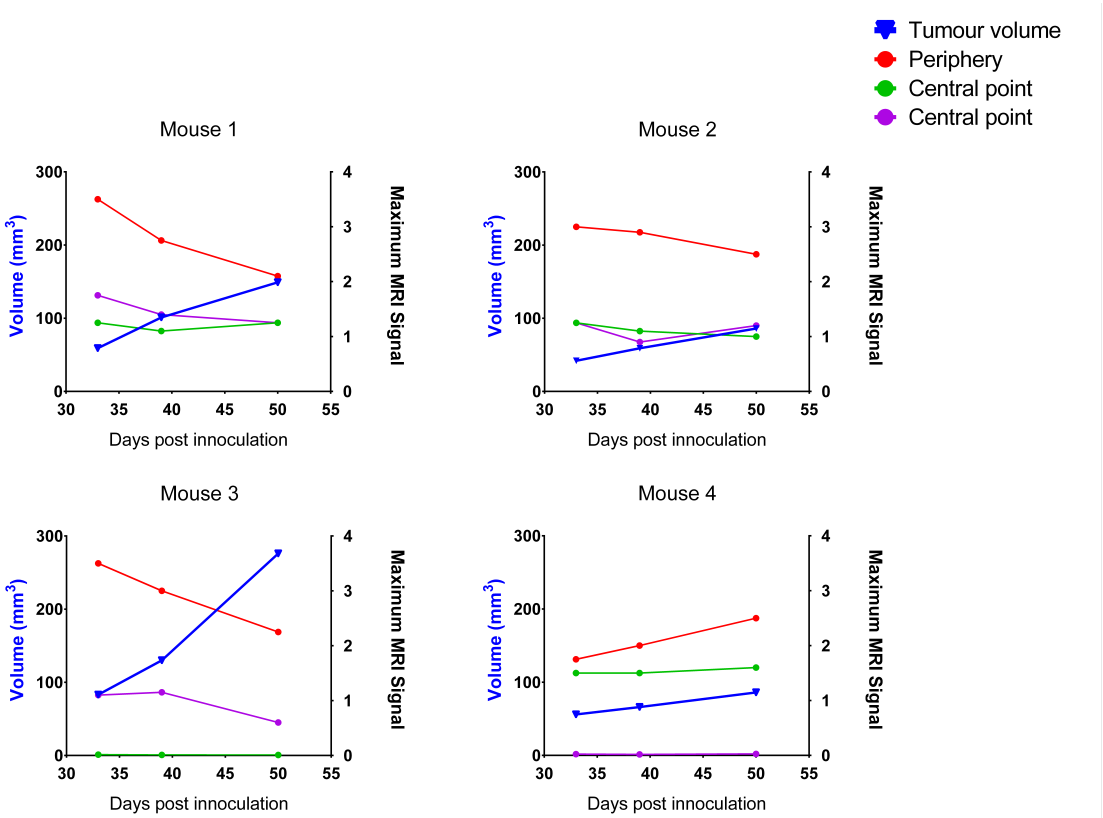


Figure 6.2: Peak perfusion at the periphery and centre of the CAPAN-2 xenografts after infusion of positive contrast enhancement agent in mice 1-4 at each imaging day. Each panel represents one mouse. The left axis shows the tumour volume (blue) at each time point and the right axis shows the maximum MRI signal at the periphery (red) and centre (green and purple) of the tumours for each time point.

centre of the tumour. Mouse 2 showed greater perfusion recorded at the rim of the tumour in comparison with the centre and again, mouse 4 continued to show the most uniform perfusion throughout the tumour.

The data suggests that CAPAN-2 xenograft tumours show reasonable perfusion throughout tumours and, as expected, the highest MRI signal values recorded were in the tumour rim. This data is summarised in the graphs showing volume and maximum MRI signal recorded at the periphery and centre of the tumour over time for individual mice (Figure 6.2). In three of the four mice, it can be seen that as the volume of the tumour increases, the maximum signal at the periphery decreases. Furthermore, the faster the increase in tumour volume is, the more distinct the drop in MRI signal at the periphery. At the centre of the tumour, there is no obvious

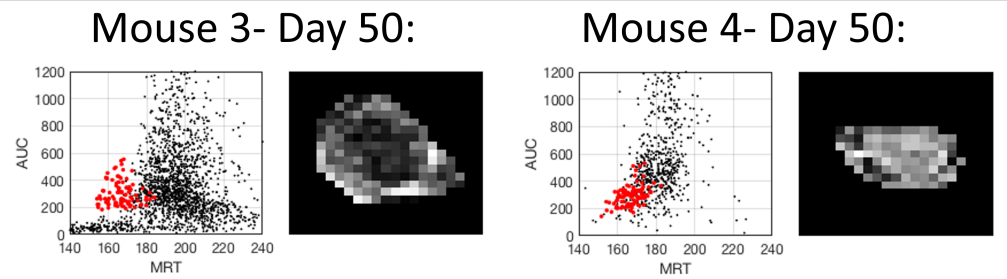


Figure 6.3: Area Under the Curve (AUC) vs Mean Residence Time (MRT) plots for CAPAN-2 xenografts on mice 3 and 4 at day 50. Images of the pixels from which points on the plots were derived are displayed on the right of the plots. Red dots represent values recorded from muscle for comparison of the tumour perfusion to normal muscle.

change in the maximum MRI signal recorded as the tumour volume increases. This suggests that the levels of perfusion remain at a relatively constant level in the centre of the tumour, despite a decrease in perfusion the periphery being recorded.

Once tumour volumes reached larger values (>250mm^3), the levels of perfusion observed throughout the tumour were impacted and the traces suggested that contrast agent was slowly diffusing into the centre of the tumour from the outer rim. [199, 229] This data is in accordance with the angiogenic switch theory in which the balance between pro- and anti-angiogenic molecules are altered. [230]

These findings were supported by area under the curve (AUC) vs mean residence time (MRT) analysis. MRT is the average time that molecules (Gd contrast agent in the work presented here) spend in the body. [231, 232] In AUC vs MRT plots, higher AUC at shorter MRT represent uncompromised perfusion and hence greater tumour blood flow at that point. Conversely, the points with a smaller AUC at longer MRT values indicate that the contrast agent is reliant on diffusion rather than convection, indicative of poor perfusion. [232] For comparison, plots for mouse 3 on day 50 and mouse 4 on day 50 are displayed in Figure 6.3.

Figure 6.3 shows that there is a clear difference in the number of "diffusion" points between mouse 3 (276 mm^3) and 4 (86 mm^3) in the AUC plots. Mouse 4 shows a tight scatter with a steeper profile and very few MRT values over 180s. Mouse 3 has a much broader scatter with a large range of MRT values and a noticeable

number of points with high MRT and low AUC, suggesting there are large areas of the tumours which show diffusion action of the contrast agent occurring.

These findings suggest that there is a clear treatment volume window of between approximately 40-150mm^3 for subcutaneous CAPAN-2 xenograft tumours (although it should be noted that the upper limit of the tumour volume is likely to be higher as perfusion of xenografts with volumes between 150-279 mm^3 were not tested). Therefore, where possible, treatment in Experiment 2, 3 and 4 occurred when tumour volumes were within this volume range and tumours over 279 mm^3 were not used in studies.

These data provide confidence in a tumour size based 'perfusion' window, however it is notable that even tumours of very similar size can have markedly different perfusion levels. This both serves to highlight both the difficulty in performing studies in xenograft tumours and the potential utility of a physical mechanism of delivery. In particular, an enhanced delivery system which can provide in-treatment feedback on the level of stimulus generated (i.e. cavitation mapping) can allow for real-time adjustments to be made based on the scale and location of the stimulus, thereby further improving the overall treatment.

6.2.2 Experiment 1: Determination of MUC1 expression in xenograft CAPAN-2 tumours

MUC1 expression in CAPAN-2 xenografts grown in nude mice has been reported in the literature [233, 234], however given its role as a tumour target in these studies, it was important to verify that CAPAN-2 xenografts grown under the conditions used here maintained MUC1 over expression. CAPAN-2 tumours were recovered at the culmination of the tumour perfusion study. The tumour with a volume of 130 mm^3 was homogenised to a 40 mg/mL concentration in 1X cell culture lysis buffer (E1531, Promega) supplemented with protease inhibitor cocktail (ab65621, abcam) and western blot analysis for MUC1 was performed as described in section 2.8.3.1.

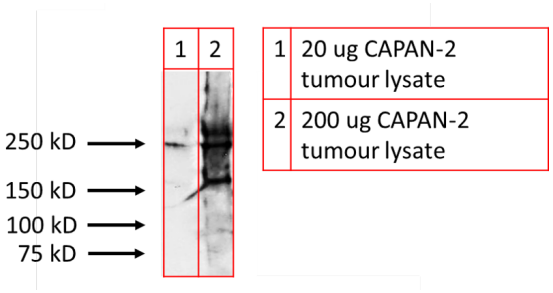


Figure 6.4: Western blot analysis of CAPAN-2 tumour homogenate to assess MUC1 protein expression and binding of aMUC1 antibody (HMFG2). CAPAN-2 homogenate was loaded at 20 µg (lane 1) and 200 µg (lane 2).

Either 20 µg (lane 1) or 200 µg (lane 2) of tumour lysate was mixed with running buffer and added to wells. SDS-PAGE was then used to separate the proteins before staining for MUC1 was performed. The results displayed in Figure 6.4.

MUC1 is a fairly heterogenous high-molecular weight glycoprotein with a core region comprising of a variable number (30 to 100) of tandem repeats of a 20 amino-acid sequence. The core protein is characterised as having a molecular weight (MW) of between 120-225 kDa but this increases depending on the extent of glycosylation which can increase the MW to range between 250-500 kDa. [235, 236] The aMUC1 antibody (HMFG2) used here binds to the MUC1 peptide epitope DTR in both the glycosylated and deglycosylated forms of the MUC1 protein backbone. In tumour cells, a more hypoglycosylated MUC1 is found and hence it is predicted to form a band of between 120-250 kDa. [145, 147, 237–239]

In 200 µg (lane 2) a broad band between 150 kDa and over 250 kDa was stained by the aMUC1 antibody. In 20 µg (lane 1) the 1:10 dilution in DPBS showed that a high concentration of a 250 kDa MW of MUC1 was present in the tumour lysate and binding of other MW MUC1 was much fainter than the band seen at 250 kDa. This agrees with the aMUC1 (HMFG2) antibody manufacturers predicted bands and with the literature.

Xenograft model	Unilateral, CAPAN-2
Number	n=1
Administration route	IV
Cavitation nuclei	1.1 mg SSPs
Group 1	$2x10^6$ pfu VV + SSP + US
Group 2	$1x10^7$ pfu + SSP VV + US
Group 3	$1x10^7$ pfu VV + SSP (without US)

Table 6.1: Experimental design details of experiment 2: dose validation for delivery and tumour growth studies.

6.3 Results: Experiment 2- Assessment of the viral dose to use in combination with ultrasound-mediated cavitation

6.3.1 Experiment 2: Experimental design

Due to the enhancements seen in PK for PCVV and aMUC1-PCVV at both the $2x10^6$ and $1x10^7$ pfu dose, and the reported success by Myers *et al* with a $1x10^6$ pfu dose on unilateral tumours, it was determined that a dose of $2x10^6$ pfu would be appropriate for the delivery and tumour growth studies reported here. However given the difference in xenografts and to ensure this dosing level gave sufficient transgene expression to measure without exceeding the linearity of the *in vivo* imaging system (IVIS) measurement capabilities an n=1 study was performed comparing (group 1: $2x10^6$ pfu + SSP + US) to (group 2: $1x10^7$ pfu + SSP + US) and (group 3: $1x10^7$ pfu + SSP (without US)) (Table 6.1). Treatments will be referred to as group 1, group 2 and group 3 through this section

The schematic of the dual transducer setup can be seen in Figure 6.5 and the ultrasound parameters are displayed in Table 6.2.

The schematic depicts two HIFU transducers (with centre frequencies of 0.5 MHz) mounted perpendicular to each other and aligned confocally. Each transducer had a rectangular cut out into which a linear transducer array was mounted. Real-time passive acoustic mapping (PAM) of cavitation events that occurred within the tumour were obtained using received signals from the linear arrays. The data was also saved, thereby allowing for both real-time treatment monitoring and post

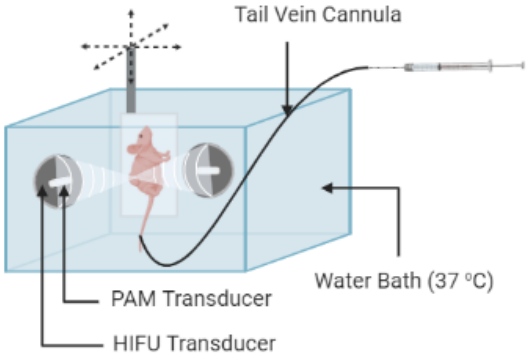


Figure 6.5: Schematic of in vivo US setup. Mice were place in a 37 °C water bath to facilitate coupling of US. The two HIFU transducers were aligned to the tumour using B-Mode images obtained from the linear arrays. Resulting cavitation signals were detected with Passive Acoustic Mapping (PAM) transducers. Whole tumours were 'painted' during the treatment using a 3D movement unit. VV, PCVV, aMUC1-PCVV or IgG-PCVV samples were pre-mixed with SSP cavitation nuclei before IV administration through a tail vein cannula.

Frequency (MHz)	PRF (Hz)	DC (%)	Cycles/Burst	PRFP (MPa)
0.5	0.5	5	50 000	1.5-2

Table 6.2: Parameters for in vivo US treatment of mice during experiment 2, 3 and 4.

treatment analysis of cavitation activity. Cavitation data acquired by the arrays was processed using custom generated MATLAB code written by Dr Christian Coviello, Dr Calum Crake and Seán Finn (Oxsonics Ltd.). The perpendicular configuration of the transducers used here allows for the best PAM resolution in both the transverse and axial directions, which means more accurate localisation of cavitation activity can be achieved. [192] Furthermore, the precision of the ultrasound cavitation is improved as the overlapping focal region of two HIFU transducers is smaller than that of a single transducer for the same focal pressure.

6.3.2 Experiment 2: Luciferase imaging to determine infection levels

Luciferase imaging using an IVIS imager was used to determine infection levels on days 1, 3, 7 and 10. Regions of interest (ROI) were drawn around tumours and the average radiance within the ROI was recorded. The average radiance is a measure of the number of photons per second recorded from within the ROI divided by the

area of the ROI per steradian (p/s/cm^2/sr). This experiment showed that persistent luciferase signal (average radiance (p/s/cm^2/sr)) was observed in both the group 1: 2x10^6 pfu + SSP + US and group 2: 1x10^7 pfu + SSP + US treated mice from day 3 to 10 post treatment. The results are displayed in Figure 6.6.

On day 1, there was a smaller luciferase signal (average radiance) in the group 1 treated mouse (5x10^5 p/s/cm^2/sr) when compared with both the group 2 (3x10^6 p/s/cm^2/sr) and group 3 (2x10^6 p/s/cm^2/sr) treated mice. This is inline with the treatment dose given. However as the days post treatment progressed, the signal in the two US treated mice became substantially stronger than the 1x10^7 pfu + SSP treated mouse. The peak average radiance for all groups was observed on day 7 with the Group 1 treated mouse displaying the highest average radiance value (8x10^9 p/s/cm^2/sr), followed by the 1x10^7 pfu + SSP + US treated mouse (5x10^9 p/s/cm^2/sr) and 1x10^7 pfu + SSP had the lowest average radiance of (5x10^7 p/s/cm^2/sr). On day 10, persistent infection was seen in both US treated mice, however the 1x10^7 pfu + SSP treated mouse continued to show 100-fold lower luciferase signals. These results therefore provided good support for the choice of 2x10^6 pfu as the dosing level, as a good and prolonged infection level was seen without the signal saturating. PK studies reported in Chapter 5 (Figure 5.22a) suggested that VV exposure (AUC) during the first 5 minutes post injection would be approximately 1.8x10^7 pfu min/mL if a 2x10^6 pfu dose is used. Therefore at this dose, a sufficient amount of virus would be circulating within the mouse to impact upon with US mediated cavitation.

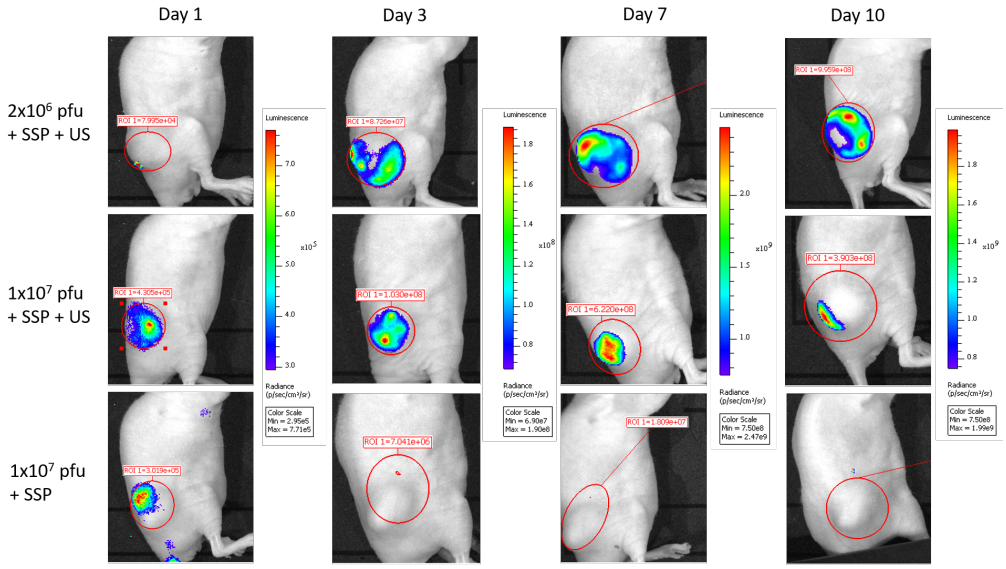


Figure 6.6: An n=1 study to assess the infection in CAPAN-2 unilateral xenografts after treatment with VV-luc in the following doses: Group 1: '$2x10^6$ pfu + SSP + US', Group 2: '$1x10^7$ pfu + SSP + US', and Group 3: '$1x10^7$ pfu + SSP (without US)'. IVIS images were taken on days 1, 3, 7 and 10 post treatment. 100 µL D-luciferin was administered IP in two 50 µL boluses to either flank. Imaging was performed 5 minutes after luciferin was administered. Data shows radiance (p/s/cm^2/sr) set to the same scale for all eaches for each day of imaging: Day 1 ($2.95x10^5$ to $7.7x10^5$), Day 3 ($6.9x10^7$ to $1.9x10^8$), Day 7 ($7.5x10^8$ to $2.5x10^9$) and Day 10 ($7.5x10^8$ to $2x10^9$).

6.4 Results: Experiment 3- In vivo delivery study- VV, PCVV, aMUC1-PCVV and IgG-PCVV with ultrasound-mediated cavitation

6.4.1 Experiment 3: Experimental design

A bilateral CAPAN-2 xenograft model was used here to isolate the effect of US and cavitation on the delivery of VV, PCVV, aMUC1-PCVV and IgG-PCVV. BALB-C nude mice were implanted with subcutaneous xenograft CAPAN-2 tumours and (as determined by the results of the tumourigenicity study, section 6.2.1), were treated in the volume range of between 40 - 180 mm^3 in size. Mice with the most closely matched bilateral tumour sizes were chosen for the study and were assigned to treatment groups so that the mean size of US and non-US treated tumours were approximately equal. This bilateral tumour model was previously used to demonstrate the improved delivery to tumours treated with 'US + cavitation

Xenograft model	Bilateral, CAPAN-2
Administration route	IV
Cavitation nuclei	1.1 mg SSPs
Group 1	$2x10^6$ pfu VV + SSP +/- US (n=3)
Group 2	$2x10^6$ pfu PCVV + SSP +/- US (n=4)
Group 3	$2x10^6$ pfu aMUC1-PCVV + SSP +/- US (n=3)
Group 4	$1x10^7$ pfu IgG-PCVV + SSP +/- US (n=4)

Table 6.3: Experimental design details of experiment 3: delivery study with SSPs and VV, PCVV, aMUC1-PCVV or IgG-PCVV with or without US.

nuclei' as opposed to 'no US' controls for the oncolytic adenovirus (Ad5) and polymer-stealthed Ad5. [116, 202] The same dual transducer setup and ultrasound parameters as those which were used in experiment 2 (section 6.3) were used here. The schematic of the dual transducer setup can be seen in section 6.3.1 Figure 6.5 and the ultrasound parameters are displayed in Table 6.2.

Virus samples were made up on the same day as treatment occurred as described in sections 2.2, 2.2.1 and 2.3.4. The cavitation nuclei were chosen based on the success of SSPs when compared with SV for *in vivo* delivery of VV reported by Myer's *et al.* Hence, 50 µL of a 22 mg/mL solution of SSPs in 5% glucose was used in this study and premixed before injection with 100 µL of each $2x10^6$ pfu virus solution.

BALB-C nude mice bearing bilateral CAPAN-2 xenografts were anaesthetised, cannulated and positioned on a custom holder submerged in the heated waterbath up to the neck. B-Mode images from the linear arrays were used to align the HIFU transducer focus with the tumour to be treated. Ultrasound treatment was started and then mice were co-injected with 1.1 mg of SSP and $2x10^6$ pfu of either VV, PCVV, aMUC1-PCVV or IgG-PCVV via the tail vein cannula (Table 6.3). A detailed description of US treatment can be found in section 2.8.7.

The US was focused on the largest part of the tumour at the beginning of the treatment and after the injection of the virus sample + SSP the mouse was moved slowly in 3 dimensions so that the HIFU transducer focus would treat all regions of the tumour. The Peak Rarefactional Pressure (PRFP) was adjusted during the treatment based on the feedback from the real time PAM feedback monitoring. The aim was to keep the PAM Magnitude constant between 10-30 units (au) for all US

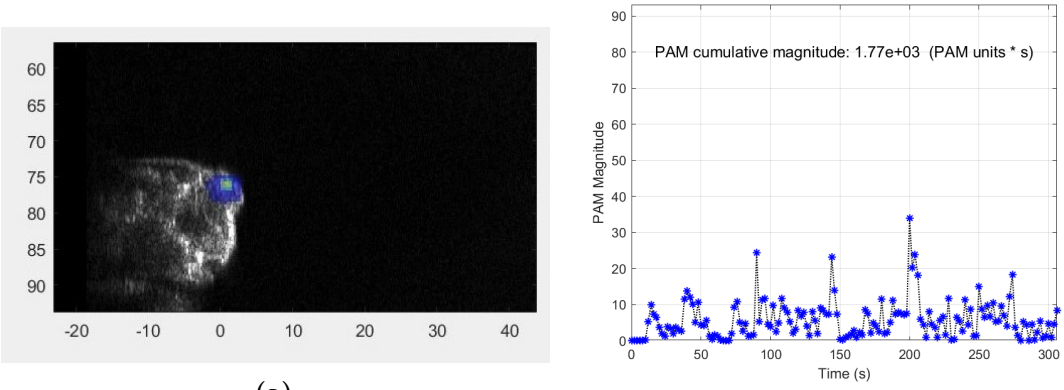
treated tumours. This was possible for most tumours, however there were some tumours that displayed low PAM Magnitude values over the entire treatment and some tumours which had spikes of high PAM magnitude peaks in certain, potentially more perfused, areas of the tumours. At the end of the treatment the tumour region was examined for signs of bruising and mice monitored as they recovered from the anaesthetic. Tumour volume was monitored post treatment to determine impact on tumour growth and on days 1, 3, 8 and 10 after treatment luciferase expression was measured in the tumours using an IVIS imager, 5 minutes after IP injection of luciferin. Mice were culled on day 10 and tumours were collected for ex vivo vaccinia genome quantification by qPCR.

6.4.2 Experiment 3: Acoustic Feedback

B-mode imaging with co-registered PAM (Figure 6.7a) was used to spatially map cavitation events, providing real-time feedback of acoustic cavitation during US treatment of tumours. The feedback seen during treatment gave the location and strength of cavitation events which occurred and the pixel with the maximum energy was extracted for each frame, denoted PAM Magnitude (AU), and plotted against time (Figure 6.7b). The PAM Magnitude plots, cavitation dose and videos produced here were shown with the help of Cameron Smith after reprocessing the PAM data recorded during experiments.

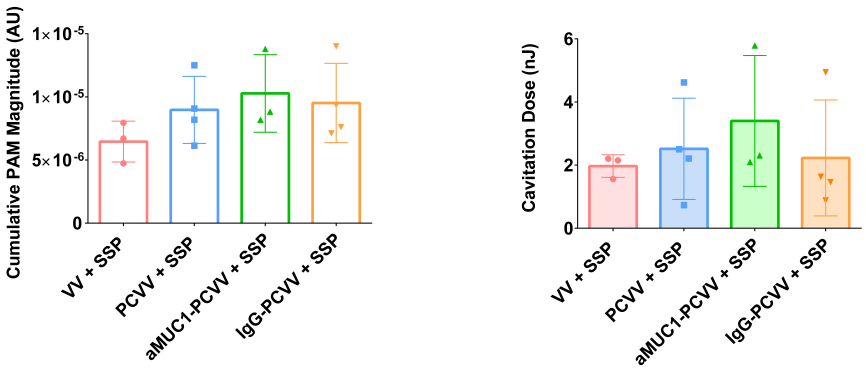
These plots depict in a clear manner a snap-shot of the maximum cavitation events occurring over time and allow the uniformity of the treatment to be determined for each mouse. From these PAM Magnitude plots metrics can be quantified to determine the amount of cavitation that occurred during treatment. As described in Chapter 3 (Sections 3.2.2 and 3.3.2), two of the metrics that can be used to quantify cavitation activity are cumulative PAM magnitude and cavitation dose.

Both metrics of cavitation were calculated for tumours treated in this experiment and the values are displayed in Figure 6.8. For the cumulative PAM Magnitude, the mean values ranged between $6.5\text{x}10^{-6}$ au (VV) and $1.0\text{x}10^{-5}$ au (aMUC1-PCVV). Differences in cumulative PAM Magnitude dose between groups were analysed by



(a) (b)

Figure 6.7: Acoustic data acquired during US treatment of CAPAN-2 tumour-bearing mice with oncolytic virus and SSPs. (a) B-mode imaging with co-registered PAM for mouse 454 (VV+SSP) at time 204s. The pixel with the maximum energy can be seen coloured yellow. That frame shown here corresponds to the point at 204s on the PAM Magnitude vs Time plot in (b). The value for the cumulative PAM Magnitude (integral of the PAM Magnitude over time) is printed at the top of the image.



(a) (b)

Figure 6.8: Quantification of acoustic data acquired during US treatment of CAPAN-2 tumour-bearing mice with VV (n=3), PCVV (n=4), aMUC1-PCVV (n=3) or IgG-PCVV (n=4) and SSPs. (a) Cumulative PAM Magnitude. (b) Cavitation Dose. The mean dose for each group is plotted overlaid with individual points for each mouse. Error bars represent SD. NS differences between any group (one-way ANOVA)

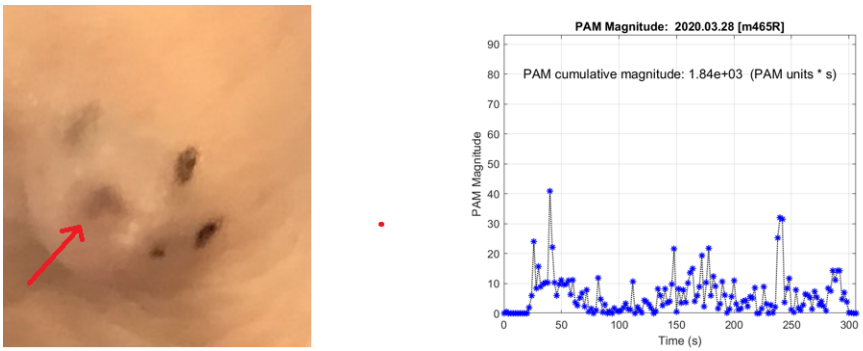


Figure 6.9: Tumour damage was assessed immediately after ultrasound treatment. A representative image of bruising seen directly after treatment for mouse 465 (IgG-PCVV). The PAM magnitude plot shows peaks in PAM magnitude at 50s and 250s. Black marks around the tumour periphery are pen marks used to demarcate the tumour boundary, the area of bruising is in the centre of the tumour (indicated by red arrow).

a one-way ANOVA and determined not to be statistically significant ($p>0.05$). For the cavitation dose, the mean values ranged between 1.97 nJ (VV) and 3.4 nJ (aMUC1-PCVV). Again, differences were analysed by one-way ANOVA and determined to not be statistically significant. There were two tumours treated which had a cavitation dose of below 1: mouse 456 (PCVV) at 0.73 nJ and mouse 471 (IgG-PCVV) at 0.88 nJ. Mouse 456 also had the second lowest cumulative PAM magnitude, however mouse 471 reported a cumulative PAM magnitude which was only 5th smallest. Both 456 and 471 had the two largest tumours of those treated with volumes of 157 mm^3 and 182 mm^3 respectively. For mouse 471 therefore, the discrepancy between the reasonable cumulative PAM Magnitude and low cavitation dose is due to its large tumour volume. Whereas for mouse 456, the PAM derived energy recorded was low and hence once its large volume was taken into account, this produced an equally low cavitation dose.

Immediately after treatment, tumours were assessed for damage within the exposed tumour area. Bruising was seen in 5 of the 14 tumours exposed to US. By visual inspection, the bruising was seen in tumours and on the skin surrounding the tumours (Figure 6.9). By determining the maximum PAM magnitude from the traces, all 5 of the mice which showed visible bruising had maximum PAM magnitude in the top 7 of the maximum PAM magnitude recorded for all mice. By day 3, all signs of damage were gone.

6.4.3 Experiment 3: Assessment of infection of VV, PCVV, aMUC1-PCVV and IgG-PCVV +/- ultrasound treatment

Mice were monitored for infection (luciferase imaging) and tumour growth for 10 days post treatment. Luciferase imaging using an IVIS imager was performed on days 1, 3, 8 and 10 post treatment to enable the infection levels over time to be determined (Figure 6.10). ROI were drawn around tumours and the average radiance within the ROI was recorded. On day 1, as can be seen in Figure 6.10a, the average radiance levels recorded in the tumours were lower than those recorded in other organs such as the lungs, liver and ovaries. This suggested that for some mice in all groups there were low levels of infection within non-tumour tissues. The minimum luminescence (radiance) displayed in Figure 6.10a is $5x10^4$ photons/second (p/s).

On day 1 the levels of luciferase expression within the tumours were very low ($<4x10^4$ p/s/cm^2/sr) for all treatment groups (Figure 6.11b). Comparing the average radiance in the non US exposed tumours on day 1 could give an indication of the accumulation achieved by VV, PCVV, aMUC1-PCVV and IgG-PCVV after IV injection and whether the enhanced PK for polymer coated VVs evident in Chapter's 4 and 5 provided enhanced early time-point infection. One-way ANOVA performed on the average radiance values for tumours that were not exposed to US found that any differences between means were not significant. It was noted however, that the highest values for average radiance in non-US treated tumours were ($>1x10^4$ p/s/cm^2/sr) were in VV + SSP and aMUC1-PCVV + SSP treated mice.

In PCVV, aMUC1-PCVV and IgG-PCVV treated mice all except one of the tumours (one mouse in the PCVV treatment group) treated with US displayed higher average radiance values at this early time point than those that were not treated with US (Figure 6.10b). In the VV treated mice, two of the three mice showed higher average radiance values in the tumour that was not treated with US when compared with the tumour that was treated with US. This was not in accordance with the findings of Myers *et al* who demonstrated 10-fold cavitation enhancements at 24 hours.

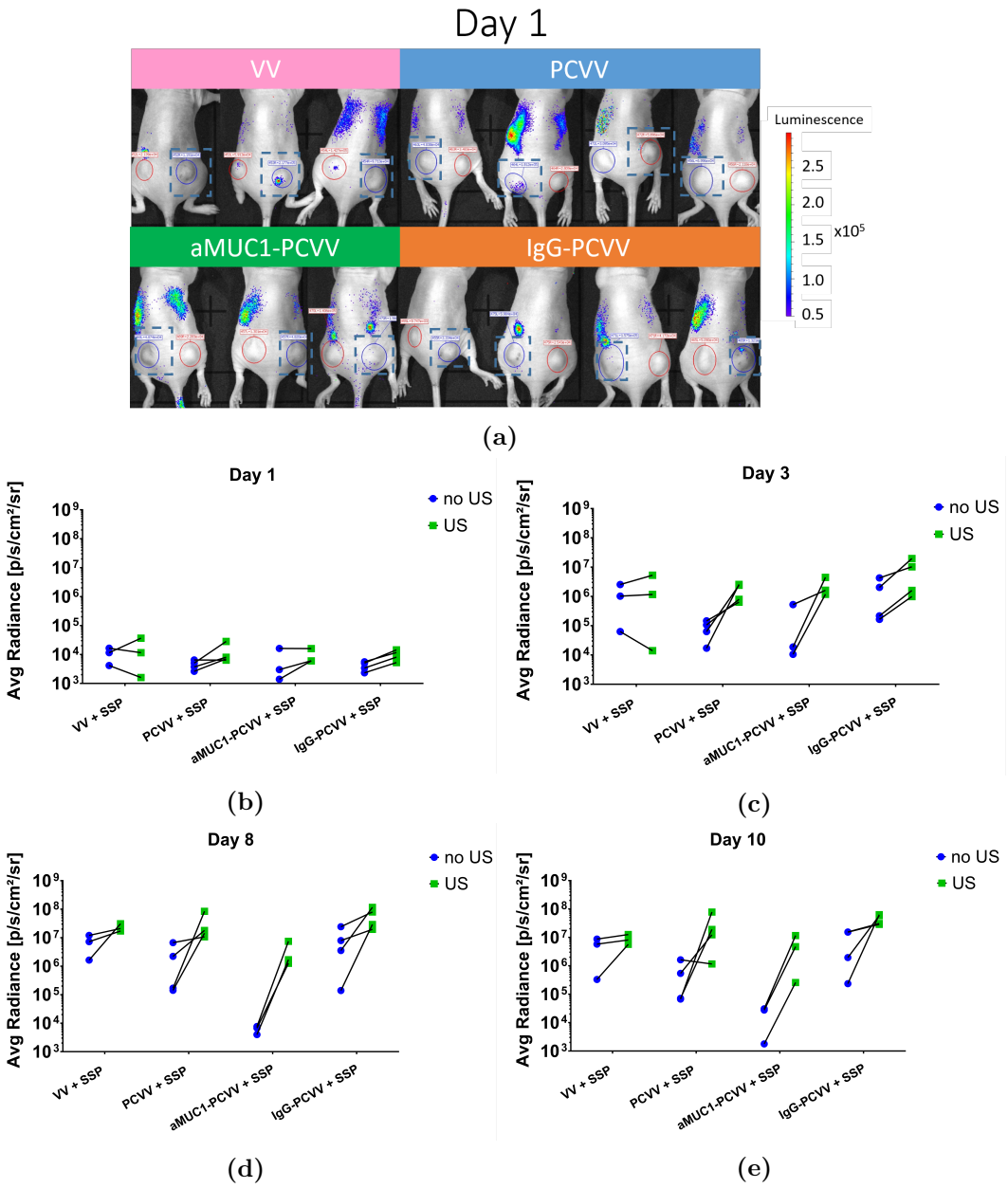
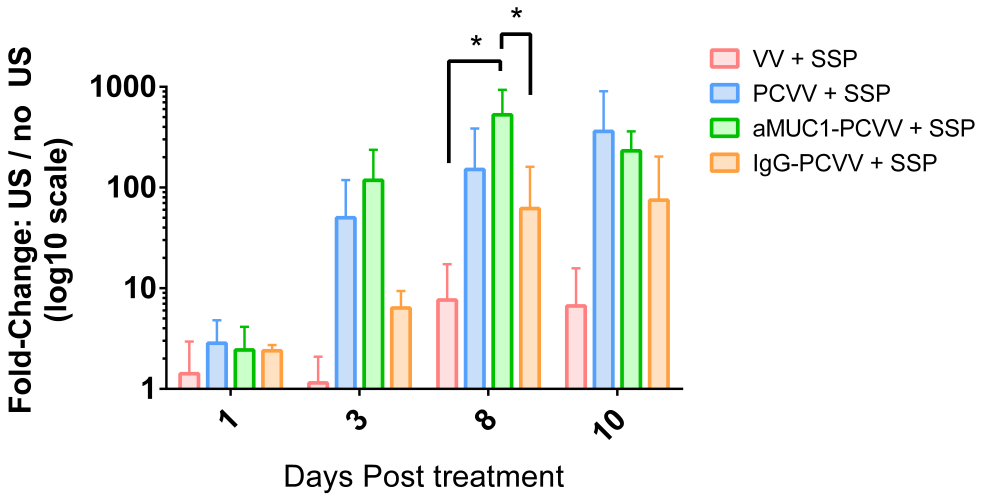
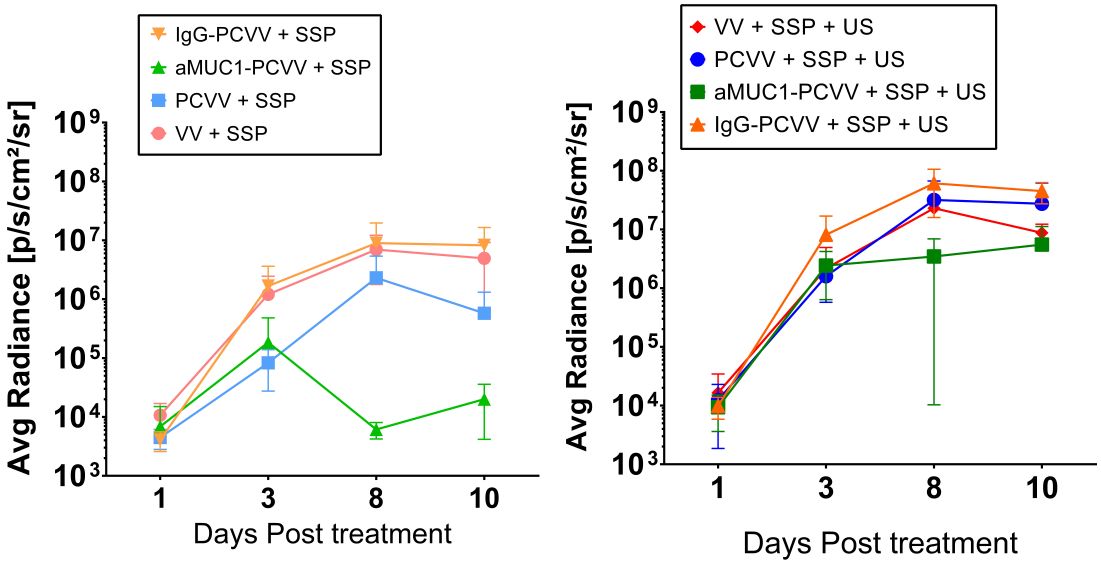


Figure 6.10: Luciferase quantification on days 1, 3, 8 and 10 after treatment with SSPs and 2x10^6 pfu of either VV (n=3), PCVV (n=4), aMUC1-PCVV (n=3) or IgG-PCVV (n=4) without (blue circle) or with (green square) US. SSPs were co-injected with either VV, PCVV, aMUC1-PCVV or IgG-PCVV into BALB-C mice bearing bilateral CAPAN-2 xenograft tumours. One of the two tumours was randomly selected for exposure to US for 5 minutes. (a) The average radiance was recorded from regions of interest (ROIs) drawn around tumours on images as depicted in images in panel 'day 1'. IVIS images were taken 5 minutes after mice were administered luciferin via intra peritonial (IP) injection. The exposure time was 30s for all images. Blue dashed boxes indicate the tumour exposed to US. (b)-(e) Individual values for the average radiance of tumours -US (blue dots) and +US (green dots) are displayed with black lines connecting tumours from the same mouse.



(a)



(b) (c)

Figure 6.11: Luciferase quantification on days 1, 3, 8 and 10 after treatment with SSPs and 2x10^6 pfu of either VV (n=3), PCVV (n=4), aMUC1-PCVV (n=3) or IgG-PCVV (n=4) without (blue circle) or with (green square) US. SSPs were co-injected with either VV, PCVV, aMUC1-PCVV or IgG-PCVV into BALB-C mice bearing bilateral CAPAN-2 xenograft tumours. One of the two tumours was randomly selected for exposure to US for 5 minutes. (a) The fold-change was calculated between US and no US tumours in each mouse and the mean fold-change for the whole treatment groups is reported at each time point. Error bars represents SD. b) mean average radiance for tumours not exposed to ultrasound, error bars represent SD, c) mean average radiance for tumours exposed to ultrasound, n= 3 or 4, error bars represent SD. Statistical significance was determined using two-way ANOVA with Sidaks tests for multiple comparisons. Statistically significant differences are displayed using * = $p<0.05$, all other differences between groups were found to be insignificant.

By day 3, infection levels had increased substantially (10-100 times) for all groups (Figure 6.11c and d) when compared to the levels of luciferase expression on day 1. This confirms that all virus groups were able to infect and replicate in the CAPAN-2 xenografts. Infection of non-tumour tissue was still observed, particularly in the ovaries for mice in all treatment groups (shown in Figure 6.12). This will be discussed in further detail below. For tumours which were not exposed to US, once again there was no significant difference (one-way ANOVA) in the average radiance values recorded when comparing the means from each of the four treatment groups. This further supports what was seen in chapter 5, where enhanced PK leading to a 5X increase in PCVV and aMUC1-PCVV circulating at 5 minutes was not sufficient to impact on passive delivery after a $2x10^6$ pfu dose (Figure 5.22c).

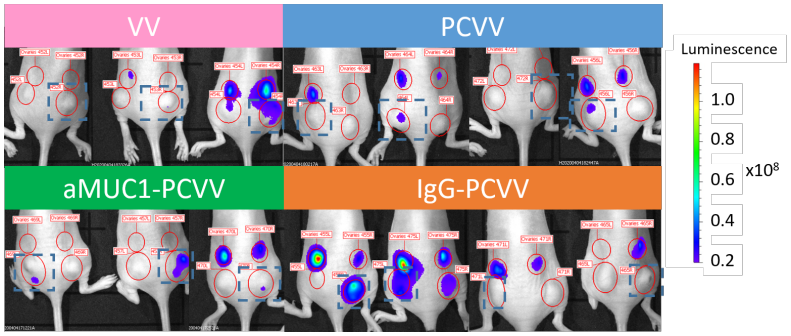
When assessing temporal changes within the same groups, the highest increase in infection between day 1 and day 3 was in the IgG-PCVV + SSP group with the tumours showing 33, 39, 879 and 1262-fold greater average radiance levels than those reported on day 1. This suggests that for two of the mice treated with IgG-PCVV, the virus was able to replicate at a markedly faster rate than the other treatment groups.

In all mice, the higher levels of infection seen on day 1 post treatment in tumours exposed to ultrasound over those not exposed became even more apparent on day 3, with exception of mouse 452 (VV+SSP) which had also failed to show enhancement at day 1 (Figure 6.10c). This was particularly true for PCVV and aMUC1-PCVV groups which had mean increases in average radiance for US vs no US of 50 and 118-fold respectively (Figure 6.11a). At these early time points, aMUC1-PCVV treated mice displayed the greatest impact from US treatment on increasing the infection levels achieved. PCVV was next greatest, followed by IgG-PCVV with an average-fold change of 6 and VV showing the lowest impact of US enhanced delivery with an average fold-change of 4 (Figure 6.11a). This suggests that for all three polymer-modified virus treatment groups, using ultrasound mediated cavitation in combination with SSPs enhances the infection ability of the virus by day 3 in this CAPAN-2 xenograft model.

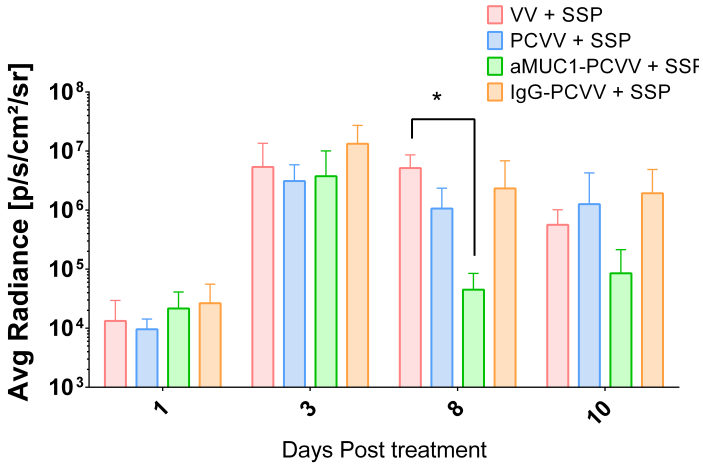
On day 8, the average radiance values for most tumours were the maximum values recorded over the 10 day monitoring period (Figure 6.11b and c). The same distinct increase in infection levels seen on days 1 and 3 in US exposed tumours was also seen here and it was noted that mouse 452 (VV + SSP) which did not share this same pattern at days 1 and 3, was now showing average radiance values of approximately 10-fold higher in US exposed tumours compared with non exposed tumours (Figure 6.10d). The greatest increase (528-fold) between US and no US tumours was observed in aMUC1-PCVV + SSP treated mice and this fold-change was shown to be statistically significant (two-way ANOVA) when compared with VV ($p=0.0115$) and IgG-PCVV ($p=0.0165$) (Figure 6.11b).

On the final day of imaging, day 10 post-treatment, average radiance levels either decreased or plateaued when compared to those recorded at day 8 (Figure 6.11b and c). The greatest difference between infection in the US and no US tumours was seen in the aMUC1-PCVV, where fold increase values of 380, 171 and 144 gave a mean 231-fold increase. Similarly in the PCVV group US treated tumours gave a mean 361-fold enhancement compared to non-US treated tumours (Figure 6.11a). PCVV and aMUC1-PCVV showed consistently enhanced infection levels in the US exposed tumours vs no US tumours when compared to VV. US exposure appeared to have a moderate effect on IgG-PCVV treated mice (mean 75-fold) but this effect was delayed when compared with aMUC1-PCVV and PCVV. US had the lowest impact on VV where US treated tumours showed a mean 7-fold increase in infection levels (Figure 6.10e).

Something which was observed in most mice across all treatment groups was infection of the ovaries. This has been reported previously for oncolytic VV. [240, 241] Positioning of the mouse during imaging and the ROI during analysis was designed to minimize the confounding impact of this as much as possible. Although there were two examples (454 VV+SSP and 475 IgG-PCVV+SSP) where its impact could not be discounted. Figure 6.12a shows the IVIS images taken on day 3 where the infection levels observed in the ovaries was highest. High levels of infection were



(a)



(b)

Treatment	Number of Ovaries Infected		Average Radiance (p/s/cm²/sr)	
	Day 3	Day 8	Day 3	Day 8
VV + SSP	3/6	4/6	5.4×10^6	5.2×10^6
PCVV + SSP	5/8	2/8	3.1×10^6	1.1×10^6
aMUC1-PCVV + SSP	2/6	0/6	3.8×10^6	4.5×10^4
IgG-PCVV + SSP	7/8	1/8	1.3×10^7	2.3×10^6

(c)

Figure 6.12: Luciferase quantification in ovaries post treatment with SSPs + VV (n=3), PCVV (n=4), aMUC1-PCVV (n=3) or IgG-PCVV (n=4). IVIS imaging on days 1, 3, 8 and 10 was used to quantify infection (luciferase) in the ovaries. (a) ROIs were drawn around the ovaries on images at each time point as shown for day 3 and the average radiance was recorded. IVIS images displayed here were taken 5 minutes after mice were administered luciferin via IP injection. The exposure time was 30s for all images. (b) Mean average radiance quantified within ROIs were plotted at each time point for each virus treatment. Error bars represent SD. Statistical significance was determined using one-way ANOVA at each time point with Tukey's tests for multiple comparisons. Statistically significant differences are displayed using * = $p<0.05$, all other differences between groups were found to be insignificant. (c) A table to summarise ovary infection in each treatment group.

reported across all groups, however they were highest in the VV + SSP and IgG-PCVV groups. IgG-PCVV treated mice had 7 out of 8 ovaries with an infection level greater than 1x10^6 p/s/cm^2/sr. Infection levels in the ovaries in the aMUC1-PCVV treated mice reduced substantially between day 3 and day 8; 3.8x10^6 p/s/cm^2/sr on day 3 to 4.5x10^4 p/s/cm^2/sr day 8. The mean average radiance in the ovaries reported for aMUC1-PCVV treated mice on day 8 was 115-fold lower than the level with VV (mean average radiance 5.2x10^6 p/s/cm^2/sr, p=0.0326) on day 8. This indicates that coating and retargeting may play a role in reducing uptake into other non-target organs as well as reducing the rate of capture in the liver. This intriguing finding has repercussions for potential clinical translation. [242]

After IVIS imaging on day 10, mice were culled and tumours were collected for viral genome (VG) quantification (Figure 6.13), to assess the level of replication that had occurred within tumours. Tumours were weighed and mixed with lysis buffer to a concentration of 75 mg/mL before being homogenised using the Precelleys tissue homogeniser (Bertin Instruments). Samples were then left at 55 °C for 2 hours until there were no visible fragments in the samples (details in section 2.7). DNA was then extracted (section 2.8.4.3) and qPCR analysis was performed.

The number of VG/ g tumour showed reasonable agreement with the average radiance calculated by IVIS images on day 10. There was large variability of VG levels detected within groups and this was particularly true for the tumours not exposed to US. In PCVV + SSP (-US) treated tumours, 3 out of 4 tumours had undetectable levels of VG in recovered tumours. In aMUC1-PCVV + SSP (-US) 1 out of 3 had undetectable levels of VG, and in IgG-PCVV 2 out of 3 had undetectable levels. Tumours not exposed to US had consistently lower VG / g tumour than tumours exposed to US in the same mice. This was in line with the IVIS imaging data, however there were no cases where 0 luciferase expression was recorded. Detection of luciferase signal when no VV genomes are detected can be explained by the half-life of luciferase protein allowing signal to outlive the presence of the VV. In the US exposed tumours, there were detectable levels of VG in all mice of all treatment groups. The highest VG / g tumour values were reported

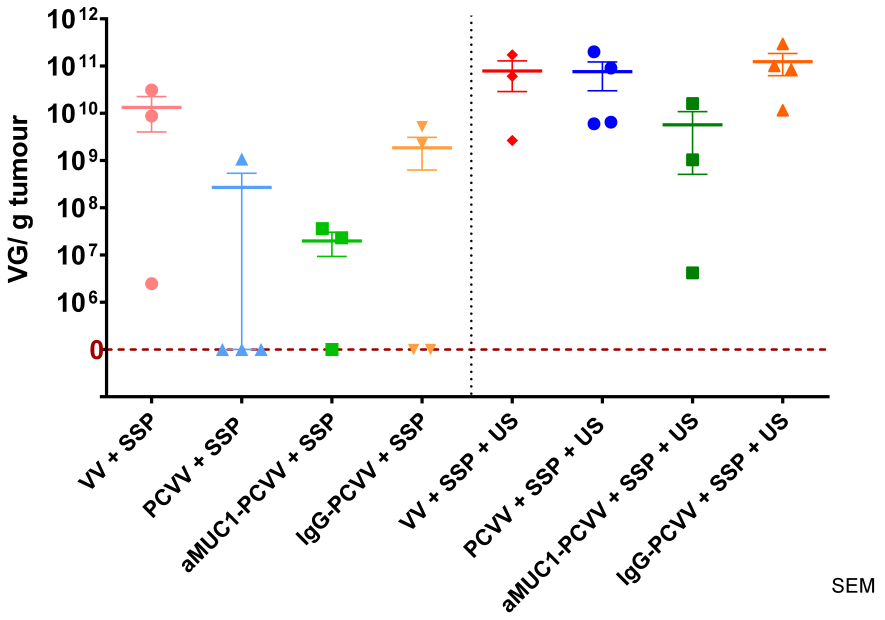


Figure 6.13: Intra-tumoural viral load on day 10 post-treatment for mice treated with SSPs + VV (n=3), PCVV (n=4), aMUC1-PCVV (n=3) or IgG-PCVV (n=4) with or without US. Tumours were collected and homogenised to 75 mg/mL before lysis and DNA extraction was performed. Quantification of viral genomes (VG) in the tumours was then done using qPCR and results are displayed as VG/g tumour. There is a superficial red line to represent points that had 0 VG detected in tumours. The dashed line separates no US tumours on the left and US tumours on the right.

in the IgG-PCVV + SSP + US treated tumours ($1.2x10^{11}$ VG/g tumour) and, as with the no US tumours, aMUC1-PCVV + SSP + US recorded the lowest mean VG / g tumour of the US treated tumour groups ($5.7x10^{9}$ VG/g tumour).

This study was designed as an investigation of the potential of US to enhance delivery and early infection levels, and so was powered accordingly. However, during the process of IVIS measurement and welfare tracking it became clear that marked effects on tumour growth were also evident and so caliper measurements were taken to capture these effects. Tumour measurements were performed on the day of treatment and then subsequently on days 3, 7 and 10. Each tumour was measured three times at each time point and the mean volume was recorded. The percentage change in tumour volume on each measurement day from the volume measured on the day of treatment was determined and the average tumour volumes for each treatment group over time can be seen in Figure 6.14. The only treatment group

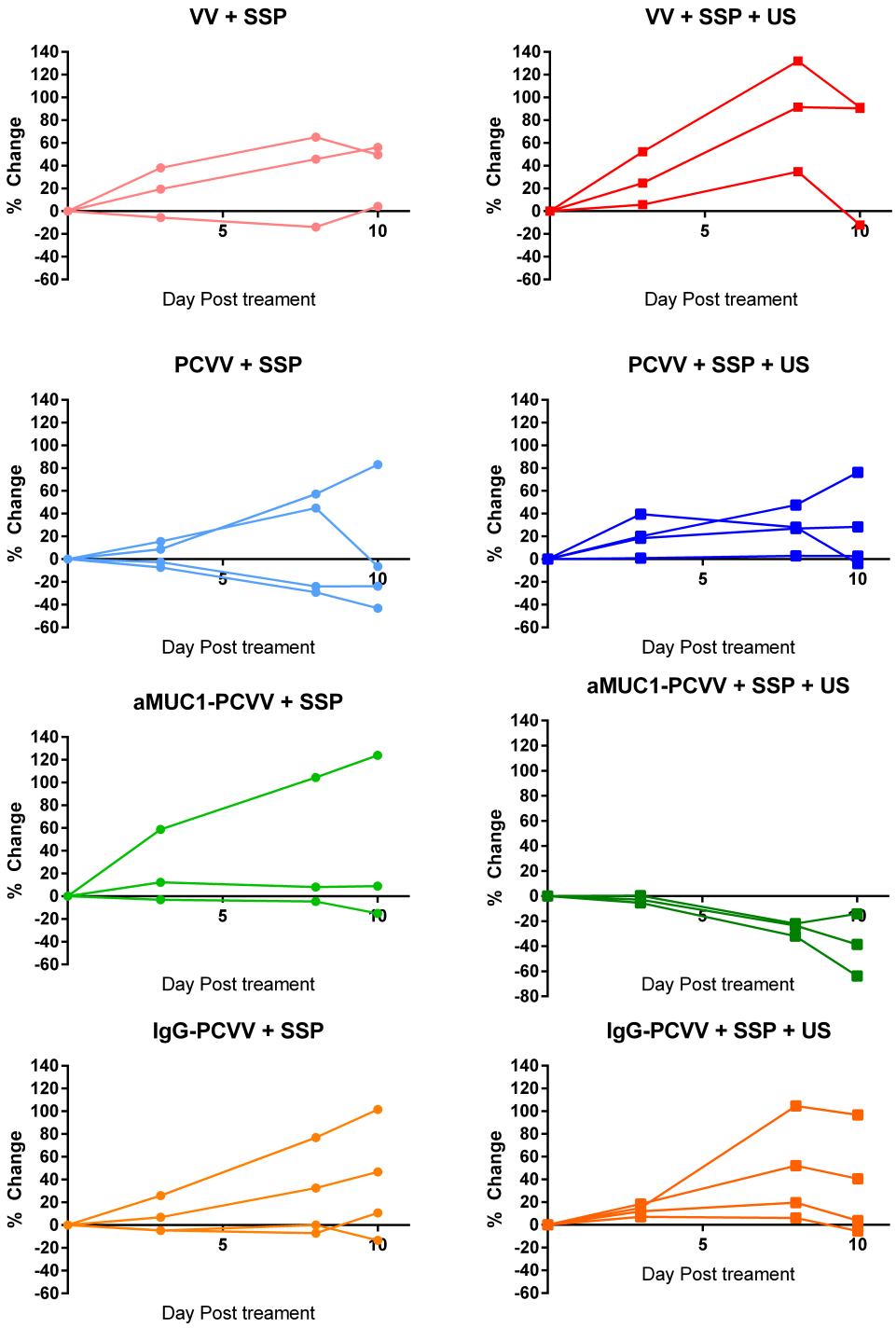


Figure 6.14: Impact of SSP + 2x10^6 pfu VV (n=3), PCVV (n=4), aMUC1-PCVV (n=3) or IgG-PCVV (n=4) with or without US on CAPAN-2 tumour growth. Tumours were measured on day 0, 3, 8 and 10 to determine the impact of treatments on tumour growth. The % change in volume of tumours at each day from day 0 for individual mice are reported for each treatment group.

in which every tumour had slowed growth and exhibited regression from the 3 day time point post treatment onwards was the US exposed aMUC1-PCVV + SSP treated tumours (Figure 6.14 (dark green)). By day 10, two of the three tumours showed marked regression (-63.8% and -38.6%). As expected, these two tumours had the two highest VG /g tumour reported in Figure 6.13, the third tumour which had a 250-fold lower VG/g tumour on day 10, showed a volume increase of 9% from the volume on the day of treatment. In aMUC1-PCVV + SSP tumours not exposed to US (light green), one tumour had substantial increase in tumour volume of +124% whilst the other two had stabilised tumour volumes over the 10 day measurement period. The tumour which had a marked increase in volume had no VG detected by qPCR at day 10 (Figure 6.13).

In the VV + SSP and the IgG-PCVV + SSP treated mice both the +US and -US tumours showed large variability in tumour change with some showing marked increases in tumour volume following treatment and others showing regression. At day 10, it appeared that tumour volume was beginning to reduce in the all of the VV + SSP + US and IgG-PCVV + SSP + US treated tumours. These measurements suggest that for aMUC1-PCVV + SSP + US treated tumours, tumour regression was consistent across all times points.

Tumours treated with SSPs + VV, PCVV, aMUC1-PCVV or IgG-PCVV in the absence of US were compared to determine whether there was any difference in mean tumour growth or regression (Figure 6.15a). PCVV + SSP treated tumours had the lowest mean % tumour growth and tumours were starting to regress in size on day 10. All other groups showed a steady mean % increase in tumour volume. Differences within groups were large and hence any differences in the mean % change were found not to be significant.

Tumours treated with US were also compared for the different treatment groups. By day 8 there was a clear difference in the mean % change of tumour volume for aMUC1-PCVV + SSP + US (-25.8 % +/- 3.1) treated tumours compared with VV + SSP + US (+86.1 % +/- 28.2, p=0.011). Differences between the mean % change in PCVV + SSP + US (26.4 % +/- 9.1) treated tumours, IgG-PCVV + SSP + US

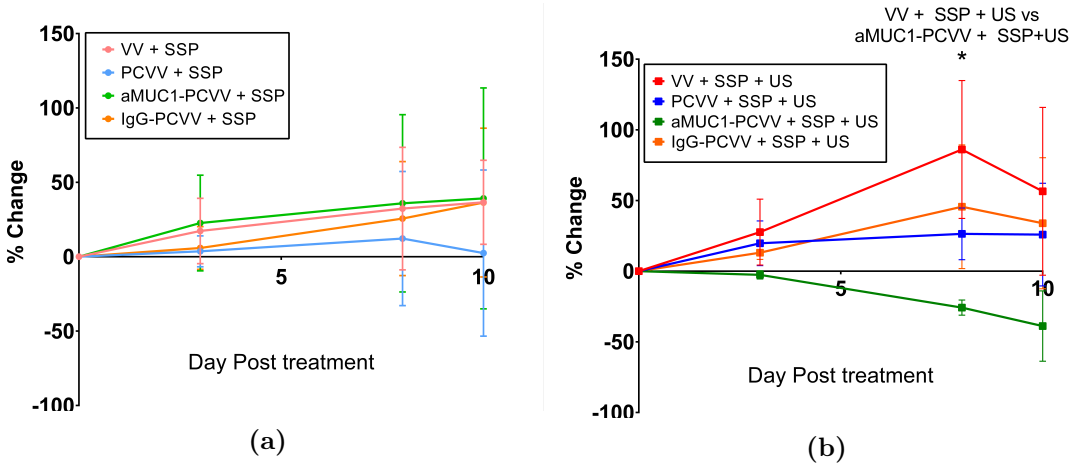


Figure 6.15: Impact of SSP + VV (n=3), PCVV (n=4), aMUC1-PCVV (n=3) or IgG-PCVV (n=4) with or without US on CAPAN-2 tumour growth. Tumours were measured on day 0, 3, 8 and 10 to determine the impact of treatments on tumour growth. The mean % change in volume from treatment day of tumours is reported for tumours not exposed to US (a) and tumours exposed to US (b). Error bars represent standard deviation (SD). Differences between groups on day's 8 and 10 were determined using a one-way ANOVA followed by Tukey's test for multiple comparisons. $p<0.05$ = *

(+45.6 % +/- 21.9) and aMUC1-PCVV + SSP + US treated tumours were shown to not be statistically significant. On day 10 the % decrease in tumour volume was even more pronounced for aMUC1-PCVV + SSP + US treated tumours. The tumours in other groups were also starting to regress in size. Differences between groups were found not to be statistically significant. It is noted that the difference observed between aMUC1-PCVV + SSP + US (-38.8 % +/- 14.4) treated tumours and VV + SSP + US (56.5 % +/- 34.3) had a p value of 0.08.

6.4.4 Relationship between PAM and delivery of VV, PCVV, aMUC1-PCVV and IgG-PCVV

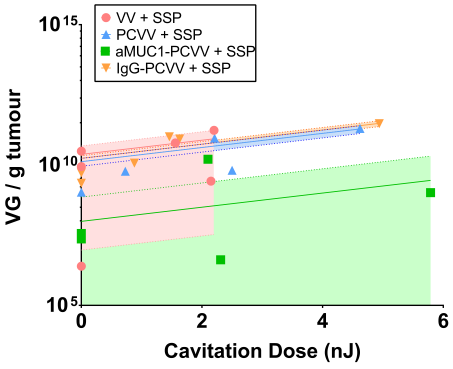
As discussed in section 6.4.3, tumours which were exposed to US showed greater luciferase expression (Figure 6.10) and intratumoural viral genome content (Figure 6.13) than their internal no US control tumour. Therefore, a relationship between the quantity of cavitation activity recorded and the delivery of VV, PCVV, aMUC1-PCVV and IgG-PCVV was probed.

Given the wealth of different metrics this experiment produces to give an overall picture of infection, there were several options for comparing the cavitation activity

with these different metrics (for example average radiance, qPCR analysis, tumour growth). Due to its accuracy and sensitivity, VG content as determined by qPCR analysis was used as the metric to describe the achieved delivery. Cavitation dose has previously been used to show good correlation with biological effects and hence was the metric for cavitation that was chosen for use here. [203] Cavitation dose was plotted against VG/ g tumour values for each tumour to determine whether it could be a predictive measure for VG content within tumours. Tumours that were not exposed to ultrasound were given a cavitation dose of 0, as they did not receive any cavitation.

Individual values for VG per g tumour are plotted against cavitation dose (Section 6.4.4). From the distribution of points seen, the trend cavitation dose (nJ) and concentration of VG/g tumour, regardless of viral treatment, was fairly weak. Assessing the tumours within each treatment group and applying a non-linear regression with an exponential growth equation ($Y = Y_0 e^{kx}$) gave a reasonable fit for both PCVV + SSP (blue) and IgG-PCVV + SSP (orange) treated mice (Section 6.4.4a) with R^2 values of 0.85 and 0.91 respectively. The Y0 values for IgG-PCVV and PCVV are displayed in Table 6.4.4a. This analysis suggests that the cavitation dose may have impacted the viral content present in tumours on day 10 post treatment with PCVV and IgG-PCVV in an exponential manner. For both aMUC1-PCVV and VV there was not a reasonable fit with this equation (R2= 0.19 and 0.31 respectively).

This exponential equation did not show reasonable fit for VV or aMUC1-PCVV treated mice. One major difference (as presented in Figure 6.15b) between all the aMUC1-PCVV + SSP + US treated tumours and the other groups was the marked tumour regression that was already occurring at day 10 when the VG content of the tumours were assessed. This may be due to considerable oncolysis occurring earlier in aMUC1-PCVV treated tumours than other groups, either directly or due to increased bystander cell death. [243] Due to the multiplicity of effects that could be at play, it was unsurprising that treatment with aMUC1-PCVV + SSP at this time point did not result in a reasonable trend.



(a)

	Y0 (VG / g tumour)
PCVV	$1.3x10^{10}$ (+/-$1.7x10^{9}$)
IgG-PCVV	$1.7x10^{10}$ (+/-$1.7x10^{9}$)

(b)

Figure 6.16: Tumour VG content as a function of cavitation dose. (a) Points show data from individual tumours (VV=6, PCVV=8, aMUC1-PCVV=6, IgG-PCVV=8) against cavitation dose with non-linear multiple regression for all treatment groups. The exponential coefficient of the cavitation dose (k) was determined to be 0.5804. (b) Table showing the non-linear multiple regression curve constants for VG/g tumour vs cavitation dose for IgG-PCVV and PCVV tumours.

In summary, using a bilateral CAPAN-2 xenograft model it was shown that treatment with US (1.5 - 2 MPa for 5 minutes exposure) using SSPs as the cavitation nuclei with VV and all three modified VV gave rise to an increase in tumour transgene expression as measured by IVIS imaging 3, 8 and 10 days after treatment. This average fold increase with US vs no US was shown to be higher for aMUC1-PCVV (529-fold +/- 404) when compared with VV (8 +/- 10, p= 0.0115) and IgG-PCVV (61 +/- 99, p= 0.0165). Genome quantification of homogenised tumours on day 10 confirmed what was observed in IVIS imaging: tumours exposed to US regardless of the viral treatment had higher levels of VG/ g tumour than the internal control tumour which was not exposed to ultrasound.

Tumour growth monitoring in the 10 days post treatment showed that in tumours that were not exposed to US, volumes increased or showed inhibited growth, in line with their particular levels luciferase levels or viral genome levels. On day 10, the PCVV + SSP treated tumours all appeared to be showing tumour regression, although differences between groups were found to be non-significantly different using a one-way ANOVA with post hoc Tukeys test for multiple comparisons. In the US treated tumours the tumour regression seen in the aMUC1-PCVV + SSP + US tumours was marked and by day 8 a mean tumour regression of -25 % +/- 3.1 was

observed. This change in tumour volume was greater than in tumours treated with VV + SSP + US (p=0.0109). Differences between the mean tumour volume change in the aMUC1-PCVV + SSP + US group and IgG-PCVV were found to be outside of statistical significance (p=0.0821). This level of regression (and presumably cell death) may account for the lower levels of luciferase expression measured at day 8 in the aMUC1-PCVV + SSP + US tumours compared to the other + US groups.

Previous experiments (Grundy *et al*, under review) have successfully sought to build a relationship between the dose of cavitation occurring within a tumour and the dose of drug delivered. Typically such studies have been performed using therapeutic antibodies and an ELISA performed immediately after delivery. In this thesis this relationship had to be built on output of viral genomes at 10 days. Unfortunately the confounding factors involved in each of these methods of 'delivery' analysis mean that a robust relationship with cavitation could not be identified. Future experiments may have explored this question by performing qPCR on tumours excised directly after US exposure.

6.5 Results: Experiment 4- Tumour growth study- VV, aMUC1-PCVV or glucose, with or without ultrasound mediated cavitation

Whilst the bilateral delivery experiment in section 6.4.3 produced a suggestion of improved tumour growth control using aMUC1-PCVV + SSP + US the experiment was not powered to fully explore this. Hence, the interesting effects on tumour growth seen at day 10 in the bilateral CAPAN-2 xenograft delivery study (Figure 6.15), led to a further study in which a unilateral CAPAN-2 xenograft model was utilised to determine the impact of ultrasound mediated cavitation on the delivery of VV and aMUC1-PCVV and ultimately the impact of these treatments on tumour volume. A unilateral CAPAN-2 xenograft model was chosen so that any impact of viral shedding into the blood stream and potential increased infection of non target tumours could be avoided in assessing the different virus groups. [25, 29]

Xenograft model	Unilateral, CAPAN-2	
Administration route	IV	
Cavitation nuclei	1.1 mg SSPs	
	Treatment	**Average tumour volume (mm^3)**
Group 1	$2x10^6$ pfu VV + SSP - US (n=6)	139
Group 2	$2x10^6$ pfu VV + SSP + US (n=5)	139
Group 3	$2x10^6$ pfu aMUC1-PCVV + SSP - US (n=5)	128
Group 4	$2x10^6$ pfu aMUC1-PCVV + SSP + US (n=5)	133
Group 5	5% Glucose + SSP + US (n=4)	129

Table 6.4: Experimental design details of experiment 4: tumour growth study with SSPs and VV, aMUC1-PCVV or glucose with or without US.

The same dual transducer setup (Figure 6.5) and parameters (Table 6.2) as were used in the delivery study were used here. The experiment was run under the same protocol as for the bilateral delivery study with $2x10^6$ pfu of VV or aMUC1-PCVV premixed with 1.1 mg SSPs before intravenous administration to female BALB-C nude mice bearing CAPAN-2 xenograft tumours. The details for the experimental protocol can be found in section 2.8.6.

As the primary endpoint of the study was an exploration of tumour growth, a glucose + SSP + US group which had not been included in the delivery study was included to exclude the impact of cavitation within the tumour impacting on its growth. Due to limitations on the number of mice which had usable tumours, not all groups could be brought forward to assess the impact on tumour growth further. In the delivery study (section 6.4.3) PCVV and IgG-PCVV did show enhanced delivery when co-administered with SSPs and US was applied, however this improved delivery did not result in marked tumour regression for either group

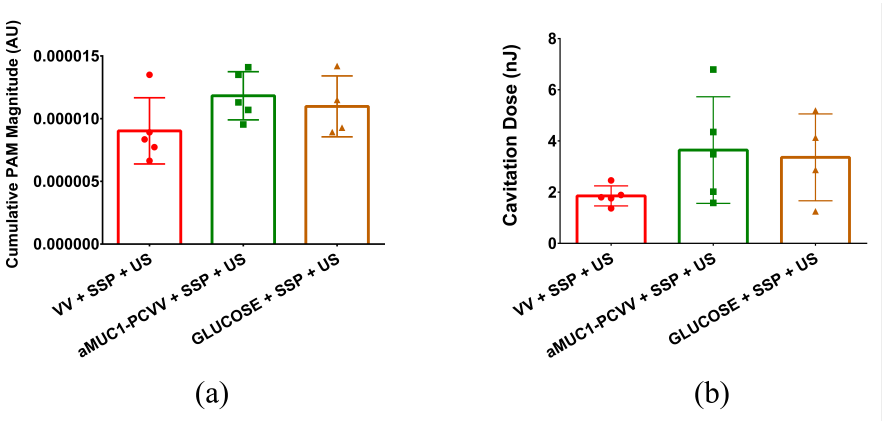


Figure 6.17: Quantification of acoustic data acquired during US treatment of CAPAN-2 tumour-bearing mice with SSPs and 2x10^6 pfu VV (n=5), aMUC1-PCVV (n=5) or glucose (n=4). (a) Cumulative PAM Magnitude. (b) Cavitation Dose. The mean dose for each group is plotted over laid with individual points for each mouse. Error bars represent SD.

when compared to that of aMUC1-PCVV. Therefore given that tumour growth was being assessed, PCVV and IgG-PCVV were not included in this further tumour growth study. Hence, this study compared the impact of US mediated cavitation on the change in tumour volume when VV was administered compared to when aMUC1-PCVV was administered.

6.5.1 Experiment 4: Acoustic Feedback

As previously (section 6.4.2), B-mode imaging with co-registered PAM (Figure 6.7a) was used to spatially map cavitation events, providing real-time feedback of acoustic cavitation during US treatment of tumours. This feedback gave the location and strength of cavitation events which occurred during treatment. The cavitation dose used here were provided with the help of Cameron Smith after reprocessing the PAM data recorded during experiments.

Both metrics for cavitation (cumulative PAM magnitude and cavitation dose) were calculated for tumours treated in this experiment and the values are displayed in Figure 6.17. For the cumulative PAM Magnitude, the mean values ranged between 9.0x10^6 au (VV) and 1.2x10^{-5} au (aMUC1-PCVV). Differences in cumulative PAM Magnitude between groups were analysed by a one-way ANOVA and determined not to be statistically significant. For the cavitation dose, the mean values ranged

between 1.9 nJ (VV) and 3.6 nJ (aMUC1-PCVV). Again, differences were analysed by one-way ANOVA and determined to not be statistically significant.

Immediately after treatment tumours were assessed for damage within the exposed tumour area. Bruising was seen in 7 of the 14 tumours exposed to US across all groups and by day 3, all signs of damage were gone.

6.5.2 Experiment 4: Luciferase imaging on Day 7 and 21 to monitor infection levels

Infection levels were assessed at two time points, day 7 and day 21, after treatment to ascertain and link the impact of infection on tumour growth in each group. It was also used to determine whether infection was still persistent in this CAPAN-2 xenograft model at later time-points.

IVIS imaging was performed and ROIs were drawn around tumours as described in section 6.4.3. Images are shown for aMUC1-PCVV + SSP and aMUC1-PCVV + SSP + US (Figure 6.18a) and VV + SSP and VV + SSP + US (Figure 6.18b). No detectable luminescence was observed during IVIS imaging for glucose + SSP + US treated tumours. Quantification of the average radiance within the tumour ROIs for each mouse was performed and the mean values with individual tumours overlaid are shown.

On day 7 (Figure 6.18c) the mean values for average radiance were highest in the VV + SSP + US ($8.7x10^7$+/- $5.3x10^7$ p/s/cm^2) and aMUC1-PCVV + SSP + US ($8.3x10^7$+/- $5.6x10^7$ p/s/cm^2) groups compared to the no US groups (9 and 23–fold increases respectively).

The 10-fold increase seen for VV + SSP + US compared with VV + SSP was in line with what was reported on day 8 for VV in the delivery study. The 22-fold increase seen for aMUC1-PCVV + SSP + US when compared with aMUC1-PCVV + SSP was lower than what was observed in the bilateral delivery study (Figure 6.11). This could be due to the difference in xenograft tumour size for the different studies (delivery study: mean volume 101 mm^3, tumour growth study: mean volume 135 mm^3). Another potential factor could be the unilateral xenograft tumour model used

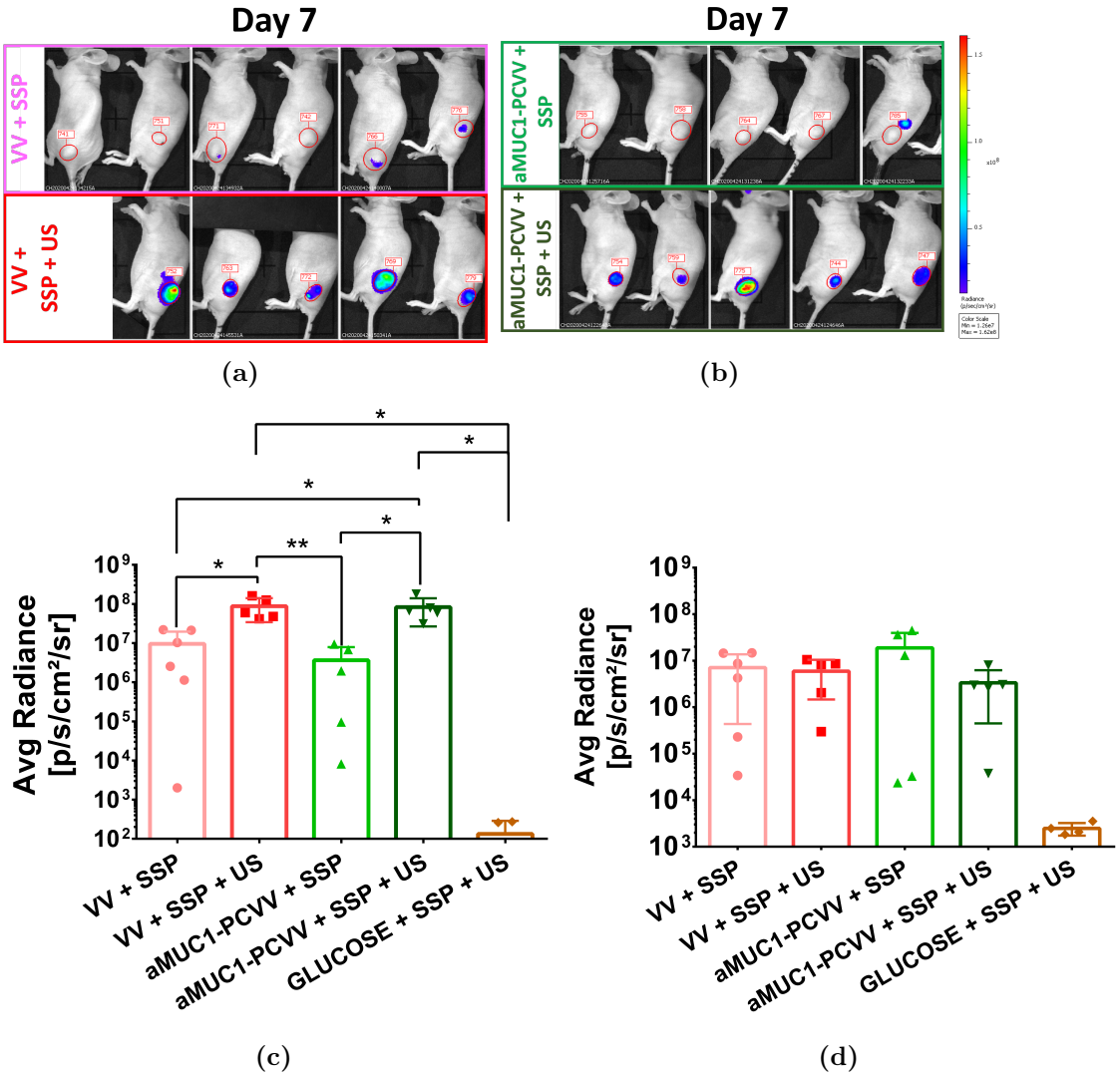


Figure 6.18: Luciferase imaging to determine infection levels post-treatment. Mice bearing unilateral CAPAN-2 xenografts were treated with SSPs and $2x10^6$ pfu VV (n=6), VV + US (n=5), aMUC1-PCVV (n=5), aMUC1-PCVV + US (n=5) or glucose + US (n=4). The average radiance was recorded from regions of interest (ROIs) drawn around tumours on images as depicted in the images for (a) VV + SSP +/- US and (b) aMUC1-PCVV +/- US on day 7. Mice which had tumours exposed to US are on the bottom of both panels. IVIS images were taken 5 minutes after mice were administered luciferin via intraperitonial (IP) injection. The mean average radiance observed for each group at both time-points are plotted with individual values shown for (c) day 7 and (d) day 21. Error bars represent SD. Statistical differences were determined using a one-way anova with Tukey's test for multiple comparisons. $p<0.05$ = *

in the tumour growth study when compared to the bilateral xenograft tumour model used for the delivery study. It may be that in the delivery study where the $2x10^6$ pfu was "shared" between the two tumours, US mediated cavitation in combination with aMUC1-PCVV resulted in a reduced circulating dose of aMUC1-PCVV during the 5 minute treatment time. This may result in a lower amount of aMUC1-PCVV being available to passively accumulate in the tumours that were not exposed to US. Given the enhanced PK of aMUC1-PCVV when compared to VV at this dose (as reported in Chapter 5), US mediated cavitation may disproportionately impact the aMUC1-PCVV circulating when compared with VV.

Another important feature is the much tighter distribution of values evident in the US groups, demonstrating that US mediated delivery provides greater reproducibility to the procedure, an observed benefit in accordance with several previous studies. [116, 190]

Glucose + SSP + US treated mice showed a background mean average radiance of $1.3x10^2$ (+/- $1.5x10^2$) p/s/cm^2/sr. All mice treated with virus displayed levels of infection above background (as determined by the average radiance signal reported for the glucose + SSP + US group). Differences between means were assessed using a one-way ANOVA with post hoc Tukey's test for multiple comparisons. The mean average radiance recorded for VV + SSP + US was found to be greater than VV + SSP ($9.6x10^6$ (+/- $1.0x10^7$) p/s/cm^2/sr, p =0.0119). The mean average radiance recorded for aMUC1-PCVV + SSP + US was found to be greater than aMUC1-PCVV + SSP ($3.7x10^6$ (+/- $4.2x10^6$) p/s/cm^2/sr, p =0.0144). There was no significant difference between the VV + SSP + US and the aMUC1-PCVV + SSP + US treated mice (p=0.999).

By day 21 (Figure 6.18d), overall infection levels were lower than those reported for day 7. This reflects the plateauing of signal that was evident at day 10 in the experiment reported in section 6.4.3. The average radiance for the two +US groups, VV + SSP + US and aMUC1-PCVV + SSP + US, had reduced to the level of those observed with the -US groups. Differences in the mean average radiance levels between groups were found to be non statistically significant.

6.5.3 Experiment 4: Tumour growth control

Tumour volume was tracked over 22 days post treatment with measurements taken every 2-3 days. At each time point, each tumour was measured three times and the mean volume was reported. The change in tumour volume from the day of treatment was calculated and mean values for each treatment group are displayed in Figure 6.19. Mice were arranged into groups so that the mean tumour volume at the start was approximately equal for all groups 135 mm^3 (+/- 5 mm^3).

In the first 10 days post-treatment, no clear differences in tumour volume change were seen between any of the treatment groups (in contrast to the data in Figure 6.14 which showed a difference as early as day 3). However, from day 13 there were differences starting to appear in tumour regression between the US treated groups and no US treated groups. Tumours treated with aMUC1-PCVV + SSP + US all demonstrated reduction in volume from their starting tumour volume by day 16. For tumours treated with VV + SSP + US, 3 out of 5 tumours showed a reduction in tumour volume on day 16. This was the same for tumours treated with aMUC1-PCVV + SSP without US which had 4 out of 5 tumours showing size reduction from the day of treatment. The majority of mice in the VV + SSP group and the glucose + SSP + US group had tumours which increased in volume (5 out of 6 and 3 out of 4 respectively). As the number of days post-treatment increased, the tumour regression in the aMUC1-PCVV + SSP + US group became even more apparent when compared with other groups and by day 22 the mean tumour regression was -73% (+/-14). VV + SSP + US and aMUC1-PCVV + SSP without US produced the next greatest level of regression with mean reductions of -30% (+/- 33) and -30% (+/-27) respectively. Both VV + SSP (+16 % +/- 31.6) and glucose + SSP + US (+38 +/- 102) tumour volumes were increasing on the final day of treatment. Differences between groups were assessed on day 22 post treatment using a one-way ANOVA with Tukey's test for multiple comparisons. aMUC1-PCVV + SSP + US was found to have significantly greater tumour volume reduction compared to VV + SSP (p=0.0360) and glucose + SSP + US (p=0.0144).

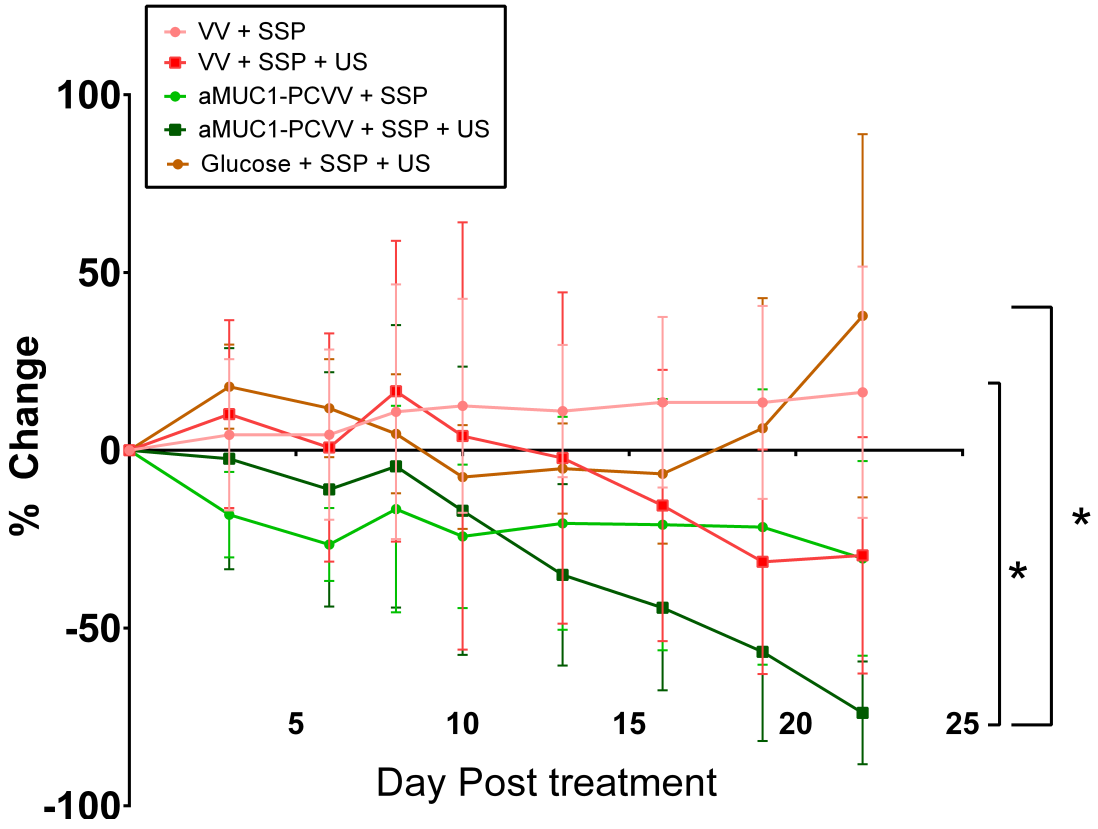
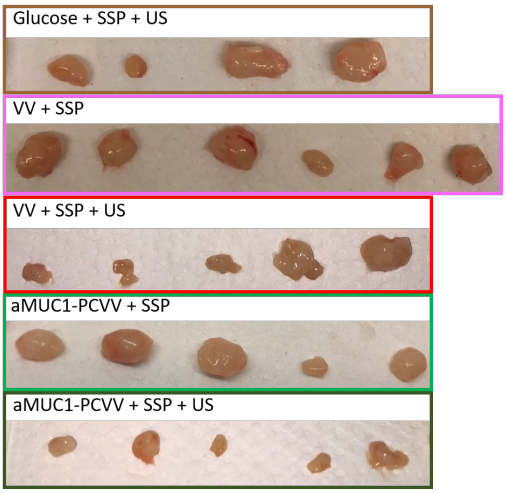


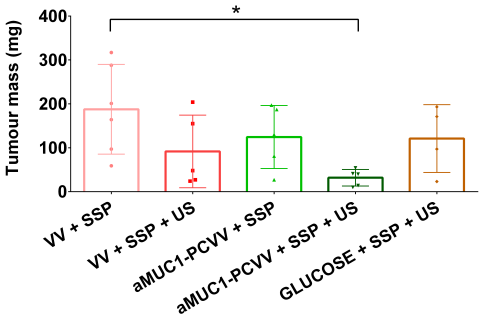
Figure 6.19: The mean tumour volume following treatment of mice bearing unilateral CAPAN-2 xenografts were treated with SSPs and $2x10^6$ pfu VV (n=6), VV + US (n=5), aMUC1-PCVV (n=5), aMUC1-PCVV + US (n=5) or glucose + US (n=4). Tumours were measured three times at each time point and the mean volume was reported for each tumour. The mean volume change from the day of treatment for tumours is displayed. Error bars represent SD. Differences between groups on day 22 was assessed for statistical significance using a one-way ANOVA and Tukey's test for multiple comparisons. $p<0.05$ = *

When the tumour volume change was assessed by one-way ANOVA with Dunnett's test for multiple comparisons of the VV + SSP + US and aMUC1-PCVV + SSP + US to the glucose + SSP + US control group, aMUC1-PCVV + SSP + US showed a statistically significant difference in tumour volume change when compared with the glucose + SSP + US control (p=0.0066) whereas VV + SSP + US showed no statistically significant difference when compared with glucose + SSP + US (p=0.1265). Differences between groups were more apparent as time passed and ideally tumour growth would have been tracked for a longer duration.

On day 22 mice were culled and tumours were recovered. Photos of tumours were taken and the mass of each tumour was recorded (Figure 6.20). As can be



(a)



(b)

Dunnett's multiple comparisons test	Adjusted P value
aMUC1-PCVV + SSP + US vs. VV + SSP	0.0116
aMUC1-PCVV + SSP + US vs. VV + SSP + US	0.5646
aMUC1-PCVV + SSP + US vs. aMUC1-PCVV + SSP	0.211
aMUC1-PCVV + SSP + US vs. GLUCOSE + SSP + US	0.2813

(c)

Figure 6.20: Assessment of tumours excised post-cull. (a) Images of tumours excised post cull for mice treated with 1.1 mg SSPs and $2x10^6$ pfu VV + SSP (n=6), VV + SSP + US (n=5), aMUC1-PCVV + SSP (n=5), aMUC1-PCVV + SSP + US (n=5) or glucose + SSP + US (n=4). (b) Tumours were weighed and the mean mass for tumours in treatment groups is displayed. Error bars represent SD. (c) Differences between groups was assessed for statistical significance using a one-way ANOVA and Dunnett's test for multiple comparisons against the aMUC1-PCVV + SSP + US treatment group. *=$p<0.05$

clearly seen in Figure 6.20a, aMUC1-PCVV + SSP + US had the smallest tumours on day 21 with a mean mass of 31.8 mg. VV + SSP + US had the second smallest tumours with greater variability in tumour sizes (and hence recorded mean mass, 91.6 mg) than that of the aMUC1-PCVV + SSP + US group. Both VV + SSP, aMUC1-PCVV + SSP and glucose + SSP + US had larger and varied tumour volumes when compared to aMUC1-PCVV + SSP + US. A one-way ANOVA was used to determine the statistical significance of differences of mean tumour mass reported between groups. Only one difference in mean tumour mass was found to be statistically significant between the VV + SSP and aMUC1-PCVV + SSP + US group (p=0.0116).

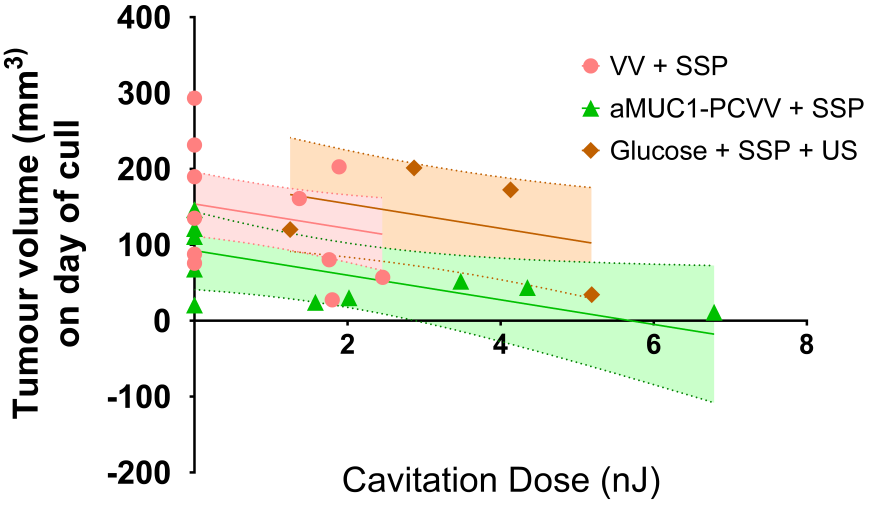


Figure 6.21: Assessment of the relationship between cavitation dose received and the final tumour volume measure on day 22 post treatment. Individual values for each tumour are displayed and a linear regression fit with a constrained slope of -16.22 mm^3/ nJ was determined.

6.5.4 Experiment 4: Relationship between PAM and tumour volume at end point

In section 6.4.4, relationship between the cavitation dose received for each tumour and the VG/ g tumour was assessed. Here, the final output of the experiment was the difference in tumour volume between groups. Therefore, the relationship between tumour volume at this later 22 day time point and the cavitation dose received by tumours treated with VV + SSP, aMUC1-PCVV + SSP and Glucose + SSP was assessed using linear regression and the results are displayed in Figure 6.21. Tumours which were not exposed to US were assigned a cavitation dose of 0 nJ.

Linear regression with a constrained slope for each group did not produce a particularly strong fit for VV (R^2=0.19), aMUC1-PCVV (R^2=0.35) or glucose (R^2=0.17). Values for the y-intercepts are shown in Table 6.5. As there were no glucose treated mice which were not exposed to US, determining a linear regression with only 4 points is not particularly strong. For both VV and aMUC1-PCVV, the large variability in volumes on day 22 for tumours that were not exposed to US hindered any reasonable fit from being determined.

	Y_{int} (mm^3)
VV (11)	154 (+/-20)
aMUC1-PCVV (10)	92 (+/-25)
Glucose (4)	187 (+/-41)

Table 6.5: Non-linear multiple regression curve constants for tumour volume vs cavitation dose for all tumours.

In summary, using a unilateral CAPAN-2 xenograft model the impact of treatments with VV and aMUC1-PCVV with and without US (1.5-2 MPa for 5 minutes of treatment) using SSP cavitation nuclei on tumour growth was determined. Cavitation activity was consistent across all groups with no differences between cumulative PAM magnitude or cavitation dose in any US treated tumours being found to be statistically significant. Glucose + SSP + US was used as the non-viral control to see the potential impact which US mediated cavitation may have on tumour growth inhibition or regression.

Transgene expression determined on day 7 showed that VV + SSP + US had a 10-fold higher transgene expression than VV + SSP (p=0.0119) and a 24-fold higher transgene expression than aMUC1-PCVV + SSP (p=0.0094). aMUC1-PCVV + SSP + US had a 22-fold increase in transgene expression over aMUC1-PCVV + SSP (p=0.0144) and a 9-fold increase over VV + SSP (p=0.0186). By day 21 transgene expression in US treated tumours had decreased to the same level as those expressed in the tumours not exposed to US, suggesting that as tumour regression occurred transgene expression also reduced.

Tumour volume was measured in the 22 days post treatment and regression was observed in the aMUC1-PCVV treated tumours both exposed to US and not exposed to US. By day 22, the regression seen in the aMUC1-PCVV + SSP + US mice was considered statistically different to the tumour volume change achieved by VV + SSP (p=0.0411) and glucose + SSP + US (p=0.0210).

A relationship between tumour volume and cavitation dose was sought using linear regression, however the goodness of fit for both aMUC1-PCVV and VV was not deemed reasonable. Further analysis to determine whether a different

model be more efficient would need to be performed to assess whether any robust correlation could be determined.

6.6 Discussion

Due to its rapid replication and large transgene coding capacity, and the multiple forms which oncolytic VV can take after cellular infection, it is heralded as an oncolytic virus with huge potential for oncolytic virotherapy, specifically with the aim of systemic injection. However, as discussed previously (sections 1.3 and 4.5) there are both bloodstream neutralisation limitations and extravasation, penetration and homogenous delivery difficulties in solid tumours. [3, 4, 77, 151]

In previous chapters, polymers were used to coat VV in an attempt to enhance its blood stream stability. It was shown that using a Cholesterol-PEG and Cholesterol-PEG conjugated to an anti-MUC1 antibody, the circulation kinetics were enhanced and specifically the amount of VV circulating at 5 minutes was significantly higher for both PCVV and aMUC1-PCVV. The use of PHPMA to polymer coat oncolytic adenovirus has previously been shown to enhance its circulation kinetics and used US in combination with cavitation nuclei (SonoVue) increased the transgene expression in tumours. [116] Despite the enhanced circulation kinetics reported in chapters 4 and 5, PCVV and aMUC1-PCVV did not result in an immediate (20 minutes) increase in intratumoural VG detected in recovered tumours. It was previously reported in the literature that tumour focused US used with an IV delivered cavitation nuclei was able to enhance the infection levels achieved by VV in a HepG2 xenograft model *in vivo*. [190] Hence, it was hypothesised that combining the enhanced circulation kinetics within the first 5 minutes after IV injection with a 5 minute US + cavitation nuclei exposure, would result in even greater infection levels and ultimately impact on tumour growth to a greater extent than naked VV with and without US mediated cavitation. The main findings in this chapter are outlined below.

1. Genetically engineered mouse (GEM) models in which tumours develop spontaneously in the pancreas of immune-competent mice have been used in many

recent preclinical studies in pancreatic cancer treatment. [244] In GEM models tumour cells are of mouse origin, growth can be slow and varied and hence treatments can be difficult to plan, and inter-tumour heterogeneity is low compared with human tumours. [244] This made them an undesirable model for the studies presented here. CAPAN-2 xenograft models have several microenvironmental characteristics in common with GEM models: the tumours develop a dense collagen-rich extracellular matrix (consistent with what is seen in human pancreatic cancer tumours) [245] and collagen fibres which appear in thick filament bundles. Therefore a CAPAN-2 subcutaneous xenograft tumour model was assessed for its suitability for an US enhanced delivery experiment using VV and modified VV. Cells from the same CAPAN-2 cell line used in the *in vitro* assessment of MUC1 retargeting of VV in Chapter 5 were subcutaneously injected into 5 BALB-C nude mice. The number of tumours that showed persistent growth was found to be 4 out of 5, suggesting a take rate of 80 %. The tumour growth produced a heterogenous tumour volume by day 50 (86-280mm3). Analysis of the literature revealed that very large intramuscular CAPAN-2 xenografts (700 mm^3) have blood vessels located in the connective tissue and display approximately 20% hypoxic regions from immunohistochemistry staining. [246] It is reported in the literature that by using direct contrast enhancement (DCE)-MRI imaging, the blood flow in tissues can be determined by acquiring a series of images during an infusion of a contrast agent. [199, 200, 229, 246] Furthermore, approximates for vascular permeability properties can be made by analysing the area under the curve (AUC) and mean resident time (MRT) plots. For AUC vs MRT plots, a steeper the gradient of the voxels recorded relates to uncompromised perfusion and visa versa. [231] Perfusion over the 50 day tumour growth was assessed to determine a suitable tumour volume treatment window in which perfusion would not be greatly hindered by large necrotic and hypoxic regions within the tumours. Perfusion levels determined by DCE-MRI imaging analysis were shown to be reasonable in tumours with a volume of between 50- 150 mm^3, however, when the tumour reached a volume of 280 mm^3, a marked reduction in perfusion was observed. It is noteworthy that the differences in origin, stromal

content and susceptibility to VV infection will be expected to create differences when data is compared to the VV delivery and infection data reported by Myers et al using HepG2 and SKOV tumours. [190]

Western blot analysis of a recovered tumour showed that MUC1 was still over expressed in CAPAN-2 xenografts and that the aMUC1 antibody used for targeting MUC1 in these studies was able to bind the MUC1 from CAPAN-2 xenografts.

2. US-mediated delivery of VV, PCVV, aMUC1-PCVV and IgG-PCVV (all expressing a luciferase transgene) using SSP cavitation nuclei was investigated in a CAPAN-2 bilateral xenograft model. This is the first report utilising ultrasound mediated cavitation for a polymer modified enveloped virus. Cavitation was detected in real-time during treatment using two perpendicularly aligned linear arrays and was mapped using PAM. Cavitation activity was assessed and good localisation within the tumours was observed. Cavitation activity was quantified as two different metrics: a cumulative PAM magnitude and a cavitation dose. Both quantification methods provided evidence for reasonably uniform treatment across US exposed tumours using SSP's as a cavitation nuclei. This agrees with what has previously been reported in the literature after a single IV injection of SSPs. [190]

A low level of bruising was observed in 5 out of the 14 tumours immediately after treatment and monitored in the days post treatment. All signs of damage had gone by day 3. It is hypothesised that the bruising was a result of a sudden peak in PAM energy resulting in a very high peak in PAM magnitude (>33 au) seen on the PAM Magnitude trace. This damage could have implications for clinical translation and so careful assessment of parameters which are chosen for clinical translation would be necessary to ensure safety. This could include changing the parameters used depending on whether you are at the periphery (more well vascularised) or the core (less well vascularised) of the tumour as shown in section 6.2.1. It is noteworthy that sectioning of tumours post SSP + US has previously shown no evidence of macroscopic or microscopic tissue damage (Katti et al, manuscript in preparation). Furthermore, when tested at depth in a more appropriately sized mammal (i.e. a pig) there was no damage evident in any internal organ (personal communication

R.Carlisle), it is believed that the surface bruising evident in some mice xenografts is not of relevance to the deployment of the system at depth in humans.

3. Infection in non-tumour tissues was seen across all groups at day 1 post treatment. These tissues included the lungs, liver and ovaries. By day 3 infection in non-tumour tissues was only seen to a detectable extent in the ovaries. This was particularly apparent in the IgG-PCVV treated mice where infection was visible in 7 out of 8 of the ovaries in these treated mice. By day 8 infection in the ovaries was still high for VV and IgG-PCVV treated mice but was substantially reduced in aMUC1-PCVV treated mice to be 100-fold lower than that in VV treated mice ($p<0.05$). This suggests that an aMUC1 polymer coated VV was able to prevent rapid replication in ovary tissues which is a feature of naked VV following IV injection into this mouse model. Infection of ovaries by VV has been reported previously in the literature with results in accordance to those reported here. [208] High infection levels have raised concerns as to whether this may prevent the treatment population clinically. [242] The ovaries express normal levels of mucin and so it was re-assuring to see that there was not high levels of infection levels seen in the aMUC1-PCVV treated mice when compared to other treatment groups. [247] Further analysis on cell death and damage would be useful to compare the over all impact of each treatment group on the ovaries which might not be determined from the transgene expression levels alone.

Transgene expression was higher in US treated tumours for all mice with the exception of one of the VV treated mice by day 3 post treatment. Ultrasound exposure had the greatest impact on PCVV and aMUC1-PCVV treated mice which showed fold-change of transgene expression in US to no US treated tumours of 50 and 118 respectively. For IgG-PCVV and VV the fold-change was just 6 and 4 respectively. This suggests that the impact of US mediated cavitation was greater for increased levels of transgene expression in PCVV and aMUC1-PCVV treated mice. This is in accordance with the hypothesis that increasing bloodstream residence time of the VV provides a higher circulating dose for the tumour focused US to impact upon: a finding which has previously been reported for a polymer coated

Adenovirus. [116] It is important to note however, that when day 3 absolute levels of tumour infection were compared between groups (one-way ANOVA on day 3) there was no statistically significant increase in any group. This suggests the improved PK profile and consequent enhanced US response achieved by the addition of a polymer coat or a polymer coat and a targeting ligand compensates for a loss of infectivity suffered as a result of the coating process. Although this is in accordance with the in vitro monolayer CAPAN-2 infection data for PCVV, which showed a 3-fold decrease in transgene expression see Figure 5.17). It is perhaps surprising that the aMUC1-PCVV did not outperform the VV, as in vitro it could match the VV and in vivo it should derive greater benefit from its enhanced PK compared to VV. It is noted that the use of 2D IVIS imaging alone to determine infection has its flaws in trying to accurately reconstruct the expression within a 3D volume. However, this discrepancy between in vitro and in vivo infection levels is most likely related to access to the cell surface required for infection. It has been reported that VV can infect both tumour cells and tumour endothelial cells. [172, 176] Even a low amount of circulating VV may still be able to achieve a level of infection of tumour vasculature during its passage. Indeed, Arunlanandam et al reported that VV tumour vasculature infection after IV administration was important for successful delivery and spread within tumours. [176] In coating VV and retargeting infection to MUC1, this endothelial infection may be lost, and whilst the enhanced circulation is provided, potential reduction of VV tumour vasculature infection may inhibit its spread within tumours by interfering with this mechanism of passage into the tumour parenchyma. However, once US mediated cavitation is added as a mechanism for aMUC1-PCVV to be driven into the tumour, contact with and infection of tumour cells is encouraged and hence the benefit is evidenced.

In accordance with this theory, aMUC1-PCVV was found to have a significantly higher fold-change of US treated tumours compared to no US treated tumours than that of VV ($p=0.0115$) and IgG-PCVV ($p=0.0165$). Differences in transgene expression between the treatment groups for tumours not exposed to ultrasound were found to not be statistically significant (one-way ANOVA at days 8 and 10). By

day 10, the mean levels of transgene expression in tumours treated with IgG-PCVV + US were higher (17-fold) than those treated with aMUC1-PCVV + US (p=0.0449). Therefore suggesting that the addition of an aMUC1 antibody resulted in a decrease in infection levels at later time points after treatment when compared to the addition of an IgG antibody. This could suggest that more efficient cell death was occurring in the aMUC1-PCVV + US treated tumours thereby detrimentally impacting on its ability to replicate, a proposal in accordance with the enhanced tumour growth control seen with aMUC1-PCVV + US (Figures 6.14 and 6.15). [243, 248]

4. Trends from the IVIS imaging were supported by qPCR analysis performed on the excised tumours recovered at day 10. Tumour treated with US all had detectable VG in their tumour homogenates whereas in the tumours which weren't exposed to US PCVV, aMUC1-PCVV and IgG-PCVV all had at least one tumours per group which had undetectable VG. Thereby confirming that delivery and persistent infection were better in the US exposed tumours at day 10 than for those not exposed to US. One of the most notable benefits of the application of SSP+US is the marked decrease in variability it provides, with much lower standard deviations in both luciferase and qPCR measurements evident when SSP+US is applied. This is in accordance with previous data [116, 190] and emphasizes that a robust controllable physical mechanism such as cavitation can help mitigate a lot of the heterogeneity in response to therapy that results from heterogeneity in tumour physiology.

5. During tumour monitoring post treatment, tumour regression occurred in all tumours treated with aMUC1-PCVV + SSP + US. On day 8, the percentage change in tumour volume was -25% (+/-3) in aMUC1-PCVV + SSP + US treated tumours the level and reproducibility of which was a marked contrast when compared to that of VV + SSP (+32% (+/- 41), p=0.0724) and VV + SSP + US (+86% (+/- 28.2), p=0.0109). By day 10, the mean % volume change in the other treatment groups (+US) began to reduce, meaning differences between groups were determined not to be statistically significant.

6. An exponential relationship was determined to give a reasonable fit between cavitation dose (x) and VG/ g tumour (Y) for both PCVV and IgG-PCVV. The

equations produced were: IgG-PCVV: $Y = 1.7\text{x}10^{10}e^{0.5804x}$ and PCVV: $Y = 1.3\text{x}10^{10}e^{0.5804x}$. However this fit was not good for VV or aMUC1-PCVV. The relationship for cavitation activity was also assessed for other metrics of infection such as luciferase expression on day 3, however no good relationship was found. Given the number of confounding factors between the cavitation measured at 0-5 minutes and both luciferase at day 3 or VG/g tumour on day 10, a lack of robust relationship is potentially unsurprising. For this to be properly defined, qPCR on tumours excised immediately after treatment (5 minute cull point) or 24 hours after treatment would be needed.

7. Motivated by the effect on tumour regression observed during the bilateral CAPAN-2 delivery study, a further study to determine the impact of US mediated cavitation with aMUC1-PCVV or VV on tumour growth was performed. The groups which were compared were VV + SSP (+ or - US), aMUC1-PCVV + SSP (+ or - US) and glucose + SSP (+US). This allowed the effect of the aMUC1-polymer coating and the effect of exposure with US on tumour growth to be assessed. In the tumours that were not exposed to US, neither VV nor aMUC1-PCVV showed marked tumour regression during this 22 day post treatment period. However, transgene expression recorded on day 20 suggested that infection in these two -US treatment groups was measurable. Therefore if the study had continued over a longer time frame, an impact on tumour volume may have been observed. Substantial tumour regression was observed in both VV + SSP + US and aMUC1-PCVV + SSP + US treated tumours with aMUC1-PCVV + SSP + US having a mean tumour regression from the day of treatment of 73%. This is in accordance with the report of Myers et al who demonstrated that a VV-luc dosed at $1\text{x}10^6$ pfu in HepG2 and SKOV tumours could provide tumour growth control when SSP + US was added. [190] Furthermore, this was shown to be significantly different to the tumour volume change observed in VV + SSP and glucose + SSP + US treated tumours. It is concluded that aMUC1-PCVV + SSP + US instigated substantial improvements to the level and reproducibility of tumour regression in this CAPAN-2 xenograft model when compared with all other groups with benefit particularly apparent in

comparisons to naked VV alone and glucose + SSP + US. This is depicted clearly in the images of the excised tumours. Given the difference in % tumour change seen compared with the glucose + SSP + US group, it can be concluded that US mediated cavitation alone is not causing the tumour regression seen here.

6.6.1 Summary and Conclusions

In summary, it was shown in this chapter that delivery could be improved for VV, PCVV, aMUC1-PCVV and IgG-PCVV viruses by using ultrasound mediated cavitation in a CAPAN-2 xenograft mouse model. The increase in transgene expression was greatest in tumours treated with aMUC1-PCVV after US exposure when compared with the internal control. This suggests that US mediated cavitation was key to enhancing the infection efficiency of a VV with a polymer coating and MUC1 antibody ligands with prolonged circulation kinetics. The reduction in infection levels seen in ovaries suggest that this aMUC1-polymer coating was also able to reduce off target effects when compared with VV and IgG-PCVV. In a tumour growth study comparing VV (+/- US), aMUC1-PCVV (+/- US) and glucose (+US) it was shown that aMUC1-PCVV + SSP + US was able to induce greater tumour regression than VV + SSP or glucose + SSP + US.

Regarding the key question of how the data presented here impacts on the likelihood of translation of these ideas into clinical practice, any safety or efficacy gains have to be weighed against the extra manufacturing and regulatory challenges presented. It is clear that the case for the addition of SSP + US, which has been made previously [190], is further supported here with strong (10-1000 fold) enhancements in infection and tumour growth control. The US + SSP technology is at an advanced manufacturing and regulatory stage and the healthcare economics case has been refined. [249] The case for the polymer coating strategy described here is not as developed, however given PEG's previous use as a tool for pegylation of drug carriers it is hoped that regulatory approval would be straightforward. The addition of targeting antibodies such as aMUC1 do pose as a regulatory challenge, however aMUC1 antibodies are involved at substantially higher concentrations in later stage

clinical trials. [148] OV have shown efficacy when delivered by direct IT injection [43, 78] (detailed in section 1.2.1), however, in order for OV to become an established tool across a range of cancers and be able to optimally infect primary and metastatic tumours, administration via IV injection is essential. [10, 77] Indeed, it has been reported that IV injection may enhance the induction of anti-tumour immune responses when compared with IT administration [79] and provides enhanced benefit in cases where metastatic variants have lost or changed their neoepitope landscape thereby rendering previous neoepitope specific treatments, and hoped for abscopal effects from IT injection of a primary tumour, non-efficacious [80, 250]. Therefore, whilst IT delivery will continue to provide a viable option for many patients, achieving successful delivery in local and disseminated cancer will be critical in the progression of OV clinically. Low-cost techniques such as the polymer coating and retargeting strategy presented here may be an important step in realising this process for VV and potentially for other enveloped OVs. Although more complete coating using a polymer such a pHPMA may be required, just as it proved more effective than PEG for Ad5 [106]. Another interesting approach may be to perform enzymatic deglyocsylation of VV virions followed by Chol-PEG coating. [126]

The following is therefore concluded for Chapter 6:

- Focused US applied to CAPAN-2 xenograft tumours coupled with IV administration of SSP cavitation nuclei resulted in prolonged cavitation and led to increased transgene production in all virus groups when compared to an internal bilateral tumour control that was not exposed to US.
- The greatest impact for enhanced transgene production was observed in PCVV and aMUC1-PCVV groups suggesting that focused US mediated cavitation was required to help realise the benefit of enhanced circulation that the polymer coating provided and enable improved delivery in xenograft tumours.
- Marked tumour regression (-73 %) was observed in the aMUC1-PCVV + SSP + US treated CAPAN-2 xenograft tumours just 22 days after treatment. This change was significantly different when compared with VV + SSP (+16

%) and glucose + SSP + US (+38 %) treated CAPAN-2 xenograft tumour bearing mice where tumours were still increasing in volume at day 22.

Chapter 7

Conclusions and Future Work

7.1 Summary of findings and conclusions

Thorough analysis of the current clinical trials underway (Chapter 1, section 1.2.1) revealed that 14 of the 25 trials investigating oncolytic VV are relying on local or intratumoural (IT) administration, a decision which is driven by the relatively poor PK of VV in human blood. [22, 28] This bloodstream limitation was emphasized by the recent 'PHOCUS' Phase III trial, which relied on IT delivery of VV, and was set to fail to meet its primary endpoint before it was terminated. [251] The only two oncolytic viruses (*H101* and *Imlygic*) that have gained regulatory approval are also both restricted to intratumoural administration.

The difficulty in establishing standardized protocols for IT administration is reflected in the variability in efficacy reported in early-phase clinical trials of oncolytic viruses after IT administration. Such variability suggests that the uniformity of infection achieved using this route is sub-optimal and, as a consequence, managing to evidence robust responses following IT administration is difficult in early phase trial. Specifically, Sauthoff et al reported patchy virus distribution of adenovirus after intralesional injection of xenograft tumours [252] and Bazan-Peregrino et al reported that large injection volumes resulted in fairly poor IT retention of adenovirus which was heavily dependent on tumour volume. [253] In 100 mm^3 tumours as little as 40% of the injected dose was retained after four 20 µL IT injections and spread of infection was enhanced only by the use of multiple injection sites [253].

Indeed, in this thesis, IT administration even in a simple readily accessible model such as murine subcutaneous xenografts, showed very poor reproducibility, with the standard deviations of GFP reporter gene expression at day 7 (SD = +/- 1.9x10^{10}) exceeding the mean level (8.2 x10^9 [p/s/cm^2/sr] / [µW/cm^2]) even when n was as high as 20. This situation was one that not even the application of US mediated-cavitation at the time of IT injection could reasonably and fully rescue. Although, in chapter 3 the use of US-mediated cavitation on a DLD xenograft tumour model did result in enhanced spread 6 days after treatment when compared with xenografts which had not been exposed to US. This resulted in the demonstration of a reasonable relationship between the % tumour area which was successfully infected and the cumulative PAM magnitude calculated (sections 3.2.3 and 3.2.4). However, when repeated in CAPAN-2 xenografts, both the ultrasound exposed and non-exposed tumours showed large variability in response and no enhancement as a result of ultrasound-mediated cavitation was reported (section 3.3.3.1).

Miller et al. and Carlisle et al. both report challenges of IT oncolytic virus spread (oncolytic VSV and polymer coated adenovirus respectively) within infected tumours, suggesting that infection occurs in "pockets" and is heavily associated with peri-vascular regions. [77, 116, 177, 201] Two approaches can be taken to try and overcome this barrier; re-dosing with more virus may seed sufficient infection foci that they can eventually overlap providing complete coverage, and/or agitating the tumour may allow better spread from established infection foci. Given the widely reported challenges associated with repeating IT dosing [254, 255], alternative methods of enhancing the spread of pre-seeded intratumoural were sought. Hence, a second intervention with US-mediated cavitation instigated within already infected tumours was investigated to try and help spread seeded VV infection within tumours (section 3.3.3.2). Infection levels were detrimentally impacted by a second intervention of US at early time points, and this was especially true for mice which had received US at intervention 1. Promising increases of infection levels and % area of infection of the US treated mice at intervention 2 (US/US and no US/US) on the final day of imaging compared with plateauing and declining infection in

the no US treated mice at intervention 2 (no US/no US and US/no US) suggested that if the study had been able to continue, an enhancement in infection levels and spread due to ultrasound mediated cavitation may ultimately have been realised.

The clinical experience of IT VV, and the intra-group variability between results reported in chapter 3 in particular, make a strong case for trying to improve the IV efficacy of VV rather than continue to rely on IT injection. The experiments reported in Chapters 4, 5 and 6 investigated strategies aimed at improving IV efficacy. However, this is no straightforward task. In addition to sharing the IT challenges that VV infection faces upon its arrival at the tumour site, IV delivery also presents a multiplicity of challenges to VV including sequestration from the blood stream by the mononuclear phagocytic system and neutralisation mediated by complement and anti-VV antibodies (Chapter 1, section 1.3). [7, 75] However, should such challenges prove to be surmountable a therapeutic approach with far greater clinical utility and potential efficacy may emerge.

Specific barriers to consider, include the fact that due to its use in the smallpox vaccination program, many of today's cancer population have been pre-exposed to VV, presenting a unique antibody-based challenge for successful IV administration. However, evolution has provided VV with multiple ways of protecting itself from bloodstream neutralisation including, most notably, the secretion of vaccinia virus complement control protein to inhibit the complement cascade. [227, 256] Despite these mechanisms, VV still suffers from variability in achieving reliable tumour delivery and efficacy in clinical trials administered IV (Chapter 1, section 1.2.1).

Conjugation of PHPMA to the Ad5 capsid has been shown to successfully reduce opsonisation and antibody binding *in vitro* and *in vivo* (section 1.3.1.2.1). Previous reports using cholesterol-PEG to enhance circulation kinetics of drug vehicles and liposomes by forming a brush like PEG coat using the cholesterol as an anchor in the lipid bilayer led to the hypothesis that the same technique could be used to enhance the circulation kinetics of VV. [136] Chapter 4 explored this hypothesis, utilising flow virometry to detect VV and further confirm, using a fluorescently conjugated cholesterol-PEG, that successful coating of VV had been achieved (section 4.2.2). In

line with other reports of polymer coated Ad, polymer coated VV (PCVV) showed reduced cancer cell infection levels when compared to VV.

The loss in infectivity was balanced by a demonstrated enhanced stability in blood components (i.e. maintained infection levels of cancer cells when incubated with VV neutralising human plasma) and an approximate 20% reduction in anti-VV antibody binding, as demonstrated by flow virometry (section 4.3.1). This work culminated in an *in vivo* PK study comparing the amount of virus circulating in HepG2 xenograft bearing CD1 nude mice which showed a substantial 6-fold increase in PCVV circulating at 5 minutes when compared with VV (section 4.4). Rojas *et al* have demonstrated that the infection profile of, and the resulting immune responses to, VV can be altered by enzymatic treatment of the VV envelope. [126] Similarly Thirunavukarasu *et al* have shown that a single point genetic modification of the A34R gene into a double deleted VV can result in the production of more progeny virus in the form of EEV, the immune-evasive and more blood stable of VV progeny (Chapter 1, section 1.2.1), resulting in reduced clearance by neutralising antibodies in pre-immunised mice and in enhanced spread within tumours. However the data reported in this thesis represents the first report of modification of VV to improve its PK.

Despite the enhanced circulation of PCVV when compared to VV, it did not result in greater passive accumulation 30 minutes after treatment, in fact the accumulation in HepG2 tumours was extremely low for both virus groups. Chapter 5 described the use of an aMUC1 antibody conjugated to Chol-PEG to produce aMUC1-PCVV with the aim of restoring the infection levels of a polymer coated VV *in vitro* whilst maintaining the potential benefit of an enhanced PK and thereby providing enhanced tumour targeting and accumulation. Chol-PEG-aMUC1 constructs were formed and shown to still have a high affinity binding to their MUC1 target (section 5.2.2). Flow virometry was again utilised to determine Chol-PEG-aMUC1 coating of VV and the formation of aMUC1-PCVV was successfully shown (section 5.12). aMUC1-PCVV was shown to restore infectivity in high MUC1 expressing CAPAN-2 cells *in vitro* when compared with

PCVV (sections 5.3.3 and 5.3.4). Such restoration may support the hypothesis that the tropism of VV has been re-directed via MUC1, in-line with previous studies showing genetic modification could achieve such MUC1 specific redirection. [130] However alternatively, restoration may result from the presence of the aMUC1 antibody reducing the efficiency with which the polymer can coat the VV thereby merely allowing restoration of normal infection. Whilst the flow virometry (Chapter 5, section) argued against this latter possibility, as it showed a high level of Chol-PEG-aMUC1 embedding, it was necessary to probe the question further. This can be done several ways all of which have limitations.

A receptor negative cell line can be chosen, but these are often hard to identify. MUC1 has been reported to have shown expression in a wide range of cancer cells [143, 144, 148], and furthermore cells differ in many other ways besides MUC1 expression which alter amenability to infection. A receptor negative cell line can be created (e.g. use of siRNA to knockdown MUC1 in CAPAN-2), but this never provides complete durable knockdown and can alter the viability and activity of the cells. Due to these weaknesses it was decided here to alter the VV rather than the cells, first by creating a polymer linked to a 'dummy' retargeting moiety (an IgG of the same isotype and from the same species as the aMUC1 antibody), and secondly by attempting to block the aMUC1-MUC1 interaction with free peptide. Unexpectedly the IgG-PCVV showed the same restored infection as aMUC1-PCVV suggesting that potentially the presence of an IgG antibody enabled enhanced infection in CAPAN-2 cells in monolayer experiments. This may be through non-specific interactions, enabled by changes to the surface charge of the PCVV as a result of the addition of any protein. Alternatively, differences in PCVV infection when compared with aMUC1-PCVV could be the result of differences in VV polymer coating when any antibody is attached, which enables restoration of infection by reducing coating density. In the second approach a "blocked" aMUC1-PCVV study was performed by incubating Chol-PEG-aMUC1 constructs with MUC1 overnight before aMUC1-PCVV formation. This showed that incubation with MUC1 peptide did reduce the infection levels recorded in CAPAN-2 cells, but the effect was not

overwhelming (section 5.3.4). It is thought that incubating MUC1 in the infection media during the infection as opposed to with antibody-polymer constructs prior to infection, a greater inhibitive effect would be observed. Paul et al reported success target specificity of a heavily attenuated genetically modified MVA targeting MUC1 by transfecting a MUC1 negative BHK cell line to express MUC1 [130], although this approach may suffer from other consequences of MUC1 expression which may increase amenability to infection by increasing cell division rate. [257, 258]

Two PK studies were then performed at a $2x10^6$ pfu dose and a $1x10^7$ pfu dose to asses the impact that the addition of aMUC1 antibodies to the polymer coating had on its circulation kinetics following IV infection (section 5.4). At both doses an increase in the amount of virus circulating at 5 minutes was evident for both PCVV and aMUC1-PCVV, however no significant increase in CAPAN-2 xenograft tumour accumulation was observed at 20 minutes, despite the addition of the aMUC1 antibody to the coating. Whilst this early time-point ensures replicated and released virus is not confused with initially delivered virus it does rely on having great sensitivity to the quantification of the dose recovered, and it is possible this sensitivity threshold was not reliably met here. The case could also be made that despite an enhanced PK and retargeting to a tumour associated antigen that is abundantly expressed in the CAPAN-2 xenografts, the challenges faced due to the tumour microenvironment, particularity given the dense stroma reported in CAPAN-2 tumours, could be preventing passive accumulation, even if blood levels can be raised.

Many techniques have been investigated to try and enhance the intratumoural delivery of therapeutics (including oncolytic viruses) after IV administration (Chapter 1, section 1.3.2). Ultrasound-mediated cavitation using SSPs as the cavitation nuclei has been shown not to impact in the structure of infection efficacy of VV *in vitro* [259] and has been shown to provide marked enhancement of intratumoural transgene expression *in vivo* [190]. Therefore it was hypothesised that ultrasound-mediated cavitation, such as that which was used in Chapter 3 to try to enhance the spread of VV after IT administration, could be used here to realise the potential

of PCVV and aMUC1-PCVV, particularly during the first 5 minutes after IV administration due to their enhanced PK. It was shown using a murine model with two bilateral CAPAN-2 xenograft tumours that when US was applied to one of the tumours after IV administration of SSPs + VV, PCVV, aMUC1-PCVV or IgG-PCVV, the US exposed tumour resulted in higher transgene expression when compared to the tumour not exposed to US, (in 14 out of 14 cases by day 8) (section 6.4.3). These results were in line with Myers et al's reports of increased transgene expression in tumours exposed to ultrasound after IV administration of VV + SSP. This was particularly true for PCVV and aMUC1-PCVV which showed the greatest fold-change in transgene expression in the US tumour compared with the no US control tumour (50-fold and 118-fold respectively). This supports the hypothesis linking VV with enhanced PK resulting in a higher circulating dose with a more marked impact of cavitation on delivery, in accordance with PC-Adenovirus studies by Carlisle *et al.* [116]

Increased transgene expression in US exposed tumours was also seen in a unilateral tumour study comparing SSPs with VV +/- US, aMUC1-PCVV +/- US or glucose + US (section 6.5.2). Notably, tumour growth regression in these mice was marked for VV + SSP + US (-30% +/-33) but more substantial for aMUC1-PCVV + SSP + US (-73% +/-14) (section 6.5.3). Regression was also seen in the aMUC1-PCVV + SSP without US (-30% +/-27) however exposure to US not only resulted in over 2 times greater tumour regression on the day of cull, but also produced a much tighter distribution in tumour regression and final tumour mass values within the aMUC1-PCVV + SSP + US treatment group. This suggests that the combination of Chol-PEG polymer coating and retargeting of VV to MUC1 in combination with ultrasound-mediated cavitation had a profound impact on tumour regression and the uniformity of treatment in this CAPAN-2 xenograft model.

7.2 Future work

The work presented here highlights the significant challenges VV faces and must over come if it is to achieve widespread impactful clinical translation. This thesis

reports strategies to enable VV to over come these delivery hurdles. Specifically the use of polymer coating and retargeting of an enveloped oncolytic vaccinia virus to the tumour associated antigen MUC1 was assessed. Furthermore, the use of ultrasound-mediated cavitation to help realise the potential of a polymer coated and retargeted VV which display enhanced circulation kinetics was also probed. Some of the limitations which were encountered and future work to overcome these challenges and further the work presented in this thesis are discussed here.

- After the second intervention with US after IT administration of VV in a CAPAN-2 xenograft tumour model, measurement of the % area of infected tumour and average radiant efficiency was shown to be increasing on the final day of imaging (day 14) when compared to day 9. A longer study which was able to further assess whether these increasing values resulted in a significant difference between tumours exposed to US at intervention 2 compared with tumours not exposed to US, would be of value. It would also be of interest to directly compare delivery of VV with non-inertial cavitation or inertial cavitation after IT administration. This could be done by using an additional cavitation nuclei such as SonoVue and adjusting the US parameters to match those which have previously been reported. [202] Particular attention should be given to the amount of damage observed after treatment between these two different cavitation conditions.
- Throughout this thesis the relationship between cavitation activity and markers of infection were probed. Many of the relationships which were assessed did not provide particularly strong relationships. Therefore a properly powered study to investigate the relationship between cavitation activity (either cumulative PAM magnitude or cavitation dose) and tumour growth or VV genome content would be needed to definitively determine these relationships.
- Infection foci were determined in tumours using 2D-IVIS imaging, which although insightful, could be better analysed using either 3D-IVIS imaging,

or, fluorescence microscopy and immunohistochemistry on recovered tumour slices. [77]

- Flow virometry was used here to determine Chol-PEG and Chol-PEG-aMUC1 coating of VV. To support this work, high resolution fluorescence imaging may be able to inform the uniformity of the coating on each VV virion. Alternatively using imaging flow cytometry may also allow the coverage to be determined. [260]
- A reduction in antibody binding is reported for PCVV here, however when compared with polymer coated Ad studies, the knockdown in infectivity (which was used to demonstrate the extent of coating) is markedly lower for the studies reported here. It therefore may be worth assessing the use of a cholesterol-PHPMA polymer, as PHPMA has previously shown greater protection for Ad than PEG [116], or perhaps combining enzymatic deglycosylation of VV's surface prior to polymer coating. [126]
- Chol-PEG-NHS conjugation to aMUC1 antibody was via a random interaction between NHS with free lysine groups on the antibody. Affinity of Chol-PEG-aMUC1 constructs to MUC1 was not hugely hindered by this non-specific method of conjugation, however, a more site-specific method may result in enhanced affinity of antibody-polymer constructs to their target. [261] It may also better shield Fc regions of the retargeting antibody thereby reducing RES mediated clearance even further.
- MUC1 specificity was probed here using an IgG antibody for comparison with aMUC1, however notable differences in the biological activity of the antibody-polymer conjugates that were formed could not be untied (beyond a much lower propensity for the aMUC1 antibody to give ovarian infection). A further study attempted to reduce the aMUC1 antibody affinity to MUC1 in cells by pre-incubating Chol-PEG-aMUC1 constructs with a blocking MUC1 peptide target. Indirect ELISA of Chol-PEG-aMUC1 incubated with the MUC1 peptide showed reduced binding to immbolised MUC1 peptide. However, once the Chol-PEG-aMUC1 + MUC1 was then incubated with VV and

subsequently purified from free polymer, the impact on reducing infectivity in CAPAN-2 cell monolayer experiments was found to be statistically non-significant. This is likely due to the incubation of aMUC1-polymer conjugates with MUC1 peptide over night before formation of aMUC1-PCVV, giving the antibody-peptide a substantial period of time and multiple rounds of dilution by washing during which disassociation is likely to have occurred. It would therefore be of merit to refine this experiment by incubating the MUC1 peptide in the infection media with the aMUC1-PCVV at the time of infection. Additionally silencing MUC1 expression in a cancer cell line and comparing the infection level achieved with aMUC1-PCVV to that achieved in the non-silenced cells, would be worthwhile.

- Given the reported impact that VV has on tumour associated vasculature during infection, it would be interesting to combine the DCE-MRI study in tumours before and after treatment to see whether there is any difference in blood flow associated with the VV, PCVV or aMUC1-PCVV viruses (with and without ultrasound-mediated cavitation).
- The impact of aMUC1-PCVV + SSP + US on tumour regression was marked and it would be of interest to complete a large survival study to see whether the impact on tumour regression here is marked enough to produce prolonged survival when compared with VV + SSP, aMUC1-PCVV + SSP or glucose + SSP + US. It would also be of interest to develop a murine model in an immunocompetent mouse so any to determine how the anti-tumour immune response may further result in even more enhanced tumour regression (i.e 'turning cold tumours hot' [262, 263]). An immunocompetent murine model would also allow the protective effect of the polymer coating to be determined in more clinically relevant multiple-dosing regimes.

References

[1] *Side Effects of Chemotherapy | Cancer.Net.*

[2] David L Bartlett M Firdos Ziaddin. *Viral Therapy of Cancer, Chapter 9: Oncolytic vaccinia.* Ed. by Pandha Harrington VIle. John Wiley & Sons, Ltd, 2008.

[3] Claudia Hill and Robert Carlisle. "Achieving systemic delivery of oncolytic viruses". In: *Expert Opinion on Drug Delivery* 16.6 (June 2019), pp. 607–620.

[4] Claudia A. P. Hill, Luca Bau, and Robert Carlisle. "Methods for Modification of Therapeutic Viruses". In: ed. by Christine Engeland. Humana, New York, NY, 2020, pp. 7–29.

[5] Elizabeth Kelly and Stephen J. Russell. *History of oncolytic viruses: Genesis to genetic engineering.* Apr. 2007.

[6] Robert L. Martuza et al. "Experimental therapy of human glioma by means of a genetically engineered virus mutant". In: *Science* 252.5007 (May 1991), pp. 854–6.

[7] Stephen J Russell, Kah-Whye Peng, and John C Bell. "Oncolytic virotherapy." In: *Nature biotechnology* 30.7 (July 2012), pp. 658–70.

[8] Sean E. Lawler et al. *Oncolytic viruses in cancer treatment a review.* June 2017.

[9] Kenneth Lundstrom. "Viral Vectors in Gene Therapy". In: *Diseases* 6.2 (May 2018), p. 42.

[10] Stephen J Russell and Kah-Whye Peng. "Oncolytic Virotherapy: A Contest between Apples and Oranges." In: *Molecular therapy : the journal of the American Society of Gene Therapy* 25.5 (2017), pp. 1107–1116.

[11] Roberto Cattaneo et al. "Reprogrammed viruses as cancer therapeutics: targeted, armed and shielded". In: *Nature Reviews Microbiology* 6.7 (July 2008), pp. 529–540.

[12] C Heise et al. "ONYX-015, an E1B gene-attenuated adenovirus, causes tumor-specific cytolysis and antitumoral efficacy that can be augmented by standard chemotherapeutic agents." In: *Nature medicine* 3.6 (June 1997), pp. 639–45.

[13] David F. Stojdl et al. "Exploiting tumor-specific defects in the interferon pathway with a previously unknown oncolytic virus". In: *Nature Medicine* 6.7 (July 2000), pp. 821–825.

[14] T Hermiston. "Gene delivery from replication-selective viruses: arming guided missiles in the war against cancer." In: *The Journal of clinical investigation* 105.9 (May 2000), pp. 1169–72.

[15] Kseniya S. Yurchenko et al. "Oncolytic effect of wild-type Newcastle disease virus isolates in cancer cell lines in vitro and in vivo on xenograft model". In: *PLOS ONE* 13.4 (Apr. 2018). Ed. by Ilya Ulasov, e0195425.

[16] Frederik H. Igney and Peter H. Krammer. "Death and Anti-Death: Tumour Resistance to Apoptosis". In: *Nature Reviews Cancer* (2002).

[17] K. J. Harrington et al. "Phase I/II Study of Oncolytic HSVGM-CSF in Combination with Radiotherapy and Cisplatin in Untreated Stage III/IV Squamous Cell Cancer of the Head and Neck". In: *Clinical Cancer Research* 16.15 (Aug. 2010), pp. 4005–4015.

[18] Howard L. Kaufman et al. "Local and Distant Immunity Induced by Intralesional Vaccination with an Oncolytic Herpes Virus Encoding GM-CSF in Patients with Stage IIIc and IV Melanoma". In: *Annals of Surgical Oncology* 17.3 (Mar. 2010), pp. 718–730.

[19] J M Markert et al. "Conditionally replicating herpes simplex virus mutant, G207 for the treatment of malignant glioma: results of a phase I trial". In: *Gene Therapy* 7.10 (May 2000), pp. 867–874.

[20] James M Markert et al. "Phase Ib Trial of Mutant Herpes Simplex Virus G207 Inoculated Pre-and Post-tumor Resection for Recurrent GBM". In: *Molecular Therapy* 17.1 (Jan. 2009), pp. 199–207.

[21] Neil N. Senzer et al. "Phase II Clinical Trial of a Granulocyte-Macrophage Colony-Stimulating Factor- Encoding, Second-Generation Oncolytic Herpesvirus in Patients With Unresectable Metastatic Melanoma". In: *Journal of Clinical Oncology* 27.34 (Dec. 2009), pp. 5763–5771.

[22] Caroline J Breitbach et al. "Intravenous delivery of a multi-mechanistic cancer-targeted oncolytic poxvirus in humans". In: *Nature* 477.7362 (Sept. 2011), pp. 99–102.

[23] R M Conry et al. "Phase I trial of a recombinant vaccinia virus encoding carcinoembryonic antigen in metastatic adenocarcinoma: comparison of intradermal versus subcutaneous administration." In: *Clinical cancer research : an official journal of the American Association for Cancer Research* 5.9 (Sept. 1999), pp. 2330–7.

[24] Timothy P Cripe et al. "Phase 1 Study of Intratumoral Pexa-Vec (JX-594), an Oncolytic and Immunotherapeutic Vaccinia Virus, in Pediatric Cancer Patients". In: *Molecular Therapy* 23.3 (Mar. 2015), pp. 602–608.

[25] Tae-Ho Hwang et al. "A Mechanistic Proof-of-concept Clinical Trial With JX-594, a Targeted Multi-mechanistic Oncolytic Poxvirus, in Patients With Metastatic Melanoma". In: *Molecular Therapy* 19.10 (Oct. 2011), pp. 1913–1922.

[26] Dc Mansfield et al. "Oncolytic vaccinia virus as a vector for therapeutic sodium iodide symporter gene therapy in prostate cancer". In: *Gene Therapy* 23.105 (2016), pp. 357–368.

[27] Michael J Mastrangelo et al. "Intratumoral recombinant GM-CSF-encoding virus as gene therapy in patients with cutaneous melanoma". In: *Cancer Gene Therapy* 6.5 (Nov. 1999), pp. 409–422.

[28] Byeong-Ho Park et al. "Use of a targeted oncolytic poxvirus, JX-594, in patients with refractory primary or metastatic liver cancer: a phase I trial". In: *The Lancet Oncology* 9.6 (June 2008), pp. 533–542.

[29] Herbert J Zeh et al. "First-in-man Study of Western Reserve Strain Oncolytic Vaccinia Virus: Safety, Systemic Spread, and Antitumor Activity". In: *Molecular therapy : the journal of the American Society of Gene Therapy* 23.1 (Jan. 2015), pp. 202–214.

[30] Kenneth N. Barton et al. "Second-Generation Replication-Competent Oncolytic Adenovirus Armed with Improved Suicide Genes and ADP Gene Demonstrates Greater Efficacy without Increased Toxicity". In: *Molecular Therapy* 13.2 (Feb. 2006), pp. 347–356.

[31] Jianhua Chang et al. "A Phase I study of KH901, a conditionally replicating granulocyte-macrophage colony-stimulating factor: armed oncolytic adenovirus for the treatment of head and neck cancers." In: *Cancer biology & therapy* 8.8 (Apr. 2009), pp. 676–82.

[32] J Randolph Hecht et al. "A phase I/II trial of intratumoral endoscopic ultrasound injection of ONYX-015 with intravenous gemcitabine in unresectable pancreatic carcinoma." In: *Clinical cancer research : an official journal of the American Association for Cancer Research* 9.2 (Feb. 2003), pp. 555–61.

[33] J-L Li et al. "A phase I trial of intratumoral administration of recombinant oncolytic adenovirus overexpressing HSP70 in advanced solid tumor patients". In: *Gene Therapy* 16.3 (Mar. 2009), pp. 376–382.

[34] Ilkka Liikanen et al. "Oncolytic Adenovirus With Temozolomide Induces Autophagy and Antitumor Immune Responses in Cancer Patients". In: *Molecular Therapy* 21.6 (June 2013), pp. 1212–1223.

[35] S. Morley et al. "The dl1520 Virus Is Found Preferentially in Tumor Tissue after Direct Intratumoral Injection in Oral Carcinoma". In: *Clinical Cancer Research* 10.13 (July 2004), pp. 4357–4362.

[36] Michael A Morse et al. "Novel adenoviral vector induces T-cell responses despite anti-adenoviral neutralizing antibodies in colorectal cancer patients." In: *Cancer immunology, immunotherapy : CII* 62.8 (Aug. 2013), pp. 1293–301.

[37] J Nemunaitis et al. "Intravenous infusion of a replication-selective adenovirus (ONYX-015) in cancer patients: safety, feasibility and biological activity". In: *Gene Therapy* 8.10 (May 2001), pp. 746–759.

[38] Jackie Nemunaitis and John Nemunaitis. "Head and neck cancer: Response to p53-based therapeutics". In: *Head & Neck* 33.1 (Jan. 2011). Ed. by David W. Eisele, pp. 131–134.

[39] Tony R Reid et al. "Effects of Onyx-015 among metastatic colorectal cancer patients that have failed prior treatment with 5-FU/leucovorin". In: *Cancer Gene Therapy* 12.8 (Aug. 2005), pp. 673–681.

[40] Cormac Sheridan. "First Oncolytic virus edges towards approval in surprise vote". In: *nature biotechnology* 33.6 (June 2015), pp. 569–570.

[41] Ken Garber. "China Approves World's First Oncolytic Virus Therapy For Cancer Treatment". In: *JNCI: Journal of the National Cancer Institute* 98.5 (Mar. 2006), pp. 298–300.

[42] B. L. Liu et al. *ICP34.5 deleted herpes simplex virus with enhanced oncolytic, immune stimulating, and anti-tumour properties*. 2003.

[43] Robert H.I. Andtbacka et al. "Talimogene laherparepvec improves durable response rate in patients with advanced melanoma". In: *Journal of Clinical Oncology* (2015).

[44] Kathryn A. Skelding, Richard D. Barry, and Darren R. Shafren. "Enhanced oncolysis mediated by Coxsackievirus A21 in combination with doxorubicin hydrochloride". In: *Investigational New Drugs* 30.2 (Apr. 2012), pp. 568–581.

[45] Robert Hans Ingemar Andtbacka et al. "CALM study: A phase II study of an intratumorally delivered oncolytic immunotherapeutic agent, coxsackievirus A21, in patients with stage IIIc and stage IV malignant melanoma." In: *Journal of Clinical Oncology* 32.15_suppl (May 2014), pp. 3031–3031.

[46] V. Bernstein et al. "A randomized phase II study of weekly paclitaxel with or without pelareorep in patients with metastatic breast cancer: final analysis of Canadian Cancer Trials Group IND.213." In: *Breast Cancer Research and Treatment* 167.2 (Jan. 2018), pp. 485–493.

[47] G L Smith and B Moss. "Infectious poxvirus vectors have capacity for at least 25 000 base pairs of foreign DNA." In: *Gene* 25.1 (Nov. 1983), pp. 21–8.

[48] R Blasco and B Moss. "Role of cell-associated enveloped vaccinia virus in cell-to-cell spread." In: *Journal of virology* 66.7 (July 1992), pp. 4170–9.

[49] Geoffrey L. Smith, Alain Vanderplasschen, and Mansun Law. *The formation and function of extracellular enveloped vaccinia virus*. 2002.

[50] Nina Tolonen et al. "Vaccinia Virus DNA Replication Occurs in Endoplasmic Reticulum-enclosed Cytoplasmic Mini-Nuclei". In: *Molecular Biology of the Cell* 12.July (2001), pp. 2031–2046.

[51] D. H. Kirn et al. “Enhancing Poxvirus Oncolytic Effects through Increased Spread and Immune Evasion”. In: *Cancer Research* 68.7 (Apr. 2008), pp. 2071–2075.

[52] Mike M Pütz et al. “Quantification of antibody responses against multiple antigens of the two infectious forms of Vaccinia virus provides a benchmark for smallpox vaccination”. In: *Nature Medicine* 12.11 (Nov. 2006), pp. 1310–1315.

[53] A Vanderplasschen et al. “Extracellular enveloped vaccinia virus is resistant to complement because of incorporation of host complement control proteins into its envelope.” In: *Proceedings of the National Academy of Sciences of the United States of America* 95.13 (June 1998), pp. 7544–9.

[54] A Vanderplasschen, M Hollinshead, and G L Smith. “Antibodies against vaccinia virus do not neutralize extracellular enveloped virus but prevent virus release from infected cells and comet formation.” In: *Journal of General Virology* 78.8 (Aug. 1997), pp. 2041–2048.

[55] Surendran Mahalingam and Gunasegaran Karupiah. “Modulation of chemokines by poxvirus infections”. In: *Current Opinion in Immunology* 12.4 (Aug. 2000), pp. 409–412.

[56] Bruce T Seet and Grant McFadden. “Viral chemokine-binding proteins.” In: *Journal of leukocyte biology* 72.1 (July 2002), pp. 24–34.

[57] A Alcamí et al. “Blockade of chemokine activity by a soluble chemokine binding protein from vaccinia virus.” In: *Journal of immunology (Baltimore, Md. : 1950)* 160.2 (Jan. 1998), pp. 624–33.

[58] R Deonarain et al. “Impaired antiviral response and alpha/beta interferon induction in mice lacking beta interferon.” In: *Journal of virology* 74.7 (Apr. 2000), pp. 3404–9.

[59] P. Najarro, P. Traktman, and J. A. Lewis. “Vaccinia Virus Blocks Gamma Interferon Signal Transduction: Viral VH1 Phosphatase Reverses Stat1 Activation”. In: *Journal of Virology* 75.7 (Apr. 2001), pp. 3185–3196.

[60] J A Symons, A Alcamí, and G L Smith. “Vaccinia virus encodes a soluble type I interferon receptor of novel structure and broad species specificity.” In: *Cell* 81.4 (May 1995), pp. 551–60.

[61] A Sahu et al. “Interaction of vaccinia virus complement control protein with human complement proteins: factor I-mediated degradation of C3b to iC3b1 inactivates the alternative complement pathway.” In: *Journal of immunology (Baltimore, Md. : 1950)* 160.11 (June 1998), pp. 5596–604.

[62] G J Kotwal et al. “Inhibition of the complement cascade by the major secretory protein of vaccinia virus.” In: *Science (New York, N.Y.)* 250.4982 (Nov. 1990), pp. 827–30.

[63] N. M. Girgis et al. “Cell Surface Expression of the Vaccinia Virus Complement Control Protein Is Mediated by Interaction with the Viral A56 Protein and Protects Infected Cells from Complement Attack”. In: *Journal of Virology* 82.9 (May 2008), pp. 4205–4214.

[64] Herbert J Zeh and David L Bartlett. “Development of a replication-selective, oncolytic poxvirus for the treatment of human cancers”. In: *Cancer Gene Therapy* 9.12 (Dec. 2002), pp. 1001–1012.

[65] E D Whitman et al. “In vitro and in vivo kinetics of recombinant vaccinia virus cancer-gene therapy.” In: *Surgery* 116.2 (Aug. 1994), pp. 183–8.

[66] Kelley A Parato et al. “The oncolytic poxvirus JX-594 selectively replicates in and destroys cancer cells driven by genetic pathways commonly activated in cancers.” In: *Molecular therapy : the journal of the American Society of Gene Therapy* 20.4 (Apr. 2012), pp. 749–58.

[67] J A McCart et al. “Systemic cancer therapy with a tumor-selective vaccinia virus mutant lacking thymidine kinase and vaccinia growth factor genes.” In: *Cancer research* 61.24 (Dec. 2001), pp. 8751–7.

[68] Jeong Heo et al. “Randomized dose-finding clinical trial of oncolytic immunotherapeutic vaccinia JX-594 in liver cancer.” In: *Nat Med* 19.3 (Mar. 2013), pp. 329–336.

[69] Stephanie Downs-Canner et al. “Phase 1 Study of Intravenous Oncolytic Poxvirus (vvDD) in Patients With Advanced Solid Cancers”. In: *Molecular Therapy* 24.8 (Aug. 2016), pp. 1492–1501.

[70] Mell L.K. et al. “Phase 1 trial of attenuated vaccinia virus (GL-ONC1) delivered intravenously with concurrent cisplatin and radiation therapy in patients with locoregionally advanced head-and-neck carcinoma”. In: *International Journal of Radiation Oncology Biology Physics* 88.2 (2014), pp. 477–478.

[71] J V Pedersen et al. “Preliminary results of a phase 1 study of intravenous administration of gl-onc1 vaccinia virus in patients with advanced solid cancer with real time imaging”. In: *Annals of Oncology* 21 (2010), p. viii175.

[72] A. Biondo et al. “Phase I clinical trial of a genetically modified oncolytic vaccinia virus GL-ONC1 with green fluorescent protein imaging”. In: *European Journal of Cancer* 47 (2011), S162.

[73] UM Lauer et al. “Phase I Clinical Trial of a Genetically Modified and Oncolytic Vaccinia Virus GL-ONC1 in patients with peritoneal carcinomatosis”. In: *Zeitschrift für Gastroenterologie* 50.08 (2012), K151.

[74] Ulrich Lauer et al. “Phase I/II clinical trial of a genetically modified and oncolytic vaccinia virus GL-ONC1 in patients with unresactable, chemotherapy-resistant peritoneal carcinomatosis.” In: *Journal of Clinical Oncology* 31.suppl 15 (2013), abstr.3098.

[75] Laura Evgin et al. “Complement inhibition prevents oncolytic vaccinia virus neutralization in immune humans and cynomolgus macaques.” In: *Molecular therapy : the journal of the American Society of Gene Therapy* 23.6 (June 2015), pp. 1066–76.

[76] K D Fisher et al. “Polymer-coated adenovirus permits efficient retargeting and evades neutralising antibodies.” In: *Gene Therapy* 8.5 (Apr. 2001), pp. 341–348.

[77] Amber Miller et al. “Reporter gene imaging identifies intratumoral infection voids as a critical barrier to systemic oncolytic virus efficacy”. In: *Molecular Therapy Oncolytics* 1 (Dec. 2014), pp. 14005–.

[78] Daniel S. Chen and Ira Mellman. *Oncology meets immunology: The cancer-immunity cycle.* 2013.

[79] Marie-Claude Bourgeois-Daigneault et al. “Neoadjuvant oncolytic virotherapy before surgery sensitizes triple-negative breast cancer to immune checkpoint therapy”. In: *Science Translational Medicine* 10.422 (Jan. 2018), eaao1641.

[80] Els M.E. Verdegaal and Sjoerd H. van der Burg. “The potential and challenges of exploiting the vast but dynamic neoepitope landscape for immunotherapy”. In: *Frontiers in Immunology* 8.SEP (Sept. 2017), p. 1113.

[81] Andrzej B. Popawski et al. “Frequent genetic differences between matched primary and metastatic breast cancer provide an approach to identification of biomarkers for disease progression”. In: *European Journal of Human Genetics* (2010).

[82] Valsamo Anagnostou et al. “Evolution of neoantigen landscape during immune checkpoint blockade in non-small cell lung cancer”. In: *Cancer Discovery* 7.3 (Mar. 2017), pp. 264–276.

[83] Irene Kuhn et al. “Directed Evolution Generates a Novel Oncolytic Virus for the Treatment of Colon Cancer”. In: *PLoS ONE* 3.6 (June 2008). Ed. by Dong-Yan Jin, e2409.

[84] Maxine Bauzon and Terry W Hermiston. “Oncolytic viruses: The power of directed evolution”. In: *Advances in Virology* 2012 (2012), p. 586389.

[85] Manish R. Patel and Robert A. Kratzke. “Genetic Engineering of Oncolytic Viruses for Cancer Therapy”. In: *Translating Gene Therapy to the Clinic* (Jan. 2015), pp. 261–279.

[86] Robert E. Edge et al. "A let-7 microRNA-sensitive vesicular stomatitis virus demonstrates tumor-specific replication". In: *Molecular Therapy* (2008).

[87] Mina Hikichi et al. "MicroRNA regulation of glycoprotein B5R in oncolytic vaccinia virus reduces viral pathogenicity without impairing its antitumor efficacy". In: *Molecular Therapy* (2011).

[88] Elizabeth J. Kelly et al. "Engineering microRNA responsiveness to decrease virus pathogenicity". In: *Nature Medicine* (2008).

[89] Mathias F. Leber et al. "MicroRNA-sensitive oncolytic measles viruses for cancer-specific vector tropism". In: *Molecular Therapy* (2011).

[90] Cleo Y F Lee, Paul S. Rennie, and William W G Jia. "MicroRNA regulation of oncolytic herpes simplex virus-1 for selective killing of prostate cancer cells". In: *Clinical Cancer Research* (2009).

[91] E. Ylosmaki et al. "Attenuation of Semliki Forest Virus Neurovirulence by MicroRNA-Mediated Detargeting". In: *Journal of Virology* 87.1 (Jan. 2013), pp. 335–344.

[92] Zahid M Delwar et al. "Tumour-specific triple-regulated oncolytic herpes virus to target glioma". In: *Oncotarget* 7.19 (May 2016), pp. 28658–28669.

[93] Biljana Petrovic et al. "Insertion of a ligand to HER2 in gB retargets HSV tropism and obviates the need for activation of the other entry glycoproteins". In: *PLoS Pathogens* 13.4 (Apr. 2017). Ed. by Peter Palese, e1006352.

[94] M H Verheije and P J M Rottier. "Retargeting of viruses to generate oncolytic agents." In: *Advances in virology* 2012 (2012), p. 798526.

[95] Takafumi Nakamura et al. "Rescue and propagation of fully retargeted oncolytic measles viruses". In: *Nature Biotechnology* 23.2 (Feb. 2005), pp. 209–214.

[96] Florian Kreppel et al. "Combined genetic and chemical capsid modifications enable flexible and efficient de- and retargeting of adenovirus vectors." In: *Molecular therapy : the journal of the American Society of Gene Therapy* 12.1 (July 2005), pp. 107–17.

[97] L. Krutzke et al. "Substitution of blood coagulation factor X-binding to Ad5 by position-specific PEGylation: Preventing vector clearance and preserving infectivity". In: *Journal of Controlled Release* 235 (Aug. 2016), pp. 379–392.

[98] Sateesh Krishnamurthy et al. "Differentially Regulated Interferon Response Determines the Outcome of Newcastle Disease Virus Infection in Normal and Tumor Cell Lines". In: *Journal of Virology* 80.11 (2006), pp. 5145–5155.

[99] Kirk W Reichard et al. "Newcastle disease virus selectively kills human tumor cells". In: *Journal of Surgical Research* 52.5 (May 1992), pp. 448–453.

[100] Arnold I. Freeman et al. "Phase I/II Trial of Intravenous NDV-HUJ Oncolytic Virus in Recurrent Glioblastoma Multiforme". In: *Molecular Therapy* 13.1 (Jan. 2006), pp. 221–228.

[101] S. A. Laurie et al. "A Phase 1 Clinical Study of Intravenous Administration of PV701, an Oncolytic Virus, Using Two-Step Desensitization". In: *Clinical Cancer Research* 12.8 (Apr. 2006), pp. 2555–2562.

[102] Andrew L Pecora et al. "Phase I trial of intravenous administration of PV701, an oncolytic virus, in patients with advanced solid cancers." In: *Journal of clinical oncology : official journal of the American Society of Clinical Oncology* 20.9 (May 2002), pp. 2251–66.

[103] Wei Song Zhongkui Wu Dan Li Hong Chen Lin Yuan et al. "Biocompatible polymer materials: role of protein-surface interactions". In: *Progress in Polymer Science* 33.33 (2008), pp. 1059–1087.

[104] Catherine R. O'Riordan et al. "PEGylation of Adenovirus with Retention of Infectivity and Protection from Neutralizing Antibody in Vitro and in Vivo". In: *Human Gene Therapy* 10.8 (May 1999), pp. 1349–1358.

[105] Maria A. Croyle et al. “PEGylation of E1-Deleted Adenovirus Vectors Allows Significant Gene Expression on Readministration to Liver”. In: *Human Gene Therapy* (2002).

[106] Nicola K. Green et al. “Retargeting polymer-coated adenovirus to the FGF receptor allows productive infection and mediates efficacy in a peritoneal model of human ovarian cancer”. In: *The Journal of Gene Medicine* 10.3 (Mar. 2008), pp. 280–289.

[107] Joanne Morrison et al. “Virotherapy of ovarian cancer with polymer-cloaked adenovirus retargeted to the epidermal growth factor receptor”. In: *Mol Ther* 16.2 (Feb. 2008), pp. 244–251.

[108] M Stevenson et al. “Incorporation of a laminin-derived peptide (SIKVAV) on polymer-modified adenovirus permits tumor-specific targeting via α6-integrins”. In: *Cancer Gene Therapy* 14.4 (Apr. 2007), pp. 335–345.

[109] Piyanuch Wonganan and Maria A Croyle. “PEGylated Adenoviruses: From Mice to Monkeys.” In: *Viruses* 2.2 (Feb. 2010), pp. 468–502.

[110] M. A. Croyle et al. “"Stealth" Adenoviruses Blunt Cell-Mediated and Humoral Immune Responses against the Virus and Allow for Significant Gene Expression upon Readministration in the Lung”. In: *Journal of Virology* 75.10 (May 2001), pp. 4792–4801.

[111] Ramon Alemany, Kaori Suzuki, and David T. Curiel. “Blood clearance rates of adenovirus type 5 in mice”. In: *Journal of General Virology* 81.11 (Nov. 2000), pp. 2605–2609.

[112] Hoyin Mok et al. “Evaluation of polyethylene glycol modification of first-generation and helper-dependent adenoviral vectors to reduce innate immune responses”. In: *Molecular Therapy* 11.1 (Jan. 2005), pp. 66–79.

[113] N K Green et al. “Extended plasma circulation time and decreased toxicity of polymer-coated adenovirus.” In: *Gene therapy* 11.16 (2004), pp. 1256–63.

[114] K D Fisher et al. “Passive tumour targeting of polymer-coated adenovirus for cancer gene therapy”. In: *Journal of Drug Targeting* 15.7-8 (Oct. 2007), pp. 546–551.

[115] Nicola K Green et al. “Tropism ablation and stealthing of oncolytic adenovirus enhances systemic delivery to tumors and improves virotherapy of cancer”. In: *Nanomedicine* 7.11 (2012), pp. 1683–1695.

[116] Robert Carlisle et al. “Enhanced tumor uptake and penetration of virotherapy using polymer stealthing and focused ultrasound.” In: *Journal of the National Cancer Institute* 105.22 (Nov. 2013), pp. 1701–10.

[117] Jan Michael Prill et al. “Traceless bioresponsive shielding of adenovirus hexon with HPMA copolymers maintains transduction capacity in vitro and in vivo”. In: *PLoS ONE* 9.1 (Jan. 2014). Ed. by Saw-See Hong, e82716.

[118] Anette Bonsted et al. “Photochemically enhanced transduction targeted to the epidermal growth factor receptor”. In: *Journal of Gene Medicine* 8.3 (Mar. 2006), pp. 286–297.

[119] Laura M. Kasman et al. “Polymer-enhanced adenoviral transduction of CAR-negative bladder cancer cells”. In: *Molecular Pharmaceutics*. Vol. 6. 5. American Chemical Society, Oct. 2009, pp. 1612–1619. arXiv: NIHMS150003.

[120] Joung Woo Choi et al. “Polymeric oncolytic adenovirus for cancer gene therapy”. In: *Journal of Controlled Release* 219 (Dec. 2015), pp. 181–191. arXiv: 15334406.

[121] Joung-Woo Choi et al. “Using a magnetic field to redirect an oncolytic adenovirus complexed with iron oxide augments gene therapy efficacy”. In: *Biomaterials* 65 (Oct. 2015), pp. 163–174.

[122] Ziyue Karen Jiang et al. “Engineering polypeptide coatings to augment gene transduction and in vivo stability of adenoviruses”. In: *Journal of Controlled Release* 166.1 (Feb. 2013), pp. 75–85.

[123] Jaesung Kim et al. “Therapeutic efficacy of a systemically delivered oncolytic adenovirus - Biodegradable polymer complex”. In: *Biomaterials* 34.19 (June 2013), pp. 4622–4631.

[124] Al Fasbender et al. “Complexes of adenovirus with polycationic polymers and cationic lipids increase the efficiency of gene transfer in vitro and in vivo”. In: *Journal of Biological Chemistry* 272.10 (Mar. 1997), pp. 6479–6489.

[125] Kaname Nosaki et al. “A novel, polymer-coated oncolytic measles virus overcomes immune suppression and induces robust antitumor activity”. In: *Molecular Therapy - Oncolytics* 3.February (Jan. 2016), p. 16022.

[126] Juan J. Rojas et al. “Manipulating TLR Signaling Increases the Anti-tumor T Cell Response Induced by Viral Cancer Therapies”. In: *Cell Reports* 15.2 (2016), pp. 264–273.

[127] Megan Grundy, Constantin Coussios, and Robert Carlisle. “Advances in systemic delivery of anti-cancer agents for the treatment of metastatic cancer”. In: *Expert Opinion on Drug Delivery* 13.7 (2016), pp. 999–1013.

[128] Helen Romanczuk et al. “Modification of an Adenoviral Vector with Biologically Selected Peptides: A Novel Strategy for Gene Delivery to Cells of Choice”. In: *Human Gene Therapy* (1999).

[129] Samuel K. Campos and Michael A. Barry. “Comparison of adenovirus fiber, protein IX, and hexon capsomeres as scaffolds for vector purification and cell targeting”. In: *Virology* 349.2 (June 2006), pp. 453–462.

[130] Stéphane Paul et al. “Specific Tumor Cell Targeting by a Recombinant MVA Expressing a Functional Single Chain Antibody on the Surface of Intracellular Mature Virus (IMV) Particles”. In: *VIRAL IMMUNOLOGY* 20.4 (2007), pp. 664–671.

[131] Robert C. Carlisle et al. “Human erythrocytes bind and inactivate type 5 adenovirus by presenting Coxsackie virus-adenovirus receptor and complement receptor 1”. In: *Blood* 113.9 (Feb. 2009), pp. 1909–1918.

[132] Steve H. Thorne et al. “Rational strain selection and engineering creates a broad-spectrum, systemically effective oncolytic poxvirus, JX-963”. In: *Journal of Clinical Investigation* 117.11 (2007), pp. 3350–3358.

[133] Weizhou Hou et al. “Oncolytic Virus-Mediated Targeting of PGE2 in the Tumor Alters the Immune Status and Sensitizes Established and Resistant Tumors to Immunotherapy”. In: *Cancer Cell* 30.1 (2016), pp. 108–119.

[134] S M Scholl et al. “Recombinant vaccinia virus encoding human MUC1 and IL2 as immunotherapy in patients with breast cancer.” In: *Journal of immunotherapy (Hagerstown, Md. : 1997)* 23.5 (), pp. 570–80.

[135] Xiaobin B. Zhao et al. “Cholesterol as a bilayer anchor for PEGylation and targeting ligand in folate-receptor-targeted liposomes”. In: *Journal of Pharmaceutical Sciences* 96.9 (2007), pp. 2424–2435.

[136] Zhi Yao He et al. *Recent development of poly(ethylene glycol)-cholesterol conjugates as drug delivery systems*. July 2014.

[137] Francesca Ercole et al. “Cholesterol Modified Self-Assemblies and Their Application to Nanomedicine”. In: *Biomacromolecules* 16.7 (July 2015), pp. 1886–1914.

[138] Anush Arakelyan et al. “Nanoparticle-based flow virometry for the analysis of individual virions”. In: *Journal of Clinical Investigation* 123.9 (Sept. 2013), pp. 3716–3727.

[139] Vera A. Tang et al. “Single-particle characterization of oncolytic vaccinia virus by flow virometry”. In: *Vaccine* 34.42 (Sept. 2016), pp. 5082–5089.

[140] J. Lizbeth Reyes Zamora and Hector C. Aguilar. *Flow virometry as a tool to study viruses*. Feb. 2018.

[141] Corina P.D. Brussaard, Dominique Marie, and Gunnar Bratbak. "Flow cytometric detection of viruses". In: *Journal of Virological Methods* 85.1-2 (Mar. 2000), pp. 175–182.

[142] Raphaël Gaudin and Natasha S. Barteneva. "Sorting of small infectious virus particles by flow virometry reveals distinct infectivity profiles". In: *Nature Communications* 6 (2015), p. 6022.

[143] J Taylor-Papadimitriou et al. "MUC1 and cancer". In: *Biochimica et Biophysica Acta (BBA) - Molecular Basis of Disease* 1455.2-3 (Oct. 1999), pp. 301–313.

[144] Sandra J. Gendler. "MUC1, The renaissance molecule". In: *Journal of Mammary Gland Biology and Neoplasia* 6.3 (2001), pp. 339–353.

[145] S Nath et al. "MUC1 induces drug resistance in pancreatic cancer cells via upregulation of multidrug resistance genes". In: *Oncogenesis* 2.6 (June 2013), e51–e51.

[146] Deepak Raina, Surender Kharbanda, and Donald Kufe. "The MUC1 oncoprotein activates the anti-apoptotic phosphoinositide 3-kinase/Akt and Bcl-xL pathways in rat 3Y1 fibroblasts". In: *Journal of Biological Chemistry* 279.20 (May 2004), pp. 20607–20612.

[147] Dahlia M. Besmer et al. "Pancreatic ductal adenocarcinoma mice lacking mucin 1 have a profound defect in tumor growth and metastasis". In: *Cancer Research* 71.13 (July 2011), pp. 4432–4442.

[148] Joyce Taylor-Papadimitriou et al. *Latest developments in MUC1 immunotherapy.* June 2018.

[149] Allan J.; Pantuck et al. "Phase I Trial of Antigen-Specific Gene Therapy Using a Recombinant Vaccinia Virus Encoding MUC-1 and IL-2 in MUC-1-Positive Patients With Advanced Prostate Cancer". In: *Journal of Immunotherapy* 27.3 (2004), pp. 240–253.

[150] H W Virgin. *Pathogenesis of viral infection. Fields' Virology, eds Fields BN, Knipe DM, Howley PM.* 2007.

[151] Andrew I. Minchinton and Ian F. Tannock. "Drug penetration in solid tumours". In: *Nature Reviews Cancer* 6.8 (Aug. 2006), pp. 583–592.

[152] Hiroshi Maeda, Tomohiro Sawa, and Toshimitsu Konno. "Mechanism of tumor-targeted delivery of macromolecular drugs, including the EPR effect in solid tumor and clinical overview of the prototype polymeric drug SMANCS". In: *Journal of Controlled Release.* Vol. 74. 1-3. 2001, pp. 47–61.

[153] Joseph W Nichols and You Han Bae. "Odyssey of a cancer nanoparticle: From injection site to site of action". In: *Nano Today* 7.6 (Dec. 2012), pp. 606–618.

[154] Jennifer H E Baker et al. "Direct visualization of heterogeneous extravascular distribution of trastuzumab in human epidermal growth factor receptor type 2 overexpressing xenografts". In: *Clinical Cancer Research* 14.7 (Apr. 2008), pp. 2171–2179.

[155] Andrew J Primeau et al. "The distribution of the anticancer drug doxorubicin in relation to blood vessels in solid tumors". In: *Clinical Cancer Research* 11.24 (Dec. 2005), pp. 8782–8788.

[156] Tina D. Tailor et al. "Effect of pazopanib on tumor microenvironment and liposome delivery". In: *Molecular Cancer Therapeutics* 9.6 (June 2010), pp. 1798–1808.

[157] Shom Goel, Andus Hon Kit Wong, and Rakesh K Jain. "Vascular normalization as a therapeutic strategy for malignant and nonmalignant disease". In: *Cold Spring Harbor Perspectives in Medicine* 2.3 (Mar. 2012), a006486.

[158] Peter Carmeliet and Rakesh K. Jain. *Molecular mechanisms and clinical applications of angiogenesis.* 2011.

[159] Bert Vogelstein and Kenneth W. Kinzler. *Cancer genes and the pathways they control.* 2004.

[160] Napoleone Ferrara. *VEGF as a therapeutic target in cancer*. 2005.

[161] H F Dvorak. "Tumors: wounds that do not heal. Similarities between tumor stroma generation and wound healing." In: *The New England journal of medicine* 315.26 (1986), pp. 1650–9.

[162] Rakesh K Jain. "Antiangiogenic therapy for cancer: current and emerging concepts." In: *Oncology (Williston Park)* 19.4 Suppl 3 (2005), pp. 7–16.

[163] Rakesh K. Jain. "Taming vessels to treat cancer". In: *Scientific American* 298.1 (2008), pp. 56–63.

[164] K. Jin Kim et al. "Inhibition of vascular endothelial growth factor-induced angiogenesis suppresses tumour growth in vivo". In: *Nature* 362.6423 (1993), pp. 841–844.

[165] Bruce J. Giantonio et al. "Bevacizumab in combination with oxaliplatin, fluorouracil, and leucovorin (FOLFOX4) for previously treated metastatic colorectal cancer: Results from the Eastern Cooperative Oncology Group Study E3200". In: *Journal of Clinical Oncology* 25.12 (2007), pp. 1539–1544.

[166] C. G. Lee et al. "Anti-vascular endothelial growth factor treatment augments tumor radiation response under normoxic or hypoxic conditions". In: *Cancer Research* (2000).

[167] Ricky T. Tong et al. "Vascular normalization by vascular endothelial growth factor receptor 2 blockade induces a pressure gradient across the vasculature and improves drug penetration in tumors". In: *Cancer Research* (2004).

[168] H. Wildiers et al. "Effect of antivascular endothelial growth factor treatment on the intratumoral uptake of CPT-11". In: *British Journal of Cancer* (2003).

[169] Paxton V. Dickson et al. "Bevacizumab-induced transient remodeling of the vasculature in neuroblastoma xenografts results in improved delivery and efficacy of systemically administered chemotherapy". In: *Clinical Cancer Research* (2007).

[170] Minah Kim et al. "Amplification of Oncolytic Vaccinia Virus Widespread Tumor Cell Killing by Sunitinib through Multiple Mechanisms". In: *Cancer Research* 78.4 (Feb. 2018), pp. 922–937.

[171] Kazuhiko Kurozumi et al. "Effect of tumor microenvironment modulation on the efficacy of oncolytic virus therapy". In: *Journal of the National Cancer Institute* 99.23 (Dec. 2007), pp. 1768–1781.

[172] Caroline J Breitbach et al. "Oncolytic vaccinia virus disrupts tumor-associated vasculature in humans". In: *Cancer Research* 73.4 (Feb. 2013), pp. 1265–1275.

[173] Weizhou Hou et al. "Oncolytic vaccinia virus demonstrates antiangiogenic effects mediated by targeting of VEGF". In: *International Journal of Cancer* 135.5 (Sept. 2014), pp. 1238–1246.

[174] Tim D. Pencavel et al. "Isolated limb perfusion with melphalan, tumour necrosis factor-Alpha and oncolytic vaccinia virus improves tumour targeting and prolongs survival in a rat model of advanced extremity sarcoma". In: *International Journal of Cancer* (2015).

[175] Takahiro Seki et al. "Tumour necrosis factor-alpha increases extravasation of virus particles into tumour tissue by activating the Rho A/Rho kinase pathway". In: *Journal of Controlled Release* (2011).

[176] Rozanne Arulanandam et al. "VEGF-Mediated Induction of PRD1-BF1/Blimp1 Expression Sensitizes Tumor Vasculature to Oncolytic Virus Infection". In: *Cancer Cell* 28.2 (Aug. 2015), pp. 210–224.

[177] Amber Miller et al. "Perfusion Pressure Is a Critical Determinant of the Intratumoral Extravasation of Oncolytic Viruses." In: *Molecular therapy : the journal of the American Society of Gene Therapy* 24.2 (Feb. 2016), pp. 306–317.

[178] Leonard W Seymour and Kerry D Fisher. *Under pressure: Elevated blood pressure enhances targeting of tumors by oncolytic viruses*. Feb. 2016.

[179] Stuart Ibsen et al. "Ultrasound Mediated Localized Drug Delivery". In: *Nano-Biotechnology for Biomedical and Diagnostic Research*. Ed. by Eran Zahavy et al. Dordrecht: Springer Netherlands, 2012, pp. 145–153.

[180] Paul C. Lyon et al. "Safety and feasibility of ultrasound-triggered targeted drug delivery of doxorubicin from thermosensitive liposomes in liver tumours (TARDOX): a single-centre, open-label, phase 1 trial". In: *The Lancet Oncology* 19.8 (Aug. 2018), pp. 1027–1039.

[181] E. P. Stride and C. C. Coussios. "Cavitation and contrast: The use of bubbles in ultrasound imaging and therapy". In: *Proceedings of the Institution of Mechanical Engineers, Part H: Journal of Engineering in Medicine* 224.2 (Feb. 2010), pp. 171–191.

[182] Costas D. Arvanitis et al. "Cavitation-Enhanced Extravasation for Drug Delivery". In: *Ultrasound in Medicine and Biology* (2011).

[183] Bassel Rifai et al. "Cavitation-enhanced delivery of macromolecules into an obstructed vessel". In: *The Journal of the Acoustical Society of America* 128.5 (2010), EL310–EL315.

[184] James Collis et al. "Cavitation microstreaming and stress fields created by microbubbles". In: *Ultrasonics* 50.2 (Feb. 2010), pp. 273–279.

[185] Steven Mo et al. "Ultrasound-enhanced drug delivery for cancer". In: *Expert Opinion on Drug Delivery* 9.12 (Dec. 2012), pp. 1525–1538.

[186] T. G. Leighton and Robert E. Apfel. "The Acoustic Bubble". In: *The Journal of the Acoustical Society of America* (1994).

[187] Candace M. Howard et al. "Ultrasound guided site specific gene delivery system using adenoviral vectors and commercial ultrasound contrast agents". In: *Journal of Cellular Physiology* (2006).

[188] Adelaide Greco et al. "Eradication of Therapy-resistant Human Prostate Tumors Using an Ultrasound-guided Site-specific Cancer Terminator Virus Delivery Approach". In: *Molecular Therapy* 18.2 (Feb. 2010), pp. 295–306.

[189] James J. Kwan et al. "Ultrasound-Propelled Nanocups for Drug Delivery". In: *Small* 11.39 (2015), pp. 5305–5314.

[190] Rachel Myers et al. "Polymeric Cups for Cavitation-mediated Delivery of Oncolytic Vaccinia Virus." In: *Molecular therapy : the journal of the American Society of Gene Therapy* 24.9 (Sept. 2016), pp. 1627–33.

[191] C.-C. Coussios and R A Roy. "Applications of acoustics and cavitation to noninvasive therapy and drug delivery". In: *Annual Review of Fluid Mechanics* 40 (2008), pp. 395–420.

[192] Delphine Elbes et al. "Sub-millimeter bistatic passive acoustic mapping". In: *The Journal of the Acoustical Society of America* 141.5 (May 2017), pp. 3550–3551.

[193] Miklós Gyöngy. "Passive Cavitation Mapping for Monitoring Ultrasound Therapy". PhD thesis. University of Oxford, 2010.

[194] Christian Coviello et al. "Passive acoustic mapping utilizing optimal beamforming in ultrasound therapy monitoring". In: *The Journal of the Acoustical Society of America* 137.5 (May 2015), pp. 2573–2585.

[195] Johann Foloppe et al. "The Enhanced Tumor Specificity of TG6002, an Armed Oncolytic Vaccinia Virus Deleted in Two Genes Involved in Nucleotide Metabolism". In: *Molecular Therapy - Oncolytics* 14 (Sept. 2019), pp. 1–14.

[196] Urara Tomita et al. "Poly(ethylene glycol)-Lipid-Conjugated Antibodies Enhance Dendritic Cell Phagocytosis of Apoptotic Cancer Cells." In: *Pharmaceuticals (Basel, Switzerland)* 5.5 (Apr. 2012), pp. 405–16.

[197] Manfred M. Kurfürst. "Detection and molecular weight determination of polyethylene glycol-modified hirudin by staining after sodium dodecyl sulfate-polyacrylamide gel electrophoresis". In: *Analytical Biochemistry* 200.2 (Feb. 1992), pp. 244–248.

[198] Demir Akin, Haibo Li, and Rashid Bashir. "Real-Time Virus Trapping and Fluorescent Imaging in Microfluidic Devices". In: *Nano Letters* (2004).

[199] Eloise Thomas et al. "Ultrasound-mediated cavitation enhances the delivery of an EGFR-targeting liposomal formulation designed for chemo-radionuclide therapy". In: *Theranostics* 9.19 (2019), pp. 5595–5609.

[200] Paul Kinchesh et al. "Prospective gating control for highly efficient cardio-respiratory synchronised short and constant TR MRI in the mouse". In: *Magnetic Resonance Imaging* (2018).

[201] Stephen Russell and Amber Miller. "Heterogeneous delivery is a barrier to the translational advancement of oncolytic virotherapy for treating solid tumors". In: *Virus Adaptation and Treatment* (July 2014), p. 11.

[202] Miriam Bazan-Peregrino et al. "Cavitation-enhanced delivery of a replicating oncolytic adenovirus to tumors using focused ultrasound". In: *Journal of Controlled Release* 169.1-2 (July 2013), pp. 40–47.

[203] Cameron A.B. Smith and Constantin C. Coussios. "Spatiotemporal Assessment of the Cellular Safety of Cavitation-Based Therapies by Passive Acoustic Mapping". In: *Ultrasound in Medicine and Biology* 46.5 (May 2020), pp. 1235–1243.

[204] Meijun Zheng et al. *Oncolytic Viruses for Cancer Therapy: Barriers and Recent Advances*. Dec. 2019.

[205] Laetitia Fend et al. "Oncolytic virotherapy with an armed vaccinia virus in an orthotopic model of renal carcinoma is associated with modification of the tumor microenvironment". In: *OncoImmunology* 5.2 (Feb. 2016).

[206] Kenneth Lundstrom. "New frontiers in oncolytic viruses: optimizing and selecting for virus strains with improved efficacy." In: *Biologics : targets & therapy* 12 (2018), pp. 43–60.

[207] J. J. Kwan et al. "Ultrasound-induced inertial cavitation from gas-stabilizing nanoparticles". In: *Physical Review E - Statistical, Nonlinear, and Soft Matter Physics* 92.2 (Aug. 2015), p. 023019.

[208] J. A. McCart et al. "Complex interactions between the replicating oncolytic effect and the enzyme/prodrug effect of vaccinia-mediated tumor regression". In: *Gene Therapy* 7.14 (July 2000), pp. 1217–1223.

[209] Sheela A. Abraham et al. "The liposomal formulation of doxorubicin". In: *Methods in Enzymology* 391.SPEC. ISS. (Jan. 2005), pp. 71–97.

[210] Rasmus Eliasen, Thomas L. Andresen, and Jannik B. Larsen. "PEG-Lipid Post Insertion into Drug Delivery Liposomes Quantified at the Single Liposome Level". In: *Advanced Materials Interfaces* 6.9 (May 2019), p. 1801807.

[211] Robert B. Gennis. *Biomembranes*. Springer Advanced Texts in Chemistry. New York, NY: Springer New York, 1989.

[212] David H. Boal. "Mechanics of the cell". In: (2012), p. 608.

[213] L. S. Ramsammy and H. Brockerhoff. "Lysophosphatidylcholine-cholesterol complex." In: *Journal of Biological Chemistry* (1982).

[214] V P Shastri. "Non-degradable biocompatible polymers in medicine: past, present and future." In: *Current Pharmaceutical Biotechnology* 4.5 (Oct. 2003), pp. 331–337.

[215] Denis E. Corpet et al. "Consistent and fast inhibition of colon carcinogenesis by polyethylene glycol in mice and rats given various carcinogens." In: *Cancer Reasearch* 60.12 (June 2015), pp. 3160–3164.

[216] Prud'homme Sonke Svenson Robert K. *Multifunctional Nanoparticles for Drug Delivery Applications: Imaging, Targeting and Delivery*. Ed. by Prud'homme Sonke Svenson Robert K. Nanostructure Science and Technology. Springer, 2012.

[217] A. K. Bajpai et al. *Responsive polymers in controlled drug delivery*. 2008.

[218] Chemindustry.ru. *Polyethylene glycol*. 2010.

[219] Edward A. Belongia and Allison L. Naleway. *Smallpox vaccine: the good, the bad, and the ugly*. 2003.

[220] F. Danhier. *To exploit the tumor microenvironment: Since the EPR effect fails in the clinic, what is the future of nanomedicine?* Dec. 2016.

[221] Joseph W. Nichols and You Han Bae. *EPR: Evidence and fallacy*. Sept. 2014.

[222] Bernard Moss. *Membrane fusion during poxvirus entry*. Dec. 2016.

[223] Mark Lyons et al. "Adenovirus Type 5 Interactions with Human Blood Cells May Compromise Systemic Delivery". In: *Molecular Therapy* 14.1 (July 2006), pp. 118–128.

[224] A. Rum Yoon et al. "Antitumor effect and safety profile of systemically delivered oncolytic adenovirus complexed with EGFR-targeted PAMAM-based dendrimer in orthotopic lung tumor model". In: *Journal of Controlled Release* 231 (June 2016), pp. 2–16.

[225] Marie C. Galmiche et al. "Expression of a functional single chain antibody on the surface of extracellular enveloped vaccinia virus as a step towards selective tumour cell targeting". In: *Journal of General Virology* 78.11 (1997), pp. 3019–3027.

[226] Benjamin Purow and Kevin Staveley-O'Carroll. "Targeting of vaccinia virus using biotin-avidin viral coating and biotinylated antibodies". In: *Journal of Surgical Research* 123.1 (Jan. 2005), pp. 49–54.

[227] S. N. Isaacs, G. J. Kotwal, and B. Moss. "Vaccinia virus complement-control protein prevents antibody-dependent complement-enhanced neutralization of infectivity and contributes to virulence". In: *Proceedings of the National Academy of Sciences of the United States of America* 89.2 (Jan. 1992), pp. 628–632.

[228] Alberto Gabizon et al. "Prolonged Circulation Time and Enhanced Accumulation in Malignant Exudates of Doxorubicin Encapsulated in Polyethylene-glycol Coated Liposomes". In: *Cancer Research* 54.4 (1994).

[229] C. A. Cuenod and D. Balvay. *Perfusion and vascular permeability: Basic concepts and measurement in DCE-CT and DCE-MRI*. Dec. 2013.

[230] Gabriele Bergers and Laura E. Benjamin. *Tumorigenesis and the angiogenic switch*. June 2003.

[231] Yu Han H. Hsu, Gregory Z. Ferl, and Chee M. Ng. "GPU-accelerated nonparametric kinetic analysis of DCE-MRI data from glioblastoma patients treated with bevacizumab". In: *Magnetic Resonance Imaging* 31.4 (May 2013), pp. 618–623.

[232] Gregory Z. Ferl et al. "An automated method for nonparametric kinetic analysis of clinical DCE-MRI data: Application to glioblastoma treated with bevacizumab". In: *Magnetic Resonance in Medicine* 63.5 (May 2010), pp. 1366–1375.

[233] Aikaterini A Kyriazis et al. *Morphological, Biological, Biochemical, and Karyotypic Characteristics of Human Pancreatic Ductal Adenocarcinoma Capan-2 in Tissue Culture and the Nude Mouse*. Tech. rep. 1986, pp. 5810–5815.

[234] Guang Wu et al. "A novel monoclonal antibody targets mucin1 and attenuates growth in pancreatic cancer model". In: *International Journal of Molecular Sciences* 19.7 (July 2018).

[235] S J Gendler and A P Spicer. "Epithelial Mucin Genes". In: *Annual Review of Physiology* 57.1 (Oct. 1995), pp. 607–634.

[236] Errin Lagow, Mary M Desouza, and Daniel D Carson. *Mammalian reproductive tract mucins*. Tech. rep. 4. 1999, pp. 280–292.

[237] W. M.C. Mulder et al. "Mucin-1-related T cell infiltration in colorectal carcinoma". In: *Cancer Immunology Immunotherapy* 42.6 (Sept. 1996), pp. 351–356.

[238] M Sahraei et al. "MUC1 regulates PDGFA expression during pancreatic cancer progression". In: *Oncogene* 31.47 (Nov. 2012), pp. 4935–4945.

[239] Joseph H. Hilgers and P. H.C. Hageman. "A review on antigens of milkfat globule membranes and their value for diagnosis and prognosis of breast cancer and other carcinomas". In: *The Keio Journal of Medicine* 35.4 (1986), pp. 235–244.

[240] Markus Puhlmann et al. "Vaccinia as a vector for tumor-directed gene therapy: Biodistribution of a thymidine kinase-deleted mutant". In: *Cancer Gene Therapy* 7.1 (May 2000), pp. 66–73.

[241] Jennifer B. Meko et al. "High Cytokine Production and Effective Antitumor Activity of a Recombinant Vaccinia Virus Encoding Murine Interleukin 12". In: *Cancer Research* 55.21 (May 1995), pp. 4765–4770.

[242] Gunasegaran Karupiah et al. "Vaccinia virus-mediated damage of murine ovaries and protection by virus-expressed interleukin-2". In: *Immunology and Cell Biology* 68.5 (Oct. 1990), pp. 325–333.

[243] Leslee Sprague et al. *Please stand by: How oncolytic viruses impact bystander cells*. 2018.

[244] Ann Richmond and Su Yingjun. *Mouse xenograft models vs GEM models for human cancer therapeutics*. 2008.

[245] Catherine S. Wegner et al. "Diffusion-weighted and dynamic contrast-enhanced MRI of pancreatic adenocarcinoma xenografts: Associations with tumor differentiation and collagen content". In: *Journal of Translational Medicine* (2016).

[246] Catherine S. Wegner et al. "Dynamic contrast-enhanced MRI of the microenvironment of pancreatic adenocarcinoma xenografts". In: *Acta Oncologica* 56.12 (Dec. 2017), pp. 1754–1762.

[247] Nigel Peat et al. "Tissue-specific Expression of a Human Polymorphic Epithelial Mucin (MUC1) in Transgenic Mice". In: *Cancer Research* (1992).

[248] Brian J Thomson. "Viruses and apoptosis". In: *International Journal of Experimental Pathology* 82.2 (2001), p. 65.

[249] *OxSonics – A breakthrough drug delivery platform*.

[250] Cory A Brennick et al. "Neoepitopes as cancer immunotherapy targets: key challenges and opportunities". In: *Immunotherapy* 9.4 (Mar. 2017), pp. 361–371.

[251] *Phase 3 Trial for Oncolytic Viral Therapy Pexa-Vec in Advanced Liver Cancer Terminated Early - Cancer Therapy Advisor*.

[252] Harald Sauthoff et al. "Intratumoral spread of wild-type adenovirus is limited after local injection of human xenograft tumors: Virus persists and spreads systemically at late time points". In: *Human Gene Therapy* 14.5 (Mar. 2003), pp. 425–433.

[253] M. Bazan-Peregrino et al. "Factors influencing retention of adenovirus within tumours following direct intratumoural injection". In: *Gene Therapy* 15.9 (May 2008), pp. 688–694.

[254] Lizhi Li et al. *Delivery and Biosafety of Oncolytic Virotherapy*. Apr. 2020.

[255] Tien V Nguyen et al. "Evaluation of polymer shielding for adenovirus serotype 6 (Ad6) for systemic virotherapy against human prostate cancers". In: *Molecular Therapy - Oncolytics* 3 (Jan. 2016), p. 15021.

[256] N. M. Girgis et al. "The Vaccinia Virus Complement Control Protein Modulates Adaptive Immune Responses during Infection". In: *Journal of Virology* 85.6 (Mar. 2011), pp. 2547–2556.

[257] Christine L. Hattrup and Sandra J. Gendler. "MUC1 alters oncogenic events and transcription in human breast cancer cells". In: *Breast Cancer Research* 8.4 (July 2006), R37.

[258] Fengli Wang et al. "Expression of human full-length MUC1 inhibits the proliferation and migration of a B16 mouse melanoma cell line". In: *Oncology Reports* 30.1 (July 2013), pp. 260–268.

[259] Rachel Myers et al. "Ultrasound-mediated cavitation does not decrease the activity of small molecule, antibody or viral-based medicines". In: *International Journal of Nanomedicine* (2018).

[260] André Görgens et al. "Optimisation of imaging flow cytometry for the analysis of single extracellular vesicles by using fluorescence-tagged vesicles as biological reference material". In: *Journal of Extracellular Vesicles* 8.1 (Dec. 2019), p. 1587567.

[261] Jonathan K Dozier and Mark D Distefano. "Site-Specific PEGylation of Therapeutic Proteins". In: *OPEN ACCESS Int. J. Mol. Sci* 16 (2015), p. 16.

[262] Arthur Dyer et al. *Turning cold tumours hot: oncolytic virotherapy gets up close and personal with other therapeutics at the 11th Oncolytic Virus Conference*. Mar. 2019.

[263] Qianqian Duan et al. *Turning Cold into Hot: Firing up the Tumor Microenvironment*. July 2020.